UNIVERSITY OF SOUTHAMPTON

FACULTY OF ENGINEERING AND THE ENVIRONMENT

Mathematical Modelling and Simulation of Biofuel Cells

by

Mohamad Hussein Osman

Thesis submitted for the degree of Doctor of Philosophy

December 2013

UNIVERSITY OF SOUTHAMPTON

ABSTRACT

FACULTY OF ENGINEERING AND THE ENVIRONMENT

MATHEMATICAL MODELLING AND SIMULATION OF BIOFUEL CELLS

by Mohamad Hussein Osman

Bio-fuel cells are driven by diverse and abundant bio-fuels and biological catalysts. The production/consumption cycle of bio-fuels is considered to be carbon neutral and, in principle, more sustainable than that of conventional fuel cells. The cost benefits over traditional precious-metal catalysts, and the mild operating conditions represent further advantages. It is important that mathematical models are developed to reduce the burden on laboratory based testing and accelerate the development of practical systems. In this study, recent key developments in bio-fuel cell technology are reviewed and two different approaches to modelling biofuel cells are presented, a detailed physics-based approach, and a data-driven regression model.

The current scientific and engineering challenges involved in developing practical bio-fuel cell systems are described, particularly in relation to a fundamental understanding of the reaction environment, the performance and stability requirements, modularity and scalability. New materials and methods for the immobilization of enzymes and mediators on electrodes are examined, in relation to performance characteristics and stability. Fuels, mediators and enzymes used (anode and cathode), as well as the cell configurations employed are discussed. New developments in microbial fuel cell technologies are reviewed in the context of fuel sources, electron transfer mechanisms, anode materials and enhanced O_2 reduction.

Multi-dimensional steady-state and dynamic models of two enzymatic glucose/air fuel cells are presented. Detailed mass and charge balances are combined with a model for the reaction mechanism in the electrodes. The models are validated against experimental results. The dynamic performance under different cell voltages is simulated and the evolution of the system is described. Parametric studies are performed to investigate the effect of various operating conditions. A data-driven model, based on a reduced-basis form of Gaussian process regression, is also presented and tested. The improved computational efficiency of data-driven models makes them better candidates for modelling large complex systems.

Contents

List of Tables

List of Figures

Accompanying Material

M.H. Osman, A.A. Shah, R.G.A. Wills, F.C. Walsh (2013). "Mathematical modelling of an enzymatic fuel cell with an air-breathing cathode". Electrochimica Acta, **112**: 386-393.

M.H. Osman, A.A. Shah, R.G.A. Wills (2013). "Detailed mathematical model of an enzymatic fuel cell". Journal of The Electrochemical Society **160** (8): F806-F814.

M.H. Osman, A.A. Shah, F.C. Walsh (2011). "Recent progress and continuing challenges in bio-fuel cells. Part I: Enzymatic cells". Biosensors and Bioelectronics **26**: 3087-3102.

M.H. Osman, A.A. Shah, F.C. Walsh (2010). "Recent progress and continuing challenges in bio-fuel cells. Part II: Microbial". Biosensors and Bioelectronics **26**: 953-963.

Author's Declaration

I, Mohamad Hussein Osman declare that the thesis entitled Mathematical Modelling and Simulation of Biofuel Cells and the work presented in the thesis are both my own, and have been generated by me as the result of my own original research. I confirm that: this work was done wholly or mainly while in candidature for a research degree at this University; where any part of this thesis has previously been submitted for a degree or any other qualification at this University or any other institution, this has been clearly stated; where I have consulted the published work of others, this is always clearly attributed; where I have quoted from the work of others, the source is always given. With the exception of such quotations, this thesis is entirely my own work; I have acknowledged all main sources of help; where the thesis is based on work done by myself jointly with others, I have made clear exactly what was done by others and what I have contributed myself; parts of this work have been published as:

- M.H. Osman, A.A. Shah, R.G.A. Wills, F.C. Walsh (2013). "Mathematical modelling of an enzymatic fuel cell with an air-breathing cathode". Electrochimica Acta, **112**: 386-393.
- M.H. Osman, A.A. Shah, R.G.A. Wills (2013). "Detailed mathematical model of an enzymatic fuel cell". Journal of The Electrochemical Society **160** (8): F806-F814.
- M.H. Osman, A.A. Shah, F.C. Walsh (2011). "Recent progress and continuing challenges in bio-fuel cells. Part I: Enzymatic cells". Biosensors and Bioelectronics **26**: 3087-3102.
- M.H. Osman, A.A. Shah, F.C. Walsh (2010). "Recent progress and continuing challenges in bio-fuel cells. Part II: Microbial". Biosensors and Bioelectronics **26**:

953-963.

The review of recent progress in biofuel cells as well as the composition of the first draft was conducted entirely by myself. The mathematical model formulation, practical implementation, and the preparation of the first draft are also a result of my own research. The final published version includes minor editing by my supervisors Dr. Akeel Shah, Prof. Frank Walsh, and Dr. Richard Wills, the co-authors of those papers.

Signed: .....

Date: .....

Nomenclature

Abbreviations

AAO	Anodized aluminum oxide
ABTS	2,2'-azinobis(3-ethylbenzothiazoline-6-sulfonate) diammonium salt
AFC	Alkaline fuel cell
AlcDH	Alcohol dehydrogenase
AlcOx	Alcohol oxidase
AQDS	Anthraquinone-1,6-disulfonic acid
BES	2-bromoethanesulfonate
BFC	Bio-fuel cell
BOD	Bilirubin oxidase
BUG	Benthic unattended generator
CDH	Cellobiose dehydrogenase
CE	Coulombic efficiency
CF	Carbon fiber
CHP	Combined heat and power
CNT	Carbon nano-tube
CoTMPP	Cobalt tetramethylphenylporphyrin
COx	Cytochrome oxidase
CP	Carbon paper

CV	Cyclic voltammetry
DET	Direct electron transfer
DMFC	Direct methanol fuel cell
EDTA	Ethylenediaminetetraacetic acid
EFC	Enzymatic fuel cell
ET	Electron transfer
$FAD(H_2)$	Flavin adenine dinucleotide, cofactor for GOx (reduced form)
FDH	Fructose dehydrogenase
FESEM	Field emission scanning electron microscope
GC	Glassy carbon
GDH	Glucose dehydrogenase
GOx	Glucose oxidase
GPR	Gaussian process regression
HQS	8-hydroxyquinoline-5-sulfonic
KB	Ketjen-Black
K_3	Menadione
LDH	Lactate dehydrogenase
MCFC	Molten carbonate fuel cell
MEA	Membrane electrode assembly
MEC	Microbial electrolysis cell
MET	Mediated electron transfer
MFC	Microbial fuel cell
MP	Microperoxidase
MWCNT	Multi-wall carbon nano-tube
NAD(H)	Nicotinamide adenine dinucleotide (reduced form)
NP	Nano-particle

NQ	1,4-Naphthoquinone
NR	Neutral red
PAFC	Phosphoric acid fuel cell
PBS	Phosphate buffer solution
PEM(FC)	Polymer electrolyte membrane (fuel cell)
PLL	Poly-L-lysine
PPy	Polypyrrole
PQQ	Pyrroloquinoline quinone
PTFE	Polytetrafluoroethylene
PVP	Polyvinylpyridine
RFB	Redox flow battery (regenerative fuel cell)
SAM	Self-assembled monolayer
SCC	Short-circuit current
SOFC	Solid oxide fuel cell
SWCNT	Single-wall carbon nano-tubes

Symbols

a^s	Specific surface area	(m^{-1})
c_i	Concentration of species i	$(\mathrm{mol\,m}^{-3})$
C	Covariance matrix	
D	Diffusion coefficient	$(\mathrm{m}^2\,\mathrm{s}^{-1})$
$\mathcal{D}$	Training data set for GPR	
E	Equilibrium (open-circuit) potential	(V)
E^0	Redox potential	(V)
$E^{0\prime}$	Reference redox potential	(V)
$\mathbb{E}(Y)$	Expected value of random variable Y	

$\boldsymbol{\mathcal{E}}$	Random vector of noise terms	
$f_Y(y)$	Probability distribution of random variable Y	
I	Current	(A)
I_M	$M \times M$ identity matrix	
j	Current density	($\mathrm{A\,m^{-2}}$)
k	Reaction rate constant	
MM	Michaelis-Menten constant	($\mathrm{mol\,m^{-3}}$)
$\mathcal{N}(\mu, \sigma^2)$	Normal (Gaussian) distribution (mean μ and variance σ^2)	
P	Power density	($\mathrm{W\,m^{-2}}$)
R	Volumetric reaction rate	($\mathrm{mol\,m^{-3}\,s^{-1}}$)
$\mathbb{R}$	Set of real numbers	
S	Source term in differential equation	
T	Temperature	(K)
V_{cell}	Cell voltage	(V)
Y	Random variable	
z	Charge number	
γ	Coefficients of basis vector expansion	
δ_{ij}	Kronecker delta function	
ϵ	Volume fraction	
$\boldsymbol{\zeta}$	Spatial coordinate	
η	Over-potential	(V)
$\boldsymbol{\theta}$	Hyperparamters used in GPR	
κ	Conductivity	($\mathrm{S\,m^{-1}}$)
κ_a, κ_d	Adsorption/desorption coefficients of water	($\mathrm{s^{-1}}$)
λ	Nafion water content	

$\boldsymbol{\mu}$	Mean (expected) value	
ρ	Resistivity	($\Omega\,\mathrm{m}$)
σ	Standard daviation (or variance σ^2)	
ϕ_e	Ionic potential	(V)
ϕ_s	Electronic potential	(V)
$\boldsymbol{\chi}$	Basis functions	
$\boldsymbol{\psi}$	Basis vectors	

Subscripts

red	Reduced state
ox	Oxidized state
e	Relating to the conductive electrolyte phase
s	Relating to the conductive solid phase

Chapter 1

Introduction

1.1 The definition of a fuel cell

Electrochemical power sources are devices that directly convert the chemical energy in a reactant or fuel into electrical energy. Fuel cells differ from other electrochemical devices, such as batteries, in that the gaseous or liquid reactants are stored externally so that a fuel cell may be operated for long time periods without the need for recharging, as long as the continual supply of reactants is maintained [1].

Direct electrochemical conversion is a desirable feature since it avoids the thermodynamic limitations associated with combustion, the direct chemical reaction of a fuel with an oxidant. A heat engine engine operates by extracting a portion of the total thermal energy released upon combustion and converting it to useful mechanical energy. For a heat engine operating at a temperature T_1 and the exhaust fluid is released at temperature T_2, the maximum theoretical efficiency is know as the Carnot limit and may be expressed as: $1 - \frac{T_2}{T_1}$, where temperatures are expressed in Kelvin. In most practical cases the efficiency is usually less than 30% and decreases with decreasing operating temperature T_1. Another portion of the total heat of combustion is lost as irretrievable heat. In fuel cells, at least two electrochemical reactions, of the fuel and oxidant, occur simultaneously

at distinct electrically conducting electrodes, directly extracting electrical from chemical energy. In contrast to heat engines, the maximum thermodynamic efficiency of fuel cells is equal to the ratio of the useful portion of electrical energy to the total enthalpy change, ΔH, of the fuel cell reaction. ΔH indicates the total heat released by the reaction at constant pressure. The useful electrical energy that may be extracted is equal to the Gibbs energy, ΔG, and the maximum theoretical efficiency for a fuel cell may be expressed as [2]: $\frac{\Delta G}{\Delta H}$. The difference between the enthalpy change and Gibbs free energy is equal to $T\Delta S$ where T is the temperature and ΔS is the entropy change which represent irreversible losses. This theoretical limit is usually much higher than that of heat engines and may reach values greater than 80% at low operating temperatures. In addition to higher theoretical efficiencies and better fuel utilization, the products of electrochemical reactions are generally less toxic than those of high temperature combustion.

Bio-fuel cells have been defined as systems capable of direct chemical to electrical energy conversion *via* biochemical pathways [3–5]. The conversion is achieved by coupling an oxidation reaction supplying electrons at the anode electrode with a reduction reaction utilizing electrons at the cathode electrode. These two reactions are electronically separated inside the system to force electrons to flow through an external circuit, while ion movement inside the system (electrolyte) maintains charge balance and completes the electrical circuit (see Fig. 1.1 for an example). A fuel cell is biological if in at least one electrode: the reactant is found in biological fluids, or the reaction catalyst is biological (enzyme, bacteria) [1].

Bio-fuel cells (BFCs) are considered to be in the early stages of development. The chemical reactions are driven by diverse and abundant bio-fuels [6] and biological catalysts. The production/consumption cycle of bio-fuels is considered to be carbon neutral and, in principle, more sustainable than that of conventional fuel cells [7]. Moreover, bio-catalysts could offer significant cost advantages over traditional precious-metal catalysts through economies of scale. The neutral pH and low temperature of operation represents further advantages [3, 5].

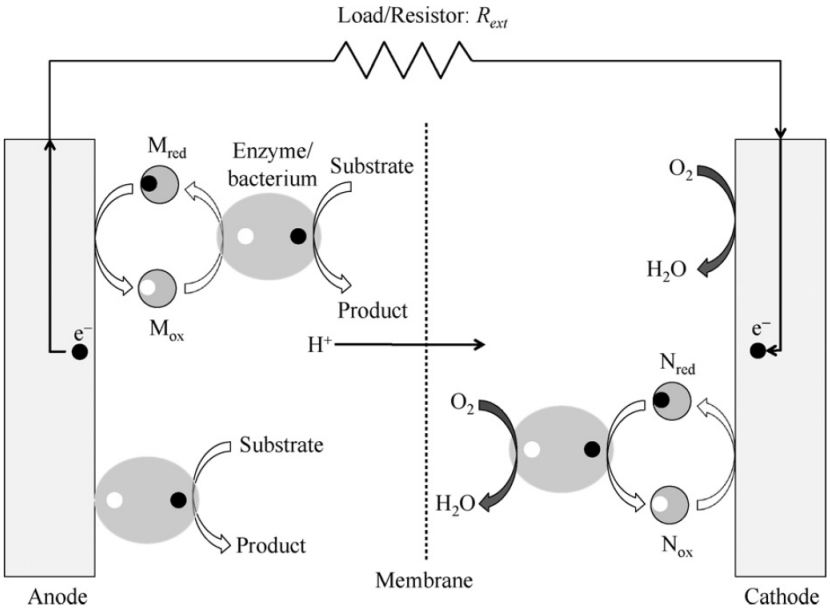

Figure 1.1: An example of a biofuel cell with oxygen reduction at the cathode. Oxidation of the substrate is catalysed by the enzymes/bacteria (preferably immobilised on the electrodes), releasing protons and electrons. The electrons released are either transferred directly to the electrode or are transferred via redox mediators, M. Oxygen reduction at the cathode can take place directly on the electrode or via enzymes/bacteria, possibly facilitated by mediators, N. The mediators can be freely suspended or immobilised on the electrode to enhance electron transfer.

Table 1.1: Electrolyte type and operating temperature of some inorganic fuel cells. [2]

Fuel cell type	**Mobile ion**	**Operating temperature**	**Application**
Alkaline (AFC)	OH^-	50-200°C	Space vehicles: Apollo, Shuttle
Proton exchange membrane (PEMFC)	H^+	30-100°C	Vehicles, mobile applications and low power CHP
Direct methanol (DMFC)	H^+	20-90°C	Low power portable electronics
Phosphoric acid (PAFC)	H^+	~220°C	Large number of 200 kW CHP systems in use
Molten carbonate (MCFC)	CO_3^{2-}	~650°C	Medium to large-scale CHP systems up to MW capacity
Solid oxide (SOFC)	O^{2-}	500-1000°C	All sizes of CHP systems, 2 kW to multi-MW

1.2 Inorganic fuel cells

Conventional fuel cells such as the polymer electrolyte membrane (PEMFC), molten carbonate (MCFC), phosphoric acid (PAFC) and solid oxide (SOFC) fuel cells have reached an advanced state in their development [1, 2]. With the exception of some direct liquid fuel

cells; direct methanol (DMFC) and direct ethanol, conventional fuel cells are essentially hydrogen fuel cells. The hydrogen gas (H_2) is usually produced by reforming hydrocarbons (C_nH_m) like petroleum and natural gas. In high temperature fuel cells this can be achieved internally without the need for an external reformer. The method commonly used is steam reforming, requiring temperatures greater than 500°C [2] and a catalyst:

$$C_nH_m + n\,H_2O \rightarrow \left(n + \frac{m}{2}\right) H_2 + n\,CO \tag{1.1}$$

Hydrogen is an attractive reactant for fuel cells. The electrochemical oxidation of hydrogen at the anode is very efficient, but it is not a natural fuel [1]. It is difficult to handle and has a low volumetric energy density even at high pressures. When produced from hydrocarbons, the fuel gas needs to be purified from contaminating material such as carbon monoxide (CO) and/or some sulphur containing compounds that can poison the catalyst[2]. The catalysts used in these fuel cells are inorganic and usually metallic. The term inorganic fuel cell is used in this context to describe these conventional devices and distinguish them from our focus, bio-fuel cells.

Table 1.1 includes some common types of inorganic fuel cells and shows their electrolyte type, typical operating temperature, and areas of applications. The alkaline fuel cell (AFC) is one of the early types that started in the 1960s with the first fuel cell boom stimulated by the space exploration race. The basicity of the electrolyte makes non-platinum catalysts possible in AFCs, but the risk of CO_2 poisoning makes them practically unusable with reformed fuels [2]. Avoiding expensive precious metal catalysts can also be achieved in high temperature fuel cells such as MCFC and SOFC.

Platinum has the highest catalytic activity among transition metals and is stable over a wide range of pH. Platinum is know to be poisoned by carbon monoxide at just 10 ppm. One method of the CO purification is the water-gas shift reaction where a mixture of water vapour and carbon monoxide reacts to produce hydrogen gas and carbon dioxide:

$$CO + H_2O \rightarrow H_2 + CO_2 \tag{1.2}$$

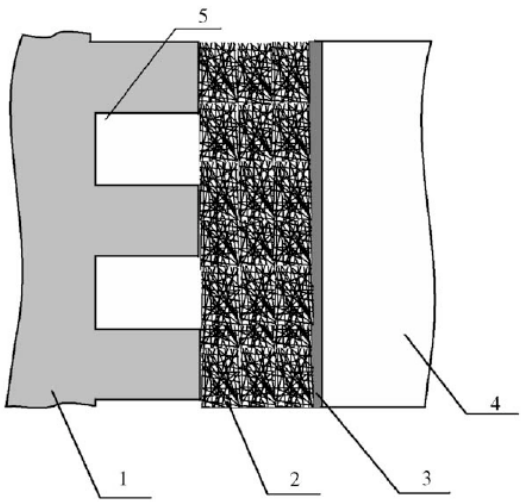

Figure 1.2: Scheme of an electrode: 1-current collector (bipolar plate); 2-gas diffusion layer; 3-catalyst layer; 4-membrane; 5-gas flow channel. [8]

In addition to purifying the fuel from carbon monoxide, this reaction also increases the efficiency of the fuel cell by the additional hydrogen produced.

The lifetime of fuel cells is limited mainly by a decrease in catalysts activity (dissolution, contamination, corrosion) and loss of ionic conductivity due to membrane degradation. Solid electrolytes reduce the risk of leakage and mixing of reactants. Between 1960 and the 1980s, Du Pont developed a proton conducting PTFE polymer with sulphonic acid groups under the trade name of Nafion. These membranes were quickly used in small fuel cells due to their chemical stability, high ionic conductivity (wet operation at $T \geq 80°C$), and overall improved cell lifetime [1]. The disadvantages of these membranes are a sensitivity to metal ion contamination and high cost. Other drawbacks include its permeability to methanol and other reactants. During the 1990s, there was an order of magnitude increase in the power density and a similar decrease in the surface density of Pt catalyst. This was due to the Nafion membrane, better surface utilization of the catalyst, and the introduction of the MEA fabrication method [1].

Electrode fabrication and catalyst utilization

The structure of the electrode is made with the purpose of providing maximum interface area between the fuel or oxygen, the electrolyte to exchange ions between the two half cells, and the actual electrode structure to transport the electron to/from the reaction sites, which is commonly referred to as 'three phase contact' [2]. The presence of some kind of catalyst to improve the reaction kinetics is common practice for most fuel cell designs, especially low temperature cells. From this, researchers distinguish two parts of the electrode, the gas diffusion layer and the catalytic layer, or the layer with catalyst reaction site in contact with the electrolyte [8]. Figure 1.2 shows a cross section of the electrode with the bipolar plate and the membrane.

In all cases, the electrode is required to be a highly porous (to increase the effective area and hence the current), yet allow sufficient reactant diffusion to reaction sites. The actual microscopic surface is area in PEMFC is actually 100 to 1000 times the macroscopic length×width area. In addition, the electrode should have minimum contact resistance with the membrane, good electrical conductivity to transport the electrons, and good mechanical and chemical stability in a relatively high temperature and corrosive environment.

In PEMFC, the electrode is part of the larger membrane-electrode assembly (MEA). This is made by first forming Pt into small particles on surface of large particles of carbon power. Then, one of two methods is used to fabricate the electrode [2]. In the separate electrode method, the carbon supported catalyst particles (Pt/C) are applied to a porous conductive material such as carbon cloth or paper that contains other additives such as hydrophobic PTFE. Teflon (the commercial name of PTFE) is needed to introduce hydrophobic properties in the electrode to prevent the flooding of the catalyst with water in addition to improving mechanical strength [9]. However, high PTFE content also increases the electrical resistance, and hence a balance is needed [9]. The carbon support provides the basic mechanical structure and allows the diffusion of the gas. These electrodes are then hot-pressed with the electrolyte to form the MEA. Alternatively, the electrode can be integrated directly into the electrolyte by applying the catalyst onto the membrane and

then layering the 'gas diffusion' section. These MEAs are then staked between bipolar plates which act as internal flow channels and current collectors between adjacent cells.

However, for catalyst sites to be active, they must be in contact with the electrolyte, so a thin layer of electrolyte is usually applied on the electrode catalyst layer (without covering it). This is found to improve the performance of PEMFC [9, 10]. The polymer usually used in PEMFC membranes is Nafion, a PTFE based cation conducting polymer with excellent characteristics. However, while a minimum amount of Nafion is need for a proper interface between the membrane and the electrode, and a high content of polymer in the catalyst layer helps to improve ionic conductivity, yet too much Nafion can have a deteriorative effect on electrode performance [9]. It was found that the performance is strongly dependent on the amount of Nafion in the electrode catalyst layer. A higher content increases the electrochemical active area and improves the overall ionic conductivity. However, there is an optimum point beyond which the porosity decreases and hence the permeability of the gases is limited [10]. Moreover, this optimum Nafion content was found to be dependant on the operating condition of the cell; at high current densities, a smaller content of Nafion increases performance and vice versa [10].

The electrode design also has an impact on the water management which is essential to keep the electrolyte hydrated yet not allow flooding of the electrode with water such that no gas can diffuse [11]. While a hydrophilic GDL will retain water in the electrode and make it more difficult to remove, but if only hydrophobic GDL is used water would be expelled from the GDL to both the gas flow channel and the catalyst layer causing flooding. However, a hydrophobic GDL can allow liquid water in the GDL to be removed by water flowing in the channel. Moreover, if hydrophobic catalyst layer is used, then it could break up the water sheets making it easier to remove. Hence a balance should be made between the hydrophobic content in both layer such that the catalyst layer has a higher content causing water expulsion in one direction

The classical use of the Pt on large carbon particle is not the only approach to producing the catalyst layer. Bessel et. al [12] investigated the potential of Pt supported on graphite nano-fibres for fuel cell electrode by testing it on the oxidation of methanol at 40°C. It was

found that at 5%wt Pt on graphite nanofibers shows the same activity of 25%wt Pt on carbon. Additionally, the result is an electrode catalyst that is considerably less susceptible to CO poisoning; a major technical challenge for Pt catalysts. These improvements have been attributed by the author [12] to be due to the more ordered or arranged crystallographic orientation of the metal particles on the 'tailored' graphite nano-fibre. These issues were later examined by Sopian and Daud [13] when they discuss the CO poisoning of Pt catalyst and the approach to alloy Pt with other elements such as Ru, Mo, or Re which helps to reduce this effect by providing oxygen containing species to oxidise CO to CO_2 [14]. The catalysts are more effective when arranged in a specific way, but when bi-functional alloy catalysts are used they tend to arrange randomly [13]. Sopian and Daud suggest that Pt-Bi is more regular and stable than the other alloys and may help solve this issue, but no extensive work has been done on this yet.

With the aim of solving the issue of high platinum loading and inactive catalyst sites, Choi et. al [15] demonstrated the electrode fabrication method for PEMFC by DC and pulse electro-deposition. The traditional methods of applying the Pt/C with PTFE on carbon cloth or paper is done by silk screening, brushing, or rolling. However, these methods create inactive catalyst sites (not on the membrane/electrode interface). Pulse electro-deposition offers more control on particle size (allowing smaller catalyst particles to be applied), stronger adhesion to the electrode, and more uniform deposition.

Platinum is not the only catalyst for fuel cell reactions. The use of other materials has been possible but with a performance lower than that of Pt and only at temperatures higher than 100°C. Heo et. al [16] demonstrated a Pt-free FC using transition metal carbides exhibiting Pt like behaviour at high temperature (ZrO_2/C for cathode and Mo_2C-ZrO_2/C for the anode) with reasonable performance above 200°C and a maximum performance, comparable to Pt, at 300°C. However, this negates the attractive feature of PEMFC low operating temperature.

Applications

To date, numerous fuel cell power plants (multiple fuel cells units with peripheral controllers, power conditioners, and fuel and thermal management devices) up to tens of mega watts (MW) in capacity have been built and operated [1]. Commercially produced fuel cells and electrochemical devices in general, including redox flow batteries (RFB) have several areas of applications:

- Grid load levelling, with large scale plants.
- Decentralized local power plants (up to hundreds of kW) with optional combined heat and power (CHP), emergency power supplies
- Provide propulsive power to vehicles (tens of kW)
- Provide power and drinking water in spacecraft, submarines or other remote locations
- Portable low power devices; personal communications, control, entertainment (mW to several Watts)

In 2011 the total power capacity of new fuel cells sold was over 100 MW. By application type, 80% of this capacity was for stationary generation. Typical technologies used for fixed units that provide electricity (and heat) are the MCFC and PEMFC [17]. SOFCs for example have an efficiency of $70-80\%$ (including heat utilisation) compared to the current $30-37\%$ in combustion, while for the transport field, PEMFC operates at about $40-50\%$ compared to the current $20-35\%$ in internal combustion engines [18]. For transport and low power applications, PEMFC and DMFC are the more common types used. In terms of the total number of shipments sold, more than 80% of these were PEMFC [17].

1.3 Bio-fuel cells

Bio-fuel cells can be classified according to the biocatalyst (Figure 1.1). Systems using specific isolated enzymes for at least part of their operation are known as enzymatic fuel cells (EFCs), while those utilizing whole organisms containing complete enzyme pathways are known as microbial fuel cells (MFC). A third, intermediate group based on organelles, namely mitochondria, has recently emerged [19]. Several operational differences between these bio-fuel cell types can be identified immediately. Isolated enzymes are substrate specific, while the diverse enzyme contents of whole organisms can be used for a wide range of fuels. Moreover, a complete breakdown of the organic fuel to carbon dioxide and water is usually only possible with several reaction steps (several enzyme catalysts). This is more easily achieved in MFCs, though it also can be achieved in EFCs with an appropriate combination and cascading of specific enzymes [20]. The micro-organism is either a specific isolated species or a mixed culture, which can be applied directly on the electrodes or used in a suspension. Alternatively, the system may be inoculated with a mixed culture in a nutrient solution under specific conditions that will allow it to form a biofilm on the electrode [21].

In MFCs, the organisms are able to regenerate the required enzymes as part of their natural functioning [22, 23], offering an advantage over EFCs, which, on the other hand, have a faster response time owing to the simpler chemical pathways. Due to the living nature of organisms, MFC systems have an initial transient operating period of bacterial growth and adaptation to the electron transport mechanism (to and from the electrodes).

A short lifetime is an inherent characteristic of enzymes, even in their natural environment [24]. This drawback is not as severe in MFCs since the organisms are able to regenerate the required enzymes as part of their natural functioning. These living systems are also able to grow and adapt, a common and advantageous phenomenon observed in MFCs [22]. Fishilevich et al. [25] recently developed a microbial fuel cell in which glucose oxidase (GOx) was displayed on the surface of yeast in the anode compartment, with glucose as the fuel and methylene blue as a mediator. The use of micro-organism in this manner

opens up the possibility of self-regenerating enzyme systems from the continuous growth and expression of enzymes on organism surfaces [26].

1.3.1 Operating principles of a bio-fuel cell

Almost all biochemical processes are catalysed by enzymes. A group of these proteins, oxidoreductases, are responsible for reactions involving electron transfer, and are the most commonly used enzymes. Different subclasses of oxidoreductases are defined based on the type of substrate they act on, as well as the reaction mechanism (*e.g.* dehydrogenases, oxidases, and peroxidases).

At each electrode in contact with the electrolyte, a potential (voltage) is setup relative to the other electrode [1]. Ideally, the cell voltage for a BFC is independent of the current drawn. In practice, the reversible cell voltage is not realized even under open-circuit (zero current) conditions due to a number of losses incurred when the cell is operated. The difference between actual cell voltage (V_{cell}) and the theoretical reversible cell voltage for the overall cell reaction (E_{cell}) at a generated current density j (current I divided by the cross-sectional area of the electrodes, A), is termed the overvoltage. As depicted in Fig. 1.3, there are three major losses that contribute towards the overvoltage (or 'overpotential', η, for a single electrode): activation overpotentials, ohmic losses and mass-transport (concentration) overpotentials [27]. The cell voltage at zero current (open-circuit voltage, OCV) E_{OCV} can also deviate from E_{cell} as a result of internal currents and fuel crossover. At steady state, and assuming spatially distributed reactants, the cell voltage can be approximated as follows:

$$V_{cell} = E_{cell} - j\sum_{i}\rho_i l_i - \eta_{act} - \eta_{conc} \tag{1.3}$$

where the second term on the right-hand side represents ohmic losses and the final two terms denote the activation and concentration overpotentials, respectively (sums of the contributions from the two electrodes). The reversible potential E_{cell} can be calculated

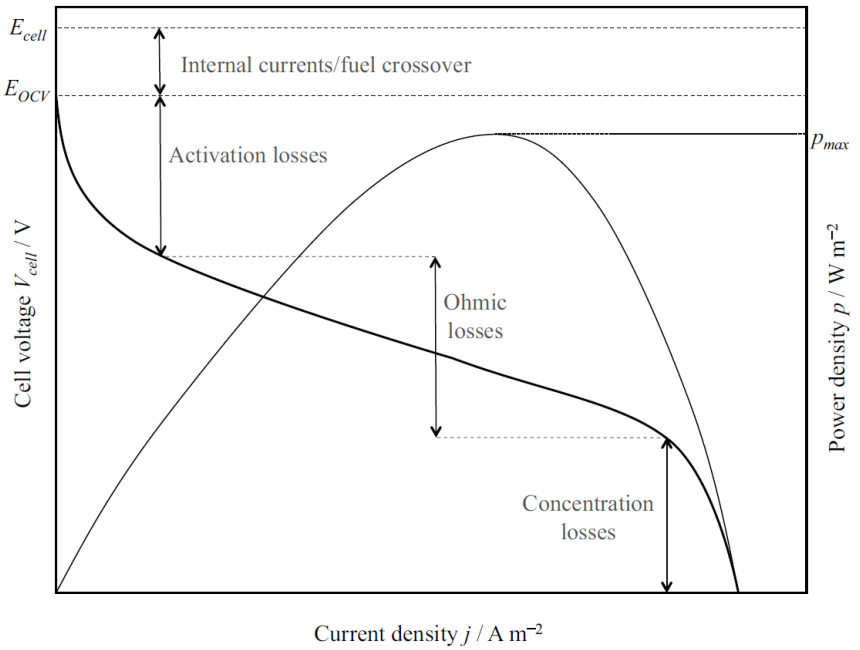

Figure 1.3: Typical variations of the cell voltage and power of an operating fuel cell with current density. The major losses of cell voltage and approximate ranges of current density in which they occur are indicated.

from the Gibbs free energy change for the anodic and cathodic reactions.

At low currents, activation (charge transfer) losses dominate; they arise from the energy barrier to charge transfer, from the mediator or bacteria/enzyme to the electrodes. These overpotentials (separate for the two electrodes) can be approximated if expressions for the reaction rates are known, *e.g.* a Tafel's or Bultler-Volmer's relation. Activation losses can be reduced by improving the electrode catalysis, increasing the electrode surface area, and by optimising the operating conditions (*e.g.* temperature and pH).

Ohmic losses are due to the resistance to charge transport through the various components in the cell, including contact resistances. They include both ionic and electronic resistances through the current collectors, electrolytes, membrane and electrodes, as well as the interfaces between these components. Assigning a characteristic resistivity ρ_i and thickness l_i to each component i, the ohmic losses may be approximated using Ohm's law, as in Eq. (1.3). To keep ohmic losses to a minimum, the membrane must possess a low resistance, the gap between the electrodes should be optimal and the components must be well contacted. The solution conductivity can also be increased by varying its

composition, but this must not affect the functioning of the bacteria/enzymes.

Concentration losses are caused by resistance to mass transport, leading to large concentration gradients, notably in the vicinity of the electrode surface. These losses tend to dominate at high current densities. They can be lowered by ensuring that the solutions are well-mixed (*e.g.* by stirring or recirculation) or, in the case of an air-breathing cathode, that the ingress of O_2 is not severely restricted. The electrical power, p of a BFC is defined as the product of the cell voltage and the generated current density: $p = IV_{cell} = V_{cell}^2/R_{ext}$, where R_{ext} is a known, fixed external resistance. The power density can be calculated by normalising the power with respect to the electrode cross-sectional area or the electrode volume. A typical profile for the power density, $P = p/A = jV_{cell}$, as a function of current density is shown in Fig. 1.3.

One of the most important measures of performance of a BFC is the coulombic efficiency, which is defined as ratio of coulombs transferred from the substrate to the anode, to the theoretical maximum coulombs produced if all of the substrate is oxidized (×100%) [28]. The major causes of reduced coulombic efficiency are (a) the occurrence of alternative reactions that do not result in current production; (b) build-up of biomass; and (c) crossover of the substrate or mixing of the anodic and cathodic reagents, a particular problem in membrane-less systems [27].

The operating voltage of a fuel cell has an upper limit dictated by the difference in potential between the oxidant and reductant and the potential difference between the final electron donor and initial acceptor at the electrodes. In bio-fuel cells, this upper limit is determined largely by the redox potential of the active sites acting on the substrate. If mediators (redox active species) are used to shuttle the electrons to/from the electrode, inevitable thermodynamic losses will occur; the mediators require a potential that is shifted from that of the active site to promote electron transfer. Mediated electron transfer can, however, yield higher currents when the mediator concentration is sufficiently large [29].

Many reports have categorized BFCs into direct and mediated electron transfer (DET and MET respectively), with often differing definitions. MET usually refers to cases where a

mediator is used to enhance electron transfer between the electrochemically active part of the enzyme and the electrode (see the top example on the anode side of Figure 1.1). Conversely, the transfer of electrons directly from the enzyme to the electrode is termed as DET. The vast majority of enzymes are not capable of DET [30–33], so most systems employ a mediator, which is usually enzyme specific.

1.3.2 Applications of bio-fuel cells

The potential applications of bio-fuel cells are diverse. Non-electrochemical applications of bacterial reactions for the production of hydrogen through fermentation, or methane via methanogens are known technologies. Although these bioreactors may be connected to conventional fuel cells for electricity production, either as an external unit supplying the fuel [34], or by incorporating the fuel production process with the oxidation reaction on the same anode [35], the biological pathway remains separate from the process of electricity production.

For stationary large-scale power generation, microbial fuel cells are the likely candidate. These systems can be fuelled by widely available, carbon-neutral complex fuels such as cellulose [35, 36]. Alternatively, they can form the basis for waste treatment systems, combined with energy generation from the organic matter found in sewage. In this application area, MFCs will have to compete with traditional anaerobic digesters producing methane or hydrogen. At present, this is not possible considering target power densities of around 1 $\mathrm{kW\,m^{-3}}$ for economic competitiveness [37, 38]. Despite these drawbacks, direct electrical output with high efficiency, low operating temperatures, and good organic treatment efficiency, with the possibility of operating on low strength wastewater, are some of the advantages of MFCs [37, 38]. Moreover, bio-electrodes can be used for the oxidation/ reduction of specific target substrates (such as nitrate, iron and sulphate) in waste removal or metal extraction from minerals [39]. The operation of MFCs on marine sediment to power remote marine instruments has also been explored in several reports.

Microbial electrolysis cells (MECs) are similar in configuration to microbial fuel cells but

require an electrical energy input to initiate a normally unfavourable reaction producing a secondary fuel. For example, hydrogen can be produced on an anaerobic cathode by the reduction of protons (the product of acetic acid oxidation at the anode) [40–42]. The electrode reactions can be written as [40]:

$$\text{Anode: } CH_3COOH + 2\,H_2O \longrightarrow 2\,CO_2 + 8\,e^- + 8\,H^+ \tag{1.4}$$

$$\text{Cathode: } 8\,H^+ + 8\,e^- \longrightarrow 4\,H_2 \tag{1.5}$$

which can be combined with the fermentation of glucose into acetate to produce hydrogen.

In another example Cheng et al. [43] produced methane at a cathode by 'electromethanogenesis' combined with the oxidation of an organic fuel at the anode. Several reports have suggested a mechanism of methane production in microbial electrochemical cells from acetate through acetoclastic methanogenesis, or from the intermediate hydrogen product. The work of Cheng et al. [43] presents preliminary evidence that methane can be produced from micro-organisms (combined with CO_2 capture). MECs that use electricity for the production of a secondary fuel may be used with renewable energy systems, such as wind turbines of photovoltaics to generate usable fuels such as hydrogen or methane that are easily transported and stored. Call and Logan [42] have projected that such systems can provide hydrogen gas at \$0.62 per kg compared to \$3.8 per kg by water electrolysis.

Another class of microbial electrochemical cells not strictly adhering to the definition of a fuel cell is that based on phototroph organisms that use light energy to produce electricity. A two-step approach where *Rhodobacter sphaeroides* converts sunlight and an organic substrate into hydrogen gas, which is then oxidized at a Pt anode, has achieved power densities up to 0.079 mW cm^{-2} in a single compartment cell [44, 45]. In an approach relying solely on light energy, Furukawa et al. [46] designed a miniature fuel cell that replicated the photosynthetic/metabolic processes to provide direct electrical energy in light/dark conditions, via alternate conversion between CO_2, H_2O and electricity. Cao et al. [47] used an enriched consortium of phototrophic bacteria from a wastewater treatment plant

in a two-chamber MFC. A maximum power density of 0.265 mW cm^{-2} was obtained. A sediment type MFC using mixed communities of photosynthetic and heterotrophic micro-organisms, capable of power production in both light and dark without the need of organic substrate additions, was recently reported by He et al. [48].

For applications on a smaller scale, EFCs operating on high energy density fuels have the potential to power portable electronic devices, though current power outputs are still far from the target figures of ~100 mW [49]. *In vivo* application of bio-fuel cells, either for powering small implantable devices or as biosensors, are more promising for the short term due to their low power requirements. Short life times are, however, a major issue.

1.4 Thesis scope

The use of biological electron transfer has been successfully applied in biosensors with a few commercial products already available. Beyond the clinical *in vivo* applications, enzymatic fuel cells have been demonstrated to power portable electronic devices using a multi-stack design [50]. These developments, and the increasing sophistication in assembling efficient bioelectrochemical electrodes are the results of both a greater understanding of the controlling factors in biological redox interactions, and improved techniques in physical electrochemistry allowing *in situ* characterization of the electrodes [51].

It is important that mathematical models are developed to reduce the burden on laboratory-based design, testing and characterization. At the cell level, models must be able to capture the distributions of charge, potentials and concentrations as well as global information such as the cell voltage. In many cases, particularly for *in situ* operation, local information can only be gained from detailed and rigorously-validated models, which in conjunction with laboratory studies, can be used to investigate the reaction environment and accelerate the development of practical systems.

The application of numerical modelling in studying enzymatic fuel cells is rare in the litera-

ture, especially on a whole system level. Mathematical approaches to bioelectrochemistry have been mainly limited to approximate steady-state analytical solutions [52, 53]. To date, only a small number of models have been developed for specific systems [54–61], which, with a few exceptions [55, 57, 58], are highly simplified and neglect crucial features such as transient performance, spatial non-uniformities, conductive losses, potential profiles, ion migration, fluid flow and a heat balance. Models for other electrochemical cells, including polymer electrolyte membrane (PEM) fuel cells and batteries [62–64] are ideal templates for further developing biofuel cell models.

In this study, two different approaches to modelling biofuel cells are presented, a detailed physics-based approach, and a data-driven regression type model. After introducing the operating principles and a background introduction, Chapter 2 presents a review of recent experimental progress and associated challenges in both enzymatic and microbial fuel cells. In Chapter 3, a brief introduction to enzyme and mediator kinetics is presented and a detailed mathematical model of an all-biological enzymatic fuel cell is developed based on the experimental work of Sakai et al. [50]. In the model system, the anode biocatalyst; an enzyme cascade of glucose dehydrogenase and diaphorase with VK3 mediator is immobilized in a porous electrically- conducting anode, while glucose and the phosphate buffer are supplied by the solution. An air-breathing bilirubin oxidase/ferricyanide cathode and a cellophane membrane complete the cell unit.

In Chapter 4, the methods used in the previous chapter are further applied to bio-anode enzymatic system. This chapter is based on the experimental work of Fischback et al. [65] and includes other commonly used components that were not included in Chapter 3, such as a diffusional mediator, platinum cathode, Nafion membrane, and an unbuffered solution.

The models developed in Chapters 3 and 4 are based on mass and charge conservation laws in addition to kinetic models for the electrochemical and biochemical reactions. In addition to providing fundamental information about the physical processes during operation which are otherwise difficult to obtain from experimental methods, these physics-based models can be used to test hypothesis of the underlying laws governing the system and validate

them against experimental results.

With increasing system complexity and size, such as in stack-level modelling or in microbial fuel cells where a large number of reactions occur, spatially-distributed physics-based models may be computationally demanding and are not feasible for optimization purposes. In Chapter 5, a data-driven approach to modelling is presented and tested using a data set obtained from the model simulations of Chapter 3.

The aim in this class of data-based models, or machine learning algorithms, is to predict quantities of interest based on what has been 'learned' from the training data. In other words, the aim is to learn or induce a relationship between a given set of inputs and outputs in order to predict the outcome of an experiment for any new unobserved input values. The method used in Chapter 5 is based on a reduced-basis form of Gaussian process regression. The main advantage of data-driven models over physics-based models is the improved computational efficiency.

Chapter 2

Literature Review

This section considers major developments in enzymatic and microbial fuel cells for power generation applications over the past five years. Earlier developments will be reviewed briefly to provide context. For more detailed reviews of this work, the reader is referred to previous reviews on the subjects of general biofuel cells [3, 66], microbial fuel cells [22, 37, 38, 67], their large scale application [68], methods of electron transfer in bacteria [69, 70], enzymatic fuel cell [52, 71, 72] and enzyme immobilization and electrode materials [24, 73–75]. Additionally, reviews specific to microfluidic fuel cells [76] and fuel cells with switchable power output that mimic electronic logic gates [77] are available. The focus here is on the application of BFCs for electrical power production (galvanic cells).

2.1 Enzymatic fuel cells

The two major problems in enzyme-based systems are the short lifetime of the enzyme caused by a reduction in its stability when functioning in a foreign environment, and the low power densities resulting from a low electron transfer rate from the enzyme active site to the electrode [24]. The bulk of the research in enzymatic fuel cells has been directed at enzyme/electrode integration methods that alleviate these problems. The short lifetime

(a few hours) is an inherent characteristic of enzymes even in their natural environment, but the lifetime may be increased to a few days by immobilization [24].

Enzymes used in fuel cells are of the oxidoreductase family (capable of catalysing oxidation and reduction reactions). They can be categorised according to the type of redox center (quinone, nicotinamide, flavin), or to the type of electrical communication [78]. The first group includes those capable of direct electrical communication through either the redox active site located at the periphery, such as in peroxidases, or through a functional domain (*e.g* heme domain in some dehydrogenases) located on the periphery that can transfer electrons to the outside. Proper orientation of the enzyme upon immobilization is essential to achieve this direct communication. One method to improve the orienatation can be achieved through the enzyme reconstruction method (subsection 2.1.3) where the enzyme active centre is first isolated and covalently linked to the electrode, then the apo-enzyme (enzyme lacking active centre) is reconstructed around the linked redox centre. The second group includes those with nicotinamide adenine dinucleotide ($NADH/NAD^+$) as their active site. In this case, the redox center is usually loosely bound and may diffuse away. This allows the enzyme to transfer electrons to the electrode by the diffusing center, although the diffusing enzyme site may be lost, especially in continuous flow systems. Covalent linking of such enzymes need to have a flexible link to allow back and forth movement between the protein structure and the electron acceptor. The third, and most difficult to extract electron from are groups of enzymes with a tightly bound redox center that is buried deep inside the protein structure. The most commonly used enzyme, glucose oxidase (GOx) belongs to this group, with a flavin adenine dinucleotide (FAD) center. Systems employing GOx are typically mediated, although it is possible to achieve DET using nanostructured electrodes as discussed later [79–82]. The different structures/functions necessitate special methods of electrically linking the enzyme. A summary of the key developments in EFCs are presented in Table 2.1 and are discussed in detail in sequel.

For biological cathodes, the enzymes are typically multi-copper oxidases, which are capable of a four-electron reduction of O_2 to water and have a high specificity towards this reaction [83]. Examples include plant and fungal laccases [84] and BOx [85]. Laccases are generally employed under slightly acidic conditions, while BOx has activity in more alkaline media,

which allows it to be used at neutral pH. Cytochrome oxidase and cytochrome *c* have also been employed. In the case of H_2O_2 reduction, microperoxidase [86, 87] and horseradish peroxidase [88] are commonly used as enzymes.

Enzymes can either transfer electrons directly (direct physical contact with the electrode or through conducting materials linking the center to the electrode), or *via* mediators. A variety of techniques for immobilisation of the enzyme on the electrode have been used [89]. These include: physical surface adsorption with diffusional mediators or mediators coadsorbed with an enzyme; entrapment in conducting polymer matrices or gels; wiring or covalent attachment to functionalised polymers (Fig. 2.1(a)) and apoenzyme reconstruction (Fig. 2.1(b)). Nano-structured elements can also be used as substrates for binding, or incorporated with one of the aforementioned techniques for enhanced electrical conductivity.

Enzyme and mediator immobilisation

Immobilisation of the enzyme has several advantages, including isolation of the enzyme for reaction, increased selectivity, improved mass transfer and long-term stability [90]. It also acts to separate the enzyme from the mixture containing the substrate, allowing for more modular cell designs. On the other hand, it can affect the stability and/or activity of the enzyme, introduce additional mass-transfer limitations on the substrate and involves additional costs. Stability is clearly a key consideration. The stability of the immobilised enzyme will depend on the nature and strength of the bonds to the support material, the conditions required for immobilisation, the degree of confinement and the conditions under which the enzyme reactions occur in a functioning electrode. The method of immobilization must be selected carefully to avoid denaturing of the enzymes and loss of structural freedom required for their activity [71, 91].

Ideally, enzymatic electrodes for power generation should maximize enzyme loading, activity and stability, while also minimizing inefficiencies due to substrate mass transport limitations and slow electron transfer from the enzyme to the electrode. While increasing

bond strength (physical adsorption/entrapment, ionic bonding, and covalent bonding) improves enzyme retention, deactivation is also more probable [92]. Simple physical binding or entrapment in polymers is sometimes complemented by ionic binding, but this imposes an operating pH depending on the type of enzyme used and the ionomer charge. Addition of a cross-linking agent is a simple and widely used method to improve the stability and increase both the concentration of the enzyme and its activity [92].

The random enzyme orientation, when physically adsorbed or covalently bonded, is unfavourable for efficient electron communication with the active site. The reconstruction of apo-enzymes around the active site bound to a redox relay provides excellent electrical communication. Monolayers of these electrically contacted enzymes have a high turnover number and sensitivity, although the enzyme loading is limited by the electrode surface area. This limitation can be relieved by a similar enzyme reconstitution but on an electrically active thin polymer film [73]. Immobilization of mediators and enzymes on polymer films is a simple and practical method for biofuel cell electrodes; however, the effective diffusion coefficient of the mediator (and hence the electron transport rate) is several orders of magnitude lower than that of a typical diffusional mediator [24].

The simplest method of enzyme immobilization is physical adsorption or entrapment. Enzymes can be adsorbed, for example, onto conductive particles such as carbon black or graphite powder [88]. The methods are straightforward and cost-effective. If the binding forces (primarily electrostatic) between the enzyme and the support are too weak, however, the enzymes can desorb and contaminate the solution; if they are too strong, denaturation can occur during the immobilisation process. Entrapment involves the confinement of the enzyme within a polymer matrix, a sol-gel [93], a redox hydrogel [94] or behind a semipermeable membrane. The structure must permit a sufficient degree of enzyme movement, while simultaneously preventing any leaching of the enzyme and/or mediator.

Isolated enzymes can be covalently bonded to supports (*e.g.* porous glass, cellulose, ceramics, and metallic oxides) via different functional groups on the support and enzyme, often in the presence of enzyme inhibitors. Reagents are used to activate the functional groups on the support. The functional groups on the enzyme, which include amino, carboxylic

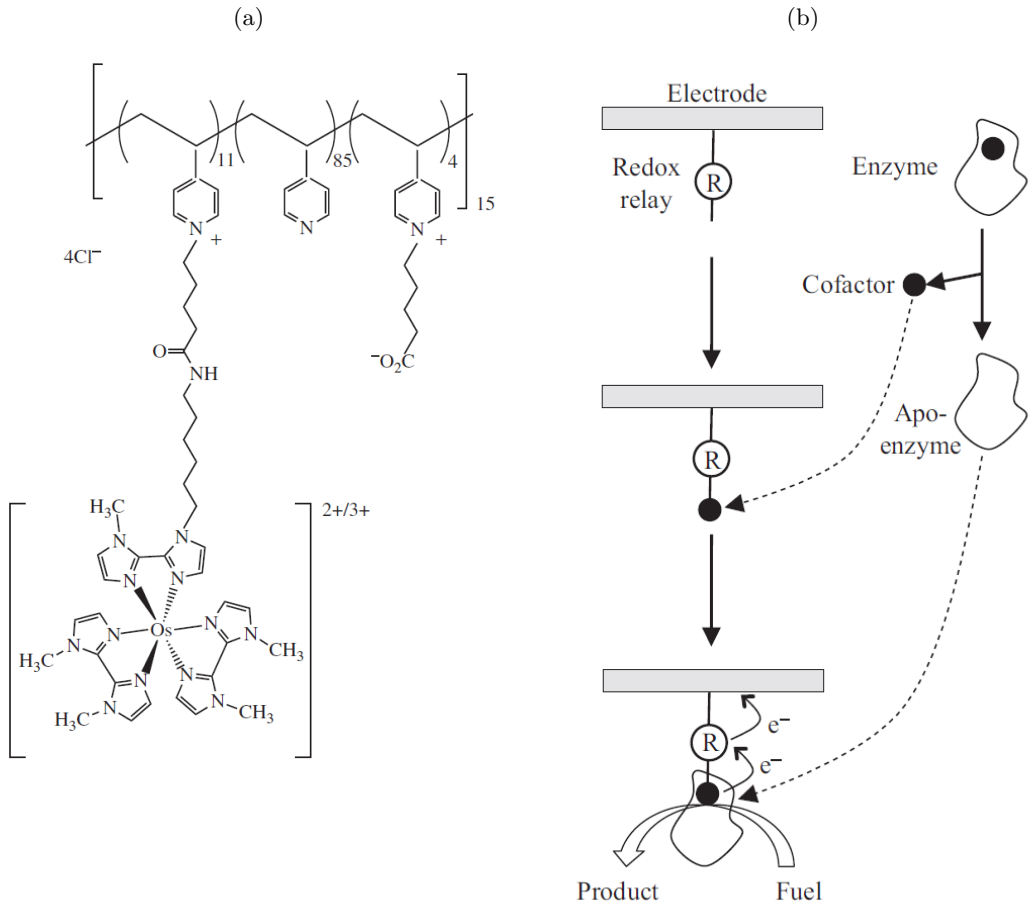

Figure 2.1: (a) The structure of polyvinylpyridine-[Os(N,N'-dialkylated-2, 2'-biimidazole)$_3$]$^{2+/3+}$ [95]. A tris-dialkylated N,N'-biimidazole $Os^{2+/3+}$ complex was tethered to the backbone of a PVP polymer via 13-atom spacers. (b) Illustration of the concept of enzyme reconstitution. An electron relay unit (molecule, redox polymer or nanoparticle) is linked to an electrode. The cofactor of the enzyme is eliminated and tethered to the relay unit. The apoenzyme is then reconstituted on the relay-cofactor monolayer. Adapted from [73].

acid and hydroxyl groups, should not be essential for catalytic activity. The conditions for this type of immobilization are important since they determine the level of enzyme activity retention. Cross-linking consists of joining enzymes to form three dimensional aggregates via covalent bonding between active groups within the enzymes. The aggregates exhibit low mechanical stability and the retained enzymatic activity can be low using this method [92].

2.1.1 Physical immobilisation of enzymes and mediators

Tasca et al. [33] investigated the direct electron transfer (DET) capabilities of different CDHs adsorbed on a graphite electrode in the presence or absence of SWCNTs. SWCNTs were found to increase the electrocatalytic current, the onset of which was shifted to more negative potentials. CDH is composed of a large flavin-associated domain and a smaller heme-binding domain that allows direct electron transfer to the electrode. A membrane-less fuel cell was constructed using *Phanerochaete sordida* CDH coadsorbed with SWCNTs, together with a Pt/C cathode. A solution with 0.1 M, 4.5 pH citrate buffer containing O_2 and 5 mM lactose was used. The open circuit voltage was 590 mV and a maximum power density of 0.032 mW cm^{-2} at 430 mV was obtained. CDH was also adsorbed on graphite in a fuel cell with laccase immobilized in a polymer [96]. The power density (0.005 mW cm^{-2}) was lower than the SWCNT system of Tasca et al. [33], but the cell voltages achieved were slightly higher.

In a similar fashion to CDH, FDH contains a heme group that should in principle allow direct electron transfer to the electrode. Previous investigations, however, were not successful in achieving practical currents. Kamitaka et al. [29] immobilized FDH from *Gluconobacter* sp. by adsorption on a Ketjen black (KB) modified carbon-paper anode that was capable of 4 mA cm^{-2}. Combined with a laccase biocatalyst from *Trametes* sp. adsorbed on a carbon aerogel cathode, a membrane-less bio-fuel cell was constructed and operated at room temperature in an O_2 saturated, 5 pH McIlvaine buffer containing 200 mM fructose. Under stirred conditions, to alleviate the O_2 mass transfer limitation, a maximum power density of 0.85 mW cm^{-2} at 410 mV was obtained and the open circuit voltage was recorded as 790 mV. The power output decreased to 63% of the maximum after 12 h of continuous operation. Under low power conditions, 4 cells connected in series continuously powered a small light-emitting diode for 60 days. Since the cell was operated at low power output for two months, the short lifetime was unlikely to be due to enzyme desorption but rather to a loss of activity during continuous operation at a high current density.

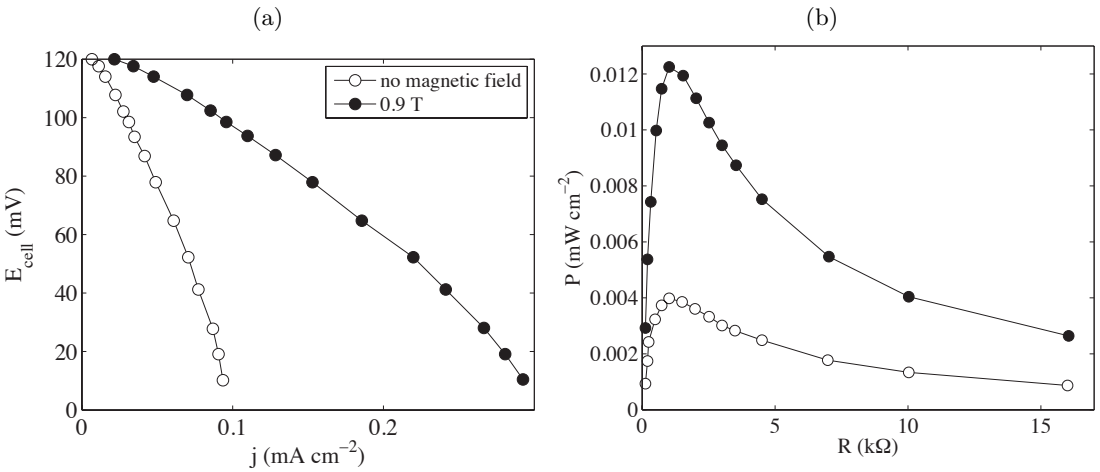

Figure 2.2: Enhancement of the performance of the biofuel cell composed of the LDH/NAD^+/PQQ-anode and COx/Cyt c-cathode: (a) shows the cell voltage *v.s.* current and (b) shows the power density *v.s.* external resistance; (∘) in the absence of magnetic field; (•) in the presence of a 0.9 T magnetic field. The biofuel cell operated upon pumping of the solution (flow rate 1 mL min^{-1}) composed of 0.1 TRIS-buffer, pH 7.0, containing $CaCl_2$ 10 mM, lactate 20 mM, and oxygen (the solution equilibrated with air). Adapted from [97].

Though stirring is not usually desired in real applications, it is often used in systems to improve mass transport and increase the power output. Katz et al. [97] investigated the effects of a constant magnetic field applied parallel to the electrode surface in surface-confined bio-electrocatalytic systems. In the two systems of GOx-FAD-PQQ and lactate dehydrogenase (LDH)/NAD^+-PQQ, in which the current was limited by mass transport, it was found that the current increased by a factor of three when a magnetic field (0.92 T) was applied (see Fig. 2.2). This improvement was brought on by a magnetohydrodynamic effect, engendering a magnetic force on the ions in solution, and thus decreasing the hydrodynamic layer thickness and increasing the current density.

Glucose dehydrogenase (GDH) was later immobilized with its cofactor, NAD^+ on KB, supported on a GC rod [98]. Together with a BOx/KB cathode, the constructed fuel cell was operated in an O_2 saturated phosphate buffer solution (PBS) containing 50 mM glucose. It achieved a maximum power density of 0.052 mW cm^{-2} at 0.3 V with an open circuit voltage (OCV) of 0.642 V.

Physical adsorption is attractive due to its simplicity, although enzyme retention is usually problematic. A review of systems employing simple adsorption shows that, despite

exhibiting 'normal' cell voltages, they have low power densities compared to alternative systems based on the same biocatalysts. This indicates either poor electron transport despite the direct capabilities, or is possibly a result of the low maximum enzyme loadings that can be achieved.

2.1.2 Enzyme immobilisation in polymers

Early hydrogel-modified electrodes in EFCs performed well over a period of a few days but suffered long-term stability issues [99]. Amongst the causes of lost activity were: leaching of components from the cross-linked matrix, and hydrogel loss [100, 101]. A recently developed method for improving stability consists of anchoring the hydrogel to the electrode surface via covalently attached tether groups [101, 102]. Boland et al. [101] compared the current densities and stabilities of pre-treated and bare graphite and Au electrodes. The pre-treated graphite electrodes were functionalised to yield the amine functional groups by electrochemical reduction of a diazonium salt from 1,4-phenylenediamine. An Os-based redox polymer was then cross-linked on the bare and pre-treated electrodes, with GOx on the anode and BOx on the cathode. For both electrodes, retention of activity was vastly improved by pre-treatment, although the test times of 48 h were still rather short. The authors postulated that the improved stability was due to the presence of amine groups on the pre-treated surfaces; these groups are amenable to anchoring of the hydrogel through reaction with the oxirane ring of the crosslinker.

Recently, Sakai et al. [49] prepared an anode by successively applying solutions of poly-L-lysine (PLL), GDH, diaphorase, NADH, vitamin K_3 and polyacrylic acid sodium salt to four separate carbon fiber (CF) sheets. A membrane electrode assembly (MEA) was constructed by combining the anode with a cellophane membrane and an air-breathing cathode, fabricated by successively treating two CF sheets with $K_3[Fe(CN)_6]$, PLL and BOx solutions. A bio-fuel cell containing the MEA and a 0.1 M, 7 pH PBS at room temperature with 0.4 M glucose yielded a power density of 1.45 mW cm^{-2} at 0.3 V with an OCV of 0.8 V and a short circuit current (SCC) of 11 mA cm^{-2}. The diaphorase biocatalyst was used for a reduced overpotential oxidation of NADH with vitamin K_3 as

the electron mediator. Two cells were then connected in series to operate a small toy car (16.5 g) for more than 2 h continuously. The assembled unit had a power output of 100 mW, a volume of 80 cm^3, and a weight of 39.7 g, of which 16.1 g was the fuel solution.

LDH is one of the many PQQ dependent enzymes capable of DET through a heme group [103]. Treu and Minteer [103] isolated PQQ-dependent LDH bound to the outer membrane of *Gluconobacter* and purified them through ion exchange chromatography. The enzyme was immobilized with a tetrabutylammoniumbromide (TBAB)-modified Nafion solution on CF paper. $CaCl_2$ was also used in the immobilization since Ca^{2+} ions are used to coordinate the PQQ cofactor with the apoenzyme. The anode was combined with a Pt cathode and a Nafion membrane.

Khani et al. [104] explored the use of alginate polymer beads in a low cost, simple method for enhanced enzyme retention. It was found that the use of pure alginate or alginate/carbon beads for the immobilization of GOx and laccase maintained 75% and 91% of the enzymatic activities, respectively, and doubled the active half-life of the enzymes. The rates of activity loss for entrapped laccase and BOx were 0.6% and 1.14% per day, respectively. While the turnover rate of GOx improved with the alginate beads (compared to a solution), the opposite was true for laccase (refer to Fig. 2.3). The Michaelis-Menten constant for GOx (a constant representing the substrate concentration needed for the reaction rate to reach half the maximum value, see subsection 3.2) in the alginate beads increased by almost a factor of four, an effect that was explained by the limited substrate concentration near the enzymes.

Polymers containing redox mediator metal complexes have been used in the immobilization of GOx [105–107], lacasse [108–111] and BOx [112]. Mano [106] used Os based metal complexes attached to a PVP polymer in addition to a crosslinking agent to wire GOx and laccase to two 7 µm diameter ×2 cm long GC electrodes. The GOx was sourced from *P. pinophilum* rather than the traditional *Aspergillus niger* since it has a lower Michaelis constant (which is needed for operating the miniature fuel cell in a glucose concentration similar to that found in physiological conditions, 5-8 mM). In a 20 mM citrate buffer with 5 mM glucose at 5 pH (optimum for GOx) and 37°C, the fuel cell was capable of producing

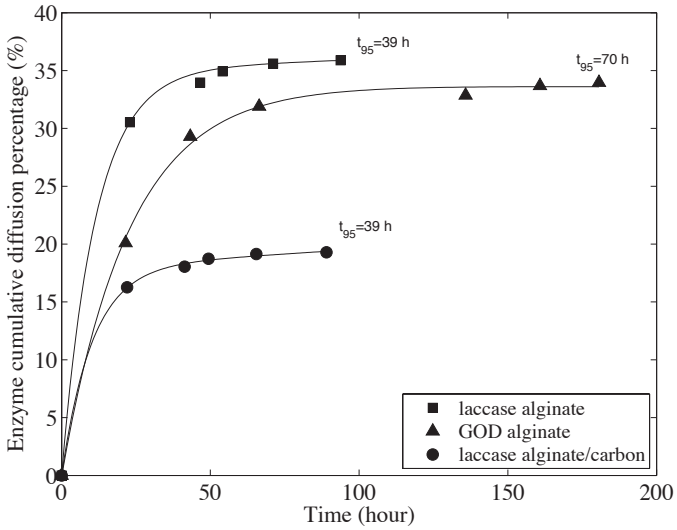

Figure 2.3: Release of the encapsulated enzymes out of the different alginate-based beads. ▪ laccase alginate, ▲ GOx alginate, • laccase alginate/carbon. Adapted from [104].

0.28 mW cm^{-2} at 0.88 V, and operated continuously for 1 month at a power loss of 3% per day for the first 2 weeks. At neutral pH, however, *Penicillium pinophilum* is unstable and denaturation of the enzyme was found to occur; the optimum pH was in the range 4-6. The GOx activity and fuel cell power output for the two enzyme sources is shown in Fig. 2.4.

A method to co-immobilise the enzyme and mediator (designed to prevent mediator leaching) was developed by Heller and coworkers, who used soluble redox hydrogels to construct biosensors and, subsequently, miniature biofuel cells [84, 109, 113–115]. In this method the enzyme is complexed with a redox polyelectrolyte forming a water soluble adduct, which is cross-linked on the electrode surface. The cross-linked polymer swells on contact with water to form a hydrogel, to which the enzymes are covalently bound. The enzymes are electrically connected to the electrode by a redox network and are said to be 'wired'; electron conduction is predominantly controlled by collisional electron transfer between the reduced and oxidized (transition metal-based) redox centers tethered to the polymer backbone. Popular choices for the polymer backbone are polyvinylimidazole, polyallylamine and polyvinylpyridine (PVP) and the redox centres are typicallyosmium (Os) or ruthenium complexes [94]. Os complexes are particularly useful due to the ease with which the redox potential can be tuned by chemical modification of the complex [116]. They can be tethered flexibly to polymer backbones, improving the electron transfer kinetics

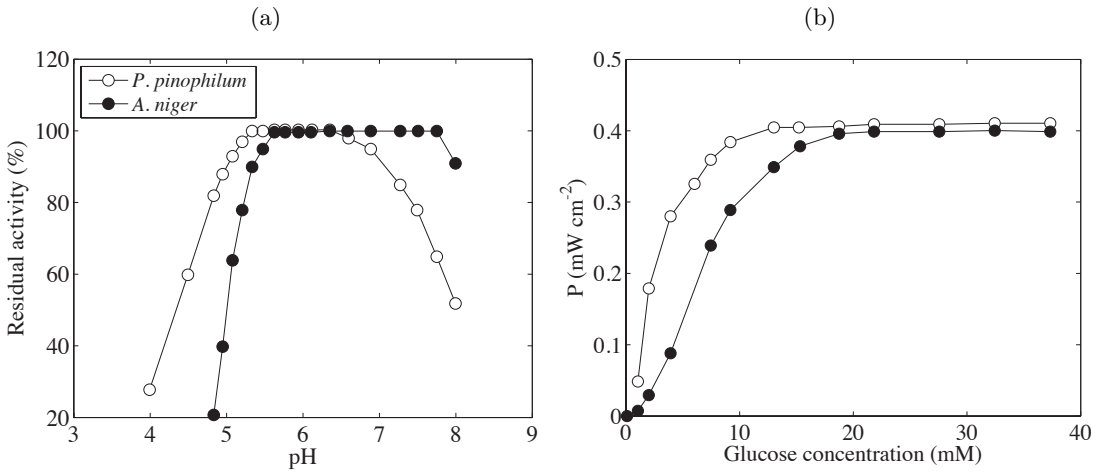

Figure 2.4: (a) pH dependence of electrodes poised at 100 mV *vs.* Ag/AgCl. 32 mM glucose, 500 rpm, 0.14 M NaCl, (b) power density of fuel cell at 0.88 V, with 20 mM citrate buffer, 5 pH, using either (∘) *P. pinophilum*, or (•) *A. niger*. Adapted from [106].

between the enzyme and electrode [117]. The mechanical strength of the hydrogels and the electron transfer rate can be improved by using spacers that connect the redox-active centers to the cross-linked networks. These spacers provide additional flexibility and improved collisional electron transfer. The lengths of the spacers are important; optimally between 8 and 15 atoms [95, 105, 115]. The redox potentials of the hydrogels are determined by the transition metal ion of their complex and by its ligands, so they can be tailored to a specific enzyme/reaction combination [115, 118]. An example of a redox polymer structure, developed by Mao et al. [95], is given in Fig. 2.1(a). The authors tethered a tris-dialkylated N,N'-biimidazole $Os^{2+/3+}$ complex to the backbone of a PVP polymer via 13-atom spacers. An order of magnitude increase in the apparent electron diffusion coefficient was observed when compared to a structure without spacers, used earlier by the authors. Furthermore, oxidation of glucose was found to occur at potentials close to the reversible potential of the $FAD/FADH_2$ centers of the enzyme.

Gao et al. [107] investigated the performance of different polymer backbones and a 7.24 pH PBS, GOx from *A. niger*, containing 15 mM glucose and atmospheric O_2. The main purpose of this study was to investigate the effect of purifying the enzyme. Commercial enzyme stocks usually contain other chemical elements whose exact composition is unknown. Purification of the stock was found to improve the specific activity and the performance of a fuel cell compared to non-purified enzymes.

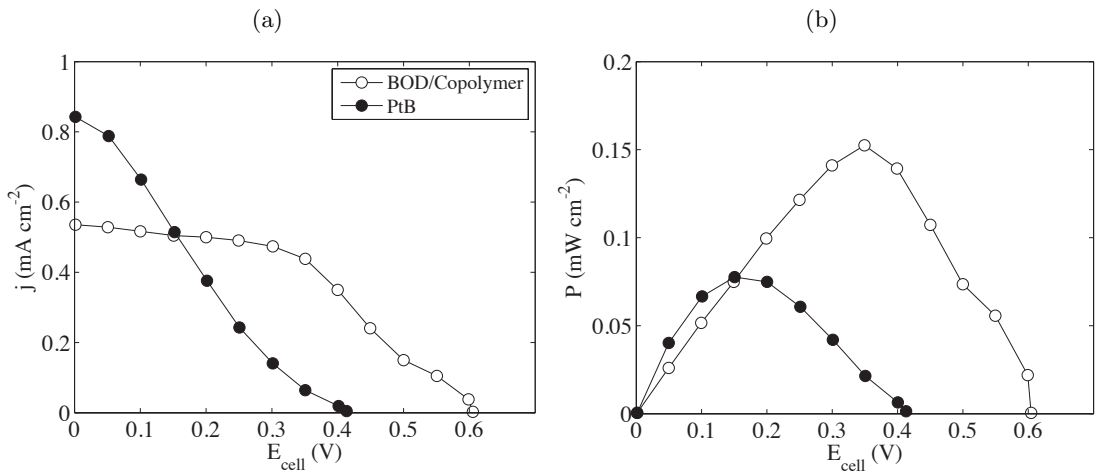

Figure 2.5: (a) current and (b) power densities versus cell voltage for two units using BOx/copolymer (∘) and Pt/C-black (•). Adapted from [119].

Organic polymers have also been used to covalently attach enzymes. In the work by Kuwahara et al. [119], 3-methylthiophene and thiophene-3-acetic acid were copolymerised into a film on a gold coated alumina plate. Subsequently, GOx and BOx were covalently attached to the carboxyl groups of the polymer. Appropriate mediators were used in the two PBS (7 pH) solutions separated by a Nafion membrane. The anolyte was saturated with nitrogen and contained 0.1 M glucose while the catholyte was saturated with O_2. The OCV and maximum current density, both higher with BOx/copolymer than with Pt/C cathodes, were 0.61 V and 0.15 mW cm^{-2} at 0.35 V (Fig. 2.5). Periodic measurements of the separate half-cell currents showed that the anodic current decreased by 50% over one month, while the cathodic current decreased by 25%.

Brunel et al. [120] made a membrane-less bio-fuel cell using porous tubes supplied internally with O_2 and containing the biocatalyst at the outer surfaces exposed to the anolyte. GOx and its mediator, 8-hydroxyquinoline-5-sulfonic (HQS) acid, were coimmobilized in polypyrrole (PPy) polymer and the cathode was similarly prepared using laccase and its mediator, 2,2'-azinobis (3-ethylbenzothiazoline-6-sulfonate) diammonium salt (ABTS), on a porous carbon tube. A solution of nitrogen saturated PBS and 10 mM glucose at 37°C was used. A separate solution containing dissolved O_2 was circulated inside the cathode. At a pH of 5, a maximum power density of 0.027 mW cm^{-2} at 0.24 V was obtained. This decreased to 0.020 mW cm^{-2} at 7 pH. Some degree of leakage of the ABTS mediator was observed. The cell was tested intermittently after being stored at 4°C and retained 80%

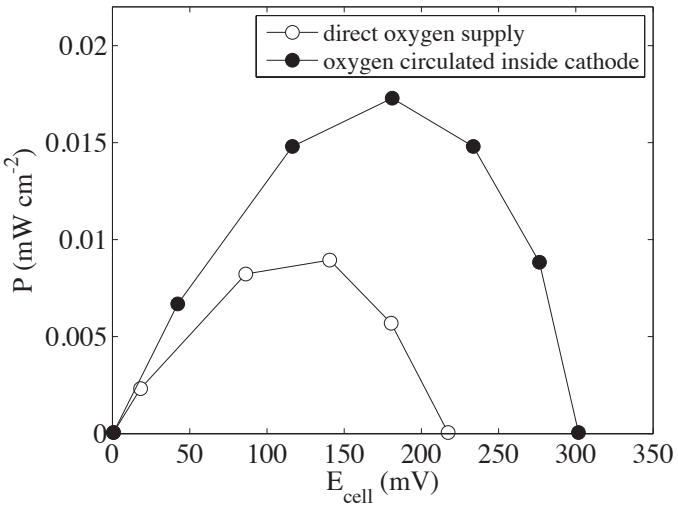

Figure 2.6: Influence of O_2 supply to the system on the power density at 37 °C in phosphate buffer 0.2M solution (pH 7.0) with 10 mM glucose, (•) oxygen saturated solution circulating inside the biocathode tube and (∘) oxygen bubbling directly in the system. Adapted from [120].

of its initial power density after 1 month. Fig. 2.6 shows the impact of the O_2 circulation in the porous cathode on the power density (at 37°C, pH 7), compared to direct oxygen bubbling.

Tamaki and Yamaguchi [121] have immobilised a quinone mediator on a flexible spacer to polymer grafted on carbon black [121, 122]. The electrode was then immersed in GOx solution, and a cross-linking agent was applied after drying. The aim was to create a three-dimensional structure where the electron conduction was divided between the carbon particles and the redox polymers.

The DET of GOx has been established using a simple anode fabrication method and without the use of nanomaterials. In the work by Wang and Chen [123], GOx was immobilized in PLL on a GC electrode, before a layer of Nafion was applied. Electrochemical tests on the Nafion-PLL-GOx anode showed reversible electrochemical behavior of the GOx and a performance similar to that using nanomaterials.

Sol-gel was employed by Lim et al. [124] for the encapsulation of GOx, using tetramethoxy silane as the precursor for the silica gel incorporating both the biocatalysts (GOx and BOx) and SWCNTs. Ferrocene methanol and ABTS were the mediators in the membrane-

separated anodic and cathodic compartments, respectively. Both compartments contained phosphate buffer solutions, with 100 mM of glucose at the anode side and saturated O_2 at the cathode side. Operating at room temperature, the fuel cell achieved a maximum power density of 0.120 mW cm^{-2} at 0.24 V, with an OCV of 0.48 V. Immobilization in a hydrogel removed any effects associated with orientation of the enzymes. Mobile enzymes diffuse in the gel, increasing the number of active enzymes and thus increasing the current, which may reach three times that for a monolayer [125]. The performance was poor when compared to other systems using the same biocatalysts and operating at a similar pH and fuel concentration.

Sol-gel glass is produced by the hydrolysis and polycondensation of organometallic compounds (typically silicon alkoxides) at low temperature [126]. Enzymes can be introduced during the formation of the sol-gel (the 'sol-gel process'), leaving them entrapped around siloxane polymer chains within an inorganic oxide network. The final matrix structure can be controlled by the pH, the temperature, the choice of solvent and the choice of catalyst, amongst other considerations. The main advantages of this method in the context of biosensor and biofuel applications are: simplicity of preparation; the ability to control the porosity; the chemical and mechanical stability of the gel; and negligible swelling [126, 127].

Rather than using polymers applied as films, Kim et al. [128] prepared an anode using PPy nanowires to immobilize GOx and its mediator, HQS, on a nanoporous anodized aluminum oxide electrode (Fig. 2.7). Different nanowire lengths, diameters, and electrode base preparation methods were tested, along with a single cathode made by immobilizing a mixture of laccase and its mediator, ABTS, in a PPy film on a gold electrode. With increasing nanowire length, the cell showed a decrease in OCV and an increase in the power density, which reached 0.28 mW cm^{-2} (at 0.15 V) using a 200 nm diameter ×16 μm length wire. This system suffered from low operating and open-circuit cell voltages, probably due to the high resistance of the long nanowires. The voltage was found to increase using 350 nm long wires grown directly on the Au surface, but the current and power output would be expected to decrease due to a decrease in the available surface area for enzyme immobilization.

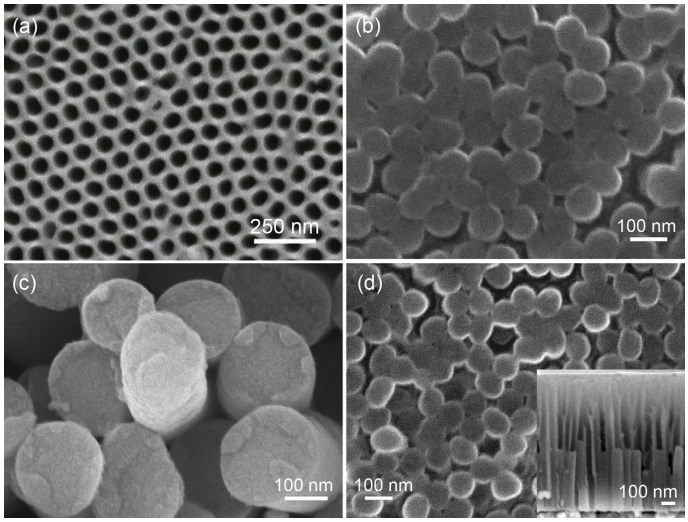

Figure 2.7: FESEM images of (a) the fabricated anodized aluminum oxide (AAO) template, (b) 80 nm diameter PPy-HQS-GOx nanowires, (c) 200 nm diameter PPy-HQS-GOx nanowires grown using free-standing AAO, and (d) 80 nm diameter PPy-HQS-GOx nanowires grown using Si substrate AAO. The inset shows a cross-sectional view of PPy-HQS-GOx nanowires grown using AAO-Si [128].

2.1.3 Covalent linking

Covalent bonding and cross-linking are commonly used to immobilise enzymes on self-assembled monolayers (SAMs) [129]. In the context of biosensors, the most studied SAMs are those formed by alkanethiols chemisorbed from solution onto gold surfaces [130]. Despite the many advantages of these SAMs (simplicity of preparation, densely packed structures and control over functional groups at the monolayer surface), they are prone to instability [131–133]. To improve stability, several research groups have used covalent modification of carbon surfaces via electrochemically reductive adsorption of aryldiazonium salts [134–137]. The resulting monolayers are highly stable over a wide potential window [134]. In recent studies, gold, graphite and glassy-carbon (GC) electrodes were functionalised using aryldiazonium salts bearing carboxylic acid groups [138, 139]. Pellissier et al. [138] grafted a GOx layer on a GC electrode modified using this method, through coupling with peripheral amine groups of the GOx. This enzyme layer was used as an anchoring base onto which a cross-linked enzyme layer was subsequently deposited, before testing the electrode using a GC rod counter electrode. The authors demonstrated that these modified electrodes retained much of their activity after 6 weeks, while control electrodes prepared by depositing the crosslinker and GOx directly onto the GC had lost

all activity within only 1 week.

Monolayers of enzymes covalently bonded through redox relay molecules have been used for the construction of anodes [73, and references therein]. Lee et al. [140] attached NAD^+-dependent LDH to PQQ electron mediators, which were in turn attached to a gold electrode by a cystamine monolayer. The novelty of the method introduced was that the final step of covalent attachment of LDH was performed in the presence of the NAD^+ cofactor, lactate substrate, and Ca^{2+}, which helped to promote a favorable orientation of the LDH after immobilization. The bioelectrochemical oxidation reactions of NADH, mediated by PQQ and leading to an electron transfer to the anode are [5]:

$$\mathrm{NADH + PQQ + H^+ \longrightarrow NAD^+ + PQQH_2} \tag{2.1}$$

$$\mathrm{PQQH_2 \longrightarrow PQQ + 2\,H^+ + 2\,e^-\ (to\ anode)} \tag{2.2}$$

The anode was combined with a cathode composed of microperoxidase (MP-11) attached to a monolayer of cystamine on a gold electrode. The anolyte consisted of 0.1 M, 7 pH, tris buffer containing optimized solution concentrations of 10 mM $CaCl_2$, 10 mM NAD^+ and 5 M lactate, while the catholyte consisted of a 0.1 M, 7 pH, PBS containing 1 mM hydrogen peroxide as the electron acceptor and ABTS as the mediator. The two compartments were separated by a Nafion membrane and the cell was operated at room temperature. The maximum power density obtained was 0.142 mW cm^{-2}. No mention was made of the cell voltage but a reading from the power and polarization plots shows that the OCV was around 0.34 V, and the maximum power density was achieved at around 0.1 V; relatively low when compared to the difference in the formal potential of the two mediators, 0.585 V ($E^0_{\mathrm{ABTS}} = 0.46$ [141] and $E^0_{\mathrm{PQQ}} = -0.125$ [142]).

Realising DET using GOx is difficult due to the deeply embedded nature of the active FAD sites. The same applies for PQQ and heme containing enzymes. In an attempt to overcome this issue, Willner and co-workers introduced a method based on reconstituting apo-enzymes on functionalised electrodes [79, 86, 143, 144] (see Fig. 2.1(b) for an illus-

tration). In one example, gold nanoparticles were linked to a gold electrode by a dithiol bridge, while amino-FAD was linked to the particles [79]. The FAD cofactor units were extracted from GOx to give the apo-enzyme, which was reconstituted on the FAD functionalised particles. The gold nanoparticles were seen to act as electron relays between the FAD redox site and the electrode. Similarly, PQQ-dependent GDH was electrically wired by the reconstitution of apo-GDH on PQQ-functionalised nanoparticles [80]. Patolsky et al. [82] instead reconstituted apo-GOx on FAD units linked to the ends of single wall carbon nanotubes (SWCNTs) assembled on a gold electrode, motivated by the efficient DET between SWCNTs and absorbed GOx redox active sites [81, 145]. The authors deduced that the SWCNTs behaved as electrical contacts between the active site of the enzyme and the electrode. Such electrodes, using either singlewalled or multi-walled CNTs [146, 147] display good stability and sensitivity [81, 148, 149].

2.1.4 Nanostructured electrodes

In recent years, the use of nanotechnology to develop biofuel cell electrodes has become widespread. Nano-structured materials have been shown to be appropriate hosts for enzyme immobilization, providing a greater surface area for attachment and improving enzyme kinetics [24]. They can also be used as electrical 'wires' between the electrode and the active redox centre of the enzyme.

Lee et al. [150] compared a fuel cell constructed using GOx and laccase with a cell containing SWCNT and a cell containing DNA-wrapped SWCNT. The use of single-stranded DNA wrapped SWCNTs was found to increase the GOx loading to 73.3 $\mu g\ mm^{-2}$ compared to approximately 19 $\mu g\ mm^{-2}$ for both SWCNT/FAD-GOx and cystamine/PQQ/FAD-GOx anodes. The electron conductivity at the three anodes was also studied and the results showed that the two electrodes containing SWCNT had similar conductivities, which were an order of magnitude greater than that of the cystamine/PQQ/FAD-GOx anode. A membrane-less fuel cell employing DNA-wrapped SWCNTs for immobilization of GOx and laccase and operating in a PBS (7 pH, 25°C) using glucose and O_2 (the fuel concentration was unspecified) achieved a maximum power density of 0.442 $mW\ cm^{-2}$ at

0.46 V, with an OCV of approximately 1.5 V. The authors suggested that DNA wrapping contributes towards decreasing the shear stress between the enzyme and the SWCNT, in addition to acting as the primary electron transfer mediator. These results are, however, questionable since the high OCV cannot be explained in terms of the redox potentials of the two biocatalysts ($E^0_{GOx} \approx -0.34$ V and $E^0_{laccase} \approx 0.54$ V *vs.* SCE [141]). The power density obtained using this pair of mediatorless biocatalysts was higher than those obtained with the same catalysts either entrapped in polymers with mediators [120], or wired through mediator activated polymers [106]. Moreover, this system [150] was operated at neutral pH, a condition that is not optimal for *Trametes versicolor* laccase activity.

These disadvantages of using laccase have been found to be source dependent. Those sourced from *Melanocarpus albomyces*, for instance, display optimum activity close to neutral conditions [116]. Kavanagh et al. immobilised laccase with an Os containing polymer, while the anode contained suspended, mediated GOx. The maximum power density was 0.052 mW cm^{-2} at 0.21 V with an OCV of 0.55 V. Ivnitski et al. [146] prepared a GOx anode using multi-walled carbon nanotubes (MWCNTs), which were grown using cobalt nanoparticles deposited on a carbon paper (CP). A mixture of GOx and polyethyleneimine was then applied to the electrode, followed by a casting of Nafion. The positively charged polycation acts as a binder between the negatively charged GOx and the CP/MWCNT electrode.

Fischback et al. [65] used enzymes in cross-linked clusters covalently immobilized on functionalised CNTs, which were than cast on a carbon felt. The preparation procedure involved immobilizing single GOx enzymes on functionalised CNTs, before adding ammonium sulfate to form enzyme clusters from the remaining freely suspended GOx. These clusters around the CNTs were then cross-linked and applied with Nafion on a carbon felt electrode. The anode was combined with a proton exchange membrane and an air-breathing Pt cathode. The cell was tested in the absence of a buffer, with an ammonium buffer and with a sodium buffer. In the absence of a buffer, the initial performance was poor, but the cell remained stable over a longer period of time and maintained almost constant power output. The maximum power density was 0.120 mW cm^{-2} at 0.1 V with an OCV of 0.33 V. The buffered cells underwent a degradation in performance due to the

presence of cations, which hinder the passage of protons through the membrane. Cross-linked enzyme clusters have previously been shown by the same group to provide good stability and high activity retention (up to 250 days). While an un-buffered solution was found to give better performance due to a lack of interference with proton transport, it may also have led to the low operating voltage (low solution conductivity). The use of an alternative membrane in the buffered cells to alleviate the problem of hindered proton transport, while not increasing the internal resistance, was not investigated.

Deng et al. [151] applied several coatings of AuNP/enzyme bilayers on macroporous gold electrodes initially treated with cystamine. Using GDH and laccase as enzymes, a membrane-less fuel cell was constructed. The cell was studied with respect to the number of bilayers and compared to one with flat gold electrodes and one bilayer. A maximum power density of 0.178 mW cm^{-2} at 226 mV was achieved using five bilayers while the OCV was 0.32 V. The current and power density were found to increase with the first 5 layers and in all cases were higher than with flat electrodes. A higher OCV (0.52 V) was observed with flat gold electrodes, and was attributed by the authors to a difference in the O_2 reduction potential compared to that for the macroporous cathode. However, CVs of these two anodes showed that a current peak occurred at a slightly higher potential with the flat electrode, indicating that the lower cell voltage is due to both electrode potentials, possibly as a consequence of the higher electrical resistance of the macroporous materials.

SWCNTs on GC have been used to attach AlcDH to covalently linked NAD^+ [152]. This anode was combined with a cathode containing both Pt and BOx in a copolymer cross-linked matrix and the cell (Fig. 2.8) was operated with 0.1 M PBS and 40 mM of ethanol at a pH of 7.0. A maximum power density of 0.2 mW cm^{-2} at 0.55 V and 0.37 mA cm^{-2} with an OCV of 0.62 V were attained. While CNTs are employed for their good conductivity and large surface area for depositing the enzymes, Zhou et al. [153] showed that a higher voltage and power density can be obtained with a mesoporous carbon based material.

The increasing use of nanostructures (such as nanoparticles, nanofibers and CNTs) has a twofold advantage: providing a greater surface area for the biocatalysts and enhancing

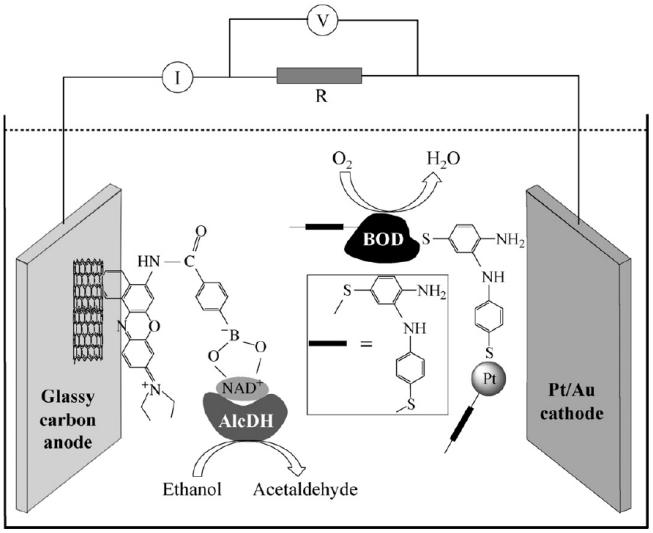

Figure 2.8: A schematic representation of a membrane-less bio-fuel cell employing bioelectrocatalytic electrodes composed of (a) alcohol dehydrogenase (AlcDH) reconstituted on a relay-NAD^+ monolayer associated with carbon nanotubes (anode); and (b) a platinum-nanoparticle/bilirubin-oxidase (BOx) crosslinked composite on a Au/Pt electrode (cathode). Adapted from Yan et al. [152].

their stability and activity [75]. These procedures are, on the other hand, relatively costly. Some reports have claimed that CNTs can have an adverse effects on the enzyme kinetics [154], indicating that the use of these structures requires a careful selection of enzymes, electrode materials and attachment methods. More generally, a careful optimization of the nanostructure size is required, since small pores can lead to mass transport limitations for the mediator/substrate and large pores can lead to leaching of the enzyme [24].

2.1.5 Fuel oxidation

In many enzymatic fuel cells, both the cathode and anode are biological, with the aim of combining the benefits of higher stability and the good catalytic activity of inorganic materials, together with improved O_2 reduction kinetics via biocatalysts at low temperatures [155–157]. Habrioux et al. [157] used Au-Pt nanoparticles supported in a Nafion/carbon-black mix, together with BOx and its mediator ABTS co-immobilized in a Nafion film to construct a concentric bio-fuel cell. A maximum power density of 0.19 mW cm^{-2} at 0.52 V was achieved at 37°C and 7.4 pH using 0.7 M glucose. An appreciable power density of 0.09 mW cm^{-2} could still be achieved at a lower glucose concentration of 10 mM.

Most fuels used in EFCs are either saccharides, such as glucose, lactose, fructose and cellobiose, or alcohols such as ethanol. Recently, glycerol has been considered due to its high energy density and abundance (it is a byproduct of biodiesel) [20, 158]. In a study by Arechederra et al. [158], a cascade of two PQQ-dependent enzymes, AlcDH and aldehyde dehydrogenase (AldDH) was immobilized in modified Nafion on a CP/Pt cathode, and the assembled fuel cell produced a maximum power density of up to 1.21 mW cm^{-2}. This cell was further developed by adding a third enzyme, oxalate oxidase [20], which allowed the complete oxidation of glycerol and slightly increased the maximum power density to 1.32 mW cm^{-2} with 100 mM of glycerol. However, the cell was less tolerant to high fuel concentrations compared to the original cell.

Another enzyme cascade system was reported by Topcagic and Minteer [159]. Ethanol was oxidized to acetate by AlcDH and AldDH and dissolved O_2 was reduced by BOx immobilized with two consecutive mediators in Nafion. In a membrane-less system employing 7.15 pH PBS with 1 mM ethanol and 1 mM NAD^+ as the anodic mediator, an OCV of 0.51 V and a maximum power density of 0.39 mW cm^{-2} were achieved. Both the voltage and power were lower than an equivalent cell employing a Nafion membrane separator. Ramanavicius et al. [160] developed a fuel cell that used ethanol as the substrate for both half reactions, with an AlcOx/MP cascade on the cathode and AlcDH on the anode. The maximum power density was 1.5×10^{-3} mW cm^{-2} with an OCV of 0.24 V.

In addition to the development of enzyme/electrode preparation methods, several studies have been aimed at optimising systems according to the buffer type and concentration, redox polymer composition, and binder-to-enzyme ratios [49, 59, 105, 117, 161]. Most of the choices were specific to the setup used and are of limited use for other designs. In the case of microfluidic fuel cells, numerical optimization of the channel dimensions has been performed by several groups [141, 162, 163].

Immobilisation of the enzymes/mediators opens up the possibility of single compartment EFCs. There are, however, very few examples of membrane-less or separator-free EFCs. The first single chamber EFC was developed by Katz et al. [87], consisting of two immiscible electrolytes separated by a liquid-liquid interface, allowing DET to take place.

GOx apo-enzyme was reconstituted on PQQ-flavin adenine dinucleotide phosphate (FAD) monolayer associated with an Au electrode. The cathode consisted of an Au electrode onto which a microperoxidase-11 monolayer was assembled and for which cumene peroxide was used as the oxidiser. Ramanavicius et al. [164] constructed a single-chamber EFC operating with immobilised alcohol dehydrogenase (AlcDH) on a carbon-rod anode and co-immobilized GOx/microperoxidase on a carbon-rod cathode. The power density, around 10 nW cm^{-2}, was low and the operational half-life was only 2.5 days. A DET, single-chamber H_2/O_2 cell with hydrogenase at the anode and fungal laccase at the cathode was constructed by Vincent et al. [165], again, however, with a low power density. A more systematic selection of the enzymes and electrode materials by Kamitaka et al. [29] led to a single-chamber, membrane-less fructose/O_2 cell capable of power densities on the order of 1 mW cm^{-2}; fructose dehydrogenase (FDH) was immobilised on a Ketjen-Black (KB) modified carbon paper and multi-copper oxidases were immobilised on a carbon paper cathode modified with KB and a carbon aerogel. Coman et al. [96] instead used cellobiose dehydrogenase (CDH) and lacasse for a glucose/O_2 system, which was capable of only 5 μW cm^{-2}. More recently, Wang et al. [166] immobilised GOx (anode) and laccase (cathode) on porous silicon substrates with pre-deposited carbon nanotubes to form a membrane-less, mediator-free glucose EFC. Again, the power density (1.38 μW cm^{-2}) was low and decreased by a factor of almost 5 after 24 h.

Membrane-less fuel cells have several attractive features, including structural simplicity, reduced cost, and a greater scope for miniaturization. There are, however, several requirements for such systems: specificity of the two half reactions occurring, such that the substrates/products of one do not interfere with the other, and acceptable operating conditions common to both biocatalysts [117]. A number of membrane-less systems have been developed, exhibiting varying degrees of electrical performance. In systems based on DET using CDH/laccase [96], CDH/BOx [167], or GOx/laccase [166], power densities of only a few μW cm^{-2} have been realised. The first two systems employing CDH exhibited relatively high operating and open cell voltages, and hence the low power was due to a low current, specifically the anodic current. This was potentially due to unfavorable orientation of CDH after immobilization; CDH has one FAD domain and one heme domain allowing DET to the electrode. Membrane-less systems employing mediators, and either

GDH/BOx [168], AlcDH/BOx [159], GDH/laccase [151], or FDH/laccase [29], can have power densities 1-2 orders of magnitude higher than those yielded by DET. The absence of soluble mediators, however, remains an essential feature of the flow type fuel cells proposed for *in vivo* applications.

Table 2.1: Summary of key enzymatic fuel cell developments

Anode	Cathode	Electrolytes/membrane	P_{max} (mW cm^{-2})	V or I at P_{max}	OCV (V)	Remarks	Reference
Mitochondria immob. in modified Nafion on C-electrode	Air-breathing **Pt**-C/membrane assembly	10 mM, 7.45 PBS, 6 M $NaNO_3$, 100 mM **pyruvate**, 1gL^{-1} ADP	0.0315†, 0.024 (average)	0.1† mA cm^{-2}	-	Air cathode/ membrane assembly	[19]
AlcDH/ AldDH/ oxalate oxidase in modified Nafion on C-paper	Air-breathing **Pt**-C/membrane assembly	7.15 pH PBS, 6M $NaNO_3$ 100 mM **glycerol**	1.32	2† mA cm^{-2} (0.66 V†)	-	Air cathode/ membrane assemble	[20]
GOx/HQS (mediator) in PPy on Carbon rod	**Laccase**/ABTS (mediator) in PPy on porous carbon tube	5 pH PBS, 10 mM **glucose**, N_2 purged, 37 °C, separate O_2 solution circulated inside cathode	0.027	0.25 V	0.41†		[120]
CDH adsorbed on graphite	**Laccase** adsorbed on graphite	0.1 M citrate buffer, 4.5 pH, 5 mM **glucose**, air saturated	5×10^{-3}	0.5 V	0.73	Membrane/ mediator-less. Enzyme desorption causes current/power loss.	[96]
5 bilayers of AuNPs/**GDH** on three dimensional ordered macroporous, cysteamine treated Au electrode	Similar to anode, using **laccase** as catalyst	0.1 M, 6 pH PBS, 5 mM NADH, 30 mM **glucose**	0.178	0.226 V	0.32	SCC=0.752 mA cm^{-2}	[151]
Cross-linked clusters of **GOx** and CNTs on CF electrode (0.332 cm^2)	Air breathing **Pt**-C cathode (0.332 cm^2)	Un-buffered, 200 mM **glucose**, 10 mM benzoquinone	0.12	0.1 V	0.33	MEA assembly. Better initial performance but degrades quickly in buffered solutions due to cation interference with proton transport.	[65]
GDH on poly(brilliant cresyl blue)/SWCNT/glassy carbon rod (3 mm diameter)	Cross-linked **BOx** on SWCNT on same carbon electrode	0.1 M PBS, 7 pH, 10 mM NAD^+, 40 mM **glucose**, ambient air	0.054	0.5 V	0.73	Membraneless. 5 % P loss in first day. 46 % loss in one week	[168]
GOx 'wired' through PVP-Os complex with cross-linking on 2 cm long, 7 µm diam. CF	**BOx** 'wired' through PAA-PVI-Os complex with cross-linking on similar electrode	20 mM PBS, 7.24 pH, 0.14 M NaCl, 15 mM **glucose**, 37 °C	0.315	0.46†V	-	Membrane-less. Commercial enzyme stock purified before usage. Operating cell for 1 week at 0.52 V lost 6 % of power output per day	[107]
Au$_{70}$Pt$_{30}$ bi-metallic nanoparticles on inner surface of carbon tube (4.4 cm^2, 1.4 cm diam.)	**BOx**/ABTS in modified Nafion on inner surface of porous carbon tube (6 mm diam.)	7.4 pH, PBS, 0.7 M **glucose**, 37 °C	0.19, 0.09 (10mM glucose)	0.52 V, 0.4 V (10mM glucose)	0.89†	Abiotic anode. Concentric design. Membrane-less	[157]
FDH adsorbed on Ketjen black (0.282 cm^2)	**Laccase** adsorbed on carbon aerogel particles (0.282 cm^2)	McIlvaine buffer, 5 pH, 200 mM **fructose**, O_2 saturated, 25 °C	0.85 (stirred), 0.39 (unstirred)	0.41 V	0.79	SCC=2.8 mA cm^{-2} (stirred), 1.1 mA cm^{-2} (unstirred). Power drops to 63 % after 12 hours. 4 cells in series operate 1.8 V LED for ~60 days.	[29]
GOx/HQS immobilized in polypyrrole nanowires (0.15 cm^2)	**BOx**/ABTS in polypyrrole film (0.35 cm^2)	7.4 pH, PBS, 15 mM **glucose**	0.28	0.15 V	0.35	SCC=2.9 mA cm^{-2} and maximum power density with 200 nm diam. 16 µm length nanowires. Membraneless	[128]
GOx covalently attached to 3-methylthiophene (3MT) and thiophene-3-acetic acid (T3A) copolymer	**BOx** covalently attached to same copolymer	0.1 M PBS, 7 pH and either 0.1 M **glucose**, 1 mM N,N,N',N'-tetramethyl-p-phenylenediamine, N_2 saturated or 1 mM ABTS, O_2 saturated in either compartment separated by Nafion membrane	0.15	0.35 V	0.61	Anodic current decreased to 50 % while cathodic current decreased to 75 % the initial values after 1 month	[119]
Au electrode-cystamine-PQQ-**LDH** monolayer	Au electrode-cystamine-**microperoxidase 11**	Anolyte: 0.1 M tris buffer, 7 pH, 20 mM $CaCl_2$, 20 mM NAD^+, 20 mM **lactate**. Catholyte 0.1 M PBS, 7 pH, 1 mM **H_2O_2**, ABTS. Nafion separator.	0.142	0.1† V	0.34†	LDH immobilization carried in presence of $CaCl_2$ promoter, NAD^+, and lactate found to increase power by 26 % compared to immobilization without.	[140]
GOx/single-stranded DNA-wrapped SWCNT on cystamine dihydrochloride treated Au electrode (0.0314 cm^2)	Similar immobilization for **laccase**	0.1 M PBS, 7 pH, **glucose**, O_2, 25 °C	0.442	0.46 V	1.5†	Cell operated for more 5 days with power in excess of 0.43 mW cm^{-2}. DNA-wrapped SWCNT found to increase enzyme loading.	[150]

GOx/SWCNTs in silica gel	**BOx**/SWCNT in silica gel	Anolyte: 4 mM ferrocene methanol, 100 mM **glucose**. Catholyte: 8 mM ABTS, O_2 saturated. Room temperature. Nafion separator.	0.12, 0.086 (ambient air)	0.24 V, 0.21 V (ambient air)	0.48		[124]
Penicillium pinophilum sourced **GOx**/PVP-Os complex, crosslinked, on 2 cm long, 7 µm diam. CF	**Laccase**/ PVP-Os complex, crosslinked on 2cm long, 7 µm diam. CF	20 mM citrate buffer, 5 pH, 37 °C, 5 mM **glucose**	0.28	0.88 V	-	GOx sourced from *P.pinophilum* allows higher power density at lower fuel concentration than tradition *A.niger* but unstable at neutral pH. 3 % power loss per day for first 2 weeks.	[106]
GDH/NAD^+ in Ketjen black on glassy carbon (0.07 cm^2)	**BOx** in Ketjen black	PBS, 50 mM **glucose**, O_2 saturated	0.052	0.3 V	0.64	SCC=0.223 mA cm^{-2}. Membrane/mediator-less	[98]
AldDH adsorbed on graphite electrode	**AlcOx/ microperoxidase-8** adsorbed on graphite electrode	50 mM sodium acetate, 6 pH, 100 mM KCl, 2mM **ethanol**	1.5×10^{-3}	-	0.24	Ethanol as substrate for both half-reactions. Power decreases to half initial value after 26 hours of operation	[160]
4 layers of (CF/ poly-L-lysine/ **GDH**/ diaphorase/ NADH/ vitamin K_3/ polyacrylic acid sodium salt) (1 cm^2 each)	air-breathing, 2 layer of (CF sheet/ $K_3[Fe(CN)_6]$/ PLL/ **BOx**) (1 cm^2 each)	0.1 M, 7 pH, (PBS), room temperature, 0.4 M **glucose**. Electrodes stacked with cellophane membrane in a single assembly.	1.45	0.3 V	0.8	SCC=11 mA cm^{-2}.	[49]
CDH/ polyvinylpyridine- Os complex/SWCNTs on graphite rods (3.05 mm diam.) with cross-linking	**Pt**-C (area≫anode area)	PBS, 7.4 pH, 37 °C, 0.1 M **glucose**, O_2 purged, non-quiescent	0.157	0.28 V	0.5		[169]
PLL-K_3/diaphorase/**GDH** on glassy carbon (0.07 cm^2)	Poly-dimethylsiloxane coated **Pt** cathode	PBS, 7 pH, 5 mM **glucose**, 1 mM NAD^+, 37 °C	0.032	0.29 V	0.55	Current drops to half initial value after 18 hours	[170]
AlcDH/ AldDH/ NAD^+/ modified Nafion on polymethylene green anode	**BOx**/modified Nafion on 1cm^2 CF paper. Dried then soaked in $Ru(bpy)_3^{2+}$ mediator	7.15 pH, PBS, 1 mM **ethanol**, 1 mM NAD^+, room temperature	0.39, 0.83 (with Nafion membrane)	-	0.51, 0.68 (with Nafion)	Power increases to a maximum of 0.46 mW cm^{-2} then rapidly drops after 20 days.	[159]
LDH/modified Nafion with $CaCl_2$ on CF paper (1 cm^2)	**Pt**-C black	Anolyte: 7.15 pH, PBS, 25 mM **lactate**. Catholyte: 1 M NaCl, dissolved O_2, 20 °C. Nafion Separator	0.022	-	0.85	Testing over 45 days without any claimed degradation in performance	[103]
Porous Si-functionalised SWCNT-**GOx**	Porous Si-functionalised SWCNT-**laccase**	PBS, 4 mM **glucose**, air bubbling, stirred. 5 mm inter-electrode distance	1.38×10^{-3}	99 mV	-	Lower power density (0.35×19^{-3} mW cm^{-2}) at higher voltage (0.357 V) when SWCNTs grown by chemical deposition followed by carboxyl group attachment rather then electrophoretic deposition of pre-functionalised SWCNTs.	[166]
Covalently linked SWCNT-NAD^+ deposited on classy carbon. **AlcDH** attached to NAD^+ through affinity, and crosslinked	Thioanaline modified **BOx** copolymerized with thioanaline capped **Pt** nanoparticles on Au electrode with thioanaline monolayer with crosslinking.	0.1 M PBS, 7 pH, 40 mM **ethanoll**, O_2 saturated	0.2	0.55† V	0.62	Maximum power at 0.37 mA cm^{-2}	[152]
GOx/ MWCNTs/ Nafion on carbon felt (0.33 cm^2)	Air-breathing **Pt** cathode	100 mM **glucose**, 10 mM 1.4-benzoquinone. Nafion/electrode assembly	0.077	0.51 V	0.57	-	[171]

† Values not explicitly reported, but estimated from graphical results

2.2 Microbial fuel cells

A summary of the key developments in microbial fuel cells is presented in Table 2.2, and are discussed in detail below.

2.2.1 Exoelectrogenesis

The use of whole cells for the biocatalysis of fuels is advantageous since it eliminates the need for enzyme isolation and allows multiple enzymes (and hence multiple fuels) to function together in conditions close to their natural environment. The working principle of MFCs is to force the microbes to shift from aerobic respiration to anaerobic respiration, in which the electrons produced during oxidation of the fuel are donated by some means to the electrode (electrode respiration or exoelectrogenesis [69]). The effect of O_2 (a natural electron acceptor) diffusion to the anode is known to lower the coulombic efficiency and several reports have noted a corresponding decrease in the power output. A more recent study on the effect of O_2 presence in the anode compartment [172] concluded that the dissolved O_2 level does not affect the power output since O_2 is scavenged by aerobic digestion. During this process, however, bacterial activity primarily takes the form of aerobic respiration of the substrate, and the voltage and power recover only after the O_2 concentration falls below a critical level. Other methods of maintaining anaerobic conditions include the use of O_2 chemical scavengers such as cysteine [173].

Forcing anoxic conditions in the anode compartment does not necessitate that the bacterium will take the respiration chemical pathway, while donating the electrons to the electrode. Bacteria will undergo the process that maximizes their energy gain, which is proportional to the potential difference between the oxidation reaction and the terminal electron acceptor. If the anodic potential is too low, organisms will switch to fermentation, which can extract only one-third of the electrons available in the substrate [38]. One recent report comparing different fuels concluded that non-fermentable substrates (*e.g.* acetate) have higher coulombic and energy efficiencies compared to fermentable substrates such as

glucose [174]. Hence, a careful balance of the anode potential is required; it must be high enough that organisms do not switch to fermentation, yet sufficiently low to maintain a high cell voltage and power output.

Several studies have investigated the effect of the anode potential on bacterial growth and power production [172, 175, 176]. At high anode potentials (by-poising), bacterial growth is encouraged, the startup time is reduced, and the overall current is reduced [175]. It has been argued, however, that there is a critical potential beyond which bacteria can no longer generate significantly more electrons due to the shortage of suitable electron acceptors [176].

The microbial cultures in fuel cells can either be suspended in the anode solution or immobilized on the electrode surface. It has been reported that the immobilization of *P. vulgaris* on graphite felt electrodes by either culturing the bacteria on the anode or chemically linking them *via* amide bonds decreases the response time of a system to fuel addition [177]. Having the biocatalyst in solution limits the operation of the system to batch-mode where fuel quantities are added at different intervals, unless the mediator is regularly replenished, increasing the cost of the system. A comparison of this operating mode with continuous-flow operation showed that the power output and efficiency were lower [177]. In continuous-feed systems, biofilm forming species are preferred since they can either use the electrode directly (through physical contact) or transfer electrons through the biofilm *via* mobile mediators [38]. Batch-mode operation, on the other hand, offers the advantage of greater mediator influence [178], particularly when mediator producing bacteria are used; this promotes accumulation of the mediators in the anodic compartment [38].

Clauwaert et al. [179] constructed an MFC using the effluent of a used MFC as inoculum for a graphite granule anode. The power density in batch operation (83 $\mu W\ cm^{-3}$) was higher than in continuous operation (65 $\mu W\ cm^{-3}$), yet the coulombic efficiency (CE) was much lower (20-40% in batch-mode compared to 90% in continuous/flow-through operation).

2.2.2 Electron transport

One of the most difficult aspects of microbial fuel cell development is tapping into the intracellular electron transport system and diverting the generated electrons from their natural electron acceptors outside the cell to the anode. The ET can be achieved either through the use of artificial or natural (produced by the bacterium) mediators or by direct contact with the electrode *via* membrane associated cytochromes. Direct contact through "nanowires" or pili produced by the bacteria has recently been attempted [69, and references there in]. This method was demonstrated with *Geobacter sulfurreducens*, where the deletion of the gene responsible for pili production stopped the current generation [180].

When mediators are used as electron shuttles, they are required to:

(i) have fast kinetics for both oxidation at the anode and reduction inside the organism;

(ii) easily penetrate the cell membrane;

(iii) be chemically stable and not interfere with other metabolic pathways;

(iv) not adsorb on the bacteria or anode, and

(v) have a potential that matches that of the reductive metabolite [5].

Different types of mediators, such as thionine, quinone, phenazines, Fe(III) ethylenediaminetetraacetic acid (EDTA), methylene blue, and neutral red (NR), have been used in MFCs. In the work by Park and Zeikus [181], the authors compared the electrical performance of two cell designs: the first with a soluble NR mediator and a woven graphite electrode and the second having covalently-linked NR on a woven graphite anode. The current in the cell containing an immobilized mediator was a factor of three higher than the current in the cell using soluble NR. Similar results were obtained when a Mn^{4+} mediator was incorporated into the anode by coordination bonding to the silica content of the graphite. On the cathode side, Fe^{3+} was incorporated into the graphite electrode following

the procedure used for Mn^{4+} in the anode. The inner surface of the cathode was coated with a 1 mm thick proton permeable layer of porcelain. Electrons reaching the cathode from the external circuit reduce the Fe(III) to Fe(II), which in turn is oxidized to Fe(III) by O_2. Operating on a bacterial culture from a sewage sludge, and using glucose as the substrate, the fuel cell with the Mn^{4+} anode achieved a power density of 78.7 μW cm^{-2} based on the theoretical surface area of the graphite felt. Graphite felt was chosen over simple graphite plates due to its higher surface area, though materials with small pore sizes usually raise concerns when used as anodes in MFCs since bacterial attachment and growth may cause blockage, leaving the active sites inaccessible to the substrate.

An alternative to using artificial mediators was made possible after the discovery that some species, *e.g.* *Clostridium butyricum* [182] and *Pseudomonas aeruginosa* [183], produce their own mediators. The latter species is known to produce phenazine derivatives that are capable of mediating ET from the bacterium to the electrode. An MFC developed by Rabaey et al. [184] using this species was capable of achieving a CE of 83% without the need for artificial mediators. The maximum power output of this system was 0.43 mW cm^{-2}. The use of these species is not restricted to the originating micro-organism; their presence in mixed cultures, or with other species not capable of DET, may enhance the electron transfer capabilities of other bacterial species [185].

Perhaps more practical bacterial species with enhanced ET capabilities are the metal reducing bacterium, namely *Rhodoferax ferrireducens* [186], *Geobacter sulfurreducens* species [180, 187] and *Shewanella oneidensis* [188]. The direct electronic communication abilities of these species with the electrode is due to the presence of enzymes on their outer membrane that can transfer the electrons directly to the anode.

Ringeisen et al. [188] used *Shewanella oneidensis* with a ferricyanide cathode to demonstrate the ability of this species to generate power in the absence of a mediator and in the presence of O_2. Power densities of 0.2 mW cm^{-2} and 0.33 mW cm^{-3} were achieved, though these could be doubled in the absence of O_2 or with the addition of a mediator. Nevin et al. [189] used *Geobacter sulfurreducens* PCA on a carbon cloth in an acetate solution along with an air-breathing Pt cathode to construct a two-chamber fuel cell. The power

densities were 0.19 mW cm^{-2} and 0.043 mW cm^{-3} when the anode chamber volume was 7 mL.

Direct ET through membrane bound enzymes has also been demonstrated for *Hasenula anomala*, a eukaryotic yeast cell [190], in a two-chamber mediatorless MFC with the microorganism immobilized by physical adsorption. In this work, a maximum power density of 2.9 μW cm^{-3} was obtained with a polyaniline-Pt coated graphite anode, using ferricyanide in the catholyte.

Xing et al. [185] used a strain of *Rhodopseudomonas palustris*, a species that has previously been used for hydrogen production, to construct a fuel cell that was capable of achieving a maximum power density of 0.272 mW cm^{-2} (at 0.99 mA cm^{-2}) in light conditions and 0.264 mW cm^{-2} in dark conditions, with respective coulombic efficiencies of 50% and 60%. The electrodes consisted of a graphite brush anode with a 30% wet-proofed carbon cloth/Pt cathode (7 cm^2) of four diffusion layers. Acetate (1 g L^{-1}) was used as the electron donor in a phosphate buffer solution. The electrical performance was higher than that with a mixed culture using the same system [185].

2.2.3 Biocatalyst source

The selection of the biocatalyst source and enrichment of the biocatalyst are important for optimising the performance of MFCs. The dominant opinion until recently was that pure cultures are better suited to the study of specific organisms (and their electrochemical performance) than they are to maximizing power generation. Mixed cultures, in contrast, are better suited for practical applications, especially when mixed fuels are used, as in wastewater treatment applications [22]. Recently, however, power densities from certain pure cultures are now comparable to those obtained from the use of mixed cultures [185, 188].

It has been observed that the bacterial population in the anodic biofilm changes during operation [22, and references therein], with the domination of specific classes such as

Geobacter [189]. Aelterman et al. [191] studied culture composition at different times during the operation of a MFC. After an initial period of stabilization, species from the *Proteobacteria* (*e.g. Geobacter, Shewanella, and Pseudomonas*) were dominant, while at maximum power generation, members of the *Bacilli* class (*e.g. Clostridium*) were dominant. The change in culture composition was also accompanied by a decrease in the internal resistance [191]. Different sources of mixed bacterial cultures have been used as inoculums in MFCs with the most common being anaerobic sewage sludge [191–193], or bacterial cultures obtained from used MFCs [179, 194–196]. Other sources such as soil and garden compost have also been investigated [197].

The question of whether microbial communities will evolve and selectively adapt to a MFC environment gave rise to a study by Kim et al. [192], where the effects of different inoculation techniques on the performance of a two-chamber MFC were investigated. Fig. 2.9 shows selected results from this study. Inocula were sourced from an anaerobic sewage sludge that was filtered and added to acetate for use as an enrichment medium, which was then replaced with a nutrient buffer for use in different settings. The performance of cells using these enriched inocula were compared to the performance of a controlled MFC with CP electrodes inoculated with the untreated sludge (the latter cell yielded a maximum power density 0.4 μW cm^{-2}). A large proportion of the micro-organisms in anaerobic sludge is believed to be methanogens, which lead to undesirable methane formation reactions that consume the substrate with no electricity generation, thus lowering the CE. Addition of 2-bromoethanesulfonate (BES), an inhibitor of methanogenic activity, was found to significantly increase the CE from 40% in the absence of BES to 70% with a correspondingly large reduction in the concentration of methane from 40 to 2%. It has recently been demonstrated that BES, which is a mild irritant to the skin, eyes and respiratory system, can inhibit the bioactivity of methanogens even at very low doses of 0.1-0.27 mM, while having no effect on exoelectrogens [198]. The authors of this report conducted batch-cycle experiments, discovering that methane production was inhibited for several cycles after a single injection of BES, suggesting that it need only be injected intermittently.

In another experiment, to promote the activity of iron-reducing bacteria (known to be

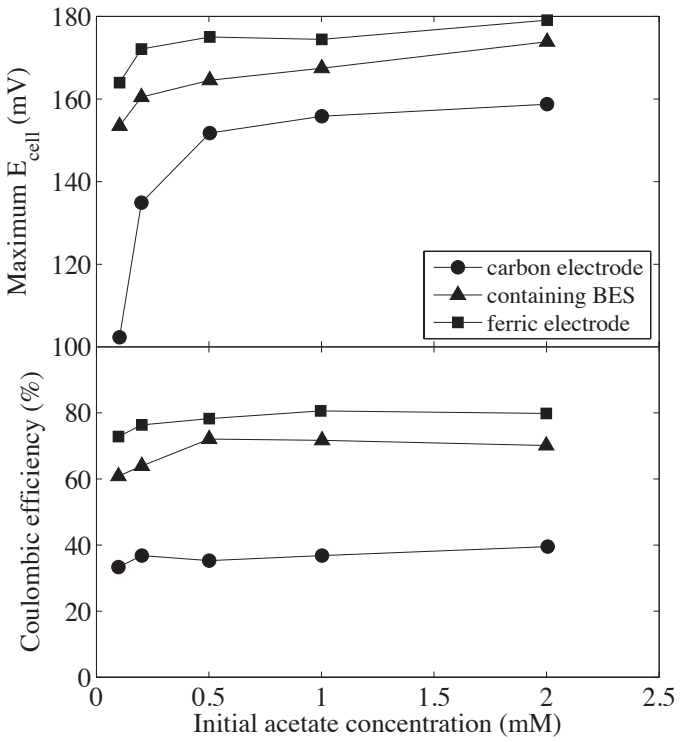

Figure 2.9: Effect of initial acetate concentration on maximum voltage and coulombic efficiency, in MFCs using a carbon electrode (•), a carbon electrode that contained BES only during the initial acclimation on wastewater (▲), and a ferric electrode (■). Adapted from Kim et al. [192].

capable of both DET and growth in the presence of acetate), Kim et al. employed an iron-oxide coated carbon paper anode. This was found to increase the power density and CE to 3 μW cm^{-2} and 80%, respectively. These increases were accompanied by a faster response to substrate addition, indicating a direct ET between the the microorganism and the electrode. Iron-reducing bacteria selectively attached to the electrode and preferentially (over methanogenic bacteria) reacted with the acetate. To further exploit the improved performance brought about by iron-reducing bacteria, their concentration was increased by successively enriching the inoculum in ferric citrate and acetate solution. This serial enrichment actually caused a negative effect on the performance and an MFC with the pre-enriched iron-reducing bacteria yielded only 0.2 μW cm^{-2}. The best performance was achieved with a biofilm scraped from the anode of a functioning MFC and applied to the new anode (4 μW cm^{-2}). None of these different techniques were found to have any effect on the startup time. While the study was useful in comparing different inoculation techniques, the power densities obtained were low, possibly due to the high internal resistance of the design.

2.2.4 Anode materials

Careful selection of anode materials is important due to its effect on both the microbial attachment and the ET [37]. Carbon or graphite based materials are frequently selected for anodes due to their large surface area, high conductivity, biocompatibility and chemical stability [67]. A recent report has demonstrated that gold, though impractical form a commerical perspective, could potentially be used as an anode with *Geobacter sulfurreducens*, yielding a performance similar to that with graphite [180]. A successful coupling of a bare gold electrode with *Shewanella putrefaciens* was only achieved by modifying the electrode with an alkanethiol self-assembled monolayer having a carboxylic acid functional head group [199], as a result of strong hydrogen bonding between the carboxylic acid groups and the cytochromes in the bacteria. This covalent linking functioned as an electrical connection between the bacteria and the electrode, and the modified electrode produced significantly higher currents than with glassy carbon. The influence of chain length and of other functional groups was also investigated. When five methylene units were added to the self-assembled monolayer, the current output was reduced, while the use of a methyl group yielded no current at all.

In another report, the anode was modified to immobilize a derivative of the anthraquinone-1,6-disulfonic acid (AQDS) mediator [200] (adsorption of AQDS, as well as 1,4- naphthoquinone (NQ), on graphite to construct bio-fuel cell anodes was previously explored by Lowy et al. [201]). Polyethyleneimine was used to bind the mediator and *Geobacter sulfurreducens* to a graphite electrode. The lifetime of this anode was reported to be more than four months (without decomposition or decrease in the current).

Numerous reports have investigated the modification of anodes with conductive polymers, mainly the organic polyanilines [37, and references therin]. This type of modification increases the current density, though it is also susceptible to microbial attack and degradation [37].

2.2.5 O_2 reduction

The complementary reduction reaction occurring at the cathode is usually achieved with O_2 as the electron acceptor. Alternative electron acceptors are hexacyanoferrate [191, 202], ferricyanide [188, 203], permanganate [204] and H_2O_2. Fuel cells using these compounds show significantly improved performance compared to O_2 based systems, as a consequence of the lower reduction potential and increased ionic strength. Due to their inherently slow oxidation kinetics, however, they need to be regenerated continually [67, 205]. Although ferricyanide has been employed as a mediator in conjunction with O_2 as an electron acceptor in an enzymatic fuel cell [206], it is doubtful that the ferricyanide functions only as a mediator, given its superior reduction kinetics compared to O_2.

The reduction of O_2 on non-catalyzed carbon based surfaces is very inefficient, occurring at an overpotential of almost 1 V below the formal reduction potential [207]. In addition to enhancing the reaction kinetics, catalysts such as platinum also decrease the critical O_2 concentration (concentration below which the reaction ceases), thus preventing O_2 diffusion to the anode [208]. The relatively well developed knowledge of O_2 reduction on platinum has been successfully applied to improve the operation of low temperature polymer electrolyte membrane fuel cells (PEMFCs), which typically operate at temperatures below 100°C.

The high cost of platinum and the possibility of poisoning by species such as CO [39] have motivated a search for alternative O_2 reduction catalysts that can function under physiological conditions and yield a similar level of performance. Cheng et al. [209] investigated the performance of a single-chamber air-breathing MFC using either cobalt tetramethylphenylporphyrin (CoTMPP) or Pt. Using carbon cloth electrodes (7 cm^2 projected area) and a Pt loading of 0.5 mg cm^{-2}, the cell produced a maximum power density of 480 mW cm^{-2}. Replacing the Pt cathode with 0.6 mg cm^{-2} CoTMPP/Nafion binder produced similar potentials but the power was reduced by 12%, with little loss in activity over 25 cycles. Comparing the CoTMPP cell to a cell with either a lower Pt loading of 0.1 mg cm^{-2} or one using PTFE binder, demonstrated consistently higher power densities.

Enzymes or whole micro-organisms could provide cost-effective and sustainable biocatalysts for O_2 reduction. A review of biocathode development up to 2006 was provided by He and Angenent [39]. Schaetzle et al. [197] implemented a bio-fuel cell using a mixed culture from soil/garden compost on a glassy carbon anode, along with laccase in a hydrogel applied at a platinum cathode with soluble 2,2'-azinobis-(3- ethylbenzothiazoline-6-sulfonate) (ABTS) as amediator. Compared to the performance using a virgin platinum electrode, the enzyme cathode led to increases in the power density and OCV from 0.46 μW cm^{-2} (at 0.2 V) and 0.6 V to 4.63 μW cm^{-2} (at 0.5 V) and 1.1 V, respectively. It must be pointed out that laccase applied as a hydrogel on a platinum cathode will be permeable to both the mediator and to O_2, making it difficult to isolate the effect of the platinum from that of the enzyme in the performance figures.

Recently, whole micro-organisms that can use the cathode as an electron donor have been investigated for use in MFCs. Clauwaert et al. [179] combined the anode of a tubular MFC with a new mixed culture, open-air, graphite felt cathode. Under continuous-feed operation, the 0.183 L MFC generated a volumetric power density of 65 μW cm−3 at 0.344 V with a CE of 90%. Under batch-fed mode the power density was 28% higher but the CE ranged between 20% and 40%. The application of a layer of manganese oxide on the cathode was observed to lower the startup time by 30% without affecting the steady-state performance. In the absence of ammonium or nitrate, the cell was operated for 7 months. Similar improvements in MFC performance and reductions in the internal resistance were also observed by Chen et al. [210].

2.2.6 Reactor design

Different design concepts and configurations have been developed to optimise the arrangement of the three basic components, anode, cathode and separator, in a functioning system [196, 211]. Four different categories can be identified [37] (see Figure 2.10):

1. the classic two-chamber setup where both the anode and cathode are placed in liquid electrolytes separated by an ion exchange membrane;

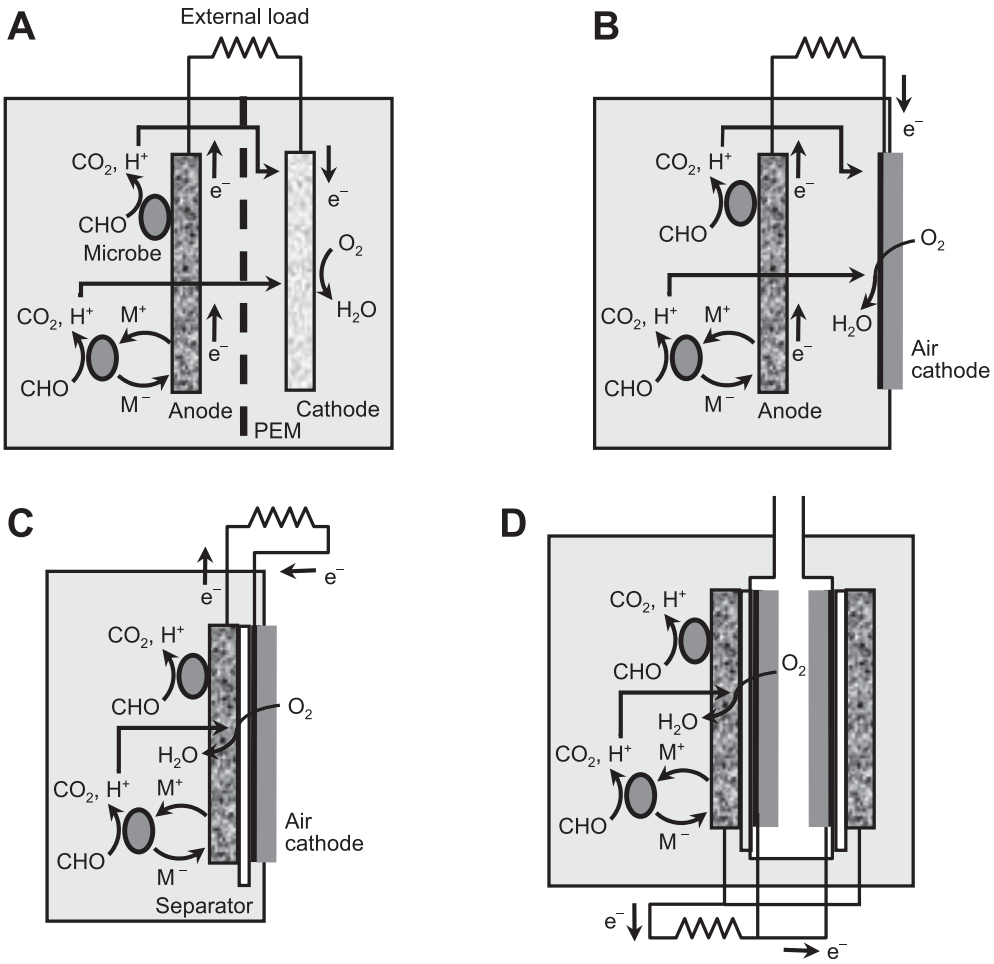

Figure 2.10: MFC reactor designs and electrochemical reactions. (A) A double-chamber MFC using oxygen as the cathode electron acceptor. (B) A single-chamber air-cathode MFC. (C) A single-chamber air cathode MFC with cloth electrode assembly separator. (D) A cassette-electrode MFC. M, Mediator; CHO, organics; PEM, proton exchange membrane. [37]

2. a single-chamber air-breathing MFC with the anode placed in the electrolyte and the cathode unit (with or without a separator) placed between open-air and the anolyte [181, 195, 212, 213];

3. a single-chamber MFC where all three components are arranged into a single unit similar to the membrane electrode assembly (MEA) of PEMFC [211];

4. a cassette-electrode arrangement where two MEAs are arranged to have a common aerated chamber on the inside and are exposed to a common anolyte on the outside [214].

An air-breathing cathode is desirable since it eliminates the need for an aerated catholyte, thus simplifying the system design, as well as reducing costs and energy requirements. Such a system was first developed by Park and Zeikus [181], using mediator-immobilized graphite electrodes. A 1 mm proton-conducting porcelain layer was applied to the inside of the cathode, which was impermeable to the liquid anolyte. This design was found to produce a maximum power density (0.078 mW cm^{-2}) which is similar to that of a more complex two-chamber configuration.

The effect of a proton exchange membrane was later investigated by Liu and Logan [212], who found that removing the PEM (and slightly reducing the Pt loading) increased the power density by 88% when using glucose as a substrate and by 420% when using wastewater. The CE, however, was significantly reduced as a consequence of increased O_2 diffusion to the anode. It is now believed that using an air-breathing cathode without a PEM increases the power output. The removal of the PEM causes a reduction in the internal resistance of the system, although care should be taken with microbial biofilm formation on the cathode [212].

Condensation in an air-breathing cathode leads to a two-phase flow. Cheng et al. [213] found that the addition of hydrophobic layers on the air side of the cathode mitigated flooding of the catalyst layer. At the same time, the CE was increased through a reduction in the rate of O_2 diffusion to the anode. Additional layers of hydrophobic PTFE will continue to increase the CE, though it is not desirable to reduce the O_2 diffusion beyond the limit of the reaction requirements. Cheng et al. [213] found the optimum number of PTFE layers (applied to a carbon cloth) to be four. The power density in this case was increased by more than 40% (0.076 mW cm^{-2}) and the CE increased from ~15% to more than 20% compared to a cathode without PTFE layers.

The classical design of an BFC is based on two chambers containing the anode and cathode, separated by a ion-selective membrane [3]. Such cells can be operated in either batch or continuous mode. For wastewater treatment (MFCs), an up-flow, two-chamber design was developed by He et al. [215], operating in continuous mode. The system exhibited an internal resistance of 84 Ω. A membrane-less version was constructed by Jang et al.

[216], with, however, a considerably higher internal resistance of 3.9 MΩ. Removing the membrane can lead to higher power outputs but the cells must be carefully designed for high reaction selectivity in order to avoid low coulombic efficiencies (due to transport of oxygen to the anode). For scale up and reduced cost, on the other hand, the concept of a membrane-less, single chamber design is highly attractive. Moreover, the use of a ferricyanide solution and aeration in the cathode compartment are not desirable. The cell exhibited a higher power density than an equivalent membrane-containing cell but with a much reduced coulombic efficiency. An alternative arrangement was developed by Rabaey and Verstraete [38], in which a granular graphite matrix anode was housed in a tubular, sealed membrane covered by a woven-graphite cathode (soaked in a ferricyanide solution).

It has recently been suggested that internal resistance due to restricted proton-transport is the dominant limiting factor in most MFC designs [22, 37, 217, 218], though some disagreement exists over the exact source of this resistance. Watanabe [37] reasoned that since proton diffusion is always slower than ET in the external circuit, proton-transport limitations dominate kinetic and reactant-transport limitations. While proton-transport limitations are often disregarded on the basis that MFCs use the same PEM as chemical fuel cells but with current densities a few orders of magnitude lower [22], new evidence suggests that a comparison to PEMFCs is not valid due to differences in the pH and electrolyte composition [22, 219]. In MFCs, there is a much higher concentration of cations (other than protons) that hinder proton diffusion through the membrane. The presence of these cations results in an increased pH in the catholyte and a decreased pH in the anolyte, which affects the solution conductivity and the overall cell performance [220] (restricted proton migration through the membrane decreases the pH in the anode solution, while simultaneously increasing the pH in the cathode solution, where protons are continuously consumed by oxygen reduction). Subsequent studies have suggested that anion exchange and bipolar membranes have better characteristics than cation exchange membranes in terms of pH management and electrical performance [23, 196, 221].

One of the practical difficulties faced in MFC design is the increased internal resistance with scale-up. Increasing the surface area increases the power output only when the system is not limited by a high internal resistance [195]. Several early reports showed

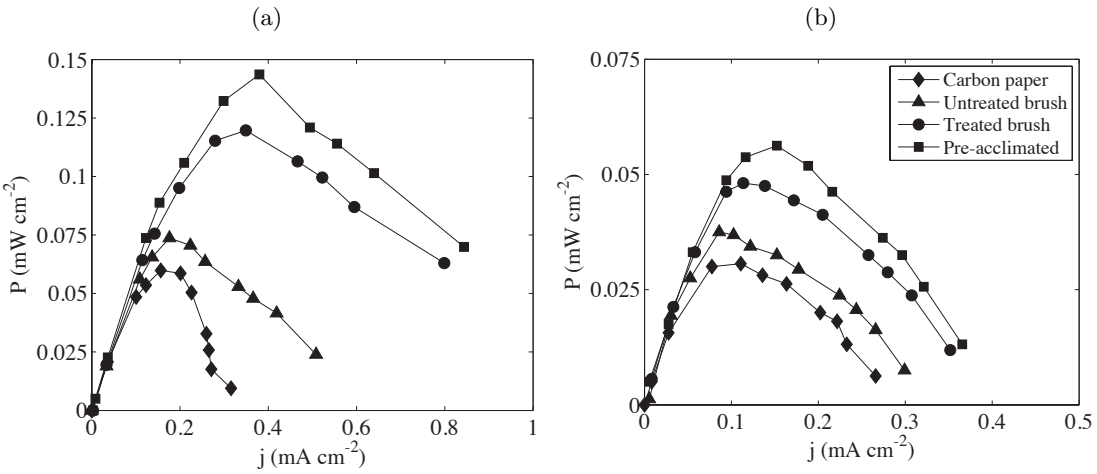

Figure 2.11: Power density curves for bottle-MFCs in (A) 200 mM PBS, and (B) 50 mM PBS. ◆ carbon paper, ▲ untreated brush, ● treated brush, ■ pre-acclimated. Adapted from [195].

that increasing the reactor volume decreases the power density [179, 211], even when the inter-electrode gap is kept constant. In contrast, Liu et al. [193] recently found that a high ratio of electrode area to reactor volume and a simultaneous decrease in the inter-electrode gap when scaling up a reactor from 28 to 520 mL increased the power density.

Logan et al. [195] designed a new graphite brush anode by winding graphite fibers around a central conductive, non-corrosive metal rod. The 2.5 cm diameter ×2.5 cm length anode (specific area 9600 m^{-1}) was used with an air-breathing carbon paper cathode containing 40% CoTMPP catalyst in a cube-design MFC. The design achieved power densities of 0.24 mW cm^{-2} (based on the projected cathode area) and 0.073 mW cm^{-3} (based on the liquid volume) with a maximum CE of 60%. The specific area of the graphite-brush anode is much higher than that of traditional graphite foam or cloth. The internal resistance of the graphite-bush fuel cell (R_{int} = 8 Ω) was lower than the equivalent resistance using a plain carbon paper electrode. Moreover, power production was not affected by biofilm growth. This anode design represents a promising concept that should, in principle, allow efficient scaling of MFCs with a wide scope for optimization (fiber density, length, and winds per unit length) [195]. A second bottle-MFC using a different anode was also constructed. The effects of the different electrode preparation methods and the buffer concentration are shown in Fig. 2.11.

The total power output can be increased and shifted to a higher voltage and current when individual cells are connected in series or in parallel [191]. With a series connection, however, voltage reversal in individual cells may occur, shifting the anode potential to positive values. This phenomenon is encountered when either high currents are drawn from the weaker cell with limited biocatalytic conversion performance, or during sudden changes in fuel demand, as occurs at startup [22, 172, 191]. The increased potential could be accompanied by O_2 evolution in the anode. The problem can be alleviated by avoiding low substrate conditions (*e.g.* batch-fed operation) [68], and by ensuring that all cultures are properly enriched before operating at a high current.

Microbial fuel cells that can harvest electricity from the organic matter in aquatic sediments have been developed by Reimers, Tender and co-workers [222, 223]. These systems, termed Benthic Unattended Generators (BUGs), can be used to power electronic devices in remote locations. The anode is buried in the marine/freshwater sediment and is connected to a cathode that is suspended in the aerobic water. *Desulfuromonas* species are considered to be the predominant species on anodes submerged in marine sediments, while *Geobacter* dominate in freshwater [7]. In a more recent design, the anode is enclosed in a so-called benthic chamber buried in the sediment, which improves mass transport of pore water to the anode by advection, either naturally or through pumping, and leads to significantly higher power densities [224, 225].

Table 2.2: Summary of key microbial fuel cell developments

Anode	**Cathode**	**Electrolytes/membrane**	P_{max} **(mW cm^{-2} or mW cm^{-3})**	V **or** I **at** P_{max}	**OCV (V)**	**Remarks**	**Reference**
Graphite rod (5 mm diam.), graphite granules (1.5-5 mm diam.) inoculated with **aerobic/anaerobic sludge mixture**	Same graphite rod/granules as anode	Anolyte: 0.75-1 gL^{-1} **acetate**. Catholyte: 50 mM **$K_3Fe(CN)_3$**, 100 mM KH_2PO_4 buffer, 1 M NaOH, 7 pH, room temperature. Ultrex membrane.	0.263 mW cm^{-3} (6 parallel cells), 0.308 mW cm^{-3} (series)	0.35 V (parallel), 2.28 V (series)	0.67 (parallel), 4.16 (series)	QE=77.8 % and 12.4 % for parallel and series respectively. Figures based on void volume fraction in cell. Maximum power occurs after 200 days of operation	[191]
C-cloth (7 cm^2) inoculated with **domestic wastewater** (7.3-7.6 pH, 200-300 mgL^{-1} COD)	**Pt**/C-cloth (7 cm^2), with 4 PTFE diffusion layers on air side	Per liter: (5 mg **glucose**, PBS: 0.31 g NH_4Cl,4.97 g $NaH_2PO_4{\cdot}H_2O$, 2.75 g $Na_2HPO_4{\cdot}H_2O$, 0.13 g KCl), and 12.5 mL each of metal and vitamin solution, 30 °C	0.0766 mW cm^{-3}	-	0.3	CE=20-27 %	[213]
Granular graphite inside tube, with previous **MFC effluent as inoculum**	Graphite felt **biocathode** on outside of tube	Electrolytes (per liter): (4.4 g KH_2PO_4, 3.4 g K_2HPO_4, 2 g $NaHCO_3$, 0.5 g NaCl, 0.2 g $MgSO_4{\cdot}7H_2O$, 0.0146 g $CaCl_2$) circulated with 2 gL^{-1} of sodium **acetate** re-added to anodic circuit upon depletion. Ultrex membrane on inner tube surface.	0.083 mW cm^{-3} (batch), 0.065 mW cm^{-3} (continuous)	0.34 V (continuous)	-	CE=20-40 % (batch), 90 % (continuous)	[179]
Carbon cloth (1 cm^2), inoculated with **pre-acclimated mixed culture** from previous MFC	Two air-breathing: **Pt** on carbon cloth (7 cm^2 each) with PTFE layers	200 mM PBS, with 30 mM acetate and per liter: (0.31 g NH_4Cl, 0.13 g KCl, 5.84 g $NaH_2PO_4{\cdot}H_2O$, 15.5 g $Na_2HPO_4{\cdot}7H_2O$. And 12.5 mL of minerals and vitamin) in batch operation mode	0.686 mW cm^{-2} (anode area), 0.098 mW m^{-2} (reactor cross section)	2.62 mA cm^{-2} (anodic)	0.7 - 0.8		[194]
Either: (i) plain porous carbon paper (22.5 cm^2) or (ii) iron oxide coated. Both inoculated with **anaerobic sewage sludge** or (iii) plain carbon paper with anode biofilm from previous MFC applied	**Pt**	Anolyte: 7 pH, buffer (per liter): 0.31 g NH_4Cl, 0.13 g KCl, 2.69 g $NaH_2PO_4{\cdot}H_2O$, 4.33 g Na_2HPO_4 and **acetate**. Stirred. Catholyte: 50 mM PBS, 7 pH, air sparged. Nafion separator. 30 °C.	(i) $0.8{\times}10^{-3}$ mW cm^{-2}, (ii) $3{\times}10^{-3}$ mW cm^{-2}, (iii) $4{\times}10^{-3}$ mW cm^{-2}	(iii) 0.2 V	-	CE= (i) 40 %, (ii) 80 %.	[192]
Carbon cloth (757 cm^2 total surface area), inoculated with **wastewater** in presence of nutrients and acetate	**Pt** on Carbon cloth (161 cm^2 total surface area) with 4 diffusion layers on the side open to air chamber	Nutrient solution with 800 mgL^{-1} **acetate** in batch mode. Membrane-less	0.016 mW m^{-3}, 0.052 mW cm^{-2}	0.18 mA cm^{-2}	-	CE=38-52 %. Power increases to 0.022 mW cm^{-3} (0.069 mW cm^{-2}) with continuous flow mode. Purpose to show higher power output in scaled-up cell when conditions of higher electrode area to reactor volume and shorter inter-electrode distance are satisfied.	[193]
Either: (i) Graphite fiber brush (9600 m^2/m^3 reactor volume), or (ii) same brush electrode (4200 m^2/m^3 reactor volume). Both inoculated using **pre-acclimated bacteria** from previous MFC	Air-breathing, (i) **Cobalt tetramethylphenylporphyric** or (ii) Pt. Both on carbon paper with 4 diffusion layers	Batch fed: 50 mM PBS, and (per liter): 4.09 g Na_2HPO_4, 2.93 g $NaH_2PO_4{\cdot}H_2O$, and 1 g of either (i) **acetate**, 30 °C or (ii) glucose, 23 °C.	(i) 0.24 mW cm^{-2}, 0.073 mW cm^{-3}, (ii) 0.143 mW cm^{-2}, $2.3{\times}10^{-3}$ mW cm^{-3}	(i) 0.82 mA cm^{-2}	(i) 0.57	CE= (i) 40-60 %, (ii)23 %. Power densities normalized by cathode area and liquid volume	[195]

***Geobacter sulfurreducens* PCA**. Carbon cloth (0.806 cm^2)	Air-breathing **Pt** on CF electrode (6.45 cm^2)	10 mM **acetate**, circulated. Nafion separator	0.19 mW cm^{-2}, 0.043 mW cm^{-3}	0.46 mA cm^{-2}		When anode volume chamber volume decreased from 7 mL to 0.336 mL volumetric power density increased to 2.15 kW m^{-3}.	[189]
***Hasenula anomala* (yeast)** adsorbed on either (i) graphite felt, or (ii) Polymer-Pt composite coated graphite	Graphite	Anolyte: PBS with nutrient broth, Catholyte: 0.1 M **ferricyanide**. Nafion separator	(i) 2.34×10^{-3} mW cm^{-3}, (ii) 2.9×10^{-3} mW cm^{-3}	-	-	-	[190]
Pseudomonas aeruginosa on rough graphite plate anodes (30 cm^2)	-	Anolyte: **glucose**, 0.5 $gL^{-1}day^{-1}$. Catholyte: 100 mM PBS, 100 mM potassium **hexacyanoferrate**, aerated at minimum of 6 mgL^{-1}	0.167×10^{-3} mW cm^{-2}	-	-	No mediator addition. Bacterial strain produces pyocyanin mediator that can also be used by other organisms for electron mediation, enhancing the performance of mixed cultures when present.	[183]
Shewanella oneidensis in solution with graphite felt electrode (2 cm^2, 1.2 cm^3 compartment volume)	Graphite felt electrode (2 cm^2, 1.2 cm^3 compartment volume)	Anolyte: (i) Suspended *S. oneidensis* with 10-30 mM sodium **lactate**, optionally with: (ii) saturated oxygen content of influent, (iii) 100 µM AQDS mediator, (iv) both oxygen and mediator. Catholyte: 7.4 PBS, 50 mM **ferricyanide**. Nafion membrane	(i) 0.3 mW cm^{-2}, 0.5 mW cm^{-3} (ii) 0.2 mW cm^{-2}, 0.333 mW cm^{-3} (iii) 0.4 mW cm^{-2}, 0.666 mW cm^{-3}, (iv) 0.27 mW cm^{-2}, 0.45 mW cm^{-3}	(i) 0.6 mA cm^{-2} (ii) 0.4 mA cm^{-2} (iii) 1 mA cm^{-2} (iv) 0.7 mA cm^{-2}	(i)0.75, (ii)0.7, (iii)0.7, (iv)0.8	CE= (ii) 3-5.5 %. SCC= (i) 1mA cm^{-2}, (ii) 0.6mA cm^{-2}, (iii) 1.79mA cm^{-2}, (iv) 1.2 mA cm^{-2}	[188]
Glassy carbon (10 cm^2), **mixed culture** from compost	Suspended *Trametes versicolor* **laccase**	Anolyte: 10 mM of glucose and lactate. Catholyte: 0.1 M **acetate** buffer, 2 mM ABT, 5 pH, air saturated. 100 mM NaCl salt bridge	4.6×10^{-3} mW cm^{-2}	0.5 V	1.1	Low power density due to cell design. Immobilizing laccase in hydrogel in the absence of mediator produces little power. No change in power after 2 days of operation	[197]
Carbon felt, inoculated with **mixed bacterial culture**	**Pt** on carbon cloth (57 cm^2) with 4 PTFE diffusion layer. Open to air chamber	Per liter: (0.1 g KCl, 0.2 g NH_4Cl, 0.6 g NaH_2PO_4) and fed with 20 mL of model **organic waste** containing starch, Bacto peptone and fish extract at 3:1:1 ratio.	0.13 mW cm^{-3} (12 series cells), 0.09 mW cm^{-2}		0.56	CE=28-48 %. Treatment efficiency of 93 % at organic loading rate of 5.8 g L^{-1} per day.	[214]
Graphite fiber brush (2235 cm^2 surface), ***Rhodopseudomonas palustris* DX-1** biofilm	Air-breathing, **Pt** on carbon paper with 4 PTFE diffusion layers	200 mM PBS, 1 gL^{-1} **acetate**, 23 °C	0.272 mW cm^{-2}, 0.087 mW cm^{-3}	0.99 mA cm^{-2}	0.56	Power density based on cross-sectional area of anode. Under dark conditions, power density slightly less (0.272 mW cm^{-2}). Electron transfer was not through self produced mediators, probably by direct communication with electrode. CE=40-60 %	[185]
CF brush, inoculated with **pre-acclimated mixed culture** from MFC	Air-breathing, **Pt** on carbon cloth with 4 PTFE diffusion layers	50 mM PBS with minerals, vitamin and **acetate** (1 g L^{-1}), 23 °C. Anion exchange membrane placed against cathode and supported with a stainless steel mesh.	0.046 mW cm^{-3}	0.34 mA cm^{-2}	0.24†	Anion exchange membrane significantly improves electrical performance by reducing the large pH gradients, and lowering internal resistance. CE lg 90 % for current densities greater than 0.2 mA cm^{-2}. Using two cathode/anion permeable membranes increases power density to 0.098 mW cm^{-3}.	[196]

† Values not explicitly reported, but estimated from graphical results

2.3 Summary and outlook

In the last few years, enzymatic fuel cells have approached power densities of ~1 mW cm^{-2}. For portable electronic applications, high energy density fuels such as ethanol [159] and glycerol [20] show great promise. Developments in the overall system design have also led to more efficient systems. For example, removing the separator membrane without significant loss in power output, and the emergence of single chamber, air-breathing systems using compact MEAs. For many proposed applications, however, further substantial improvements in performance are required (higher power densities and energy efficiencies).

Research targets for microbial fuel cells are generally different from those for enzymatic fuel cells. MFC systems are typically discussed in the context of large-scale applications using wastewater or mixed organic compounds as fuels. Power densities have rapidly increased in the last few years to a few W m^{-2} and over 1 kW m^{-3} (of reactor volume). Most of the systems developed are ≤1 L in volume, though new understanding of the important parameters affecting reactor scale-up has successfully led to larger scale systems with similar performance characteristics. These developments have also been enabled by better insight into the species and processes responsible for electricity generation in biofilms. A direct electrical output with high efficiency, low operating temperatures, and good organic treatment efficiency (with the possibility of operating on low-strength wastewater) make MFCs ideal for waste treatment technologies [37, 38].

For both MFC and EFC, electrode materials need to be more catalytic while maintaining their performance, particularly in the face of problems caused by fouling of the active surfaces and loss of enzyme activity. It is also important to study time-dependent performance over practical periods, particularly with a focus on long-term changes in the enzyme activity.

A greater understanding and characterisation of the reaction environment can be achieved through studies of the reactant and charge distribution, mass transport and mass transfer, as well as the bio-electrochemical reaction kinetics. Carefully validated models can be used

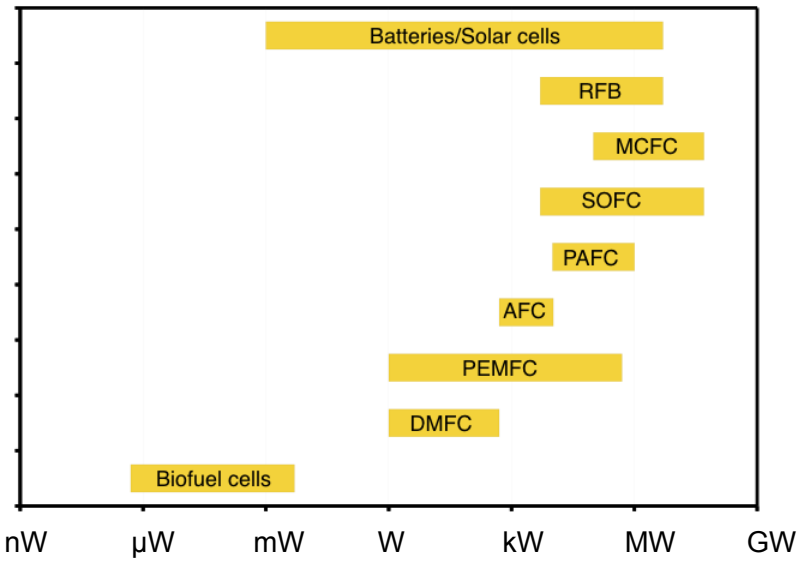

Figure 2.12: Power output of some electrochemical systems. (RFB) redox flow battery, (MC) molten carbonate, (SO) solid oxide, (PA) phosphoric acid, (AFC) alkaline fuel cell, (PEM) polymer electrolyte membrane, (DM) direct methanol. Adapted from [2, 3]

in conjunction with laboratory studies to investigate these processes (particularly *in situ* and to accelerate the development of practical systems.

A vitally important aspect of bio-fuel cell performance and stability is the immobilization of the enzyme/mediator on the electrode. Maintaining a continuous supply of fuel to the active sites and ensuring an efficient electron-transfer process from the enzyme/bacteria to the electrode via the mediator are crucial. While previous research was mainly targeted at developing the enzyme chemistries [3], the past 5 years can be marked by efforts to develop new methods and materials for integrated enzyme electrodes that maximize enzyme loading and move from the classic two-dimensional loading to highly ordered three dimensional structures with improved enzyme stabilization [75]. These use of nanostructures shows great promise, though it should be kept in mind that for application purposes the materials must be safe and cost effective, and the fabrication techniques must be practical.

From an engineering perspective, cells with chemistries that allow single-compartment operation and possess constructional simplicity would be highly advantageous. It is important that low-cost, modular and scalable designs are developed, particularly if they are to form the basis for multi-plate (*e.g.* bipolar) cell stacks. At the present time, there are very few examples of BFC stacks [49, 191]. In this respect, much could be learned from the

rapid progress in PEM fuel cell MEA/stack performance over the past two decades [226]. Cell construction has been improved to optimise the cell voltage through comprehensive modelling/experimental studies of the electrode overpotentials and all cell resistances; there is a vast body of literature on the electrical, thermal, transport and mechanical properties of electrode, plate and membrane materials.

High temperature systems such as MCFC and SOFC have certainly benefited from computer aided design. Fuel cells, including large CHP stations running on reformed fuels, are already making an important contribution towards the environmental and economic concerns of a sustainable energy supply, and there is no doubt that this contribution will continue to increase [1]. For low operating temperatures, PEMFC dominates the market. A large incentive for the research into PEMFCs today is fuelled by the automotive sector. Almost 30% of the worldwide energy demand comes from the transportation (including commercial) sector and the need for both better fuel efficiency and lower emissions is critical. The more promising shift towards sustainability in the transport sector will come from second generation biofuels produced from non-food crops. Algal biofuels from waste treatment plants require neither agricultural land nor freshwater. World biofuel production increased from 10 million tonnes oil equivalent (toe) in 2001 to almost 60 million toe in 2011 [227]. Transport fuel in 2030 will be dominated by oil (87%) and biofuels (7%) [228].

Figure 2.12 shows typical power output ranges of various types of electrochemical power sources. It is clear that biofuel cells are still far from competing with classical fuel cell applications due to their limited power, and differing ranges of application. While a few micro-watts (μW) output or less is sufficient for biosensors, for power generation purposes, biofuel cells need to be improved to cover the range from mW up to a few watts required for portable electronics. Experimental enzymatic cells are currently only a few cm^2 in area with power densities up to ~1 mW cm^{-2}. With proper scaling of some successful designs this gap may be bridged. Mathematical modelling can help construct efficient three-dimensional stacks by designing passive fuel cells and minimizing the volumetric footprint. In addition to providing useful information about the chemical and electrochemical kinetics, the use of numerical simulation can aid in the design of a proper heat

flux within the stack and the bipolar plates separating individual cells.

Despite the rapid progress in bio-fuel cells, cost-effective, modular designs that can be handled safely (and are environmentally friendly) are still some way from being realised. Two promising applications for the near future are (domestic and industrial) wastewater treatment/electricity production [229–231], and providing power to marine instruments, such as a meteorological buoy, using benthic MFCs [232]. Several of the critical challenges to be overcome in the development of MFC technology are listed below.

1. A step-change improvement in performance is required for many applications. This includes much higher power densities and energy efficiencies.

2. Electrode materials need to be more catalytic while maintaining their performance in the face of problems caused by fouling of the active surfaces, loss of enzyme activity, corrosion and other degradation mechanisms.

3. Cell construction needs to be improved to maximize the cell voltage by paying appropriate attention to electrode overpotentials and all cell resistances, including those arising in the positive and negative electrodes, the separator/membrane and the electrolytes.

4. Time dependent performance (and hence energy density) must be studied over practical periods (≤1000 h) due to long-term changes in the enzyme activity, electrode fouling, membrane blockage, the build-up of metabolites and the breakdown of products. Sludge production can block flow paths as well as foul electrodes and membranes.

5. Many investigations have naturally involved small, laboratory scale unit cells. The importance of the reaction environment and of scale-up necessitate studies of (i) the fluid flow and active species transport/mass transfer, (ii) the bio-electrochemical reaction kinetics and (iii) the distributions of the current density, charge and reactant concentrations (including that of dissolved O_2). Fractional conversion in larger, multi-plate (*e.g.* bipolar) cell stacks is also of importance. Cells with chemistries that allow single-compartment operation and possess constructional simplicity would

be highly advantageous.

6. A crucial aspect of bio-fuel cell development is the immobilization of the enzyme/mediator on the electrode. Maintaining a continuous supply of fuel to the active sites and ensuring an efficient electron transfer process from the enzyme/bacteria to the electrode *via* the mediator are crucial. The development of new techniques for immobilization, including on nano-structures substrates, could provide significant improvements in both performance and stability. These techniques must be both practical and cost-effective.

7. It is important that mathematical models are developed to reduce the burden on laboratory-based design, testing and characterization. At the cell level, models must be able to capture the distributions of charge, potentials and concentrations as well as global information such as the cell voltage, as in PEM fuel cell modelling [64, 233, 234]. In many cases, particularly for *in situ* operation, local information can only be gained from detailed and rigorously validated models. Although a small number of models have been developed for specific systems [55, 57, 59, 111, 235–240], with the exception of Picioreanu et al. [55], they are highly simplified and neglect crucial features such as transient performance, spatial non-uniformities, conductive losses, potential profiles, ion migration, fluid flow and a heat balance.

Chapter 3

Numerical model of an all biological enzymatic fuel cell

3.1 Introduction

Biofuel cells operate on the same principles as conventional fuel cells, directly converting chemical energy in a fuel and oxidant into electrical energy. Despite the significantly lower power outputs of biofuel cells compared to conventional cells, they have a number of highly attractive properties: they use renewable bio-catalysts, the can operate under benign pH and temperature conditions, they are able to operate on a much broader range of fuels, tolerating limited impurities in the feedstock [241–243]. Enzymatic fuel cells (EFCs) employ enzymes in isolated and purified forms, which enables the construction of relatively well-defined systems that exhibit a high specificity towards the desired reactions, and avoids the use of dangerous micro-organisms such as *e-coli*.

The concept of biological electron transfer has been applied successfully in biosensors, which are widely available commercially. Much the interest in enzymatic fuel cells (EFCs) has been motivated by *in-vivo* medical applications, which require very low power densities. Recent developments, however, have shown that power densities approaching the mW

cm^{-2} scale are feasible, with multi-stack designs capable of powering small portable electronic devices [50]. These developments, and the increasing sophistication in assembling efficient bioelectrochemical electrodes are the results of both a greater understanding of the controlling factors in biological redox interactions, and improved techniques in physical electrochemistry allowing *in situ* characterization of the electrodes [51].

Modelling and simulation could play vital roles in further understanding and developing biofuel cells [242, 243]. Carefully validated models can be used in conjunction with laboratory studies to investigate the reaction environment, design new electrode architectures and accelerate the development of practical systems. To date, however, only a small number of models have been developed and with a few notable exceptions [54–61] models are highly simplified, neglecting crucial features such as transience, spatial non-uniformities, ion migration, fluid flow and heat transport. In contrast, the modelling and simulation of batteries and conventional fuel cells, such the polymer electrolyte membrane (PEM) fuel cell [64] are mature areas of research.

In this chapter, a multi-dimensional, transient framework for modelling EFCs is developed. The particular cell chosen contains a biological anode and a biological cathode, as well as a multiple enzyme system in the anode. Detailed mass and charge balances are combined with models for the multistep reaction mechanisms in the electrodes. The model results are rigorously fitted to half-cell experimental data and validated against whole cell data, demonstrating excellent agreement. The framework developed is general and can be applied to other EFC systems.

3.2 Enzyme kinetics

For a single-substrate, enzyme catalysed reaction, the simplest and most common model is the Michaelis-Menten kinetics [244, 245]. The mechanism of enzyme action assumed is shown in Eq. (3.1). The substrate, S, binds to the enzyme, E, in a reversible step to produce the enzyme-substrate complex, ES. This complex then breaks down irreversibly

to produce the product, P, and regenerates the enzyme.

$$\mathrm{S} + \mathrm{E} \underset{k_r}{\overset{k_f}{\rightleftharpoons}} \mathrm{ES} \xrightarrow{k_{cat}} \mathrm{E} + \mathrm{P} \tag{3.1}$$

Assuming a steady-state concentration of ES ($\mathrm{d}c_{\mathrm{ES}}/\mathrm{d}t = 0$), the rate of reaction (product formation, ν), is related to the concentration of substrate c_{S} by [246]:

$$\nu = \frac{\nu_{\max}\, c_{\mathrm{S}}}{K + c_{\mathrm{S}}} = \frac{k_{cat}\, c_{\mathrm{E}}^{0}}{1 + \dfrac{K}{c_{\mathrm{S}}}} \tag{3.2}$$

where ν_{max}, the maximum enzymatic rate (assuming saturated substrate conditions), is the product of the constant total enzyme concentration, $c_{\mathrm{E}}^{0} = c_{\mathrm{E}} + c_{\mathrm{ES}}$, and the turnover rate, k_{cat}. This quasi-steady state assumption is the most commonly used to describe the Michaelis-Menten enzyme kinetics. The constant K is then defined as:

$$K = \frac{k_r + k_{cat}}{k_f} \tag{3.3}$$

For oxidoreductase enzyme reactions involving electron transfer, Eq. (3.1) is modified to include the oxidized and reduced states of the enzyme, E_{ox} and E_{red} respectively. Assuming an anodic reaction the substrate oxidation reaction is as follows:

$$\text{Enzyme reduction:} \qquad \mathrm{S} + \mathrm{E}_{ox} \underset{k_{-1}}{\overset{k_1}{\rightleftharpoons}} \mathrm{ES} \xrightarrow{k_2} \mathrm{E}_{red} + \mathrm{P} \tag{3.4}$$

For mediated electron transfer, a similar reaction would occur in the presence of a suitable electron acceptor (oxidized mediator, M_{ox}):

$$\text{Enzyme oxidation:} \qquad \mathrm{M}_{ox} + \mathrm{E}_{red} \underset{k_{-3}}{\overset{k_3}{\rightleftharpoons}} \mathrm{EM} \xrightarrow{k_4} \mathrm{E}_{ox} + \mathrm{M}_{red} \tag{3.5}$$

Equations (3.4) and (3.5) are termed the 'ping-pong' or two-substrate mechanism [53, 236, 247]. EM is the enzyme mediator complex. The reduced mediator M_{red} transfers the

electrons to the electrode by a direct electrochemical reaction (Eq. 3.6). Alternatively, in the case of DET, Eq. (3.4) would be followed by a similar electron transfer from E_{red}, thus regenerating the oxidized enzyme.

$$\mathrm{M}_{red} \overset{k_{anod}}{\rightleftharpoons} \mathrm{M}_{ox} + m\,\mathrm{H}^+ + n\,e^- \tag{3.6}$$

Assuming steady-state on the two enzyme complexes ES and EM (Michaelis-Menten kinetics), the rates of enzyme reduction and oxidation, ν_{red} and ν_{ox} respectively, are given by:

$$\nu_{red} = k_{red}\, c_{\mathrm{S}}\, c_{\mathrm{E}_{ox}} = \frac{k_1\, k_2}{k_{-1} + k_2}\, c_{\mathrm{S}}\, c_{\mathrm{E}_{ox}} \tag{3.7}$$

$$\nu_{ox} = k_{ox}\, c_{\mathrm{M}_{ox}}\, c_{\mathrm{E}_{red}} = \frac{k_3\, k_4}{k_{-3} + k_4}\, c_{\mathrm{M}_{ox}}\, c_{\mathrm{E}_{red}} \tag{3.8}$$

where k_{red} and k_{ox} are the second order rate constants for Eqs. (3.4) and (3.5) respectively.

At steady-state, due to the constant total enzyme concentration, the two enzymatic rates are equal. This overall enzymatic rate for the two substrate case may then be expressed in terms of the total enzyme concentration, c^0_{E}, as [236]:

$$\nu = \frac{k_{cat}\, c^0_{\mathrm{E}}}{1 + \dfrac{K_S}{c_{\mathrm{S}}} + \dfrac{K_M}{c_{\mathrm{M}_{ox}}}} \tag{3.9}$$

where the turn-over rate, k_{cat}, is now defined as [236]:

$$k_{cat} = \frac{k_2\, k_4}{k_2 + k_4} \tag{3.10}$$

and the Michaelis constants for the substrate and mediator, K_S and K_M respectively, are defined as [236]:

$$K_S = \frac{k_{cat}}{k_{red}} = \frac{k_4\,(k_{-1} + k_2)}{k_1\,(k_2 + k_4)} \tag{3.11}$$

$$K_M = \frac{k_{cat}}{k_{ox}} = \frac{k_2\left(k_{-3} + k_4\right)}{k_3\left(k_2 + k_4\right)} \tag{3.12}$$

The simplified extension of the Michaelis-Mentin kinetics to two-substrate enzyme reactions (Eq. (3.9)) appears in different forms in the literature according to a range of additional assumptions [53, 54, 61, 247]. While it is sufficient for steady-state models, in order to properly capture the dynamics of the enzymatic reactions the two reactions should be treated separately and explicitly in terms of E_{red} and E_{ox} (Eqs. (3.7) and (3.8)). This is necessary if competing side reactions are to be included.

3.3 Model development

The model presented here is of a system reported by Sakai et al. [50]. The bioanode was composed of immobilized layers of: a hydrophilic cationic polymer, poly-lysine; two enzymes, glucose dehydrogenase (GDH) and diaphorase (DI); their intermediate cofactor, NADH; an electrode mediator, menadione (vitamin K3); and a hydrophilic anionic polymer, polyacrylic acid sodium salt. Solutions of each component were added in the order mentioned on four stacked carbon fibre sheets (10 mm square, 2.11 mm total thickness), and drying of the anode followed each step.

Similarly, the air-breathing biocathode, made of two similar carbon sheets (0.905 mm thick), employed a ferricyanide mediator ($K_3[Fe(CN)_6]$), poly-lysine as an electrolyte, and bilirubin oxidase (BOD). The hydrophilic polymer poly-lysine coated the carbon fibre and BOD was subsequently immobilized on the poly-lysine. The two electrodes were separated by a permeable cellophane membrane, and titanium meshes were used as current collectors. The anode side of the cell was fed with a solution containing a phosphate buffer (1 M, pH 7) and glucose (0.4 M).

Different configurations were constructed to study the separate half cells. The single unit design studied, along with the reaction mechanism is presented in Figure 3.1. The

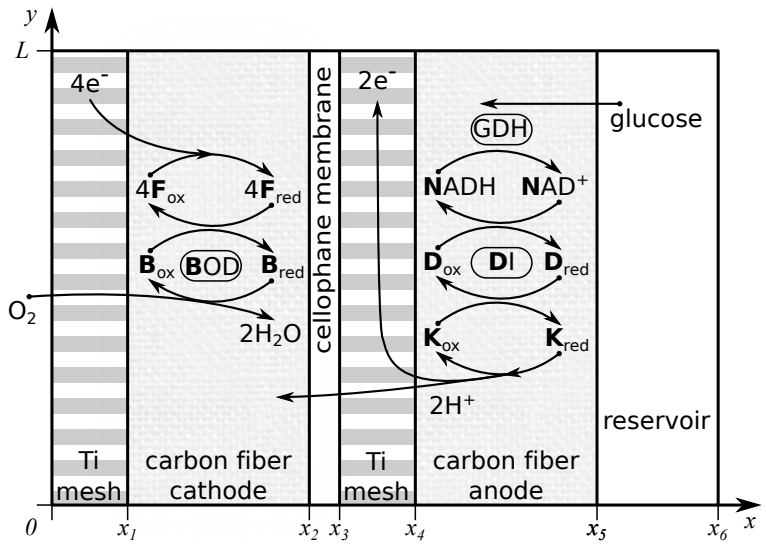

Figure 3.1: Schematic representation of the fuel cell showing the reaction mechanism. Adapted from Sakai et al. [50].

thickness of the Ti meshes and cellophane were assumed to be 1 mm and 60 μm.

The use of multiple enzyme electrodes as a way to increase the overall efficiency in biofuel cells is receiving increasing attention [248]. It has been used to achieve the complete oxidation of fuels such as methanol [249, 250] or glycerol [20] to carbon dioxide. Other systems, such as the diaphorase/NAD^+-dependent dehydrogenases [170, 251–254] are used to complement the individual properties of each enzyme. The optimum pH for GDH is near neutral, while the activity of dissolved glucose oxidase (GOx) in solution is more favourable under slightly acidic conditions [255]. The optimum pH does depend on the chosen mediator and the immobilisation method, as in the case for an anode using GOx wired to a redox polymer which is capable of producing maximum current at a wide range of pH from 6 to 10 [105]. A fuel cell utilising dehydrogenases are incapable of utilizing dioxygen, a natural electron acceptor of glucose oxidase [256]. The dependence on the NAD^+ cofactor makes it necessary to use an intermediate enzyme for NADH oxidation since the direct chemical (*via* a mediator) or electrochemical regeneration of the cofactor proceed at low rates and large overpotentials [252, 257]. The use of diaphorase is an efficient method to accelerate NADH oxidation [252, 258]. With a great variety of NAD^+-dependent dehydrogenases, the system modelled in this chapter can be adapted readily to operate on different types of fuels.

Bilirubin oxidase, a multi-copper enzyme like laccase, can catalyze the four electron reduction of O_2 to water in the presence of a suitable electron donor. This group of enzymes is superior to Pt in cathodes since the electrochemical reduction proceeds at a lower overpotential [109], without formation of hydrogen peroxide. While laccase exhibits very little activity above pH 5, BOD yields a high mediated biocatalytic current at neutral pH [259–264].

It is noted that research and development by Sony has increased the power output by using a lower potential anode mediator that is less reactive with DI [265], by replacing the sodium phosphate with an imidazole buffer [266], and by adding another enzyme to break down the gluconic acid product, alongside other electrode and enzyme modifications.

3.3.1 Reaction kinetics

Glucose dehydrogenase catalyses the oxidation of glucose in the presence of NAD^+ *via* the following reaction [267]:

$$GN: \quad \mathrm{G} + \mathrm{N}_{ox} \longrightarrow \mathrm{N}_{red} + \mathrm{H}^+ + \mathrm{P} \tag{3.13}$$

where N_{ox} and N_{red} represent NAD^+ and NADH respectively. G represents glucose, and P is the product, glucono-lactone. The forward reaction rate can be expressed as follows:

$$R_{GN} = \frac{k_{GDH}}{1 + \mathrm{MM}_G/c_G + \ \mathrm{MM}_N/c_{\mathrm{N}_{ox}}} \tag{3.14}$$

in which MM_G and MM_N are the Michaelis-Menten constants, and c_G and $c_{N_{ox}}$ are the concentrations of glucose and NAD^+, respectively. k_{GDH} is the enzymatic rate, calculated by dividing the experimentally measured enzyme unit, U, by the total anodic volume.

The reactions of diaphorase with the NADH and the mediator K3 follow a 'ping-pong' mechanism involving the oxidized and reduced forms of the diaphorase enzyme (D_{ox} and

D_{red}, respectively), as shown below [253]:

$$ND: \quad D_{ox} + N_{red} + H^+ \rightleftharpoons D_{red} + N_{ox} \tag{3.15}$$

$$DK: \quad D_{red} + K_{ox} \rightleftharpoons D_{ox} + K_{red} \tag{3.16}$$

where K_{ox} and K_{red} are the oxidized and reduced forms of the mediator, K3 (2-methyl-1,4-naphthoquinone).

Following Takagi et al. [252], the reaction kinetics of the diaphorase enzymes with their electron mediators (reactions (3.15) and (3.16)) can be written in a Butler-Volmer form:

$$R_{ND} = k_{DI}\left[c_{D_{ox}} c_{N_{red}} \exp\left(\frac{2\beta_D F(E_D^0 - E_N^0)}{RT}\right) - c_{D_{red}} c_{N_{ox}} \exp\left(\frac{2\alpha_D F(E_D^0 - E_N^0)}{RT}\right)\right] \tag{3.17}$$

$$R_{DK} = k_{DI}\left[c_{D_{red}} c_{K_{ox}} \exp\left(\frac{2\alpha_D F(E_K^0 - E_D^0)}{RT}\right) - c_{D_{ox}} c_{K_{red}} \exp\left(\frac{2\beta_D F(E_K^0 - E_D^0)}{RT}\right)\right] \tag{3.18}$$

in which c_i is the concentration of species i, k_{DI} is the (common) rate constant, α_D and β_D are the oxidation and reduction charge-transfer coefficients, respectively, and E_N^0, E_K^0 and E_D^0 are the equilibrium redox potentials for the NADH, K3 mediator and the diaphorase enzyme, respectively. The latter can be calculated using the Nernst equation (equation (3.29) presented below). The factor of two in the exponential terms represents the number of electrons transferred. The direct electrochemical oxidation of diaphorase, and the mediated electron transfer between NADH and the oxidized K3 are relatively small [258]. They are, therefore, neglected.

The final electrochemical reaction transferring the electrons to the anode is:

$$K: \quad \mathrm{K}_{red} \rightleftharpoons \mathrm{K}_{ox} + 2\mathrm{H}^+ + 2e^- \tag{3.19}$$

The rate of this reaction can be expressed in Butler-Volmer form as follows:

$$R_K = a_a^s \, k_K \, c_{\mathrm{K}_{red}}^{\alpha_K} \, c_{\mathrm{K}_{ox}}^{(1-\alpha_K)} \left[\exp\left(\frac{2(1-\alpha_K) F \eta_a}{RT} \right) - \exp\left(\frac{-2\alpha_K F \eta_a}{RT} \right) \right] \tag{3.20}$$

in which a_a^s is the specific surface area of the anode, k_K is the rate constant, α_K is the charge transfer coefficient, and η_a is the anodic overpotential, defined as:

$$\eta_a = \phi_s - \phi_e - E_K^0 \tag{3.21}$$

In this expression, ϕ_s and ϕ_e are the electronic and ionic potentials, respectively.

At the cathode, the action of BOD can be divided into a two step mechanism of irreversible reactions [259]:

$$OB: \quad \mathrm{O}_2 + 4\mathrm{H}^+ + \mathrm{B}_{red} \longrightarrow \mathrm{B}_{ox} + 2\mathrm{H}_2\mathrm{O} \tag{3.22}$$

$$BF: \quad 4\mathrm{F}_{red} + \mathrm{B}_{ox} \longrightarrow 4\mathrm{F}_{ox} + \mathrm{B}_{red} \tag{3.23}$$

where F_{red} and F_{ox} are the reduced and oxidized forms of the ferro/ferri-cyanide mediator couple ($[\mathrm{Fe(CN)_6}]^{-4}$ and $[\mathrm{Fe(CN)_6}]^{-3}$, respectively), and B_{red} and B_{ox} are the reduced and oxidized forms of the BOD enzyme, respectively. The rates of reactions (3.22) and (3.23) are assumed to take the following forms:

$$R_{OB} = k_{BOD} \, c_{\mathrm{B}_{red}} \left(\frac{c_{\mathrm{H}^+}}{c_{\mathrm{H}^+}^0} \right) \left(\frac{c_{\mathrm{O}_2}}{c_{\mathrm{O}_2}^0} \right) \tag{3.24}$$

$$R_{BF} = k_{BOD}\, c_{\mathrm{B}_{ox}} \left(\frac{c_{\mathrm{F}_{red}}}{c^0_{\mathrm{F}}} \right) \tag{3.25}$$

where c_i is the concentration of species i and c_i^0 is the reference concentration of species i. The mediator is regenerated at the electrode surface by a one electron transfer:

$$F: \quad \mathrm{F}_{ox} + e^- \rightleftharpoons \mathrm{F}_{red} \tag{3.26}$$

The rate of this electrochemical reaction can be expressed in Butler-Volmer form as shown below:

$$R_F = a_c^s\, k_F\, c_{\mathrm{F}_{red}}^{\alpha_K}\, c_{\mathrm{F}_{ox}}^{(1-\alpha_K)} \left[\exp\left(\frac{-\alpha_F F \eta_c}{RT} \right) - \exp\left(\frac{(1-\alpha_F) F \eta_c}{RT} \right) \right] \tag{3.27}$$

in which a_c^s is the cathode specific surface area, k_F is the rate constant, α_F is the transfer coefficient, and η_c is the cathode overpotential, defined as:

$$\eta_c = \phi_s - \phi_e - E_F^0 \tag{3.28}$$

E_F^0 is the equilibrium potential for reaction (3.26).

The equilibrium potentials for the redox reactions, E_i^0 are approximated using the Nernst equation, i.e., in terms of deviations from the standard values, $E_i^{0\prime}$ (referenced to Ag/AgCl electrode at reference pH 7 in Table 3.1):

$$E_i^0 = E_i^{0\prime} - \frac{RT}{n_e F} \log\left(\frac{c_{i_{red}}}{c_{i_{ox}}} \right) - 0.03\, n_{\mathrm{H}} (\mathrm{pH} - 7) \tag{3.29}$$

the number of electrons and protons transferred are denoted by n_e and n_{H}, respectively. For the NADH/NAD$^+$ couple, $n_e = 2$ and $n_{\mathrm{H}} = 1$ (reactions (3.13) and (3.15)). For the

Constant	Description	Value
$E_N^{0\prime}$	Standard equilibrium potential of NADH	-0.54 V [253]
$E_D^{0\prime}$	Standard equilibrium potential of diaphorase	-0.456 V [253]
$E_K^{0\prime}$	Standard equilibrium potential of K3	-0.23 V [253, 268]
$E_F^{0\prime}$	Standard equilibrium potential of ferricyanide	0.29 V [269, 270]
k_{GDH}	Estimated rate constant for GDH	0.8 mol m^{-3} s^{-1}
MM_G	Glucose michaelis-menten constant (GDH)	2 mol m^{-3} [271]
MM_N	NAD^+ michaelis-menten constant (GDH)	2 mol m^{-3}
k_{DI}	Rate constant for diaphorase	15 m^3 mol^{-1} s^{-1} [252]
α_D	Diaphorase oxidation charge-transfer coefficient	0.5 [252]
β_D	Diaphorase reduction charge-transfer coefficient	0.2 [252]
k_{BOD}	Rate constant of BOD reactions	205 s^{-1} [262]
k_F	Exchange rate for ferri/ferro-cyanide (equation 3.27)	5.5×10^{-7} m s^{-1} (fitted)
k_K	Exchange rate for K3 mediator (equation 3.20)	2.9×10^{-8} m s^{-1} [272]
α_F	Transfer coefficient for ferricyanide (equation 3.27)	0.25 [273]
α_K	Transfer coefficient for K3 (equation 3.20)	0.87 (fitted)

Table 3.1: Reaction kinetics parameters

mediator K (reaction (3.19)), $n_e = n_H = 2$. For the diaphorase enzyme (reactions (3.15) and (3.16)), $n_e = n_H = 2$; one free proton and one proton attached to N_{red}. For the mediator F (reaction (3.26)), $n_e = 1$ and $n_H = 0$. The reaction rate constants are listed in Table 3.1.

3.3.2 Reactant mass balances

It is assumed that the carbon fibre anode and the carbon fibre cathode were fully impregnated with the respective ionomer, enzyme(s) and mediator. This amounts to an assumption of uniform (but different) volume fractions of each constituent in the electrode.

The anode electrolyte was composed of glucose and a phosphate buffer (concentration $c_{Bfr} = 1$ M). With a pH ranging from near neutral to slightly basic, the ionic species of the buffer considered here (negative log dissociation constant $pK_a \equiv 7.21$) are the weak acid $H_2PO_4^-$ (denoted 'HA'), the conjugate base HPO_4^{2-} (denoted 'A'), sodium ions (Na^+), and free protons (H^+). Buffer solutions resist changes in pH by maintaining an equilibrium between the weak acid and conjugate base, via the dissociation reaction $HA \rightleftarrows A + H^+$.

Mass balances for glucose, A and HA that take into account transport by diffusion and electro-migration (in the case of the charged species), together with consumption or generation via the reactions, can be written as follows:

$$\epsilon \frac{\partial c_i}{\partial t} + \nabla \cdot \left(-D_i^{\text{eff}} \nabla c_i - \frac{z_i F D_i^{\text{eff}} c_i}{RT} \nabla \phi_e \right) = S_i \tag{3.30}$$

in which c_i, D_i^{eff}, z_i and S_i are the concentration, effective diffusion coefficient, charge and source term for species i. ϵ is the volume fraction occupied by the phase in which the species moves. In the anode, the species moves through the electrolyte solution, so that the porosity $\epsilon = \epsilon_{CF}$ in the carbon felt. Similarly, $\epsilon = \epsilon_{Ti}$ in the anode Ti mesh, in which the source terms are zero. In the cathode $\epsilon = \epsilon_{EL}$, the volume fraction of poly-lysine electrolyte. Finally, in the membrane $\epsilon = 1$. In each of the regions, the effective diffusion coefficient for each species is approximated using a Bruggeman correction [274]:

$$D_i^{\text{eff}} = \epsilon^{3/2} D_i \tag{3.31}$$

where D_i is the corresponding free-space value.

Using equation (3.30) to solve for HA and A, the pH and the concentration of protons are determined by:

$$-\log_{10}\left(c_{\text{H}^+}\right) \equiv \text{pH} = \text{pK}_a + \log_{10}\left(\frac{c_A}{c_{HA}}\right) \tag{3.32}$$

The sodium concentration is then found from the electro-neutrality condition in the electrolyte:

$$\sum_i z_i c_i = 0 \tag{3.33}$$

A mass balance for oxygen (in gaseous phase) in the cathode carbon fibre and the Ti mesh can be written as follows:

Source term	Cathode	Anode
S_G	-	-R_{GN}
$S_{N_{red}}$	-	R_{GN}-R_{ND}
$S_{D_{red}}$	-	R_{ND}-R_{DK}
$S_{K_{red}}$	-	R_{DK}-R_K
S_{O_2}	-R_{OB}	-
$S_{B_{ox}}$	R_{OB}-R_{BF}	-
$S_{F_{ox}}$	4R_{BF}-R_F	-
S_{HA}	-4R_{OB}	R_{GN}-R_{ND}+2R_K
S_ϕ	-F R_F	2F R_K

Table 3.2: Source terms in mass and charge balances

$$\epsilon \frac{\partial c_{O_2}}{\partial t} - \epsilon^{3/2} D_{O_2} \nabla^2 c_{O_2} = S_{O_2} \tag{3.34}$$

in which c_{O_2}, D_{O_2} and S_{O_2} are the concentration, free-space diffusion coefficient, charge and source term for O_2, respectively, and ϵ is the porosity of the relevant region. In the carbon fibre cathode, $\epsilon = \epsilon_{CF} - \epsilon_{EL}$, and in the Ti mesh, $\epsilon = \epsilon_{Ti}$. Note that a Bruggeman correction is again used.

For the immobilized enzymes and mediators in both carbon electrodes, the molar flux is equal to zero, and equation (3.30) simplifies to:

$$\frac{\partial c_i}{\partial t} = S_i \tag{3.35}$$

where c_i is the concentration of N_{red}, D_{red}, K_{red}, B_{ox}, or F_{ox}. The concentrations of the opposite states are found from the fixed total concentration each species i, c_i^0:

$$c_{i_{red}} + c_{i_{ox}} = c_i^0 \tag{3.36}$$

The source terms appearing in equation (3.30), (3.34) and (3.35) can be found in Table 3.2. The parameters appearing in these mass balances can be found in Table 3.3.

3.3.3 Charge balance

The flow of a charged species i in the electrolyte gives rise to a current density $\vec{j}_i = z_i F \vec{N}_i$, where z_i is the charge and $\vec{N}_i$ is the molar flux (driven by diffusion and electro-migration in the present case). Therefore, the total current density in the electrolyte, $\vec{j}_e$ satisfies:

$$\vec{j}_e = \sum_i \vec{j}_i = -\kappa_e \nabla \phi_e - F \sum z_i D_i^{\text{eff}} \nabla c_i \tag{3.37}$$

where the effective conductivity κ_e is given by:

$$\kappa_e = \epsilon^{3/2} \frac{F^2}{RT} \sum z_i^2 D_i^{\text{eff}} c_i \tag{3.38}$$

in which $\epsilon = \epsilon_{CF}$ (the free space) in the anode carbon fibre electrode, $\epsilon = \epsilon_{EL}$ in the cathode carbon fibre electrode, $\epsilon = \epsilon_{Ti}$ in the anode titanium mesh, and $\epsilon = 1$ in the cellophane membrane. The charge balances in these ion-conducting regions are now given by:

$$-\nabla \cdot \vec{j}_e = -S_\phi \tag{3.39}$$

where the charge source terms S_ϕ are defined in Table 3.2. This source term represents the volumetric transfer current density and is, therefore, equal to zero in regions where electrochemical reactions do not occur.

The electronic current, $\vec{j}_s$ is governed by Ohm's law. Conservation of charge within the porous regions ($\nabla \cdot \vec{j}_s + \nabla \cdot \vec{j}_e = 0$) leads to:

$$-\nabla \cdot \vec{j}_s = -\nabla \cdot \left(\epsilon^{3/2} \kappa_s \nabla \phi_s \right) = S_\phi \tag{3.40}$$

where κ_s is the conductivity of the electron conducting phase of volume fraction ϵ: $\epsilon = 1 - \epsilon_{CF}$ in the CF electrodes and $\epsilon = 1 - \epsilon_{Ti}$ in the titanium mesh.

Constant	Description	Value
c_{G}^0	Initial glucose concentration	400 mol m^{-3} [50]
c_{HA}^0	Initial weak acid concentration	618 mol m^{-3}
c_{A}^0	Initial weak acid concentration	382 mol m^{-3}
c_{N}^0	Total (NADH + NAD$^+$) concentration	119 mol m^{-3} [50]
c_{K}^0	Total K3 concentration	77 mol m^{-3} [50]
c_{D}^0	Total diaphorase concentration	3.16×10^{-5} mol m^{-3} (fitted)
c_{B}^0	Total BOD concentration	6.26×10^{-3} mol m^{-3} (fitted)
c_{F}^0	Total ferricyanide concentration	88.4 mol m^{-3} [50]
$D_{\mathrm{O_2}}$	Oxygen gas diffusion coefficient	2×10^{-5} m^2 s^{-1} [275]
D_i	Diffusion coefficient of electrolyte ions	2×10^{-9} m^2 s^{-1}
D_{G}	Glucose diffusion coefficient	2×10^{-9} m^2 s^{-1}
ϵ_{Ti}	Porosity of titanium mesh	0.9
ϵ_{CF}	Porosity of carbon felt	0.7
ϵ_{EL}	Electrolyte volume fraction in cathode	0.5
κ_{Ti}	Conductivity of titanium	2×10^6 S m^{-1}
κ_{CF}	Conductivity of carbon fiber sheet	1250 S m^{-1}
a_a^s	Anode specific surface area	9600 m^{-1} [50]
a_c^s	Cathode specific surface area	11000 m^{-1} [50]

Table 3.3: Mass and charge balance parameters

The dynamic model developed above is transformed into a steady-state model by neglecting the time derivative and the initial conditions presented below.

3.3.4 Initial and boundary conditions

The cell is considered to be operated in potentiostatic mode, i.e., a cell voltage, V_{cell} was imposed (applied through equipotential surfaces at the top boundaries of the two Ti mesh current collectors shown in Figure 3.1):

$$\phi_s = \begin{cases} V_{cell} & (0 \le x \le x_1;\, y = L) \\ 0 & (x_3 \le x \le x_4;\, y = L) \end{cases} \tag{3.41}$$

The output current density relative to the electrode area, j_{cell}, is measured along the top surface of the Ti mesh current collector in the cathode (see Figure 3.1), where the current is purely electronic:

$$j_{cell} = \left(\frac{1}{L}\right)\int_0^{x_1}\left(-\kappa_s\frac{\partial\phi_s}{\partial y}\right)dx \tag{3.42}$$

The electronic current is carried in the Ti meshes and carbon fibre electrodes. With the exception of the two equipotential surfaces specified above, all exterior boundaries are electrically insulating:

$$-\vec{n}\cdot\left(-\kappa_s\nabla\phi_s\right) = 0 \tag{3.43}$$

where $\vec{n}$ is the normal unit vector pointing outwards. Similarly, insulation conditions also apply for the exterior boundaries of the ionic current ($x = x_1, x_6$; $y = 0, L$)

The (homogeneous) initial conditions for the immobilized species in the electrodes are assumed to correspond to equilibrium conditions:

$$c_{i_{red}} = c_{i_{ox}} = c_i^0 \tag{3.44}$$

The concentration of oxygen at the air inlet, $x = 0$, and the concentrations of the soluble anolyte species (glucose, acid, base) at the inlet to the anode electrode, $x = x_6$ (0.5 mm from the anode edge, x_5), are given by (consistent with the initial concentrations):

$$c_i = c_i^0 \quad (x = 0, x_6) \tag{3.45}$$

For the soluble anolyte species, insulation conditions (no mass flux) are imposed at all other exterior boundaries (x_1, $y = 0, L$):

$$-\vec{n}\cdot\left(-D_i^{\text{eff}}\nabla c_i - \frac{z_i F D_i^{\text{eff}} c_i}{RT}\nabla\phi_e\right) = 0 \tag{3.46}$$

Similarly, insulation conditions are imposed at the exterior boundaries of gaseous oxygen

$(x_2,\ y = 0, L)$.

Continuity of mass and charge flux is applied at all interior boundaries.

3.3.5 Half-cell models

In addition to the whole cell model described above, separate half-cell models were setup similar to the experimental half-cell by separating the cathode ($0 \le x \le x_3$) and the anode ($x_2 \le x \le x_5$) and simulating a reference/counter electrode for each half-cell placed 1 mm away from x_3 for the cathode and x_5 for the anode. The potential at the reference electrodes was fixed to zero ($\phi_s = E^0_{\mathrm{Ag/AgCl}} = 0$), and the electrode potential was imposed (applied through equipotential surfaces at the top boundaries of the Ti mesh current collectors for the cathode ($0 \le x \le x_1;\ y = L$) and anode ($x_3 \le x \le x_4;\ y = L$).

The half-cell current for the cathode was calculated using equation (4.37) and a similar equation was used for the half-anode current:

$$j_{cell} = \left(\frac{1}{L}\right) \int_{x_3}^{x_4} \left(\kappa_s \frac{\partial \phi_s}{\partial y}\right) dx \tag{3.47}$$

In order to conserve charge, a surface source term for the ionic charge is applied at each counter electrode:

$$-\vec{n} \cdot \left(-\kappa_e \nabla \phi_e\right) = \begin{cases} -j_{cell} & (x = x_5) \\ j_{cell} & (x = x_3) \end{cases} \tag{3.48}$$

The concentrations of the soluble species (acid, base, and glucose in the case of the anode) were fixed at the reference electrode:

$$c_i = c_i^0 \quad (x = x_3, x_5) \tag{3.49}$$

3.4 Results and discussion

The system of equations described above was solved using COMSOL Multiphysics. In order to match the simulation results to the experimental data of Sakai et al. [50] the following parameters were estimated using a rigorous nonlinear least-squares analysis implemented by applying the MATLAB function `lsqcurvefit` and using the default settings:

1. In the anode: the DI concentration, c_{D}^0, and the K3 transfer coefficient, α_K.

2. In the cathode: the concentration, c_{B}^0, the mediator exchange rate, k_F.

These constants were estimated by comparing separate half-cell models (described above) simulations to half-cell experimental data contained in the Supplementary Data of Sakai et al. [50] (shown in Figure 3.2(a)). The parameter estimation (implemented in Matlab) was performed through a nonlinear least-squares fit of the simulation results to the half-cell polarization data (minimization of the least-square error) and the quality of the eventual fit is depicted in Figure 3.2. The estimated parameter values are given in Tables 3.1 and 3.3. The glucose dehydrogenase rate constant, k_{GDH}, was estimated to be 10% of the experimentally reported GDH activity in solution, and the fitted total BOD concentration, c_{B}^0, was approximately 1% of the reported amount of immobilized enzyme [50]. When approximating the total amount of enzyme in the ping-pong mechanism, values were found to be lower than the experimental values due to both a lower activity of the immobilized enzyme, and the definition of the total enzyme, which excludes the enzyme-substrate complexes (equation (3.36)). In both cases, these values are in agreement with the reduction of immobilized enzymatic activity reported in the literature. The cathodic transfer coefficients, α_K and α_F in equations (3.20) and (3.27) represent the portion of the overpotential or energy that goes towards driving the cathodic reaction. These values are usually close to 0.5 but can range between 0 and 1. When the cathodic transfer coefficient is equal to zero the electrochemical reaction occurs almost purely in the anodic direction, and the rate of the cathodic reaction is negligible for any value of overpotential.

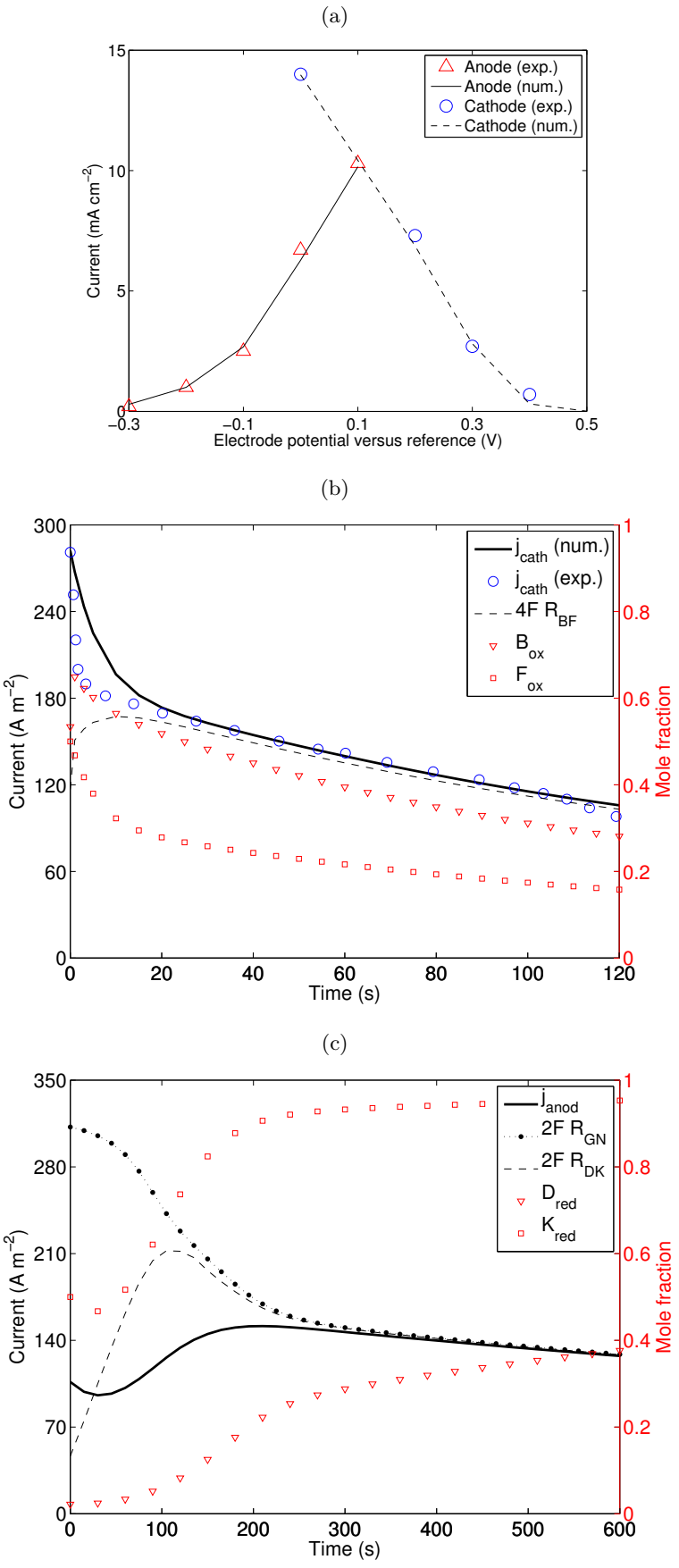

Figure 3.2: (a) Fitted half-cell simulations with experimental results. And transient half-cell response of (b) the cathode at 0 V and (c) the anode at 0.1 V.

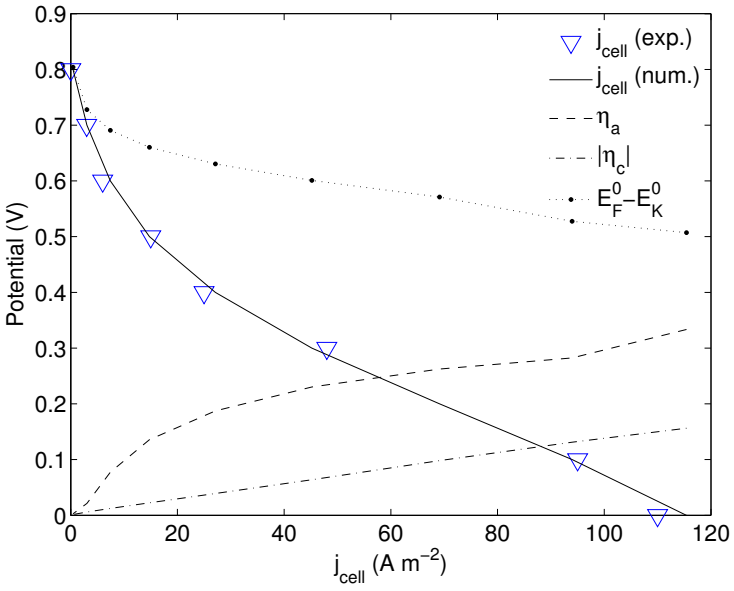

Figure 3.3: Numerical simulations and experimental polarization curve.

To understand the limitations and transient behaviour of the full cell, it is useful to first investigate the performance of each half cell. Figure 3.2(b) compares the numerically simulated cathodic half-cell current density j_{cath} (at 0 V *v.s* reference electrode) for the first two minutes to the reported experimental half cell data. The simulated initial cathodic current density is approximately 28 mA cm^{-2} and drops rapidly to around 18 mA cm^{-2}. This indicates a relatively faster electrochemical rate compared to the enzymatic regeneration of the oxidized mediator, F_{ox}. The difference between the simulated and experimental curves (a more rapid drop in the current density in the latter case) is probably due to the fact that the BOD enzyme and the active carbon-fibre surface area are separated by a poly-L-lysine layer (not included in the model), and in reality the mediator at the carbon fibre side is rapidly depleted. After the initial drop, the current continues to steadily decrease from 18 to 10 mA cm^{-2} after 2 minutes of potentiostatic operation. This slower decrease is due to proton depletion in the cathode, leading to a reduction in the concentration of oxidized enzyme and consequently a drop in the oxidized mediator concentration, accompanied by a significant drop in the current density. After 10 minutes of operation, the cathodic current approaches the steady-state value of 3 mA cm^{-2}, which represents the proton mass transport limit in the cathode.

Numerical simulations of the anodic half-cell current density at 0.1 V potentiostatic operation are depicted in Figure 3.2(c). Corresponding experimental results were not available

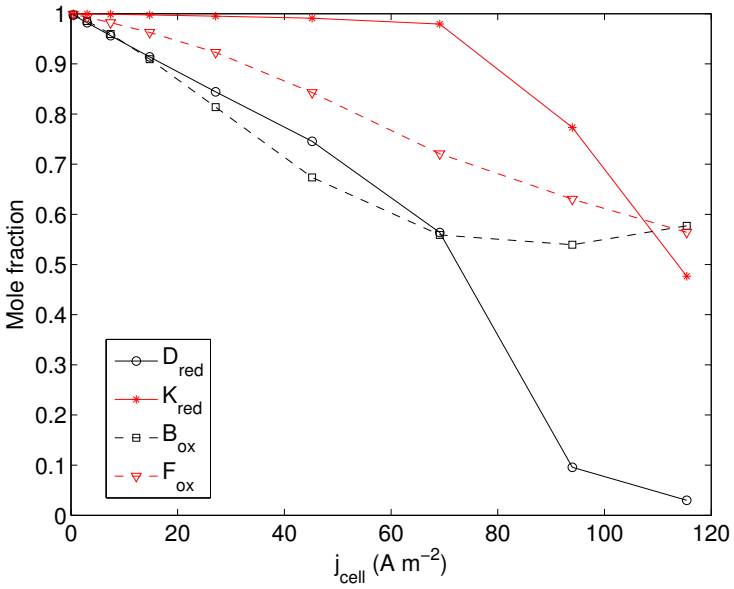

Figure 3.4: Normalized concentrations vs. j_{cell}.

for comparison. The initial anodic current density remains at around 10 mA cm^{-2} during the first minute, and is limited by both a relatively slower electrochemical rate of the K3 mediator and an initially low diaphorase reaction rate. The equilibrium potential difference between DI and K3 is a factor of 2.7 greater than that between DI and NAD$^+$, leading to a higher rate of reaction DK than that of ND ((3.17) and (3.18)). Hence, the diaphorase species is in an almost completely oxidized state in the initial stages (as indicated by the low value of D_{red}). As the initially high GDH rate (see reaction (3.13)) increases the concentration of N_{red}, the diaphorase rates also increase and the anodic current reaches almost 15 mA cm^{-2} after 3 minutes of operation at 0.1 V. The steady drop in current that follows is due to a pH decrease in the anode.

The results discussed below pertain to the full-cell model. The default model parameters used in the simulations are given in Tables 3.1 and 3.3.

A potential sweep was simulated by increasing V_{cell} in steps of 0.1 V from 0 to 0.8 V. The cell voltage was held constant at each potential for 60 s, and the current density and other quantities were estimated at the end of each 60 s constant-voltage period, as in the equivalent laboratory experiments [50]. The numerical simulations and the experimental data are plotted in Figure 3.3, which shows that the model captures the experimental data extremely well (using the parameters obtained from the least-squares fitting described

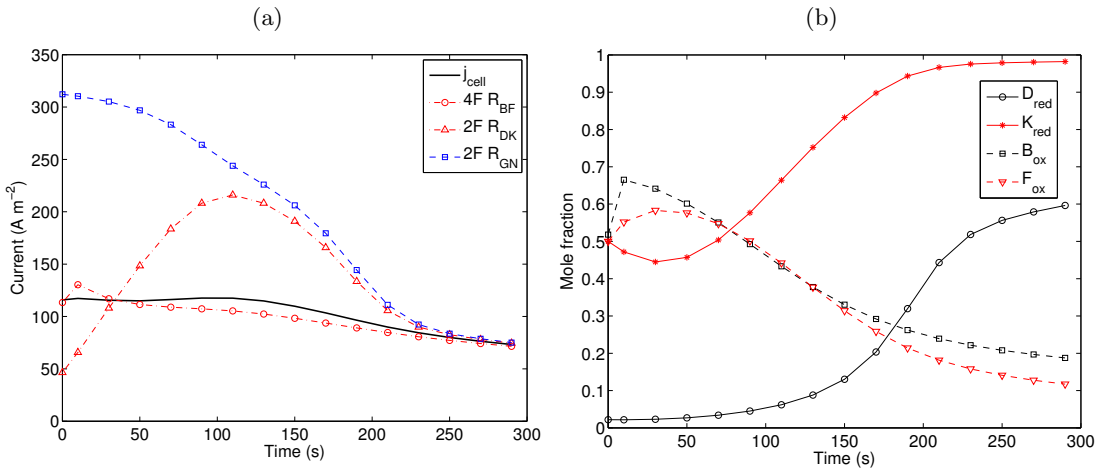

Figure 3.5: Time evolution at short-circuit (V_{cell} = 0 V) of (a) j_{cell} and enzymatic rates and (b) averaged mole fractions.

above). The experimental error in the maximum power density of 1.45 mW cm^{-2} at 0.3 V was reported to be ± 0.24 mW cm^{-2} (± 0.8 mA cm^{-2}). Both the experimental and simulated polarization curves suggest a short-circuit current density of around 11 mA cm^{-2} (after 60 s at V_{cell} = 0 V). The simulated anode and cathode overpotentials are also displayed in Figure 3.3. These plots show that the transient cell performance is influenced more by the anode than the cathode. The limiting anode process is discussed in detail below. The steady-state current is limited by proton mass transport to 3 mA cm^{-2} at cell voltages lower than 0.4 V.

Since the mediators and enzymes are immobilized, their concentrations are determined solely by the relevant reaction rates (Table 3.2). The electrode averaged mole fractions of the reactants ($c_{i_{ox}}/c_i^0$ or $c_{i_{red}}/c_i^0$) as functions of the current density during the potential sweep are shown in Figure 3.4. Deviations from the equilibrium value (0.5) of the mole fraction of a reduced or oxidized species is an indicator of its net rate of production/consumption. The mole fraction of N_{red} is greater than 0.8 at all current densities. From the relative concentrations in Figure 3.4 (and from the reaction rate calculations directly), it is possible to distinguish two regions of anodic performance.

1. For current densities below 7 mA cm^{-2}, the rates of the reactions can be ordered as follows: $R_{ND} > R_{DK} > R_K$ (see reactions (3.15), (3.16) and (3.19)). In this region, K_{red} is in excess.

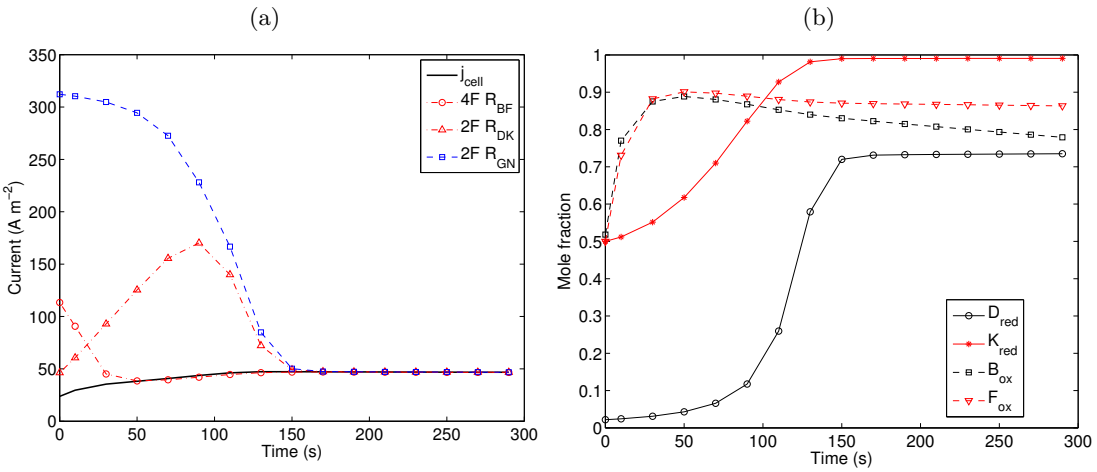

Figure 3.6: Time evolution at V_{cell} = 0.3 V of (a) j_{cell} and enzymatic rates and (b) averaged mole fractions.

2. For current densities in the range 7–11.5 mA cm^{-2}, the rates of the reactions can be ordered as follows: $R_{ND} < R_{DK}$ and $R_{DK} > R_K$. This leads to a decrease in the mole fraction of D_{red} below 0.5, while the mole fraction of K_{red} remains above the equilibrium value of 0.5.

If higher short-circuit current densities could be achieved by the mediator reaction (3.19), with rate R_K, a third region would exist where the rates of the reactions can be ordered as follows: $R_{ND} < R_{DK} < R_K$. In this range, only N_{red} remains in excess, while the mole fraction of K_{red} drops below 0.5 and the reduced diaphorase fraction approaches zero.

While the potential sweep results with 1 minute intervals show that the short-circuit current is limited to the maximum anodic current, longer operating times indicate that the the BOD reactions (3.22) and (3.23) are also limiting. Figure 3.5(a) shows the evolution of the cell current density and of the current densities associated with reactions (3.13), (3.16) and (3.23) for V_{cell} = 0 V. After 2 minutes of operation, j_{cell} begins to decrease due to a relatively low value of R_{BF}. This can also be seen from the decrease in the oxidized mole fractions ($c_{i_{ox}}/c_i^0$) of the enzyme and mediator in the cathode, as shown in Figure 3.5(b). As the rate of reaction (3.23) continues to fall, the mediator F_{ox} is increasingly depleted, which lowers the rate of electron transfer step (3.26). At this cell voltage, the cathodic pH rapidly increases to a value in excess of 8 after 5 minutes of operation.

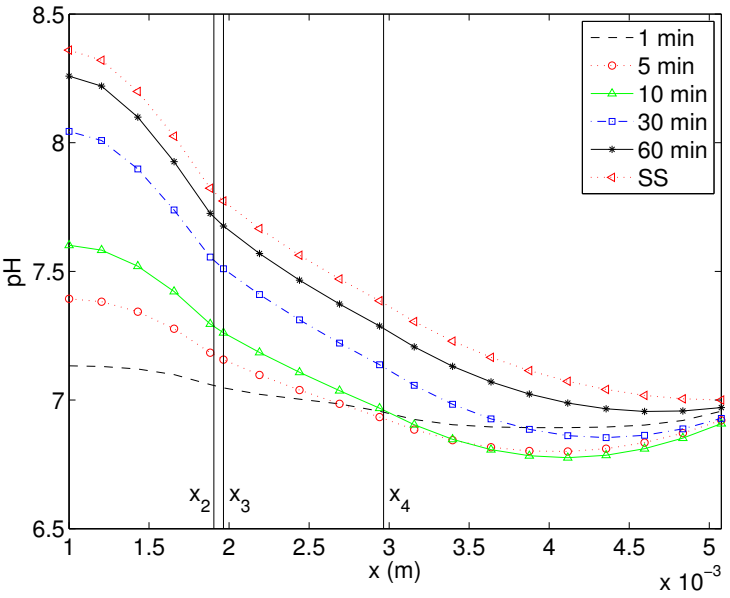

Figure 3.7: pH variation across the cell (V_{cell}=0.3 V) compared to steady-state.

When calculating the oxidized and reduced enzyme concentrations using the ping-pong mechanism, the low enzyme concentrations, compared to those of the mediators and co-factors, limit the deviation from equilibrium of the two enzyme reactions. $S_{\mathrm{D}_{red}}$, and $S_{\mathrm{B}_{ox}}$ remain very close to zero, or undergo a rapid and short-lived change that rapidly alters the distribution in the enzyme state. For this reason, separate rates for reactions (3.15)/(3.16) and (3.22)/(3.23), i.e., R_{ND}/R_{DK} and R_{OB}/R_{BF}, are not shown (they are approximately equal except for short durations), and the enzyme state is interpreted from the enzyme mole fractions.

When the cell is operated at 0.3 V, j_{cell} is limited by the rate of the electron transfer step (3.19) involving the K3 mediator in the anode (Figure 3.6), as discussed above in relation to the half cell results; Figure 3.6(a) clearly demonstrates that the enzymatic reaction rates are not limiting. As shown in Figure 3.6(b), after 3 minutes of operation the mole fractions of reduced diaphorase and K3 mediator in the anode and the mole fractions of oxidized BOD and mediator in the cathode exceed values of 0.7, indicating that the electron transfer steps (3.19) and (3.26) are slow.

The cell performance for longer operating times is still limited by the pH increase in the cathode (as found in the half-cells results), though the rise in pH at low current densities is slower. Figure 3.7 shows the pH variation across the cell ($x_1 \leq x \leq x_5$ as defined in Figure

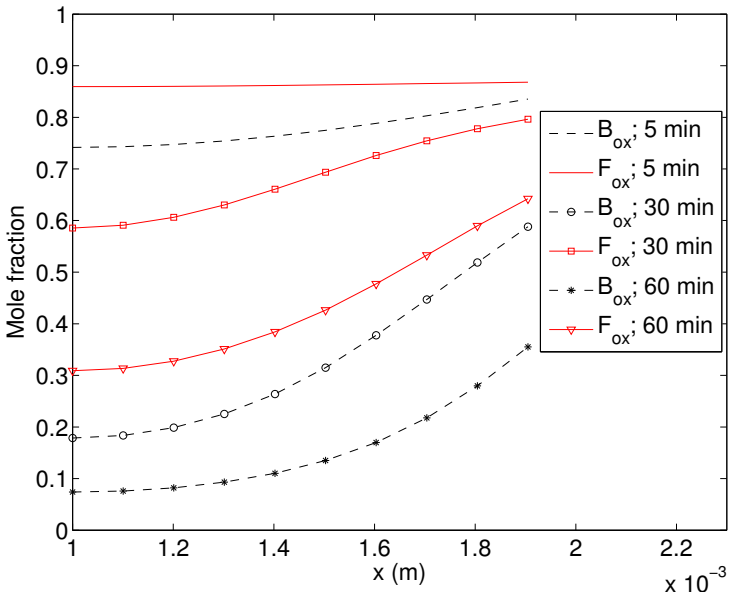

Figure 3.8: Oxidized mole fraction of BOD and mediator, F, in the cathode at V_{cell}=0.3 V.

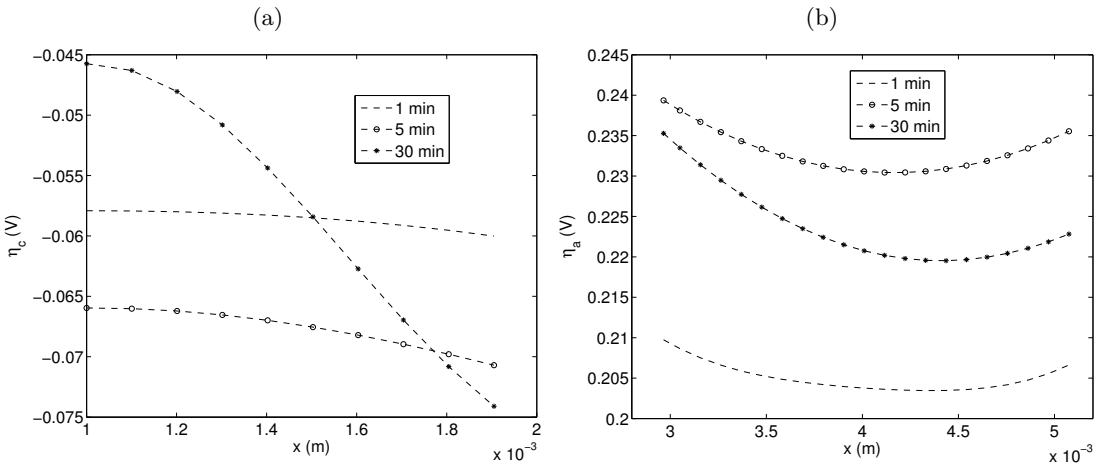

Figure 3.9: Overpotentials in (a) the cathode and (b) the anode at V_{cell}=0 V.

3.1) at V_{cell} = 0.3 V. Steady-state and transient simulations longer than 1 hour show that the limiting current is around 3 mA cm^{-2} for all cell voltages below 0.4. The pH rise in the cathode reduces the oxidized fractions of BOD and cathode mediator, as seen in Figure 3.8, which shows the values across the cathode ($x_1 \leq x \leq x_2$ in Figure 3.1). The drop in the F_{ox} concentration, particularly close to the Ti mesh/carbon fibre interface ($x = x_1$), leads to a large increase in the cathodic overpotential. The limiting current does not change considerably if the anode reservoir boundary conditions are changed to accommodate a time-varying, acidic buffer in a 3 mL reservoir.

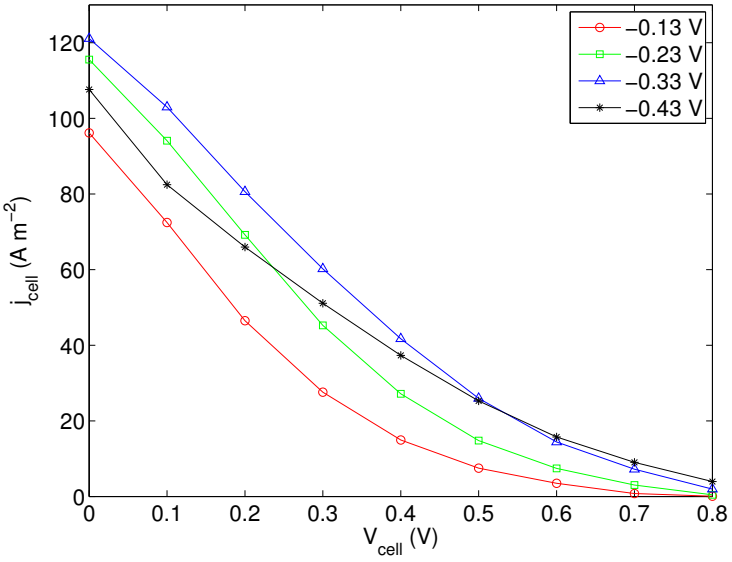

Figure 3.10: Current curves for different mediator potentials ($E_K^{0\prime}$).

Figure 3.9 shows the variation in the cathodic and anodic overpotentials at different times in the respective electrodes ($x_1 \leq x \leq x_2$ and $x_4 \leq x \leq x_5$ in Figure 3.1). In these simulations the cell is operated at short-circuit (0 V). Similar to the previous results pertaining to V_{cell} = 0.3 V, after 30 mins of operation the depletion of oxidized species in the cathode is greater at the air side ($x = x_1$). The electrochemical reaction is then concentrated at the membrane side of the cathode where the proton and F_{ox} concentrations are relatively high. After 30 mins of operation, the overpotential at x_2 is almost 30 mV more negative than the value at x_1. The variation in the overpotential across the anode is less pronounced, although the electrochemical reaction is slightly more active on the current-collector side of the anode, which is favourable for proton generation and migration to the cathode. Variations in the species concentrations and potentials across the y-dimension are negligible.

The choice of K3 as a mediator for DI is based on its high reactivity, which is partly due to its equilibrium potential, around 0.22 V higher than DI. A mediator with a lower potential will be less reactive with DI (lower R_{DK}) but, on the other hand, would increase the reversible open-circuit cell voltage. Figure 3.10 shows the potential sweep curves (V_{cell} = $0, 0.1, 0.2, \cdots, 0.8$ V, with hold for 60 s at each potential difference) for four cells with different hypothetical $E_K^{0\prime}$ = −0.13, −0.23 (default value), −0.33 and −0.43 V; the last potential is only 26 mV more positive than that of diaphorase. With the exception of this

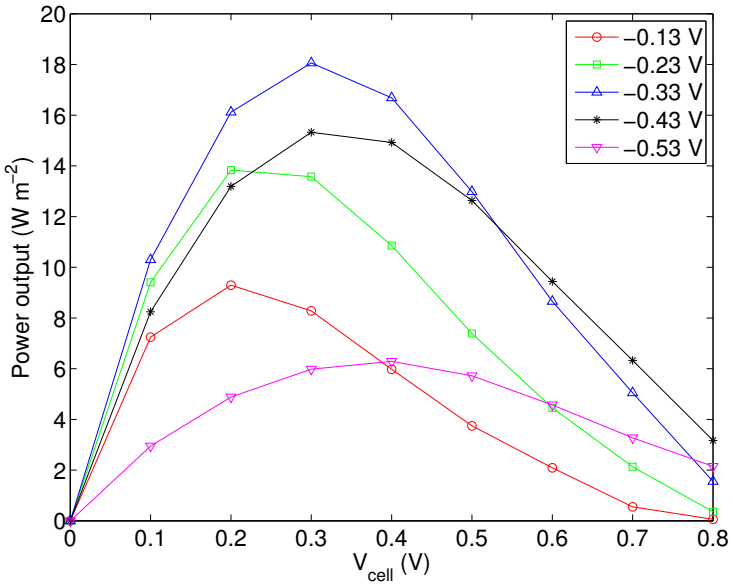

Figure 3.11: Power curves for different mediator potentials ($E_K^{0\prime}$).

last case, the cell current density is higher at all voltages as $E_K^{0\prime}$ is made more negative. When the standard equilibrium potentials of DI and K3 are almost equal ($E_K^{0\prime}$ = −0.43 V), however, j_{cell} is lower in almost the entire range of cell voltages compared to $E_K^{0\prime}$ = −0.33 V. The net effect on the output power density curves is shown in Figure 3.11. Clearly, the optimum peak power is achieved when $E_K^{0\prime} \approx -0.33$ V, rather than the default value of −0.23 V.

Figure 3.12 shows the mole fractions of the oxidized DI and reduced K3 at three mediator equilibrium potentials. For increasingly negative values of $E_K^{0\prime}$, K_{red} is lower for any given current density. At values of $E_K^{0\prime}$ more positive than −0.23 V, the rate R_{DK} of reaction (3.16) increases and the fraction of reduced K3 mediator remains high at all current densities. The point of cross-over (0.5 mole fraction) in the state of the K3 mediator changes from 11.5 to 1 mA cm^{-2} as $E_K^{0\prime}$ is lowered from −0.23 V to−0.43 V. The oxidized DI enzyme fraction at short-circuit is also lowered as the mediator equilibrium potential is reduced. When $E_K^{0\prime}$ = −0.43 V, the rate R_{DK} decreases significantly compared to R_{ND}, and the fraction of oxidized DI enzyme remains below its equilibrium value (0.5) at all current densities.

In a bioanode, the oxidized electrode mediator is continually consumed by the enzyme. At low electrical currents this results in a near-zero oxidized fraction, effectively reducing the

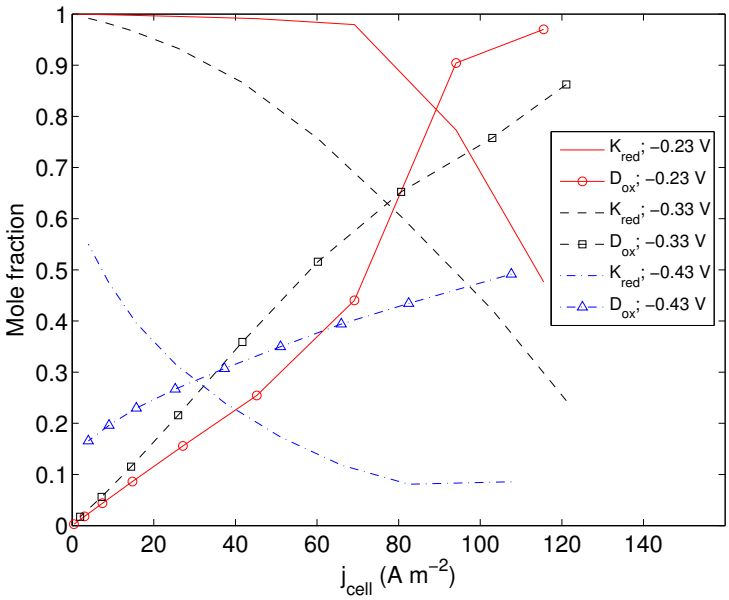

Figure 3.12: Concentrations of K_{red}, D_{ox} versus current for different mediator potentials ($E_K^{0\prime}$).

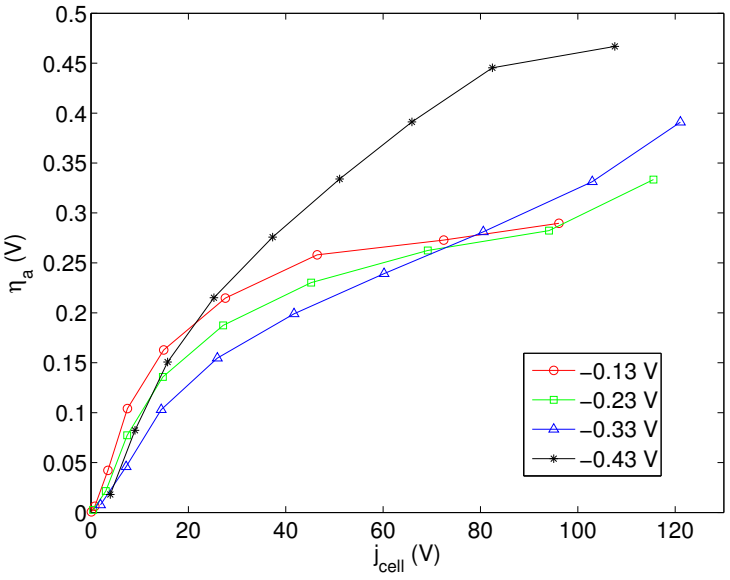

Figure 3.13: Anodic overpotential versus current for different mediator potentials ($E_K^{0\prime}$).

exchange current density (equation (3.20)). This effect is seen in the anodic overpotential in Figure 3.13 and explains the poor performance using the default value of R_{DK}. If the rate constant K_{red} is in less excess at low current and the electrochemical reaction is effectively faster.

3.5 Conclusions

Very few detailed models of biofuel cells have been developed, despite the considerable efforts directed towards the development of these technologies. In this chapter, a detailed, two-dimensional, dynamic model of a complete biofuel cell based on an enzyme cascade anode and biocathode was presented. Comparisons to experimental data have demonstrated that the model is able to capture the complex physical and bio-electrochemical phenomena within the cell to a good degree of accuracy.

The main drawback of the system modelled here is the rapid drop in the power output which is due to limitations in the mass transport of protons to the cathode. Provided that proton transport limitations can be resolved this setup proves very promising as a template for future biofuel cell designs that will achieve power outputs of several mW cm^{-2} using only biological catalysts. The anodic mediator (VK3) was probably chosen due to its high reactivity with the diaphorase enzyme, which is partly due to its equilibrium potential, around 0.22 V higher than diaphorase. A potential improvement would be to change the mediator for one with a lower equilibrium potential. Although this would consequently lower its reactivity with the enzyme, results have shown that the overall outcome is a higher power output due to a higher reversible cell voltage.

The simulations presented have revealed details regarding the temporal behaviour of the cell. These details depend to some extent on the values of the fitting parameters used. With the availability of rate constants and other measurable parameters, the methodology can provide more accurate predictions. The model presented here can be extended to other enzymatic and microbial systems, applying the same principles of mass, charge and momentum conservation. Perhaps the most challenging aspect of biofuel cell modelling lies in capturing the loss of biochemical activity that is an inevitable feature of these systems. In future work, the long-time performance of biofuel cell systems will be investigated.

Other improvements planned for this model include; incorporating the acid dissociation constants of the electrode polymers in calculating the pH, and introducing the electrolyte

thin film in the gas-diffusion cathode. The former addition is aimed at capturing the initial experimental pH which differs from that of the buffer, while the latter addition increases the time-scale accuracy of the cathodic current and allows to study the effect of the carbon fibre diameter and film thickness on the electrode performance.

Chapter 4

Numerical model of Pt-cathode and enzymatic-anode fuel cell

4.1 Introduction

In Chapter 3 a brief introduction to enzyme and mediator kinetics was presented and a detailed mathematical model of an all-biological fuel cell with multiple enzymes in the anode was presented. In this chapter, these methods are further applied to bio-anode enzymatic system which includes other commonly used components that were not included in Chapter 3, namely a diffusional mediator, platinum cathode, Nafion membrane, and an unbuffered solution.

Despite their name, many reported biofuel cells still rely on inorganic metal catalysts, mainly Pt, for the oxygen reduction reaction, while focusing on the biological anode. Another common practice that has been adopted from PEMFC and DMFC is the use of Nafion as the separator due to its high proton conductivity. New evidence suggests that this membrane will behave differently in BFCs and a comparison to PEMFCs is not valid due to differences in the pH and electrolyte composition [22, 219]. In BFCs, the concentration of cations (other than protons) is usually much higher causing an obstruc-

tion in the proton diffusion through the membrane by occupying the charge sites in the membrane [220]. For this reason, concentrated buffer solutions should not be used with a Nafion membrane. Studies have suggested that anion exchange and bipolar membranes have better characteristics than cation exchange membranes in terms of pH management and electrical performance [23, 196, 221].

4.2 Fuel cell model

4.2.1 Reaction kinetics

The system under consideration was reported by Fischback et al. [65] (see also [276, 277]). The developed miniature fuel cell (12 × 12× 9 mm) comprised a Nafion membrane/cathode electrode assembly (MCEA) stacked with an enzymatic (glucose oxidase) carbon felt anode, as depicted in Figure 4.1. Glucose oxidase was covalently attached to functionalized carbon nano-tubes (CNTs) before excess GOx was made to precipitate near the CNTs. Finally, a cross-linking agent was added to form crosslinked enzyme clusters on the surface of the CNTs. This mixture was then cast on a carbon felt. The anode was placed between the MCEA and a gold mesh, for improved electrical conductivity. The current collectors were made from titanium plates, with current being drawn from the top side (Figure 4.1). Slits were machined into these plates to provide the anolyte on the anode side and air on the cathode side. The anode was continuously fed with a solution containing glucose and the mediator benzoquinone. The air-breathing Pt/Nafion cathode was prepared by applying a Nafion/Pt-black layer on a Nafion 115 membrane [65]. The fuel cell was capable of operating continuously at maximum power for 16 hours with no significant drop in performance.

For a mediated enzymatic anode, the two chemical reactions occurring are the two-substrate 'ping-pong' reactions involving the reduction and oxidation of the enzyme [53, 236, 247]:

$$\text{Enzyme reduction:} \quad \mathrm{E}_{ox} + \mathrm{S} \xrightarrow{k_{red}} \mathrm{E}_{red} + \mathrm{P} \tag{4.1}$$

$$\text{Enzyme oxidation:} \quad \mathrm{E}_{red} + \mathrm{M}_{ox} \xrightarrow{k_{ox}} \mathrm{E}_{ox} + \mathrm{M}_{red} \tag{4.2}$$

where E_{ox} and E_{red} (i.e., FAD and $FADH_2$) are the oxidized and reduced states of the enzyme (i.e., glucose oxidase) respectively. M_{ox} and M_{red} are the oxidized and reduced forms of the quinone mediator: benzoquinone and hydroquinone respectively [247]. S and P are the glucose substrate and glucono-lactone product, respectively. A third electrochemical reaction regenerates the mediator at the electrode:

$$\mathrm{M}_{red} \overset{k_{anod}}{\rightleftharpoons} \mathrm{M}_{ox} + 2\mathrm{H}^+ + 2e^- \tag{4.3}$$

This reaction is assumed to be a two-proton/two-electron process[278]. There is disagreement in the literature on the chemical pathway of the benzoquinone reduction reaction, and the stability of some of the intermediate radicals [279]. Ions formed by a single-electron transfer are found to be more stable in unbuffered solutions for pH > 2.5 [280]. In this work, the hydroquinone oxidation is assumed to proceed by reaction (4.3).

When studying the influence of a third substrate, dissolved oxygen (O_d), which competes with the mediator for the oxidation of the GOx, a third enzymatic reaction is included:

$$\mathrm{E}_{red} + \mathrm{O}_d \xrightarrow{k_{\mathrm{O}_d}} \mathrm{E}_{ox} + \mathrm{H}_2\mathrm{O}_2 \tag{4.4}$$

Unless stated otherwise, the competing enzyme oxidation reaction (equation (4.4)) is neglected.

The anode is treated as an electrically conducting porous matrix in which the immobilized enzyme resides and participates in the bio-electrochemical reactions. Applying steady-state approximations to the intermediate enzyme complexes (*i.e.*, Michaelis-Mentin

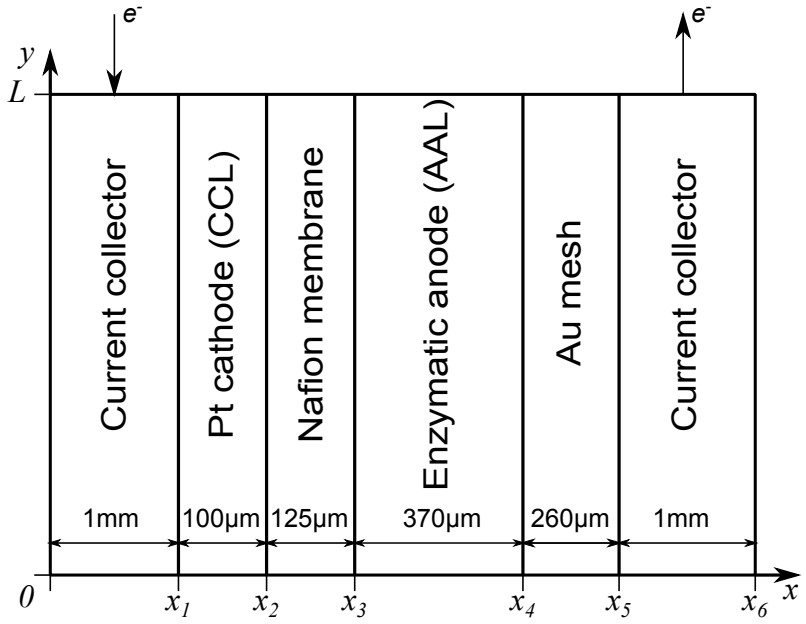

Figure 4.1: A schematic of the modelled cell.

kinetics), the reaction rates of the two enzymatic reactions (4.1) and (4.2) can be expressed as (in the anode active layer (AAL) only):

$$R_{red} = k_{red}\, c_{\mathrm{gluc}}\, c_{\mathrm{E}_{ox}} \tag{4.5}$$

$$R_{ox} = k_{ox}\, c_{\mathrm{M}_{ox}}\, c_{\mathrm{E}_{red}} \tag{4.6}$$

respectively, where c_i represents the concentration of species i ('gluc' representing glucose). k_{red} and k_{ox} are the pH dependent bimolecular rate constants, which were interpolated from the experimental data in [255, 281] (see Figure 4.2).

When assuming the presence of dissolved oxygen the rate of enzyme oxidation by the third substrate is expressed as:

$$R_{\mathrm{O}_d} = k_{\mathrm{O}_d}\, c_{\mathrm{O}_d}\, c_{\mathrm{E}_{red}} \tag{4.7}$$

The rate of reaction (4.3), occurring on the carbon anode, is expressed in Butler-Volmer form, assuming a two-electron reaction:

$$R_{anod} = k_{anod}\, c^{\beta}_{\mathrm{M}_{red}} c^{1-\beta}_{\mathrm{M}_{ox}} \left[\exp\left(\frac{2(1-\beta)F\eta_a}{RT} \right) - \exp\left(\frac{-2\,\beta\,F\eta_a}{RT} \right) \right] \tag{4.8}$$

where k_{anod} is the rate constant (s^{-1}), η_a is the anode overpotential, β is the charge transfer coefficient, T is the system temperature, F is Faraday's constant and R is the molar gas constant.

In the cathode catalyst layer (CCL), oxygen undergoes a four-electron reduction to water on Pt:

$$\mathrm{O_2} + 4\mathrm{H^+} + 4e^- \overset{k_{cath}}{\rightleftharpoons} 2\mathrm{H_2O_{(d)}} \tag{4.9}$$

Given the location of the reaction sites (simultaneous contact between ionomer, Pt and carbon [62, 63]) it is assumed that the water enters the ionomer phase, *i.e.*, is in a dissolved form (denoted with a subscript '(d)'). The rate of reaction (4.9) is expressed in Butler-Volmer form, assuming equal charge transfer coefficients:

$$R_{cath} = \frac{i^{ref}_{\mathrm{O_2}}}{F} \left(\frac{c_{\mathrm{O_2}}}{c^0_{\mathrm{O_2}}} \right) \left[\exp\left(\frac{-2F\eta_a}{RT} \right) - \exp\left(\frac{2F\eta_a}{RT} \right) \right] \tag{4.10}$$

where $i^{ref}_{\mathrm{O_2}}$ is the reference exchange current density and η_c is the cathode overpotential. The overpotentials are defined as ($j = c$ for the cathode and $j = a$ for the anode):

$$\eta_j = \phi_s - \phi_e - E^0_j \tag{4.11}$$

where ϕ_e and ϕ_s are the ionic and electron potentials. The half-cell equilibrium potentials are calculated from the Nernst equation:

$$E^0_a = E^{0\prime}_a - \frac{RT}{2F} \ln\left(\frac{c_{\mathrm{M}_{red}}}{c_{\mathrm{M}_{ox}}} \right) - 0.06 \times \mathrm{pH} \tag{4.12}$$

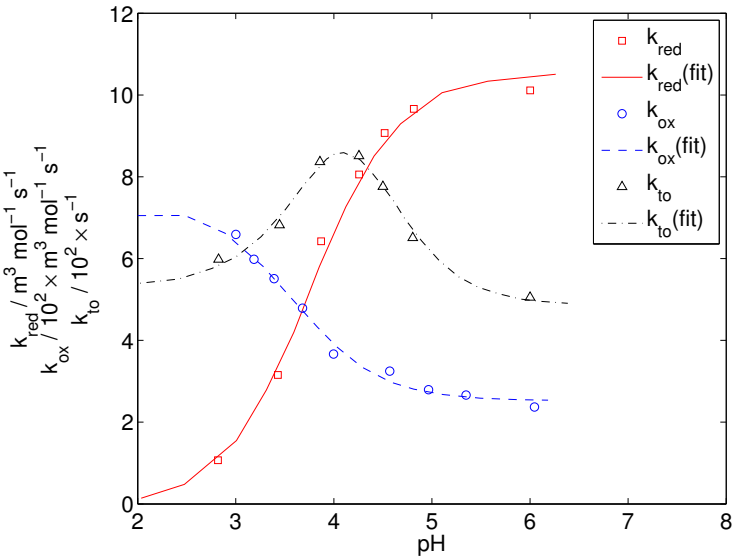

Figure 4.2: The pH dependence of enzymatic rate constants (determined from the results in [255, 281].

$$E_c^0 = E_c^{0\prime} - 0.06 \times \mathrm{pH} \tag{4.13}$$

where $E_j^{0\prime}$ are the standard potentials referenced at pH = 0, with a change of 60 mV per pH unit.

4.2.2 Reactant mass balances

The mass balance for the reduced immobilized enzyme in the absence of dissolved oxygen is as follows:

$$\frac{\partial c_{\mathrm{E}_{red}}}{\partial t} = R_{red} - R_{ox} \tag{4.14}$$

In the presence of dissolved oxygen, the source term for the reduced enzyme is modified to: $R_{red} - R_{ox} - R_{\mathrm{O}_d}$, where R_{O_d} is the rate of the reaction of the reduced enzyme with the dissolved oxygen (equation (4.7)). The fixed total concentration of enzyme, c_{E_Σ}, is

Source	Cathode catalyst layer	Anode enzyme layer
S_{O_2}	$-R_{cath}$	-
$S_{H_2O_{(v)}}$	$\nu\, h_{dv}\,(c_d - c_d^{eq})$	-
$S_{H_2O_{(d)}}$	$2\,R_{cath} - \nu\, h_{dv}(c_d - c_d^{eq})$	-
S_{H^+}	$-4R_{cath}$	$2R_{anod}$
$S_{M_{red}}$	-	$-(R_{anod} - R_{ox})$
$S_{M_{ox}}$	-	$(R_{anod} - R_{ox})$
S_{gluc}	-	$-R_{red}$
S_{ϕ_s}	$4FR_{cath}$	$-2FR_{anod}$

Table 4.1: Source terms for mass balances (4.16), (4.20) and (4.21), and the charge balances (4.32) and (4.33).

distributed between the two states: oxidized (GOx-FAD), reduced (GOx-$FADH_2$):

$$c_{E_\Sigma} = c_{E_{red}} + c_{E_{ox}} \tag{4.15}$$

Having calculated the reduced enzyme concentration (equation (4.14)), and knowing the total enzyme concentration, the oxidized enzyme concentration can then be calculated using equation (4.15)

The mass balance for a mobile species i in the porous regions (AAL, gold mesh and CCL) takes into account the accumulation of reactant species, transport by diffusion, electromigration under a potential field ϕ_e (Nernst-Planck equation) and generation/consumption during the reactions:

$$\epsilon\frac{\partial c_i}{\partial t} + \nabla\cdot\left(-D_i^{\text{eff}}\nabla c_i - \frac{z_i F D_i^{\text{eff}} c_i}{RT}\nabla\phi_e\right) = S_i \tag{4.16}$$

where c_i, D_i^{eff}, z_i and S_i are the concentration, effective diffusion coefficient, charge, and source term for species i. ϵ is the porosity of the porous region: $\epsilon = \epsilon_{al}$ in the AAL, $\epsilon = \epsilon_{Au}$ in the gold mesh and $\epsilon = \epsilon_{cl}$ in the CCL. The source terms, arising from the reactions and phase changes, are given in Table 4.1.

In the anolyte, the mobile species are glucose, M_{red}, M_{ox}, $H_2O_{(l)}$, H^+, a negatively charged

counter ion, and in some cases $O_{2(d)}$. The pH is defined as: pH= $-\log_{10}(c_{H^+})$ (in mol L^{-1}). Assuming that protons are the only cations in the anolyte, electro-neutrality is maintained by the counter ions, which, for simplicity, are assumed to have a unit charge. Denoting the counter ions by A^-, electroneutrality, which is given by:

$$\sum_i z_i c_i = 0 \tag{4.17}$$

then demands that $c_{A^-} = c_{H^+}$. In the CCL, equation (4.16) applies to O_2 and $H_2O_{(v)}$ in the CCL. In each of the regions, the effective diffusion coefficient for each species is approximated using a Bruggeman correction:

$$D_i^{\text{eff}} = \epsilon^{3/2} D_i \tag{4.18}$$

where D_i is the corresponding free-space value.

The mass balances for the species within the membrane and the ionomer (polymer electrolyte) of the CCL, namely water and protons, are treated separately, using the model of Springer et al. [282] developed for PEM fuel cells. The water moves as protonated water complexes, with the number of water molecules per proton characterized by a 'drag number' [282]:

$$n_{drag} = \frac{5\lambda}{44} \tag{4.19}$$

where λ is the membrane water content, *i.e.,* mol H_2O per mol SO_3^-. For convenience, the dissolved water concentration is normalized with respect to the fixed charge site concentration of the membrane, ν, to define $c_d = c_{H_2O_{(d)}}/\nu$. The normalized-water and proton concentrations are then given by:

$$\epsilon \frac{\partial c_d}{\partial t} + \nabla \cdot \left(-D_d^{\text{eff}} \nabla c_d - \frac{n_{drag}}{\nu} \frac{\kappa_e}{F} \nabla \phi_e \right) = S_i \tag{4.20}$$

$$\epsilon \frac{\partial c_{\mathrm{H}^+}}{\partial t} + \nabla \cdot \left(-D_{\mathrm{H}^+}^{\mathrm{eff}} \nabla c_{\mathrm{H}^+} - \frac{\kappa_e}{F} \nabla \phi_e \right) = S_i \tag{4.21}$$

respectively. In these equations, ϵ represents the volume fraction for dissolved-water and proton transport: $\epsilon = 1$ in the membrane and $\epsilon = \epsilon_{clp}$ (the volume fraction of ionomer) in the CCL. The electro-migration terms in equations (4.20) and (4.21) formally reduce to the familiar Nernst-Planck form through the relation between ion mobility and conductivity. The conductivity is obtained from an empirical relation [282]:

$$\kappa_e = \exp\left[1286 \left(\frac{1}{303} - \frac{1}{T} \right)\right] (0.514\lambda - 0.326) \tag{4.22}$$

The membrane water content is related to the dissolved water concentration as follows, with a correction for swelling of the hydrated membrane [63]:

$$\lambda = \frac{c_d}{1 - 0.0216 c_d} \tag{4.23}$$

The diffusion coefficient of dissolved water depends on λ through the following empirical relation [283]:

$$D_d^{\mathrm{eff}} = \begin{cases} \epsilon^{3/2} \left(3.1 \times 10^{-7} \lambda \left(\exp^{0.28\lambda} - 1 \right) \exp^{-2436/T} \right) & (0 < \lambda \leq 3) \\ \epsilon^{3/2} \left(4.17 \times 10^{-8} \lambda \left(1 + 161 \exp^{-\lambda} \right) \exp^{-2436/T} \right) & (3 < \lambda \leq 22) \end{cases} \tag{4.24}$$

The mass transfer of water between the vapour and dissolved phases (in the CCL) is driven by the deviation from the equilibrium concentration of dissolved water, c_d^{eq}. The corresponding equilibrium water content, λ^{eq} is related to the water vapour activity in the CCL, a_w by [63]:

$$\lambda^{eq} = 0.3 + 10.8\, a_w - 16\, a_w^2 + 14.1\, a_w^3 \tag{4.25}$$

The water activity (equilibrium relative humidity) is defined as:

$$a_w = \frac{c_{\mathrm{H_2O_{(v)}}} RT}{P_{sat}} \tag{4.26}$$

where P_{sat} is the saturation pressure at a temperature T [282]:

$$\log_{10} P_{\mathrm{sat}} = -2.1794 + 0.02953\Delta T - 9.1837 \times 10^{-5}\Delta T^2 + 1.4454 \times 10^{-7}\Delta T^3 \tag{4.27}$$

in which $\Delta T = T - 273$. The contributions of the phase change to the source terms of vapour and dissolved water are given in Table 4.1. The proportionality constant, h_{dv}, representing the coefficient of adsorption/desorption between the vapour and dissolved phases, is given by [63]:

$$h_{dv} = \begin{cases} \kappa_a \lambda & (c_d - c_d^{eq} < 0) \\ \kappa_d \lambda & (c_d - c_d^{eq} < 0) \end{cases} \tag{4.28}$$

in which κ_a and κ_d are adsorption and desorption coefficients.

4.2.3 Charge balances

The flow of a charged species i gives rise to a current density $\vec{j}_i = z_i F \vec{N}_i$, where z_i is the charge and $\vec{N}_i$ is the molar flux (driven by diffusion and electro-migration in the present case). Therefore, the total current density in the anolyte, $\vec{j}_e$ satisfies:

$$\vec{j}_e = \sum_i \vec{j}_i = -\kappa_e \nabla \phi_e - F \sum z_i D_i^{\mathrm{eff}} \nabla c_i \tag{4.29}$$

in which the effective conductivity κ_e is given by:

$$\kappa_e = \frac{F^2}{RT} \sum z_i^2 D_i^{\mathrm{eff}} c_i \tag{4.30}$$

The ionic current in the Nafion membrane and the proton-conducting ionomer of the CCL is governed by Ohm's law:

$$\vec{j}_e = -\epsilon^{3/2}\kappa_e \nabla\phi_e \tag{4.31}$$

where κ_e is defined in equation (4.22) and ϵ represents the volume fraction of the proton-conducting phase: $\epsilon = 1$ in the membrane and $\epsilon = \epsilon_{clp}$ (the volume fraction of ionomer) in the CCL. A steady-state charge balance in the ion-conducting regions is given by:

$$-\nabla \cdot \vec{j}_e = -S_\phi \tag{4.32}$$

in which the charge source S_ϕ is defined in Table 4.1. This source term is zero in regions where electrochemical reactions do not occur.
The electronic current, $\vec{j}_s$ is governed by Ohm's law. Conservation of charge within the porous regions ($\nabla \cdot \vec{j}_s + \nabla \cdot \vec{j}_e = 0$) leads to:

$$-\nabla \cdot \vec{j}_s = -\nabla \cdot \left(\epsilon^{3/2}\kappa_s \nabla\phi_s\right) = S_\phi \tag{4.33}$$

in which κ_s is the conductivity of the electron conducting phase and ϵ is its volume fraction: $\epsilon = 1 - \epsilon_{al}$ in the AAL, $\epsilon = 1 - \epsilon_{Au}$ in the gold mesh, $\epsilon = 1$ in the current collectors and $\epsilon = 1 - \epsilon_{cl} - \epsilon_{clp}$ in the CCL.

4.2.4 Initial and boundary conditions

The cell can be modelled as either operating in galvanostatic mode or potentiostatic mode. In the first case, it was assumed that a fixed current was drawn outwards from the top edge of the cathode current collector and into the cell at the top edge of the anode current collector:

Parameter	**Description**	**Value**
T	System temperature	298 K
c_{E_Σ}	Total enzyme concentration (fitted)	0.96×10^{-3} mol m^{-3}
$c^0_{\mathrm{M}_{red}}/c^0_{\mathrm{M}_{ox}}$	Initial reduced/oxidized mediator concentration [65]	5 mol m^{-3}
c^0_{gluc}	Initial glucose concentration [65]	200 mol m^{-3}
$c^0_{\mathrm{H^+}}$	Initial proton concentration (3.2 pH [65])	0.63 mol m^{-3}
$c^0_{\mathrm{H_2O_{(v)}}}$	Initial water vapour concentration	0.89 mol m^{-3}
$c^0_{\mathrm{O_2}}$	Initial oxygen concentration	8.58 mol m^{-3}
$c^0_{\mathrm{H_2O_{(l)}}}$	Initial liquid water concentration	55.5 kmol m^{-3}
c^{*0}_d	Initial (normalized) dissolved water concentration	17.22
$D_{\mathrm{H^+}}$	Diffusion coefficient of protons in anolyte	2×10^{-9} m^2 s^{-1}
D_{M_r} /D_{M_o}	Mediator diffusion coefficient [284]	2×10^{-9} m^2 s^{-1}
D_{gluc}	Diffusion coefficient of glucose [285]	0.7×10^{-9} m^2 s^{-1}
$D_{\mathrm{H_2O_{(l)}}}/D_{\mathrm{O}_d}$	Diffusion coefficient of liquid water/dissolved oxygen	2×10^{-9} m^2 s^{-1}
$D_{\mathrm{H_2O_{(v)}}}/D_{\mathrm{O_2}}$	Diffusion coefficient of water vapour/gaseous oxygen	1×10^{-5} m^2 s^{-1}
k_{O_d}	Rate constant of enzyme-dissolved oxygen reaction [255]	2×10^3 m^3 mol–1 s^{-1}
κ_a (κ_d)	Water adsorption (desorption) coefficient [63]	1.11 (3.33) [$\times10^{-6}$ s^{-1}]
k_{anod}	Rate constant for mediator oxidation (fitted)	0.15 s^{-1}
β	Anodic transfer coefficient (estimated)	0.57
$i^{ref}_{O_2}$	Reference current density of oxygen reduction (fitted)	0.093 A m^{-3}
$E^{0\prime}_a$	Benzoquinone equilibrium potential [286]	0.7 V
$E^{0\prime}_c$	Oxygen reduction equilibrium potential (fitted)	0.955 V
ϵ_{cl}	Void fraction in cathode catalyst layer (CCL)	0.2
ϵ_{clp}	Polymer (ionically conducting) fraction in CCL	0.6
ϵ_{al}	Void fraction of carbon felt anode [287]	0.9
ϵ_{Au}	Void fraction of gold mesh	0.6
κ_{al}	Carbon felt electronic conductivity [287]	30 S m^{-1}
κ_{cc} (κ_{Au})	Ti current collector (gold mesh) electronic conductivity	2 (45)[$\times10^6$ S m^{-1}]

Table 4.2: The default parameters values used in the simulations.

$$-\vec{n}\cdot\left(-\kappa_s\nabla\phi_s\right) = \begin{cases} -\left(\dfrac{L}{x_1}\right) j_{cell} & (0 \le x \le x_1;\, y = L) \\ \left(\dfrac{L}{x_6 - x_5}\right) j_{cell} & (x_5 \le x \le x_6;\, y = L) \end{cases} \tag{4.34}$$

where j_{cell} is the fixed, applied current density, relative to the anode geometrical area and $\vec{n}$ is the unit normal vector pointing into the membrane. All other external boundaries were assumed to be insulated. The cell voltage was evaluated as the difference between the averages of the electronic potential of the cathode and anode, evaluated at the top boundaries of the current collectors:

$$V_{cell} = \overline{\phi}_{s,c} - \overline{\phi}_{s,a} \tag{4.35}$$

in which the bar denotes a spatial average. For operation in potentiostatic mode, a cell voltage was imposed (applied through equipotential surfaces at the top boundaries of the two current collectors):

$$\phi_s = \begin{cases} V_{cell} & (0 \le x \le x_1;\ y = L) \\ 0 & (x_5 \le x \le x_6;\ y = L) \end{cases} \tag{4.36}$$

The current density, j_{cell} (expressed relative to the electrode area) measured at the top of the current collector:

$$j_{cell} = \frac{1}{L} \int_0^{x_1} \left(-\kappa_s \frac{\partial \phi_s}{\partial y} \right) dx \tag{4.37}$$

The concentrations of gaseous species at the air inlet ($x = x_1$), and the concentration of soluble species at the anolyte inlet ($x = x_5$) were assumed to be constant and equal to the initial concentrations:

$$c_i = c_i^0 \quad (x = x_1, x_5) \tag{4.38}$$

At the membrane/anode interface ($x = x_3$), the water in the anode solution was constrained in order to maintain a membrane water content of $\lambda = 22$ (fully liquid saturated, as would be expected for contact with an aqueous solution [63]). The mass balance of water across this interface was maintained by setting the flux of liquid water into the membrane equal to that of the dissolved water at that boundary:

$$-\vec{n} \cdot \left(-D^{\text{eff}}_{\text{H}_2\text{O}_{(l)}} \nabla c_{\text{H}_2\text{O}_{(l)}} \right) = -\nu D_d^{\text{eff}} \frac{\partial c_d}{\partial x} - \frac{5 \lambda \kappa_e}{44F} \frac{\partial \phi_e}{\partial x} \quad (x = x_3) \tag{4.39}$$

At time $t = 0$ the total enzyme concentration is assumed to be distributed equally between

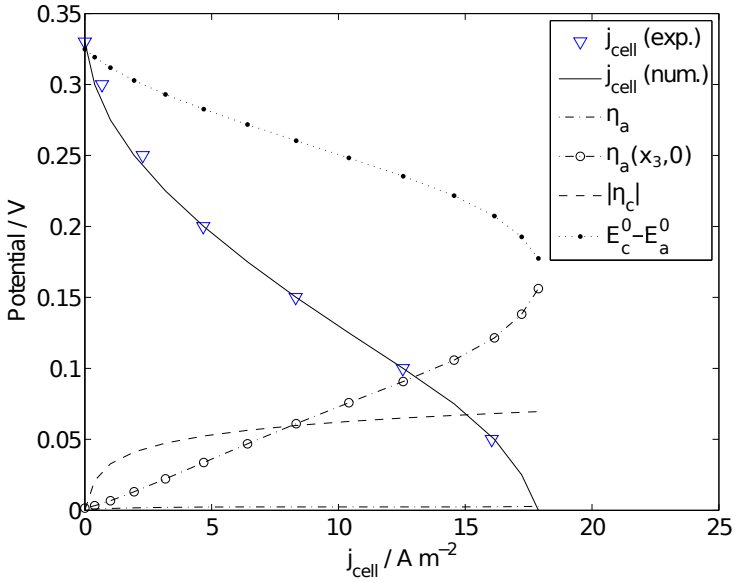

Figure 4.3: Simulated and experimentally determined polarization curves.

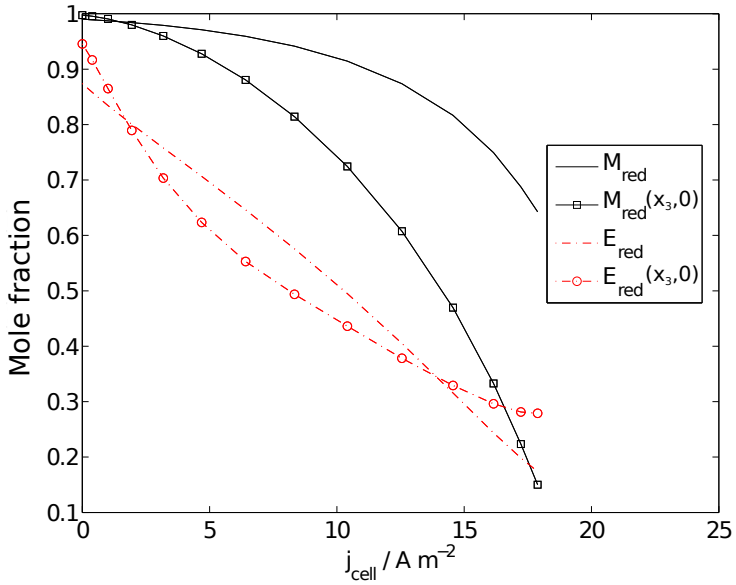

Figure 4.4: Enzyme and mediator mole fractions versus cell current density.

the reduced and oxidized states such that the initial concentration of oxidized enzyme is:

$$c^0_{\mathrm{E}_{ox}} = \frac{c_{\mathrm{E}_\Sigma}}{2} \tag{4.40}$$

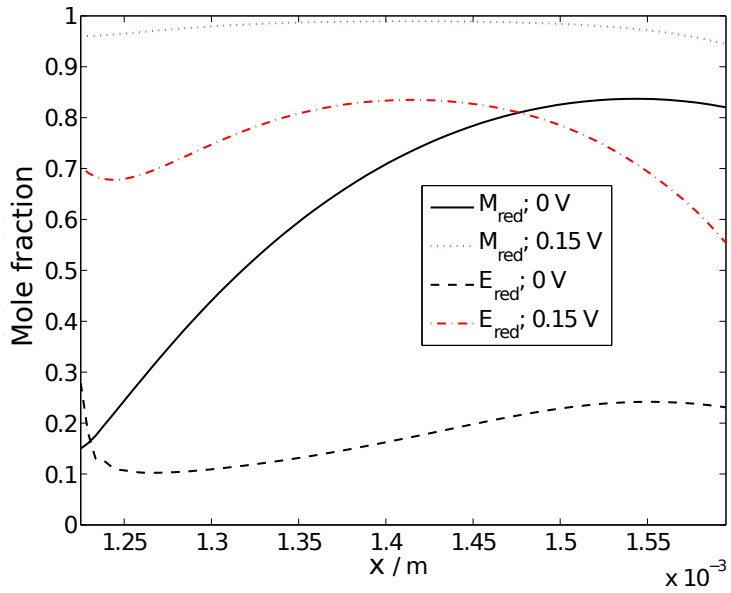

Figure 4.5: Enzyme and mediator mole fractions across the anode at different cell voltages.

4.3 Results and discussion

In order to match the simulation results to the experimental data, a number of fitting parameters were used, a standard procedure for models of complex systems. The default parameter values are given in Table 4.2. The dimensions of the gold mesh, current collectors and and Pt/Nafion cathode were assumed since specific details of the materials were not provided in Fischback et al. [65]. The AAL thickness is 370 μm [276]. The values used did not qualitatively affect the results. The three fitting parameters were the unknown total concentration of the enzyme (c_{E_Σ}), and two electrochemical rate constants for the anode mediator and cathode oxygen reduction (k_{anod} and $i_{O_2}^{ref}$ respectively). The parameter estimation (implemented in Matlab) was performed through a least-squares fit of the simulation results to the experimental polarization data (minimization of the total square error).

To obtain polarization curves (current density *vs.* cell voltage), the potentiostatic model was solved at steady-state. The results were consistent with transient operation simulations, in which the cell voltage was decreased in steps, maintaining the value at each step for 10 minute intervals and measuring the current at the end of the interval (the same procedure was used in the experiments [65]). The 10 minute interval is long enough for

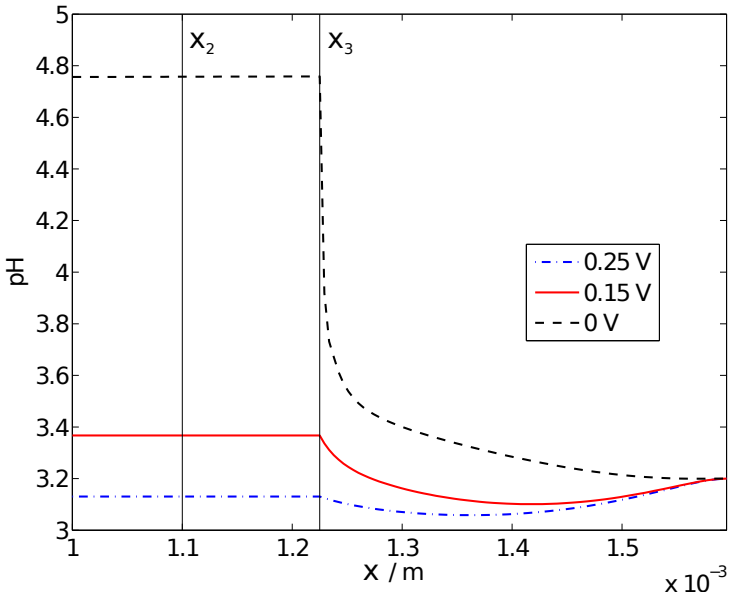

Figure 4.6: pH variation across the cell at different cell voltages. The boundaries of the Nafion membrane with the cathode and anode, x_2 and x_3 respectively, are indicated.

transient results to reach steady-state values. The results were also in agreement with equivalent galvanostatic simulations.

Figure 4.3 compares the polarization curves from the experimental cell to those from the numerical model. The match is very good, indicating that the model is able to capture the physical processes in the cell to a good degree of accuracy. The short-circuit current (SCC) density is equal to 17.5 A m^{-2}, the open-circuit voltage is 0.33 V, and the maximum power density is 1.27 W m^{-2}, at approximately 0.15 V. The cell performance can be characterized by two main factors: a relatively large drop in the reversible open-circuit potential (150 mV, of which approximately 100 mV is due to the decrease in E_c^0 as a result of the pH rise), and a relatively large anodic overpotential at the membrane boundary, x_3, compared to the average η_a which remains less than 5 mV at all currents.

Figure 4.4 shows the mole fractions of the mediator and the enzymes *vs.* the cell current density. The overall performance of the cell is strongly dependent on the reduced enzyme fraction at the membrane boundary, x_3, which quickly drops to 0.5 at 8 A m^{-2}. The anode-averaged reduced fraction of enzyme shows a linear relationship with current and at short-circuit conditions the low mole fraction of M_{red} at the membrane boundary (x_3) is due to both the diffusion limit of M_{red} and the depletion of E_{red}, whose local and average

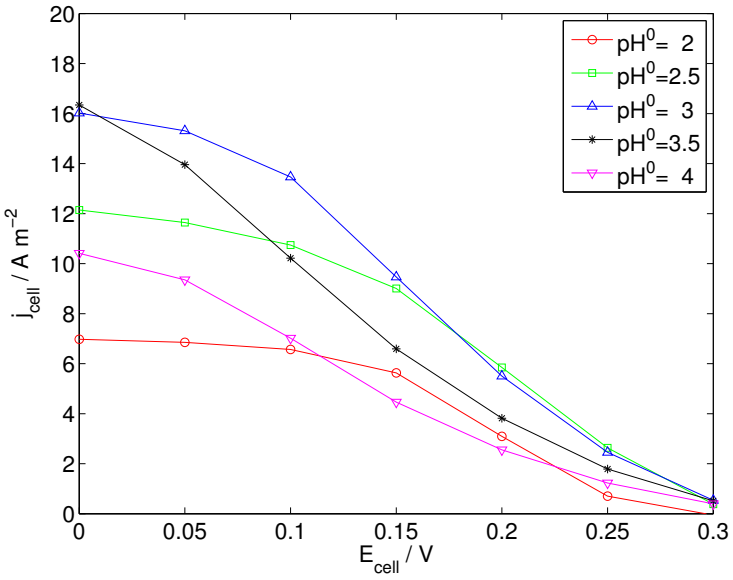

Figure 4.7: Polarization curves for different initial pH.

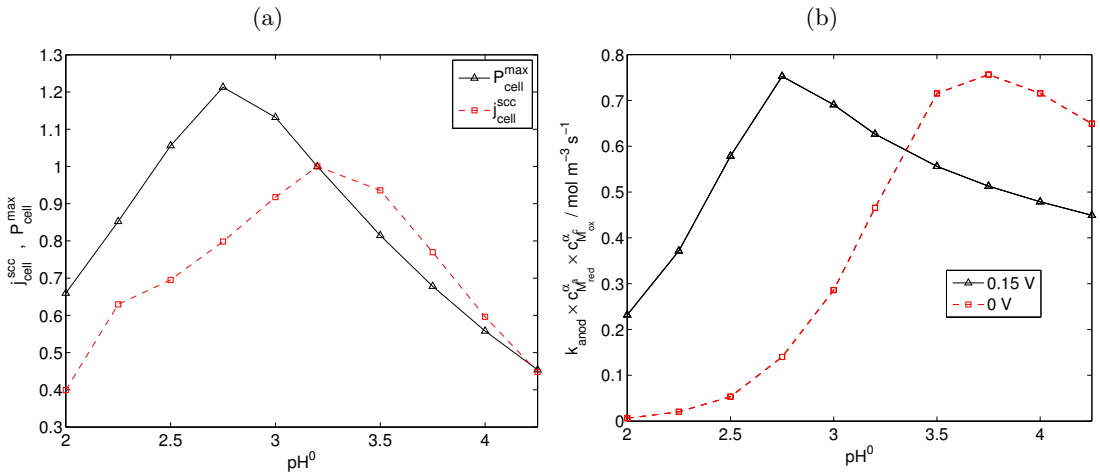

Figure 4.8: (a) Maximum power output and short-circuit current (normalized by default case of 3.2 pH), (b) electrochemical reaction rate for different cell voltages (evaluated at $(x_3, 0)$) versus initial pH.

mole fractions are around 0.25 and 0.1 at short circuit conditions. The limiting factor of mediator mass transport is evident from the profile of the reduced mediator fraction across the anode (Figure 4.5), which reaches a maximum of 0.82 near the anode inlet, x_4, but drops to nearly 0.15 at the membrane boundary. Profiles of M_{ox} are not shown since the sum of the reduced and oxidized states is equal to the total mediator concentration when the two species have equal diffusion coefficients. Variations along the y direction were negligible and are not, therefore, reported.

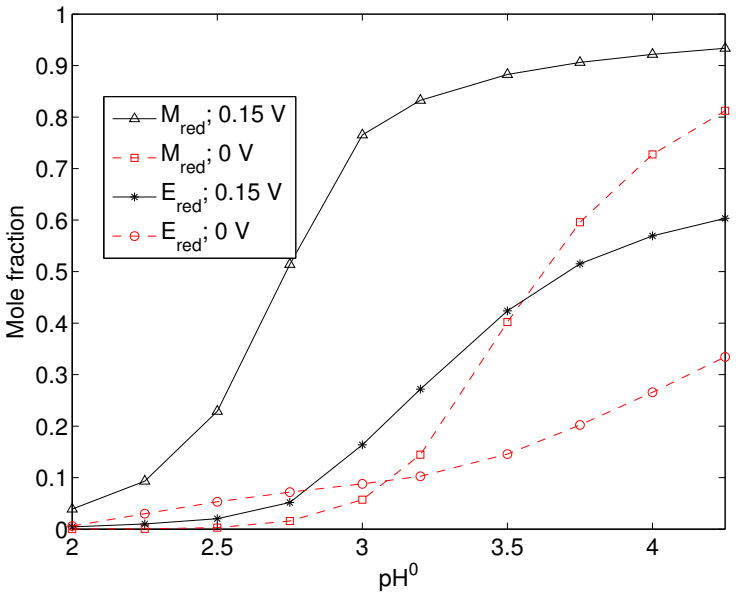

Figure 4.9: Mediator and enzyme mole fractions for different cell voltages (evaluated at $(x_3, 0)$) versus initial pH.

Figure 4.6 shows the variation in the pH across the cell at $y = 0$ for different operating cell voltages. The negligible drop in pH across the MCEA indicates that the rise in cathodic pH is not caused by proton mass transport limitations through the Nafion but is instead due to a limitation in the rate of proton generation from the anodic reaction, which is confined to a very thin region near the membrane, as evident from the sharp rise in pH at the boundary x_3. The anodic overpotential drops from nearly 150 mV at x_3 to less than 5 mV in a thin region of approximately 35 μm thickness, an indication that the electrochemical reaction is confined to a region in the vicinity of the membrane that is less than 10% of the anode thickness.

The activity of free GOx at pH = 7 is one order of magnitude greater than that at 3.2 pH, measured by UV-visible spectroscopy [65]. These results were obtained using o-dianisidine as the redox indicator which is recycled using a second enzyme, horseradish peroxidase (HRP). In this GOx-HRP setup, the two substrates for GOx are glucose and molecular oxygen, while the product is hydrogen peroxide. The rate of GOx is indirectly obtained by measuring the rate of peroxide reaction with the redox indicator, dianisidine. The pH profiles of enzyme activities are known to depend on the specific mediator used, and those obtained using the GOx-HRP system will generally be different than that used in the fuel cell. To study the effect of pH on the GOx activity with the benzoquinone mediator,

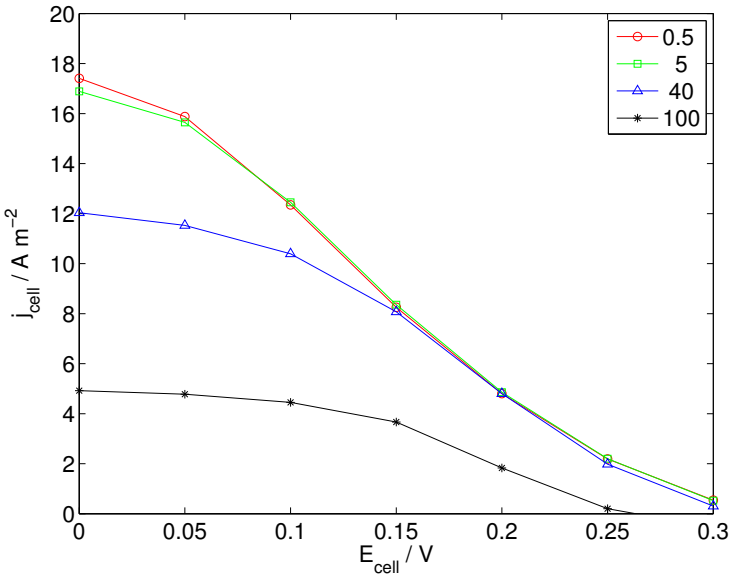

Figure 4.10: Cell polarization curves for different concentrations of dissolved oxygen, $c^0_{O_d}$.

the initial pH was varied from 2 to 4. The polarization and power curves for different pH^0 (initial pH) are shown in Figure 4.7. With increasing pH up to 3, j_{cell} is higher for all cell voltages. At even greater values of pH the cell performance quickly deteriorates. Figure 4.8 shows the maximum power and current *vs.* initial pH. The optimum value for maximum power production is around pH = 3. The enzyme reduction and oxidation rates increase and decrease respectively with an increasing pH (Figure 4.2), which results in an increase in the reduced enzyme fraction at higher pH values. From pH = 2 to pH = 3, the cell current is higher at all voltages but the reduced mediator fraction still increases with pH. This suggests that the rate of M_{red} production is limited by the amount of (reduced) enzyme and not the rate constant k_{ox}, which decreases at higher pH, but remains two orders of magnitude greater than k_{red}. For pH > 3 (Figure 4.9), the maximum power decreases due to a depletion of M_{ox} (excess of M_{red}), which reduces the concentration dependent term in the Butler-Volmer expression (4.8) and in turn leads to an increase in the anodic overpotential.

When using enzymes such as GOx that are reactive towards oxygen, it is common practice to bubble the solution with nitrogen to remove traces of the dissolved oxygen. Any dissolved oxygen in the solution competes with the mediator for oxidation of the enzyme, according to equation (4.4). Figure 4.10 shows the cell polarization curves at different concentrations of dissolved oxygen. Assuming the solution is fully saturated with oxygen

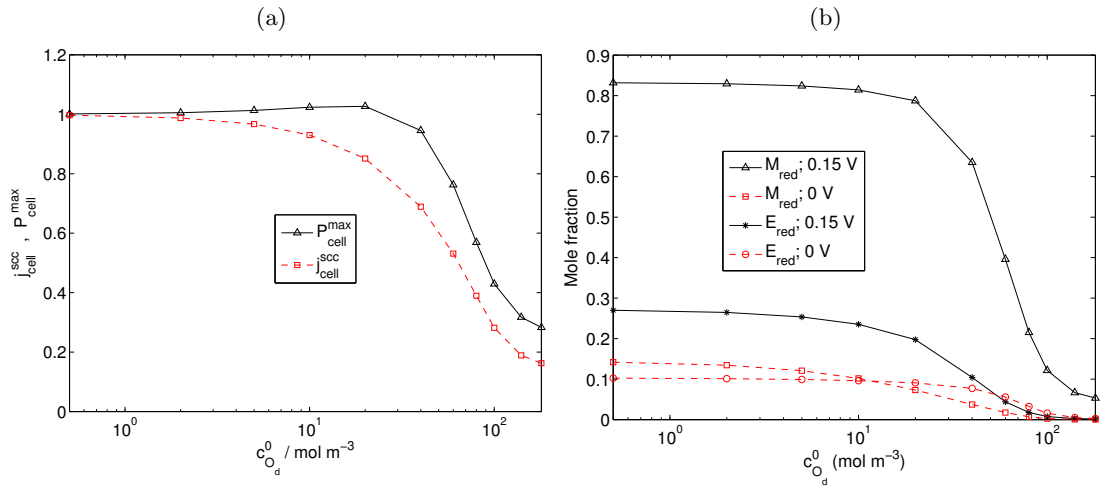

Figure 4.11: (a) Maximum power output and short-circuit current (normalized by default case, $c^0_{O_d} = 0$), (b) mediator and enzyme mole fractions for different cell voltages (evaluated at $(x_3, 0)$) versus dissolved oxygen concentration.

($c^0_{O_d}$ = 0.5 mol m^{-3}), the effect of the competing reaction (4.4) on the cell performance is negligible, even though the rate of reaction E_{red} with molecular oxygen is more than two-fold that of E_{red} with the mediator. At sufficiently high enzyme concentrations (10^{-3} mol m^{-3} in this case), the competing side reaction will proceed to consume the dissolved oxygen with a negligible effect on the current output or the enzyme/mediator mole fractions. Even at 10% of the fitted enzyme concentration, the presence of a third competing substrate has an insignificant effect on the cell performance. When the dissolved oxygen concentration is increased to almost ten-fold the saturation value, the oxygen side reaction begins to affect the availability of E_{red}, which in turn reduces the fraction of M_{red} and the output cell current, as shown in Figure 4.11(a).

One major research focus in enzymatic fuel cells is an increase in enzyme loading while maintaining long-term stability. Fischback et al. [65] demonstrated that cross-linked GOx clusters on carbon nano-tubes lead to a high enzyme loading, while retaining the initial activity for 250 days. Figure 4.12 shows the dependence of the simulated maximum power and current densities on the total enzyme concentration. The fitted concentration corresponds to the maximum power output. At 10% of the default enzyme concentration, the maximum power output drops to 40% of the maximum value, while at higher enzyme concentrations (greater than 5 to 10 times the default value) the maximum power and current actually decrease. The cause of this deteriorating performance is similar to that

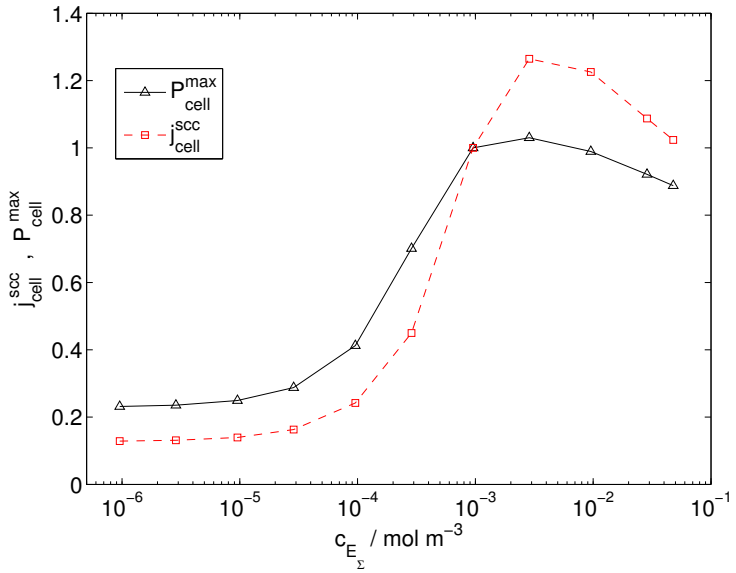

Figure 4.12: Maximum power output and short-circuit current (normalized by default fitted case) versus total enzyme concentration.

seen in the case of operation at high pH values; the increased biological reaction rates (equations (4.1) and (4.2)) lead to a depletion in M_{ox}, which in turn leads to a rise in the anodic overpotential (due to the Butler-Volmer form of the current density/reaction rate (4.8)). Thus, increasing the enzyme loading beyond a certain (optimal) value is not beneficial to performance unless the electrochemical limit of the cell is simultaneously altered (e.g., using a different mediator).

4.4 Conclusions

In this chapter, a detailed, dynamic model of a biofuel cell based on an enzymatic anode and air-breathing Pt cathode was developed and presented. The model developed can simulate steady-state as well as dynamic performance, under galvanostatic or potentiostatic conditions. The overall performance of the cell is strongly influenced by the reduced enzyme fraction in the vicinity of the membrane and the diffusion limitation associated with the mediator. Due to the higher ionic conductivity of the Nafion membrane compared to that of the unbuffered solution, the anodic reaction is confined to a very thin region near the membrane. If the mediator had been immobilized, the maximum current output would have been significantly lower due to a depletion of the reduced mediator

at the membrane boundary. The use of a diffusional redox couple allows the biological reaction to recycle the mediator throughout the anode even though the electron transfer reaction is restricted to a small region.

The spatial variations in the y (vertical direction) in Figure 4.1 were shown to be small when compared to variations in the x (through plane) direction. There is also a strong dependence on the local pH in the anode, and the pH dependance of the enzymatic rates. The effect of the initial pH was investigated and results show that for pH > 3, the maximum power is decreased due to a depletion of M_{ox} (excess M_{red}) which reduces the exchange current density in the Butler-Volmer equation. A similar result (excess of M_{red}) was obtained when the enzyme loading was increased beyond an optimal value, demonstrating that the cell in this case is limited electrochemically.

Glucose oxidase is known to be able to utilize dissolved oxygen as an electron acceptor. The effect of such a competing reaction was examined and showed little influence on the performance of the fuel cell for oxygen concentrations up to 20 mM even though the enzyme rate with the competing oxygen was more than two times greater than that with the mediator. At sufficiently high enzyme concentrations, the side reaction will proceed to consume the dissolved oxygen with a negligible effect on the current output or the enzyme and mediator mole fractions.

Chapter 5

Data-driven model using Gaussian process regression

5.1 Introduction

Mathematical models are important in the development of fuel cells for providing crucial information such as the distributions of potentials and concentrations during operation which are otherwise difficult to obtain from experimental methods. With increasing system complexity and size, such as in stack-level modelling or in microbial fuel cells where a large number of reactions occur, spatially-distributed physics-based models may be computationally demanding and are not feasible for optimization purposes.

Another approach to modelling is inductive machine learning where the aim is to learn or induce a relationship between a given set of inputs and outputs. In most cases this data is generated from experiments, but can also be generated from numerical simulations to serve as training data for these computationally efficient surrogate models. After finding a suitable function or mapping that describes the given training data set, the goal is to predict the outcome of an experiment for any new unobserved input values. Data-driven models are useful cross-disciplinary tools for analysis and prediction. Applied to fuel

cell research, such models are useful in studying experimental data-sets without making assumptions on the physical laws underlying the system.

One of the common machine learning approach that has been applied to model classical fuel cells such as SOFC and PEMFC are based on artificial neural networks [288–290]. Despite their flexibility in modelling a wide variety of functions, neural networks can be difficult to apply in practice due to the lack of a principled framework for deciding the architecture of the neural network [291, 292]. There is also no natural method for quantifying confidence (or error) in the solutions.

An alternative to artificial neural networks is Gaussian process regression (GPR). Gaussian processes are a generalisation of the Gaussian multivariate distribution to infinite dimensionality. The key assumption in GPR is that such a function or mapping can be represented as a Gaussian stochastic process. The assumption of a Gaussian process is used as prior in the context of Bayesian inference. In fact, many models commonly employed in machine learning are special cases of, or restricted kinds of Gaussian processes [291].

In this chapter, an introduction to GPR is presented and then combined with a dimensionality reduction technique for improved computational efficiency. The reduced-basis GPR presented here was developed by Shah and Nair [293] and applied in studying the polarization curves of PEMFCs. In this chapter, the method is applied to simulation data from the enzymatic fuel cell model described in Chapter 3 to study concentration and potential profiles in the cathode.

5.2 Model development

A stochastic process is a collection of random variables, Y_t, indexed by elements t, that is, for each t, Y_t is a random variable. Such a process is called Gaussian if any finite collection of Y_t (with indices $t_1, t_2, \ldots, t_n$) has a multivariate normal distribution. Moreover, any

linear combination of the random variables in the finite subset is Gaussian distributed with a univariate probability density function. Consider a Gaussian distributed random vector $\mathbf{Y}=(Y_1, Y_2, \ldots, Y_n)$. The joint probability density function of such a random vector is given by:

$$f_Y(y_1, \ldots, y_n) = \frac{1}{(2\pi)^{n/2}\sqrt{|C|}} \exp\left(-\frac{1}{2}(\mathbf{y}-\boldsymbol{\mu})^T C^{-1}(\mathbf{y}-\boldsymbol{\mu})\right) \tag{5.1}$$

where $\mathbf{y} \in \mathbb{R}^n$ is a realization of $\mathbf{Y}$ and $\boldsymbol{\mu} = (\mu_1, \ldots, \mu_n)$ is the mean vector of $\mathbf{Y}$ ($\mu_i = \mathbb{E}[Y_i]$). The matrix C is the covariance matrix, whose entries C_{ij} correspond to the covariance of Y_i and Y_j, i.e. $C_{ij} = C_{ji} = \text{cov}[Y_i, Y_j] = \mathbb{E}[Y_i Y_j] - \mathbb{E}[Y_i]\mathbb{E}[Y_j] = \mathbb{E}[Y_i Y_j] - \mu_i \mu_j$. Any Gaussian process is completely specified by its mean function and covariance function, in the sense that they entirely determine the joint probability density function on a finite subset of T.

5.2.1 General linear regression

Given a data set $\mathcal{D} = \{(\mathbf{x}^{(i)}, y^{(i)})\}_{i=1}^M$ generated from a series of laboratory or numerical experiments, containing M 'training inputs' $\mathbf{x}^{(i)} \in \mathbb{R}^L$ and M scalar outputs or 'targets' $y^{(i)}$, the objective in regression is to find a function relating the inputs to the outputs. The data is usually corrupted to some degree by errors arising from the measurement technique. The targets are assumed to be realizations of random variables $Y^{(i)}$, $i = 1, \ldots, M$, which are sums of an underlying mapping $h(\mathbf{x}^{(i)})$ from the inputs to outputs and a noise term $\mathcal{E}^{(i)}$. The regression model is thus:

$$Y^{(i)} = h(\mathbf{x}^{(i)}) + \mathcal{E}^{(i)} \quad i = 1, \ldots, M \tag{5.2}$$

The noise terms $\mathcal{E}^{(i)}$ are assumed to be independent and identically distributed (i.i.d) random variables having a normal distribution with mean zero and variance σ^2:

$$\boldsymbol{\mathcal{E}} \sim \mathcal{N}(\mathbf{0}, \sigma^2 I_M) \tag{5.3}$$

The notations I_M is used to denote the $M \times M$ identity matrix. The classical analysis of the linear regression model in equation 5.2 seeks to find a parametrized form of the underlying function, $h(\mathbf{x}; \mathbf{w})$, by estimating the linear coefficients of $\mathbf{w} = (w_1, w_2, \ldots, w_L)^T$. This function need not be linear in $\mathbf{x}$, but, crucially, it must be linear in the parameters $\mathbf{w}$. In general, the function can take the form of a linear combination of known basis functions $\{\chi_i(\mathbf{x})\}_{i=1}^K$, i.e., $h(\mathbf{x}; \mathbf{w}) = \sum_{j=1}^K w_j \chi_j = \mathbf{w}^T \boldsymbol{\chi}$, where now $\mathbf{w} \in \mathbb{R}^K$ and $\boldsymbol{\chi} = (\chi_1, \ldots, \chi_K)^T$.

In Bayesian regression, a prior distribution is placed on $\mathbf{w}$, which becomes a realization of a random vector $\mathbf{W}$. This vector of parameters is assumed to be a multivariate Gaussian:

$$\mathbf{W} \sim \mathcal{N}(\mathbf{0}, \xi^2 I_K) \tag{5.4}$$

in which case the individual coordinates are independent. Since any linear combination of the coordinates of $\mathbf{W}$ is, by definition, Gaussian, the dot product $\mathbf{W}^T \boldsymbol{\chi}(\mathbf{x})$ is a univariate Gaussian. The noise terms $\mathcal{E}^{(i)}$ are assumed to be independent of $\mathbf{W}$, and the random variables $Y^{(i)}$ are also assumed to be conditionally independent given $\mathbf{W}$. The distribution of $Y^{(i)}$, conditional on an outcome of $\mathbf{W}{=}\mathbf{w}$, is Gaussian with mean $h(\mathbf{x}; \mathbf{w}) = \mathbf{w}^T \boldsymbol{\chi}(\mathbf{x})$ and variance σ^2:

$$Y^{(i)} | (\mathbf{W} = \mathbf{w}) \sim \mathcal{N}(\mathbf{w}^T \boldsymbol{\chi}, \sigma^2) \tag{5.5}$$

The Bayesian approach to linear regression is essentially equivalent to specifying an underlying function that is the realization (for some $\mathbf{W}{=}\mathbf{w}$) of a Gaussian process indexed by the inputs $\mathbf{x}$. The observation that $\mathbf{W}^T \boldsymbol{\chi}$ is a Gaussian process is one motivation for Gaussian process regression, which consists, essentially, of directly specifying the mean and covariance matrix of a general Gaussian process, $G_{\mathbf{X}}$.

5.2.2 Gaussian process regression

The mean function of $G_{\mathbf{X}}$ can be taken as zero by centring the data. The covariance function must generate a symmetric, positive semi-definite covariance matrix when evaluated at any finite collection of points $\mathbf{x} \in \mathbb{R}^L$ in the input space. The method is 'parameter free' in the sense that a parametric form of the underlying function is not specified. The covariance function does, on the other hand, involve hyperparameters that are required to fully specify the covariance function. The problem of learning in GPR is finding the hyperparameters $\boldsymbol{\theta}$ that best describe the given data set.

A common choice of covariance function is the squared exponential:

$$k(\mathbf{x}, \mathbf{x}') = \mathbb{E}[G_{\mathbf{x}} G_{\mathbf{x}'}] = \theta_1 \exp\left(-\frac{1}{2}\sum_{l=1}^{L}\frac{(x_l - x_l')^2}{\theta_{l+1}}\right) \tag{5.6}$$

The squared exponential enforces a rapid decay in the covariance of underlying function values when evaluated at increasingly distant inputs $\mathbf{x}$. The strictly positive hyperparameters $\theta_2, \ldots, \theta_{L+1}$ introduce different degrees of decay in each component of the input. A further hyperparameter θ_{L+2}, which does not appear in equation 5.6, is defined as σ^2, the unknown variance of the noise term. The hyperparameters are collected together to form a vector $\boldsymbol{\theta} = (\theta_1, \ldots, \theta_{L+2})$. For the moment, the hyperparameters are assumed to be given.

By the definition of a Gaussian process, the joint density of $G_{\mathbf{X}}$ on a finite subset of the index set is Gaussian. In particular, this is true of the joint density on the set of inputs $\{\mathbf{x}^{(i)}\}_{i=1}^{M}$ corresponding to the targets. The regression model becomes:

$$\mathbf{Y} = \mathbf{G} + \boldsymbol{\mathcal{E}} \quad (\text{or: } Y^{(i)} = G_{\mathbf{X}^{(i)}} + \mathcal{E}^{(i)}) \tag{5.7}$$

The distribution of $\mathbf{G}$, assuming the data has been centred, is $\mathcal{N}(\mathbf{0}, \widehat{C})$, where $\widehat{C} \in \mathcal{R}^{M\times M}$ is the covariance matrix found by evaluating the squared exponential covariance function 5.6 on the index set $\{\mathbf{x}^{(i)}\}_{i=1}^{M}$. Given, therefore, that the random vectors $\mathbf{G}$ and $\boldsymbol{\mathcal{E}}$ are independent, $\mathbf{Y}|\boldsymbol{\theta} \sim \mathcal{N}(\mathbf{0}, C)$, where $C = \widehat{C} + \sigma^2 I_M$, i.e.,

$$(C)_{ij} = \theta_1 \exp\left(-\frac{1}{2}\sum_{l=1}^{L}\frac{(x_l^{(i)} - x_l^{(j)})^2}{\theta_{l+1}}\right) + \delta_{ij}\theta_{L+2}; \quad i,j = 1,\ldots,M \tag{5.8}$$

Here, δ_{ij} is the kronecker delta function ($\delta_{ij} = 0$ if $i \neq j$; $\delta_{ij} = 1$ if $i = j$); recall that $\theta_{L+2} = \sigma^2$.

5.2.3 Determining the hyperparamters

Before determining the mean and variance of a target output Y_* at a new given input $\mathbf{x}_*$, we first need to determine the hyperparameters θ_i. These parameters have to be deduced from the given data and the assumed model. The value of $\boldsymbol{\theta}$ that maximizes the posterior probability distribution ($f(\boldsymbol{\theta}|\mathbf{y})$) can be used as a substitute for the true value. Such an estimate is known as a point estimate and is interpreted as the value that is most likely to have generated the given data.

According to Baye's rule, the posterior distribution is proportional to the likelihood $f(\mathbf{y}|\boldsymbol{\theta})$ and the prior $f(\boldsymbol{\theta})$:

$$f(\boldsymbol{\theta}|\mathbf{y}) = \frac{f(\mathbf{y}|\boldsymbol{\theta})f(\boldsymbol{\theta})}{f(\mathbf{y})} \tag{5.9}$$

Since the marginal likelihood over the hyperparameters ($f(\mathbf{y})$) is independent of $\boldsymbol{\theta}$, then the value of $\boldsymbol{\theta}$ that maximises the posterior can be expressed as:

$$\text{argmax}_{\boldsymbol{\theta}} f(\boldsymbol{\theta}|\mathbf{y}) = \text{argmax}_{\boldsymbol{\theta}} f(\mathbf{y}|\boldsymbol{\theta})f(\boldsymbol{\theta}) \tag{5.10}$$

If we assume that the random vector $\boldsymbol{\theta}$ is uniformly distributed where each value is equally likely, i.e. $f(\boldsymbol{\theta})$ is independent of $\boldsymbol{\theta}$, then $\text{argmax}_\theta f(\boldsymbol{\theta}|\mathbf{y}) = \text{argmax}_\theta f(\mathbf{y}|\boldsymbol{\theta})$. $\mathcal{L}(\boldsymbol{\theta}) = f(\mathbf{y}|\boldsymbol{\theta})$ is termed the likelihood function, which attains its maximum at the maximum likelihood estimate (MLE) for $\boldsymbol{\theta}$. The MLE, which is equivalent to $\text{argmin}_{\boldsymbol{\theta}}(-\ln[\mathcal{L}(\boldsymbol{\theta})])$ improves

the numerical stability. The value of $\boldsymbol{\theta}$ is therefore determined by minimizing the negative log-likelihood:

$$-\ln\left[\mathcal{L}(\boldsymbol{\theta})\right] = \frac{1}{2}\mathbf{y}_M^T C_M^{-1}\mathbf{y}_M + \frac{1}{2}\ln|C_M| + \frac{M}{2}\ln 2\pi \tag{5.11}$$

5.2.4 Predicting a new output

Consider a test input $\mathbf{x}_*$, at which a predicted output is sought. Define $\mathbf{y}' = (\mathbf{y}, y_*)$, where $\mathbf{y}$ is the vector of observed outputs (targets). The corresponding random vector is $\mathbf{Y}' = (\mathbf{Y}, Y_*)$. One of the key properties of Gaussian distributions is that conditional distributions (over a subset of random variables Y_i) are also Gaussian. The conditional distribution of $\mathbf{Y}'$ is given by $\mathbf{Y}'|\boldsymbol{\theta} \sim \mathcal{N}(\mathbf{0}, C')$. The new covariance matrix C' is found by augmenting to the matrix C in 5.8, the extra terms arising from the inclusion of another data point $\mathbf{x}_*$:

$$C' = \begin{bmatrix} C & \mathbf{k} \\ \mathbf{k}^T & k_* \end{bmatrix} \tag{5.12}$$

where $\mathbf{k}$ is formed from the covariance between the test input $\mathbf{x}_*$ and the training input $\{\mathbf{x}^{(i)}\}_{i=1}^M$:

$$\begin{gathered} \mathbf{k} = (k(\mathbf{x}_*, \mathbf{x}^{(1)}), \ldots, k(\mathbf{x}_*, \mathbf{x}^{(M)}))^T \\ k_* = k(\mathbf{x}_*, \mathbf{x}_*) + \theta_{L+2} \end{gathered} \tag{5.13}$$

Having found the hyperparameters $\boldsymbol{\theta}$ we now need to find the conditional distribution of y_* given $\mathbf{y}$. The joint probability density function of $\mathbf{Y}'$ (with a zero mean vector) can be expressed using equation 5.1:

$$f(\mathbf{y}'|\boldsymbol{\theta}) = \frac{1}{\sqrt{(2\pi)^{M+1}|C'|}} \exp\left(-\frac{1}{2}\begin{bmatrix} \mathbf{y} \\ y_* \end{bmatrix}^T C'^{-1} \begin{bmatrix} \mathbf{y} \\ y_* \end{bmatrix}\right) \tag{5.14}$$

Using the Schur complement, $H = k_* - \mathbf{k}^T C^{-1}\mathbf{k}$, of the matrix C in the partitioned matrix

C', the covariance matrix C' may be expressed as:

$$C' = \begin{bmatrix} I_M & 0 \\ \mathbf{k}^T C^{-1} & 1 \end{bmatrix} \begin{bmatrix} C & 0 \\ 0 & H \end{bmatrix} \begin{bmatrix} I_M & C^{-1}\mathbf{k} \\ 0 & 1 \end{bmatrix} \tag{5.15}$$

and its inverse is given by:

$$C'^{-1} = \begin{bmatrix} I_M & -C^{-1}\mathbf{k} \\ 0 & 1 \end{bmatrix} \begin{bmatrix} C^{-1} & 0 \\ 0 & H^{-1} \end{bmatrix} \begin{bmatrix} I_M & 0 \\ -\mathbf{k}^T C^{-1} & 1 \end{bmatrix} \tag{5.16}$$

Substituting equation 5.16 into 5.14 and multiplying the outer triangular matrices we get:

$$f(\mathbf{y}'|\boldsymbol{\theta}) = Q \exp\left(-\frac{1}{2} \begin{bmatrix} \mathbf{y} \\ y_* - \mathbf{k}^T C^{-1}\mathbf{y} \end{bmatrix}^T \begin{bmatrix} C^{-1} & 0 \\ 0 & H^{-1} \end{bmatrix} \begin{bmatrix} \mathbf{y} \\ y_* - \mathbf{k}^T C^{-1}\mathbf{y} \end{bmatrix} \right) \tag{5.17}$$

Using the Schur complement, we may factor the determinant outside the exponential as: $|C'| = |C| \times |H|$. Therefore, $Q = \left[\sqrt{(2\pi)^{M+1}|C| \times |H|}\right]^{-1}$.

$$f(\mathbf{y}'|\boldsymbol{\theta}) = Q \exp\left[-\frac{1}{2}\mathbf{y}^T C^{-1}\mathbf{y}\right] \exp\left[-\frac{1}{2}\left(y_* - \mathbf{k}^T C^{-1}\mathbf{y}\right)^T H^{-1}\left(y_* - \mathbf{k}^T C^{-1}\mathbf{y}\right)\right] \tag{5.18}$$

Since the random variables Y_i are assumed conditionally independent given the hyper-paramters, then dividing the joint conditional probability of $\mathbf{y}'$ (given $\boldsymbol{\theta}$) by that of $\mathbf{y}$, we get the conditional probability of y_* given $\mathbf{y}$ and $\boldsymbol{\theta}$:

$$f(y_*|\mathbf{y}, \boldsymbol{\theta}) = \frac{f(\mathbf{y}'|\boldsymbol{\theta})}{f(\mathbf{y}|\boldsymbol{\theta})} = \frac{1}{\sqrt{2\pi|H|}} \exp\left[-\frac{1}{2}\left(y_* - \mathbf{k}^T C^{-1}\mathbf{y}\right)^T H^{-1}\left(y_* - \mathbf{k}^T C^{-1}\mathbf{y}\right)\right] \tag{5.19}$$

Thus, the mean of Y_* provides an estimate for y_* and variance of Y_* serves as a measure of the confidence in this prediction. It is clear that the expected value and covariance of the Gaussian distributed Y_* are:

$$\begin{aligned} \mu_* &= \mathbb{E}(Y_*) = \mathbf{k}^T C^{-1} \mathbf{y} \\ \sigma_*^2 &= k_* - \mathbf{k}^T C^{-1} \mathbf{k} \end{aligned} \tag{5.20}$$

5.2.5 Reduced-basis approach

Consider for now only a single target output, the cathodic overpotential profile, η_c. The inputs $\mathbf{x}'$ can contain any number of operating parameters. The following vector of input parameters is chosen:

$$\mathbf{x}' = (\boldsymbol{\zeta}, k_{\mathrm{OB}}, k_{\mathrm{BF}}, k_{\mathrm{F}}, k_{\mathrm{K}}, k_{\mathrm{GDH}}) \tag{5.21}$$

where $\boldsymbol{\zeta}$ represents a spatial coordinate that indexes the coefficients of η_c. The remaining 5 inputs represent rate constants for the reaction of: oxygen-bilirubin, bilirubin-ferricyanide, ferricyanide electron-transfer, VK3 electron-transfer, and glucose dehydrogenase (refer to chapter 3 for a detailed description).

For each set of input conditions, the outputs consist of the values of η_c at each of d equally-spaced spatial coordinates ζ_j, $j = 1, \ldots, d$. That is, a series of M vectors η_c, with d measurements in each. The aim of the reduced basis method is to eliminate the spatial dimension $\boldsymbol{\zeta}$ from the basic GPR method.

A modified set of inputs is defined as:

$$\mathbf{x}^{(i)} = (k_{\mathrm{OB}}^{(i)}, k_{\mathrm{BF}}^{(i)}, k_{\mathrm{F}}^{(i)}, k_{\mathrm{K}}^{(i)}, k_{\mathrm{GDH}}^{(i)}); \quad i = 1, \ldots, M \tag{5.22}$$

The profile of outputs can be considered as a function of the vector of design variables $\mathbf{x}$, indexed by ζ_j. The output vector containing the values of η_c at the values of $\boldsymbol{\zeta}$ is denoted $\mathbf{u} \in \mathbb{R}^d$. The given data contains M such vectors, $\mathbf{u}^{(i)}$, where $i = 1, \ldots, M$ signifies the sample number. The reduced basis methodology is to find an orthonormal basis

$\{\boldsymbol{\psi}_j\}_{j=1}^{d}$, $\boldsymbol{\psi}_j \in \mathbb{R}^d$, that can represent the known data set exactly, and accurately approximate η_c at new test inputs. To form a complete basis, we need exactly d such vectors. In the new basis, each $\mathbf{u}^{(i)}$ can be represented as a linear combination of those basis vectors:

$$\mathbf{u}^{(i)} = \sum_{j=1}^{d} \gamma_j^{(i)} \boldsymbol{\psi}_j \tag{5.23}$$

where the superscript $i = 1, \ldots, M$ in the coefficients $\gamma_j^{(i)}$ refers to the sample number. Since the basis vectors $\{\boldsymbol{\psi}_j\}_{j=1}^{d}$ are orthonormal ($\boldsymbol{\psi}_j^T \boldsymbol{\psi}_i = 1$ if $i = j$ and zero otherwise), then the coefficients $\gamma_j^{(i)}$ can be determined by taking the inner product of both sides of equation 5.23 with $\boldsymbol{\psi}_k$:

$$\boldsymbol{\psi}_k^T \mathbf{u}^{(i)} = \sum_{j=1}^{d} \gamma_j^{(i)} \boldsymbol{\psi}_j^T \boldsymbol{\psi}_k = \gamma_k^{(i)} \boldsymbol{\psi}_k^T \boldsymbol{\psi}_k = \gamma_k^{(i)} \tag{5.24}$$

The full expansion ($j = 1, \ldots, d$) of equation 5.23 is exact for each $\mathbf{u}^{(i)}$. With an optimal choice of basis vectors, and provided that these vectors are ordered in terms of the variance of the observed data along these directions, or, equivalently, that the coefficients $\gamma_j^{(i)}$ satisfy $\gamma_1^{(i)} \geq \gamma_2^{(i)} \geq \ldots \gamma_d^{(i)}$ for each i, then we may truncate expansion 5.23 to the first $j = 1, \ldots, J$ terms. By using this approximation, and performing GPR on the coefficients $\gamma_j^{(i)}$ ($j = 1, \ldots, J$), the number of inputs to the GPR are therefore reduced from $M \times d$ to $M \times J$ using the reduced basis method. This can be interpreted as projecting the vectors $\mathbf{u}^{(i)}$ onto a low dimensional subspace, or finding the directions (principal components $\{\boldsymbol{\psi}_j\}_{j=1}^{J}$) along which the data $\mathbf{u}^{(i)}$ exhibits the greatest variance. The validity of truncating the expansion should of course be checked as discussed below.

For a new input $\mathbf{x}_*$, the predicted output is then approximated by:

$$\mathbf{u}_* \approx \sum_{j=1}^{J} \gamma_j(\mathbf{x}_*) \boldsymbol{\psi}_j \tag{5.25}$$

where $\gamma_j(\mathbf{x}_*)$ is the GPR prediction of the coefficient corresponding to the j^{th} basis vector.

This ordered set of basis vectors with the desired properties can be found by singular value decomposition (SVD) of the data matrix $\mathcal{D}$:

$$\mathcal{D} = \left[\mathbf{u}^{(1)}, \mathbf{u}^{(2)}, \ldots, \mathbf{u}^{(M)}\right]^T \in \mathbb{R}^{M \times d} \tag{5.26}$$

The SVD of the data matrix $\mathcal{D}$ can be expressed as follows:

$$\mathcal{D} = USV^T \tag{5.27}$$

where $U \in \mathbb{R}^{M \times M}$ and $V \in \mathbb{R}^{d \times d}$ are orthogonal matrices, the columns of which are referred too as the left and right 'singular vectors' of $\mathcal{D}$ respectively. The columns of V provide the required basis vectors $\{\boldsymbol{\psi}_j\}_{j=1}^{d}$ for the expansion 5.23. $S \in \mathbb{R}^{M \times d}$ is a diagonal matrix, with $q = \min(M, d)$ non-negative diagonal elements s_i (referred to as 'singular values') that are arranged in decreasing order.

The squares of the diagonal elements (s_j^2) are eigenvalues of $\mathcal{D}^T\mathcal{D}$, and are sometimes referred to as 'energies'. One measure of the information contained in the first J terms in relation to the total information contained in the data set is given by the 'modal energy':

$$E(J) = \frac{\sum_{i=1}^{J} s_i^2}{\sum_{i=1}^{d} s_i^2} \tag{5.28}$$

Provided that the modal energy decays rapidly as a function of J, i.e. that $E(J)$ rapidly approaches 1, then the first J column vectors of V may be used to obtain the reduced-order approximations of the data (equation 5.24).

Essentially, the data $\mathbf{u}^{(i)},\ i = 1, \ldots, M$, is replaced with an equivalent set of 'data' $\gamma_j^{(i)},\ i = 1, \ldots, M,\ j = 1, \ldots, J$ corresponding to the coefficients in the new basis. The coefficients are first centred by subtracting the mean vector over the sample number, $\overline{\gamma_j} = (1/M)\sum_{i=1}^{M} \gamma_j^{(i)}$:

$$\hat{\gamma}_j^{(i)} = \gamma_j^{(i)} - \overline{\gamma_j} \tag{5.29}$$

One-dimensional GPR is then performed on the data sets $\{\hat{\gamma}_j^{(i)}, \mathbf{x}^{(i)}\}_{i=1}^{M}$, separately for each $j \leq J$. The outputs of the GPR are the expected value of the centred coefficients at the new input, $\hat{\gamma}_j(\mathbf{x}_*)$, and the variance, $\sigma_{\gamma_j}^2$. Restoring the un-centred coefficient, $\gamma_j(\mathbf{x}_*)$, the expected value of the target out, $\mathbf{u}_*$, is then found using equation 5.25.

Let u_*^n and ψ_j^n be the n^{th} component of the target output vector $\mathbf{u}_*$ and the j^{th} basis vector $\boldsymbol{\psi}_j$ respectively. Since the individual random variables, $\gamma_j(\mathbf{x}_*)\psi_j^n$, $j = 1, \ldots, J$, are assumed uncorrelated, then the variance at each individual element, n, of $\mathbf{u}_*$ is:

$$\text{Var}[u_*^n] \approx \sum_{j=1}^{J} \text{Var}\left[\gamma_j(\mathbf{x}_*)\psi_j^n\right] \tag{5.30}$$

By virtue of the property of variance in relation to multiplication by a constant, this may be expressed as:

$$\text{Var}[u_*^n] \approx \sum_{j=1}^{J} \left(\psi_j^n\right)^2 \text{Var}\left[\gamma_j(\mathbf{x}_*)\right] \tag{5.31}$$

The variance of the target output, $\sigma_{\mathbf{u}_*}^2$, may then be expressed in terms of the variance of the coefficients $\sigma_{\gamma_j}^2$ obtained from the GPR as:

$$\sigma_{\mathbf{u}_*}^2 \approx \sum_{j=1}^{J} \sigma_{\gamma_j}^2 (\boldsymbol{\psi}_j \circ \boldsymbol{\psi}_j) \tag{5.32}$$

where the symbol $\circ$ is used to denote the element-wise multiplication of the coefficients of $\boldsymbol{\psi}_j \in \mathbb{R}^d$.

Summary of the reduced basis GPR

The reduced basis GPR technique presented above can be summarised in the following procedure:

1. Construct the data matrix $\mathcal{D}$, in which the rows contain the vectors of outputs $\mathbf{u}^{(i)}$ (5.26).

2. Perform SVD on the data matrix $\mathcal{D}$ (5.27). The columns of V are the basis vectors ψ_j.

3. Choose an appropriate number of principal components (J basis vectors) based on the modal energy (5.28).

4. For the first J basis vectors, find the corresponding coefficients $\{\gamma_j^{(i)}\}_{j=1}^{J}$ (5.24).

5. After centring the coefficients (5.29), perform GPR on the reduced basis training set $\{\hat{\gamma}_j^{(i)}, \mathbf{x}^{(i)}\}$ for each $j \leq J$:

   5.1. Assume an initial value for the hyperparameters $\boldsymbol{\theta}$ and construct the covariance matrix C (5.8).

   5.2. Using the matrix C and and the targets $\hat{\gamma}_j^{(i)}$, find the MLE estimate for $\boldsymbol{\theta}$ (5.11).

   5.3. Recalculate the covariance matrix C with the new values of $\boldsymbol{\theta}$.

   5.4. For a new test input $\mathbf{x}_*$, calculate the augmented covariance matrix C' (5.12).

   5.5. Calculate the predicted estimate of the coefficient, $\hat{\gamma}_j(\mathbf{x}_*)$, and corresponding variance, $\sigma^2_{\gamma_j}$ (5.20).

6. Find the expected value, $\mathbf{u}_*$, and variance, $\sigma^2_{\mathbf{u}_*}$ (5.25 and 5.32).

5.3 Results and discussion

Simulations from the model developed in Chapter 3 are used here in the application of the reduced-basis GPR framework described above. The data set consists of a series of M output vectors which are a function of the vector of design variables $\mathbf{x}$ (5.22). The outputs can be of any dimension (*e.g.* 3 dimensional spatial profiles). To avoid confusion, the symbol $\boldsymbol{\zeta}$ is used here to represent the x-location in the cathode, $x_1 \leq x \leq x_2$, at $y = L/2$ (see Figure 3.1).

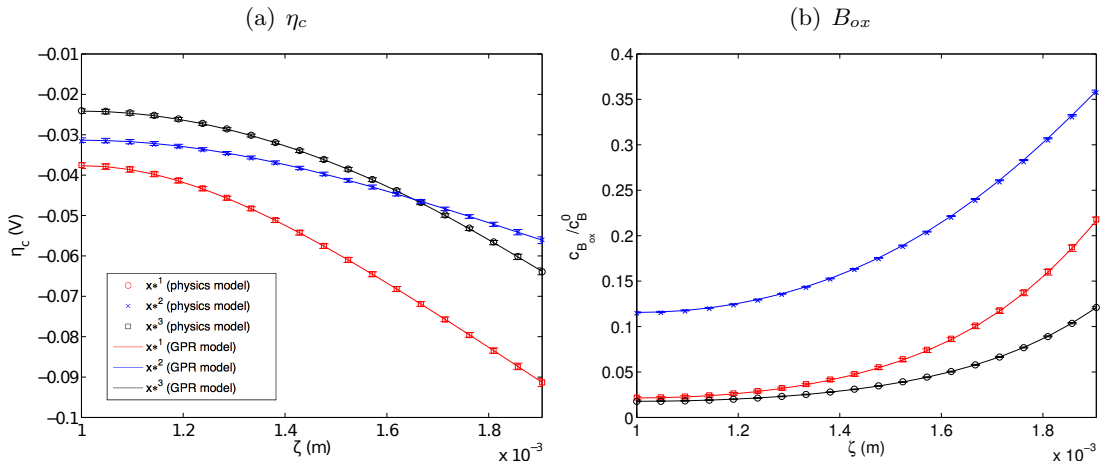

Figure 5.1: Comparison of the cathodic profiles of (a) η_c and (b) B_{ox} from GPR predictions (solid lines with $\pm\sigma$ error bars), with the expected values from the physical model simulations (markers) at 3 different test inputs using a training data set of $M = 70$ samples, and approximated using $J = 3$ principal components.

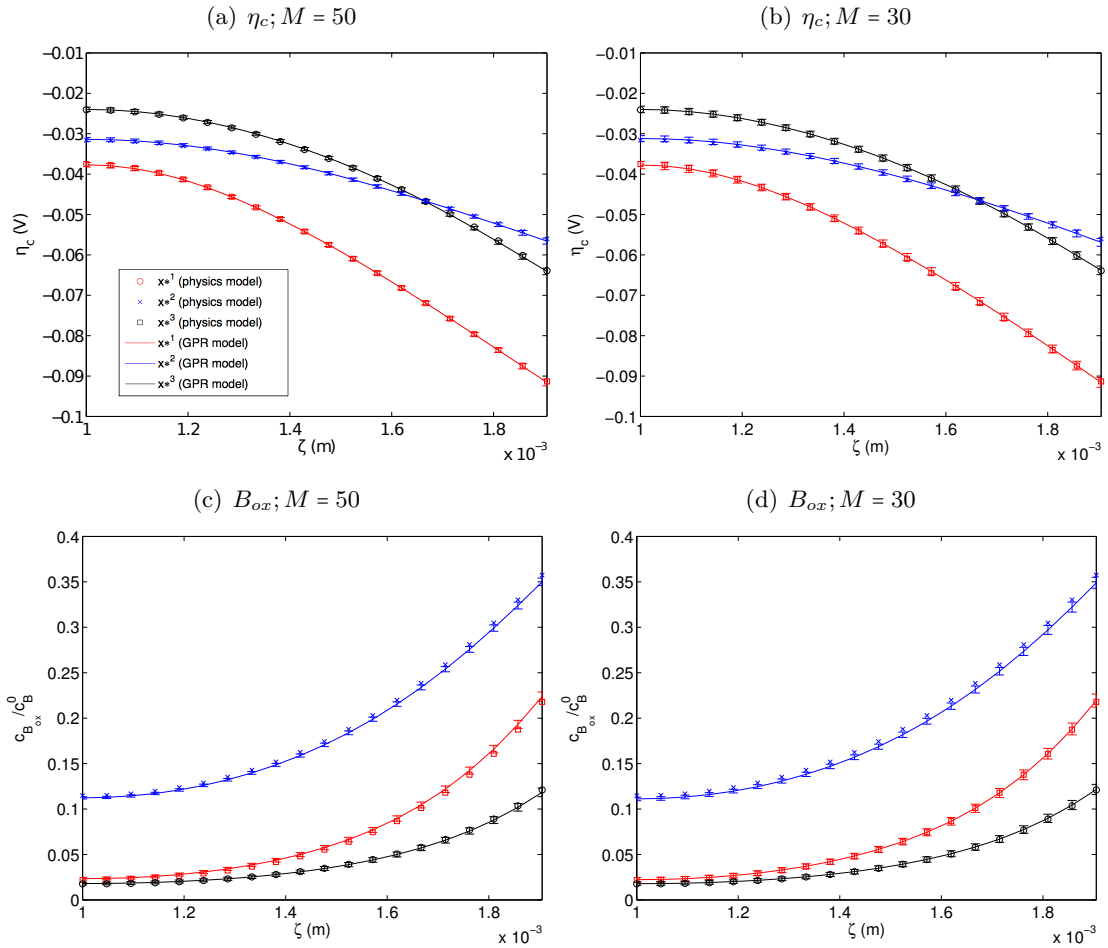

Figure 5.2: Effect of the number of training points, M, on the accuracy of the GPR model, using $J = 3$ principal components. Expected values from the physical model are shown in markers and GPR out in solid lines with error bars

The steady-state simulation results were obtained using potentiostatic operation at V_{cell} = 0.15 V. The outputs examined are the profiles of: the cathodic overpotential, η_c, and the oxidized mole fraction of enzyme, $B_{ox} = c_{B_{ox}}/c_B^0$ at equally spaced coordinates. Three different test inputs were used to compare the GPR model results to those of the physical model. For the first input the values of the parameters were; $\mathbf{x}_*^{\mathbf{1}} = [k_{\mathrm{OB}} = 205\ \mathrm{s}^{-1}, k_{\mathrm{BF}} = 205\ \mathrm{s}^{-1}, k_{\mathrm{F}} = 5.5 \times 10^{-7}\ \mathrm{m\ s}^{-1}, k_{\mathrm{K}} = 2.9 \times 10^{-8}\ \mathrm{m\ s}^{-1}, k_{\mathrm{GDH}} = 0.8\ \mathrm{mol\ m}^{-3}\ \mathrm{s}^{-1}]$. Similarly, the parameter values for the remaining two test inputs are; $\mathbf{x}_*^{\mathbf{2}} = [89\ \mathrm{s}^{-1}, 406\ \mathrm{s}^{-1}, 1.24 \times 10^{-6}\ \mathrm{m\ s}^{-1}, 7.8{\times}10^{-8}\ \mathrm{m\ s}^{-1}, 0.3\ \mathrm{mol\ m}^{-3}\ \mathrm{s}^{-1}]$ and $\mathbf{x}_*^{\mathbf{3}} = [519\ \mathrm{s}^{-1}, 491\ \mathrm{s}^{-1}, 9.5{\times}10^{-7}\ \mathrm{m\ s}^{-1}, 3.92{\times}10^{-8}\ \mathrm{m\ s}^{-1}, 0.89\ \mathrm{mol\ m}^{-3}\ \mathrm{s}^{-1}]$. Figure 5.1 compares the predicted outputs from the GPR model to those expected from the physical model at these 3 different test inputs. Results show a high degree of accuracy of the GPR model for all three test inputs.

The GPR results of Figure 5.1 were obtained using a training data set of M = 70 samples. Figure 5.2 shows a comparison at the same test inputs using a reduced data set. The overall response, as expected, is a slightly lower precision with smaller sample sizes. With 50 training samples, the GPR exhibits excellent accuracy. Even when the number of samples is reduced to 30, the the regression model functions reasonably well considering that the number of independent input variables is 5.

The results presented so far used an approximation of J = 3 principal components for reducing the dimensionality of the profiles $\mathbf{u} \in \mathbb{R}^{20}$. This choice was based on the fast decay in the modal energy (equation 5.28) whose value for the third principal component is greater than 99.99% for both outputs. Figure 5.3 shows the predicted GPR output using different approximations for the reduced basis method. At J = 2 basis vectors, the output is almost exactly the same as using 3 bases (Figure 5.1). The reason for the negligible change is that the increase in the modal energy from the second to the third basis is approximetly 0.01% and 0.1% for the η_c and B_{ox} outputs respectively. When the profile of outputs are projected onto a single dimension (J = 1), the regression model is unable to capture the exact shapes of the curves, and the outputs at different test inputs appear to have the same form but with different scaling factors.

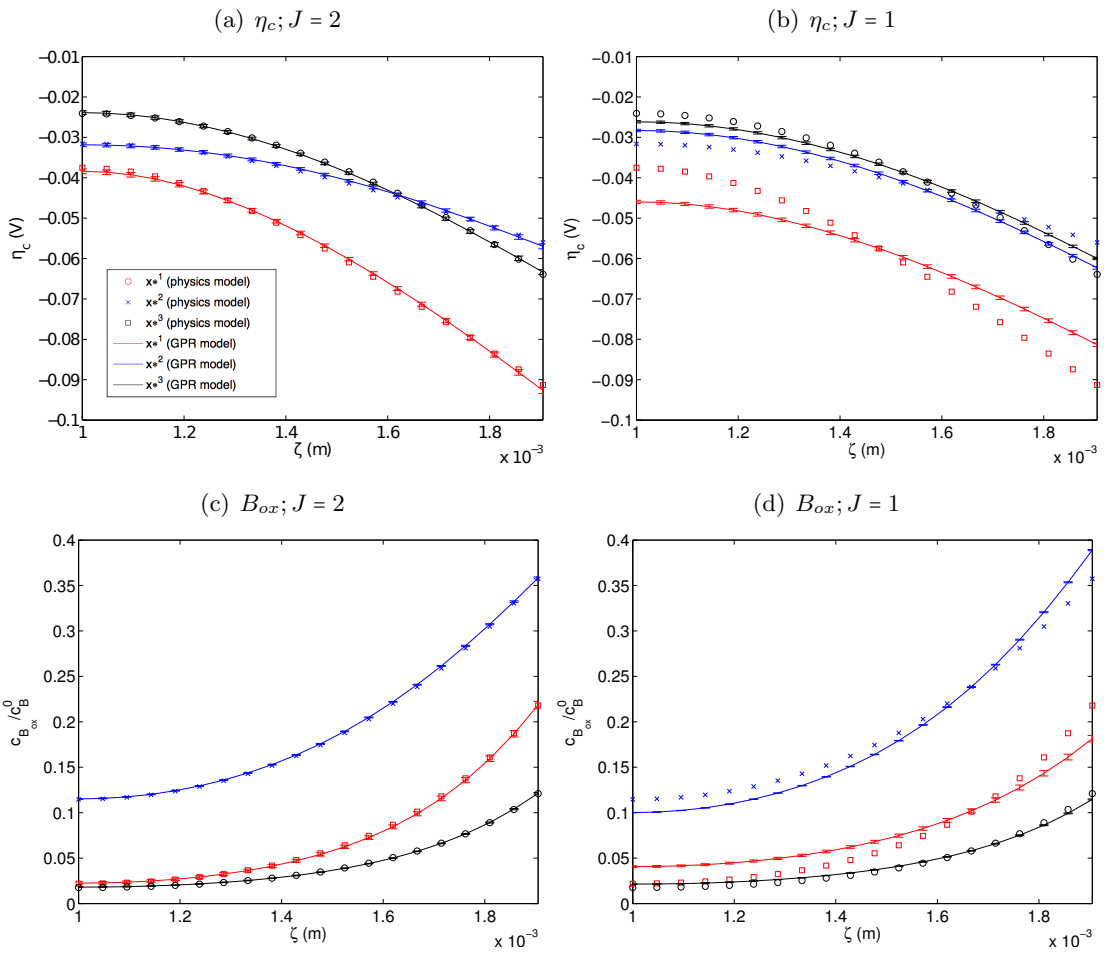

Figure 5.3: Effect of the number of principal components J in the reduced-basis approximation using $M = 70$ samples.

5.4 Conclusion

In this chapter a data-driven regression model was presented. The model is based on the method of Gaussian process regression combined with a principal component analysis for dimensionality reduction. The model was tested on simulation results of cathodic profiles but may also be used to model fuel cell polarisation curves. Results show that the method presented here has a high degree of accuracy even with relatively small training data-sets.

The improved computational efficiency over the physical model make this method a better candidate for modelling large complex systems, or for other purposes such as optimization. To optimize with respect to a large number of design variables would require extremely long computational times when using full multi-dimensional transient models. In such

cases, a surrogate model would be beneficial and optimal.

Chapter 6

Conclusions

While previous research was mainly targeted at developing the enzyme chemistries [3], the past 5 years can be marked by efforts to develop new methods and materials for integrated enzyme electrodes that maximize enzyme loading and move from the classic two-dimensional loading to highly ordered three dimensional structures with improved enzyme stabilization [75]. A vital aspect of bio-fuel cell performance and stability is the immobilization of the enzyme/mediator on the electrode. Maintaining a continuous supply of fuel to the active sites and ensuring an efficient electron-transfer process from the enzyme/bacteria to the electrode via the mediator are crucial.

Electrode materials need to be more catalytic while maintaining their performance, particularly in the face of problems caused by fouling of the active surfaces and loss of enzyme activity. A greater understanding and characterisation of the reaction environment can be achieved through studies of the reactant and charge distribution, mass transport and mass transfer, as well as the bio-electrochemical reaction kinetics. Carefully validated models can be used in conjunction with laboratory studies to investigate these processes (particularly *in situ* and to accelerate the development of practical systems.

Developments in the overall system design have also led to more efficient systems. From an engineering perspective, cells with chemistries that allow single-compartment operation

and possess constructional simplicity would be highly advantageous. It is important that low-cost, modular and scalable designs are developed, particularly if they are to form the basis for multi-plate (*e.g.* bipolar) cell stacks. Cell construction has been improved to optimise the cell voltage through comprehensive modelling/experimental studies of the electrode overpotentials and all cell resistances.

Power densities have rapidly increased in the last few years to a few W m^{-2} and over 1 kW m^{-3} (of reactor volume). Despite the rapid progress in bio-fuel cells, cost-effective, environmentally friendly modular designs are still some way from being realised. For many proposed applications, however, further substantial improvements in performance are required (higher power densities and energy efficiencies). One promising application for the near future is domestic or industrial wastewater treatment/electricity production.

It is important that mathematical models are developed to reduce the burden on laboratory-based design, testing and characterization. In many cases, particularly for *in situ* operation, local information about the distributions of charge, potentials and concentrations can only be gained from detailed and rigorously-validated models. This fundamental insight into the reaction environment together with global information such as the power output would enable the characterization of the limiting processes in different cell designs and/or under different operating conditions. In addition to investigating systems at the cell level, models can also be used to study half-cell or electrode subsystems. This is particularly useful in identifying the separate contribution of each electrode in the whole-cell.

The application of numerical modelling in studying biofuel cells is rare in the literature, especially on a whole system level. Mathematical approaches have been mainly limited to approximate steady-state analytical solutions [52, 53]. To date, only a small number of models have been developed, which, with a few exceptions [55, 57, 58], are highly simplified and neglect crucial features such as transient performance, spatial non-uniformities, conductive losses, potential profiles and ion migration.

The physical modelling framework presented in Chapters 3 and 4 can be easily adapted to other enzymatic or microbial systems. Comparisons to experimental data have demon-

strated that the model is able to capture the complex physical and bio-electrochemical phenomena within the cell to a good degree of accuracy. The simulations presented have revealed details regarding the spatial and temporal behaviour of the cell. With the availability of rate constants and other measurable parameters, the methodology can provide more accurate predictions.

The main drawback of the system modelled in Chapter 3 is the rapid drop in the power output which is due to limitations in the mass transport of protons to the cathode. Provided that proton transport limitations can be resolved this setup proves very promising as a template for future biofuel cell designs that will achieve power outputs of several mW cm^{-2} using only biological catalysts. By including detailed kinetics of the enzyme-mediator reactions, a potential improvement was identified. Results have shown that substituting the anodic mediator for one with a lower equilibrium potential that is closer to that of the enzyme would increase power output.

The overall performance of the system modelled in Chapter 4 is strongly influenced by the reduced enzyme fraction in the vicinity of the membrane and the diffusion limitation associated with the mediator. Due to the higher ionic conductivity of the Nafion membrane compared to that of the unbuffered solution, the anodic reaction is confined to a very thin region near the membrane. The use of a diffusional redox couple allows the biological reaction to recycle the mediator throughout the anode even though the electron transfer reaction is restricted to a small region.

The strong influence of the reduced enzyme fraction can also be seen from a parametric study on the solution pH which affects the rates of enzyme reduction and oxidation. The cell performance is more strongly dependant on the enzyme reduction reaction than the oxidation reaction with the mediator. A parametric study of the enzyme concentration was also performed in Chapter 4. Results demonstrated an optimal value of the enzyme loading beyond which the cell is limited electrochemically by the excess amount of reduced mediator due to higher enzyme concentration. These valuable investigations can only be performed with detailed kinetic models that properly capture the dynamics of the enzymatic reactions by treating the two reactions separately and explicitly in terms of the

reduced and oxidized states of the enzyme. This is necessary if competing side reactions are to be included (see Chapter 4 for an example of the effect of dissolved oxygen as an electron acceptor competing with the mediator).

Clearly, this is just the beginning for physics-based modelling of biofuel cells. More work needs to be done to validate models, which requires more fundamental characterisation of cells under different conditions and designs, but this work has shown that a framework for modelling biofuel cells is feasible and valuable.

For some purposes, a data-driven approach may be more appropriate, especially for optimization, in which case the full multi-dimensional and transient models are too computationally intensive. To optimize with respect to a large number of design/operating variables would require extremely long computational times. In this case, data-driven surrogate models would be beneficial and optimal. They can also be used as standalone models for experimental data to inform experiments. The data-driven model presented in Chapter 5 is based on the method of Gaussian process regression combined with a principal component analysis for dimensionality reduction. Results show that the method presented here has a high degree of accuracy even with relatively small training data-sets.

Taking this work forward, there are many possibilities for further developments:

- Three-dimensional models looking at more realistic geometries (*e.g.*multi-plate cell stacks with fluid flow channels).
- Including a thermal balance in the model.
- Meso-scale models (*e.g.* lattice Boltzmann method and dissipative particle dynamics) to investigate flow in electrodes in detail in order to optimize flow geometries to avoid mass transport limitations and to avoid detachment of enzymes.
- Modelling other systems, especially microbial fuel cells.
- Optimization using surrogate models, *e.g.* genetic algorithm using surrogate model as a black-box function.

Bibliography

[1] Bagotsky, V. S. *Fuel Cells: Problems and Solutions*. John Wiley & Sons, New Jersey, 2009.

[2] Larminie, J. and Dicks, A. *Fuel cell systems explained*. John Wiley & Sons, 2003.

[3] Bullen, R. A., Arnot, T. C., Lakeman, J. B., and Walsh, F. C. *Biosens. Bioelectron.*, 21:2015–2045, 2006.

[4] Katz, E., Shipway, A. N., and Willner, I. chapter Biochemical fuel cells. John Wiley & Sons Ltd, 2003.

[5] Shukla, A. K., Suresh, P., Berchmans, S., and Rajendran, A. *Curr. Sci. Ind.*, 87(4): 455–468, August 2004.

[6] Pant, D., Van-Bogaert, G., Diels, L., and Vanbroekhoven, K. *Bioresour. Technol.*, 101:1533–1543, 2010.

[7] Lovley, D. R. *Curr. Opin. Biotech.*, 17:327–332, 2006.

[8] Baranov, I. E., Grigoriev, S. A., Ylitalo, D., Fateev, V. N., and Nikolaev, I. I. *International Journal of Hydrogen Energy*, 31:203–210, 2006.

[9] Dhathathreyan, K. S., Sridhar, P., Sasikumar, G., Ghosh, K. K., Velayutham, G., Rajalakshmi, N., Subramaniam, C., Raja, M., and Ramya, K. *International Journal of Hydrogen Energy*, 24:1107–1115, 1999.

[10] Passos, R. R., Paganin, V. A., and Ticianelli, E. A. *Electrochimica Acta*, 51:5239–5245, 2006.

[11] Jiao, K. and Zhou, B. *Journal of Power Sources*, 175:106–119, 2008.

[12] Bessel, C. A., Laubernds, K., Rodriguez, N. M., and Baker, R. T. K. *Journal of Physical Chemistry. B*, 105(6):1115–1118, 2001.

[13] Sopian, K. and Daud, W. R. W. *Renewable Energy*, 31:719–727, 2006.

[14] Sasaki, K., Wang, J. X., Balasubramanian, M., McBreen, J., Uribe, F., and Adzic, R. R. *Electrochimica Acta*, 49:3873–3877, 2004.

[15] Choi, K. H., Kim, H. S., and Lee, T. H. *Journal of Power Sources*, 75:230–235, 1998.

[16] Heo, P., Shibata, H., Nagao, M., and Hibino, T. *Solid State Ionics*, 179:1446–1449, 2008.

[17] The fuel cell industry review 2012, September 2012. Online: `http://www.fuelcelltoday.com/media/1713685/fct_review_2012.pdf` retrieved on: 5 Sep 2012.

[18] Song, C. *Catalysis Today*, 77:17–49, 2002.

[19] Arechederra, R. L., Boehm, K., and Minteer, S. D. *Electrochim. Acta*, 54:7268–7273, 2009.

[20] Arechederra, R. L. and Minteer, S. D. *Fuel Cell*, 9:63–69, 2009.

[21] Mohan, S. V., Raghavulu, S. V., and Sarma, P. N. *Biosens. Bioelectron.*, 24:41–47, 2008.

[22] Kim, B. H., Chang, I. S., and Gadd, G. M. *Appl. Microbiol. Bioetchnol.*, 76:485–494, 2007.

[23] Kim, J. R., Cheng, S., Eun Oh, S., and Logan, B. E. *Environ. Sci. Technol.*, 41: 1004–1009, 2007.

[24] Kim, J., Jia, H., and Wang, P. *Biotechnol. Adv.*, 24:296–308, 2006.

[25] Fishilevich, S., Amir, L., Fridman, Y., Aharoni, A., and Alfonta, L. *J. Am. Chem. Soc.*, 131:12052–12053, 2009.

[26] Boder, E. T. and Wittrup, K. D. *Nat. Biotechnol.*, 15:553–557, 1997.

[27] Clauwaert, P., Aelterman, P., Pham, T. H., De Schamphelaire, L., Carballa, M., Rabaey, K., and Verstraete, W. *Appl. Microbiol. Technol.*, 79:901–913, 2008.

[28] Liu, H., Cheng, S., and Logan, B. E. *Environ. Sci. Technol.*, 39:5488–5493, 2005.

[29] Kamitaka, Y., Tsujimura, S., Setoyama, N., Kajino, T., and Kano, K. *Phys. Chem. Chem. Phys.*, 9:1793–1801, 2007.

[30] Sucheta, A., Cammack, R., Weiner, J., and Armstrong, F. A. *Biochemistry*, 32: 5455–5465, 1993.

[31] Ghindilis, A. L., Atanassov, P., and Wilkins, E. *Electroanalysis*, 9:661–674, 1997.

[32] Ferapontova, E. E., Ruzgas, T., and Gorton, L. *Anal. Chem.*, 75:4841–4850, 2003.

[33] Tasca, F., Gorton, L., Harreither, W., Haltrich, D., Ludwig, R., and Nöll, G. *J. Phys. Chem. C*, 112:9956–9961, 2008.

[34] Ishikawa, M., Yamamura, S., Takamura, Y., Sode, K., Tamiya, E., and Tomiyama, M. *Int. J. Hydrogen Energy*, 31:1484–1489, 2006.

[35] Niessen, J., Schröder, U., Harnisch, F., and Scholz, F. *Lett. Appl. Microbiol.*, 41: 286–290, 2005.

[36] Ishii, S., Shimoyama, T., Hotta, Y., and Watanabe, K. *BMC Microbiol.*, 8(6): In–press, 2008.

[37] Watanabe, K. *J. Biosci. Bioeng.*, 106(6):528–536, 2008.

[38] Rabaey, K. and Verstraete, W. *Trends Biotechnol.*, 23(6):291–298, 2005.

[39] He, Z. and Angenent, L. T. *Electroanalysis*, 18(19-20):2009–2015, 2006.

[40] Liu, H., Grot, S., and Logan, B. E. *Environ. Sci. Technol.*, 39:4317–4320, 2005.

[41] Rozendal, R. A., Hamelers, H. V. M., and Euverink, G. J. W. *Int. J. Hydrogen Energy*, 31:1632–1640, 2006.

[42] Call, D. and Logan, B. E. *Environ. Sci. Technol.*, 42:3401–3406, 2008.

[43] Cheng, S., Xing, D., Call, D. F., and Logan, B. E. *Environ Sci. Technol.*, 43: 3953–3958, 2009.

[44] Cho, Y. K., Donohue, T. J., Tejedor, I., Anderson, M. A., McMahon, K. D., and Noguera, D. R. *J. Appl. Microbiol.*, 104:640–650, 2008.

[45] Rosenbaum, M., Schroöder, U., and Scholz, F. *Environ. Sci. Technol.*, 39:6328–6333, 2005.

[46] Furukawa, Y., Moriuchi, T., and Morishima, K. *J. Micromech. Microeng.*, 16:S220–S225, 2006.

[47] Cao, X., Huang, X., Boon, N., Liang, P., and Fan, M. *Electrochem. Commun.*, 10: 1392–1395, 2008.

[48] He, Z., Kan, J., Mansfeld, F., Angenent, L. T., and Nealson, K. H. *Environ. Sci. Technol.*, 43:1648–1654, 2009.

[49] Sakai, H., Nakagawa, T., Tokita, Y., Hatazawa, T., Ikeda, T., Tsujimura, S., and Kano, K. *Energy & Environ. Sci.*, 2:133–138, 2009.

[50] Sakai, H., Nakagawa, T., Tokita, Y., Hatazawa, T., Ikeda, T., Tsujimura, S., and Kano, K. *Energy Environ. Sci.*, 2:133–138, 2009.

[51] Bartlett, P. N., editor. *Bioelectrochemistry*. John Wiley & Sons, Ltd, 2008.

[52] Ivanov, I., Vidakovi-Koch, T., and Sundmacher, K. *Energies*, 3:803–846, 2010.

[53] Bartlett, P. N., Toh, C. S., Calvo, E. J., and Flexer, V. chapter Modelling Biosensor Responses, pages 267–326. Wiley, 2008.

[54] Tamaki, T., Ito, T., and Yamaguchi, T. *Fuel Cell*, 9:37–43, 2009.

[55] Picioreanu, C., van Loosdrecht, M. C. M., Curtis, T. P., and Keith, S. *Bioelectroch.*, 78:8–24, 2010.

[56] Picioreanu, C., Katuri, K. P., van Loosdrecht, M. C. M., Head, I. M., and Scot, K. *J. Appl. Electrochem.*, 40:151–162, 2010.

[57] Picioreanu, C., Head, I. M., Katuri, K. P., van Loosdrecht, M. C. M., and Scott, K. *Water Res.*, 41:2921–2940, 2007.

[58] Bedekar, A. S., Feng, J. J., Krishnamoorthy, S., Lim, K. G., Palmore, G. T. R., and Sundaram, S. *Chem. Eng. Comm.*, 195:256–266, 2008.

[59] Kjeang, E., Sinton, D., and Harrington, D. A. *J. Power Sources*, 158:1–12, 2006.

[60] Kar, P., Wen, H., Li, H., Minteer, S. D., and Calabrese-Barton, S. *J. Electrochem. Soc.*, 158(5):B580–586, 2011.

[61] Martens, N. and Hall, E. A. *Anal. Chem.*, 66(17):2763–2770, 1994.

[62] Shah, A. A., Kim, G. S., Gervais, W., Young, A., Promislow, K., Li, J., and Ye, S. *J. Power Sources*, 160:1251–1268, 2006.

[63] Shah, A. A., Kim, G. S., Sui, P. C., and Harvey, D. *J. Power Sources*, 163:793–806, 2007.

[64] Shah, A. A., Ralph, T. R., and Walsh, F. C. *J. Electrochem. Soc.*, 156:B465–B484, 2009.

[65] Fischback, M. B., Youn, J. K., Zhao, X., Wang, P., Park, H. G., Chang, H. N., Kim, J., and Ha, S. *Electroanalysis*, 18:2016–2022, 2006.

[66] Davis, F. and Higson, S. P. J. *Biosens. Bioelectron.*, 22:1224–1235, 2007.

[67] Logan, B. E., Hamelers, B., Rozendal, R., Schröder, U., Keller, J., Freguia, S., Aelterman, P., Verstraete, W., and Rabaey, K. *Environ. Sci. Technol.*, 40(17):5181–5192, 2006.

[68] Logan, B. E. *Appl. Microbiol. Biotechnol.*, 85:1665–1671, 2010.

[69] Logan, B. E. *Nat. Rev. Microbiol.*, 7:375–381, 2009.

[70] Lovley, D. R. *Curr. Opin. Bioech.*, 19:564–571, 2008.

[71] Cooney, M. J., Svoboda, V., Lau, C., Martin, G., and Minteer, S. D. *Energy Environ. Sci.*, 1:320–337, 2008.

[72] Willner, I., Yan, Y. M., Willner, B., and Tel-Vered, R. *Fuel Cell*, 9(1):7–24, 2009.

[73] Zayats, M., Willner, B., and Willner, I. *Electroanalysis*, 20:583–601, 2008.

[74] Sarma, A. K., Vatsyayan, P., Goswami, P., and Minteer, S. D. *Biosens. Bioelectron.*, 24:2313–2322, 2009.

[75] Kim, J., Grate, J. W., and Wang, P. *Trends Bioechnol.*, 26:639–646, 2008.

[76] Kjeang, E., Djilali, N., and Sinton, D. *J. Power Sources*, 186:353–369, 2009.

[77] Katz, E. *Electroanalysis*, In-press, 2009.

[78] Heller, A. *J. Phys. Chem.-US*, 96:3579–3587, 1992.

[79] Xiao, Y., Patolsky, F., Katz, E., Hainfeld, J. F., and Willner, I. *Science*, 21:1877–1881, 2003.

[80] Zayats, M., Katz, E., and Willner, I. *J. Am. Chem. Soc.*, 127:12400–12406, 2005.

[81] Cai, C. and Chen, J. *Anal. Biochem.*, 332:75–83, 2004.

[82] Patolsky, F., Weizmann, Y., and Willner, I. *Ang. Chem.*, 43:2113–2117, 2004.

[83] Solomon, E. I., Sundaram, U. M., and Machonkin, T. E. *Chem. Rev.*, 96:2563–2606, 1996.

[84] Chen, T., Calabrese-Barton, S., Binyamin, G., Gao, Z., Zhang, Y., Kim, H. H., and Heller, A. *J. Am. Chem. Soc.*, 123:8630–8631, 2001.

[85] Mano, N., Fernandez, J. L., Kim, Y., Shin, W., Bard, A. J., and Heller, A. *J. Am. Chem. Soc.*, 125:15290–15291, 2003.

[86] Willner, I., Arad, G., and Katz, E. *Bioelectrochem. Bioener.*, 44:209–214, 1998.

[87] Katz, E., Willner, I., and Kolyar, A. B. *J. Electroanal. Chem.*, 479:64–68, 1999.

[88] Pizzariello, A., Stredansky, M., and Miertus, S. *Bioelectrochemistry*, 56:99–105, 2002.

[89] Tischer, W. and Wedekind, F. chapter Immobilized Enzymes: Methods and Applications, pages 95–126. Springer-Verlag, 2000.

[90] Cao, L. *Curr. Opin. Biotechnol.*, 9:217–226, 2005.

[91] Moehlenbrock, M. J. and Minteer, S. D. *Chem. Soc. Rev.*, 37:1188–1196, 2008.

[92] Sheldon, R. A. *Adv. Synth. Catal.*, 349:1289–1307, 2007.

[93] Kandimalla, V. B., Tripathi, V. S., and Ju, H. X. *Crit. Rev. Anal. Chem.*, 36:73–106, 2006.

[94] Gregg, B. A. and Heller, A. *J. Phys. Chem.*, 95:5970–5975, 1991.

[95] Mao, F., Mano, N., and Heller, A. *J. Am. Chem. Soc.*, 125:4951–4957, 2003.

[96] Coman, V., Vaz-Domínguez, C., Ludwig, R., Harreither, W., Haltrich, D., DeLacey, A. L., Ruzgas, T., Gorton, L., and Shleev, S. *Phys. Chem. Chem. Phys.*, 10:6093–6096, 2008.

[97] Katz, E., Lioubashevski, O., and Willner, I. *Am. Chem. Soc.*, 127:3979–3988, 2005.

[98] Miyake, T., Oike, M., Yoshino, S., Yatagawa, Y., Haneda, K., Kaji, H., and Nishizawa, M. *Chem. Phys Lett.*, 480:123–126, 2009.

[99] Calabrese-Barton, S. A., Gallaway, J. W., and Atanassov, P. *Chem. Rev.*, 104: 4867–4886, 2004.

[100] Binyamin, G. and Heller, A. *J. Electrochem. Soc.*, 146:2965–2967, 1999.

[101] Boland, S., Jenkins, P., Kavanagh, P., and Leech, D. *J. Electroanal. Chem.*, 626: 111–115, 2009.

[102] Lehr, J., Williamson, B. E., Barrière, F., and Downward, A. J. *Bioelectrochemistry*, 79:142–146, 2010.

[103] Treu, B. L. and Minteer, S. D. *Bioelectroch.*, 74:73–77, 2008.

[104] Khani, Z., Jolivalt, C., Cretin, M., Tingry, S., and Innocent, C. *Biotechnol. Lett.*, 28:1779–1786, 2006.

[105] Mano, N., Mao, F., and Heller, A. *J. Elecrtoanal. Chem.*, 574:347–357, 2005.

[106] Mano, N. *Chem. Commun.*, pages 2221–2223, 2008.

[107] Gao, F., Courjean, O., and Mano, N. *Biosens. Bioelectron.*, 25:356–361, 2009.

[108] Calabrese-Barton, S., Kim, H. H., Binyamin, G., Zhang, Y. C., and Heller, A. *J. Am. Chem. Soc.*, 123:5802–5803, 2001.

[109] Soukharev, V., Mano, N., and Heller, A. *J. Am. Chem. Soc.*, 126:8368–8369, 2004.

[110] Barrière, F., Ferry, Y., Rochefort, D., and Leech, D. *Electrochem. Commun.*, 237: 237–241, 2004.

[111] Gallaway, J. W. and Calabrese-Barton, S. A. *J. Am. Chem. Soc.*, 130:8527–8536, 2008.

[112] Mano, N., Kim, H. H., Zhang, Y. C., and Heller, A. *J. Am. Chem. Soc.*, 124: 6480–6486, 2002.

[113] Mano, N., Mao, F., and Heller, A. *J. Am. Chem. Soc.*, 124:12962–12963, 2002.

[114] Heller, A. *Phys. Chem. Chem. Phys.*, 6:209–216, 2004.

[115] Heller, A. *Curr. Opin. Chem. Biol.*, 10:664–672, 2006.

[116] Kavanagh, P., Boland, S., Jenkins, P., and Leech, D. *Fuel Cell*, 9:79–84, 2009.

[117] Stoica, L., Dimcheva, N., Ackermann, Y., Karnicka, K., Guschin, D. A., Kulesza, P. J., Rogalski, J., Haltrich, D., Ludwig, R., Gorton, L., and Schuhmann, W. *Fuel Cell*, 9:53–62, 2009.

[118] Kim, H. H., Mano, N., Zhang, Y., and Heller, A. *J. Electrochem. Soc.*, 150:209–213, 2003.

[119] Kuwahara, T., Homma, T., Kondo, M., and Shimomura, M. *Synth. Met.*, 159: 1859–1864, 2009.

[120] Brunel, L., Denele, J., Servat, K., Kokoh, K. B., Jolivalt, C., Innocent, C., Cretin, M., Rolland, M., and Tingry, S. *Electrochem. Commun.*, 9:331–336, 2007.

[121] Tamaki, T. and Yamaguchi, T. *Ind. Eng. Chem. Res.*, 45:3050–3058, 2006.

[122] Tamaki, T., Ito, T., and Yamaguchi, T. *J. Phys. Chem. B*, 111:10312–10319, 2007.

[123] Wang, D. and Chen, L. *Electrochim. Acta*, 54:4316–4320, 2009.

[124] Lim, J., Malati, P., Bonet, F., and Dunn, B. *Electrochem. Soc.*, 154(2):A140–A145, 2007.

[125] Tsujimura, S., Kano, K., and Ikeda, T. *J. Electroanal. Chem.*, 576:113–120, 2005.

[126] Lin, J. and Brown, C. W. *Trends Anal. Chem.*, 16:200–211, 1997.

[127] Wang, J. *Anal. Chim. Acta*, 399:21–27, 1999.

[128] Kim, J., Kim, S. I., and Hwa Yoo, K. *Biosens. Bioelectron.*, 25:350–355, 2009.

[129] Gooding, J. J. and Hibbert, D. B. *Trac-Trend Anal. Chem.*, 18:525–533, 1999.

[130] Dubois, L. H. and Nuzzo, R. G. *Ann. Rev. Phys. Chem.*, 43:437–463, 1992.

[131] Schoenfisch, M. H. and Pemberton, J. E. *J. Am. Chem. Soc.*, 120:4502–4513, 1998.

[132] Delamarche, E., Michel, B., Kang, H., and Gerber, C. *Langmuir*, 10:4103–4108, 1994.

[133] Gooding, J. J., Mearns, F., Yang, W., and Liu, J. *Electroanalysis*, 15:81–96, 2003.

[134] Allongue, P., Delamar, M., Desbat, B., Fagebaume, O., Hitmi, R., Pinson, J., and Savéant, J. M. *J. Am. Chem. Soc.*, 119:201–207, 1997.

[135] Saby, C., Ortiz, B., Champagne, G. Y., and Bélanger, D. *Langmuir*, 13:6805–6813, 1997.

[136] Kariuki, J. K. and McDermott, M. T. *Langmuir*, 17:5947–5951, 2001.

[137] Brooksby, P. A. and Downward, A. J. *Langmuir*, 20:5038–5045, 2004.

[138] Pellissier, M., Barrière, F. ., Downward, A. J., and Leech, D. *Electrochem. Commun.*, 10:835–838, 2008.

[139] Boland, S., Foster, K., and Leech, D. *Electrochim. Acta*, 54:1986–1991, 2009.

[140] Lee, J. Y., Shin, H. Y., Lee, J. H., Song, Y. S., Kang, S. W., Park, C., Kim, J. B., and Kim, S. W. *J. Mol. Catal. B:Enzym.*, 59:274–278, 2009.

[141] Zebda, A., Renaud, L., Cretin, M., Pichot, F., Innocent, C., Ferrigno, R., and Tingry, S. *Electrochem. Commun.*, 11:592–595, 2009.

[142] Katz, E., Filanovsky, B., and Willner, I. *New J. Chem.*, 23(5):481–487, 1999.

[143] Willner, I., Heleg-Shabtai, V., Blonder, R., Katz, E., and Tao, G. *J. Am. Chem. Soc.*, 118:10321–10322, 1996.

[144] Willner, I., Katz, E., Patolsky, F., and Bückmann, A. F. *J. Chem. Soc. Perkin Trans*, 2:1817–1822, 1998.

[145] Guiseppi-Elie, A., Lei, C., and Baughman, R. H. *Nanotechnology*, 13:559–564, 2002.

[146] Ivnitski, D., Branch, B., Atanassov, P., and Apblett, C. *Electrochem. Commun.*, 8: 1204–1210, 2006.

[147] Zhang, S. G. W. Q., Wang, R., and Yoona, S. F. *Biochem. Biophys. Res. Commun.*, 311:572–576, 2003.

[148] Wang, J., Musameh, M., and Lin, Y. *J. Am. Chem. Soc.*, 125:2408–2409, 2003.

[149] Lin, Y., Lu, F., Tu, Y., and Ren, Z. *Nano Lett.*, 4:191–195, 2004.

[150] Lee, J. Y., Shin, H. Y., Kang, S. W., Park, C., and Kim, S. W. *J. Power Sources*, 195:750–755, 2010.

[151] Deng, L., Wang, F., Chen, H., Shang, L., Wang, L., Wang, T., and Dong, S. *Biosens. Bioelectron.*, 24:329–333, 2008.

[152] Yan, Y.-M., Baravik, I., Tel-Vered, R., and Willner, I. *Adv. Mater.*, 21:4275–4279, 2009.

[153] Zhou, M., Deng, L., Wen, D., Shang, L., Jin, L., and Dong, S. *Biosens. Bioelectron.*, 24:2904–2908, 2009.

[154] Zhao, X., Jia, H., Kim, J., and Wang, P. *Bioechnol. Bioeng.*, 104:1068–1074, 2009.

[155] Choi, Y., Wang, G., Nayfeh, M. H., and Tung Yau, S. *Biosens. Bioelectron.*, 24: 3103–3107, 2009.

[156] Habrioux, A., Sibert, E., Servat, K., Vogel, W., Kokoh, K. B., and Alonso-Vante, N. *J. Phys. Chem. B*, 111:10329–10333, 2007.

[157] Habrioux, A., Servat, K., Tingry, S., and Kokoh, K. B. *Electrochem. Commun.*, 11: 111–113, 2009.

[158] Arechederra, R. L., Treu, B. L., and Minteer, S. D. *J. Power Sources*, 173:156–161, 2007.

[159] Topcagic, S. and Minteer, S. D. *Electrochim. Acta*, 51:2168–2172, 2006.

[160] Ramanavicius, A., Kausaite, A., and Ramanaviciene, A. *Biosens. Bioelectron.*, 24: 761–766, 2008.

[161] Kontani, R., Tsujimura, S., and Kano, K. *Bioelectroch.*, 76:10–13, 2009.

[162] Zebda, A., Renaud, L., Cretin, M., Innocent, C., Pichot, F., Ferrigno, R., and Tingry, S. *J. Power Sources*, 193:602–606, 2009.

[163] Togo, M., Takamura, A., Asai, T., Kaji, H., and Nishizawa, M. *J. Power Sources*, 178:53–58, 2008.

[164] Ramanavicius, A., Kausaite, A., and Ramanaviciene, A. *Biosens. Bioelectron.*, 20: 1962–1967, 2005.

[165] Vincent, K. A., Cracknell, J. A., Lenz, O., Zebger, I., Friedrich, B., and Armstrong, F. A. *Proc. Natl. Acad. Sci. U.S.A*, 102:16951–16954, 2005.

[166] Wang, S. C., Yang, F., Silva, M., and Zarow, A. *Electrochem. Commun.*, 11:34–37, 2009.

[167] Coman, V., Ludwig, R., Harreither, W., Haltrich, D., Gorton, L., Ruzgas, T., and Shleev, S. *Fuel Cell*, 2009.

[168] Gao, F., Yan, Y., Su, L., Wang, L., and Mao, L. *Electrochem. Commun.*, 9:989–996, 2007.

[169] Tasca, F., Gorton, L., Harreither, W., Haltrich, D., Ludwig, R., and Nöll, G. *J. Phys. Chem. C*, 112:13668–13673, 2008.

[170] Togo, M., Takamura, A., Asai, T., Kaji, H., and Nishizawa, M. *Electrochim. Acta*, 52:4669–4674, 2007.

[171] Zheng, W., Zhou, H. M., Zheng, Y. F., and Wang, N. *Chem. Phys. Lett.*, 457: 381–385, 2008.

[172] Oh, S. E., Kim, J. R., Joo, J. H., and Logan, B. E. *Water Sci. Technol.*, 60: 1311–1317, 2009.

[173] Logan, B. E., Murano, C., Scott, K., Gray, N. D., and Head, I. M. *Water Res.*, 39: 942–952, 2005.

[174] Sool Lee, H., Parameswaran, P., Kato-Marcus, A., Torres, C. I., and Rittmann, B. E. *Water Res.*, 42:1501–1510, 2008.

[175] Aelterman, P., Freguia, S., Keller, J., Verstraete, W., and Rabaey, K. *Appl. Microbiol. Biotechnol.*, 78:409–418, 2008.

[176] Cheng, K. Y., Ho, G., and Cord-Ruwisch, R. *Environ. Sci. Technol.*, 42:3828–3834, 2008.

[177] Allen, R. M. and Bennetto, H. P. *Appl. Biochem. Biotechnol.*, 39-40(1):27–40, 1993.

[178] Rabaey, K., Ossieur, W., Verhaege, M., and Verstraete, W. *Water Sci. Technol.*, 52 (1-2):515–523, 2005.

[179] Clauwaert, P., van-der Ha Nico Boon, D., Verbeken, K., Verhaege, M., Rabaey, K., and Verstraete, W. *Environ. Sci. Technol.*, 41(21):7564–7569, 2007.

[180] Richter, H., McCarthy, K., Nevin, K. P., Johnson, J. P., Rotello, V. M., and Lovley, D. R. *Langmuir*, 24(8):4376–4379, 2008.

[181] Park, D. H. and Zeikus, J. G. *Biotechnol. Bioeng.*, 81:348–355, 2003.

[182] Park, H. S., Kim, B. H., Kim, H. S., Kim, H. J., Kim, G. J., Kim, M., Chang, I. S., Park, Y. K., and Chang, H. I. *Anaerobe*, 7:297–306, 2001.

[183] Rabaey, K., Boon, N., Höfte, M., and Verstraete, W. *Environ. Sci. Technol.*, 39(9): 3401, 2005.

[184] Rabaey, K., Boon, N., Sicilia, S. D., Verhaege, M., and Verstraete, W. *Appl. Environ. Microbiol.*, 70(9):5373–5382, 2004.

[185] Xing, D., Zuo, Y., Cheng, S., Regan, J. M., and Logan, B. E. *Environ. Sci. Technol.*, 42:4146–4151, 2008.

[186] Chaudhuri, S. K. and Lovley, D. R. *Nat. Biotechnol.*, 21(10):1229–1232, 2003.

[187] Bond, D. R. and Lovley, D. R. *Appl. Environ. Microbiol.*, 69(3):1548–1555, 2003.

[188] Ringeisen, B. R., Ray, R., and Little, B. *J. Power Sources*, 165:591–597, 2007.

[189] Nevin, K. P., Richter, H., Covalla, S. F., Johnson, J. P., Woodard, T. L., Orloff, A. L., Jia, H., Zhang, M., and Lovley, D. R. *Environ. Microbiol.*, 10(10):2505–2514, 2008.

[190] Prasad, D., Arun, S., Murugesan, M., Padmanaban, S., Satyanarayanan, R. S., Berchmans, S., and Yegnaraman, V. *Biosens. Biotechnol.*, 22:2604–2610, 2007.

[191] Aelterman, P., Rabaey, K., Pham, H. T., Boon, N., and Verstraete, W. *Environ. Sci. Technol.*, 40:3388–3394, 2006.

[192] Kim, J. R., Min, B., and Logan, B. E. *Appl. Microbiol. Bioetchnol.*, 68:23–30, 2005.

[193] Liu, H., Cheng, S., Huang, L., and Logan, B. E. *J. Power Sources*, 179:274–279, 2008.

[194] Fan, Y., Sharbrough, E., and Liu, H. *Environ. Sci. Technol.*, 42:8101–8107, 2008.

[195] Logan, B. E., Cheng, S., Watson, V., and Estadt, G. *Environ. Sci. Technol.*, 41: 3341–3346, 2007.

[196] Zhang, X., Cheng, S., Huang, X., and Logan, B. E. *Biosens Bioelectron.*, 11:2177–2180, 2009.

[197] Schaetzle, O., Barrière, F., and Schröder, U. *Energy Environ. Sci.*, 2:96–99, 2009.

[198] Chae, K. J., Choi, M. J., Kim, K., Ajayi, F. F., Park, W., Kim, C. W., and Kim, I. S. *Bioresour. Technol.*, 101:5350–5357, 2010.

[199] Crittenden, S. R., Sund, C. J., and Sumner, J. *Langmuir*, 22:9473–9476, 2006.

[200] Adachi, M., Shimomura, T., Komatsu, M., Yakuwa, H., and Miya, A. *Chem. Commun.*, 7:2055–2057, 2008.

[201] Lowy, D. A., Tender, L. M., Zeikus, J. G., Park, D. H., and Lovley, D. R. *Biosens. Bioelectron.*, 21:2058–2063, 2006.

[202] Pham, T. H., Boon, N., Aelterman, P., Aelterman, P., Clauwaert, P., Schamphelaire, L. D., Vanhaecke, L., Maeyer, K. D., Höfte, M., Verstraete, W., and Rabaey, K. *Appl. Microbiol. Biotechnol.*, 77:1119–1129, 2008.

[203] Ringeisen, B. R., Henderson, E., Wu, P. K., Pietron, J., Ray, R., Little, B., Biffinger, J. C., and Jones-Meehan, J. M. *Environ. Sci. Technol.*, 40:2629–2634, 2006.

[204] You, S., Zhao, Q., Zhang, J., Jiang, J., and Zhao, S. *J. Power Sources*, 162:1409–14115, 2006.

[205] Chae, K. J., Choi, M., Ajayi, F. F., Park, W., Chang, I. S., and Kim, I. S. *Energy Fuels*, 22:169–176, 2008.

[206] Kim, J., Parkey, J., Rhodes, C., and Gonzalez-Martin, A. *J. Solid State Elecrochem.*, 13:1043–1050, 2009.

[207] Freguia, S., Tsujimura, S., and Kano, K. *Electrochim. Acta*, 55:813–818, 2010.

[208] Pham, H. T., Jang, J. K., and Kim, I. S. *J. Microbiol. Biotechn.*, 14(2):324–329, 2004.

[209] Cheng, S., Liu, H., and Logan, B. E. *Environ. Sci. Technol.*, 40:364–369, 2006.

[210] Chen, G.-W., Choi, S.-J., Lee, T.-H., Lee, G.-Y., Cha, J.-H., and Kim, W. *Appl. Microbiol. Biotechnol.*, 79:379–388, 2008.

[211] Fan, Y., Hu, H., and Liu, H. *J. Power Sources*, 171:348–354, 2007.

[212] Liu, H. and Logan, B. E. *Environ. Sci. Technol.*, 38:4040–4046, 2004.

[213] Cheng, S., Liu, H., and Logan, B. E. *Electrochem. Commun.*, 8:489–494, 2006.

[214] Shimoyama, T., Komukai, S., Yamazawa, A., Ueno, Y., Logan, B. E., and Watanabe, K. *Appl. Microbiol. Biotechnol.*, 80:325–330, 2008.

[215] He, Z., Minteer, S. D., and Angenent, L. T. *Environ. Sci. Technol.*, 39:5262–5267, 2005.

[216] Jang, J. K., Pham, T. H., Chang, I. S., Kang, K. H., Moon, H., Cho, K. S., and Kim, B. H. *Proc. Biochem.*, 39:1007–1012, 2004.

[217] He, Z., Wagner, N., Minteer, S. D., and Angenent, L. T. *Environ. Sci. Technol.*, 40: 5212–5217, 2006.

[218] Eun Oh, S. and Logan, B. E. *Appl. Microbiol. Biotechnol.*, 70:162–169, 2006.

[219] Fan, Y., Hu, H., and Liu, H. *Environ. Sci. Technol.*, 41:8154–8158, 2007.

[220] Rozendal, R. A., Hamelers, H. V. M., and Buisman, C. J. N. *Environ. Sci. Tehcnol.*, 40:5206–5211, 2006.

[221] Rozendal, R. A., Sleutels, T. H. J. A., Hamelers, H. V. M., and Buisman, C. J. N. *Water Sci. Technol.*, 57:1757–1762, 2008.

[222] Tender, L. M., Reimers, C. E., Fertig, S., and Wang, W. *Environ. Sci. Technol.*, 35: 192–195, 2001.

[223] Reimers, C. E., Tender, L. M., Stecher, H. A., Holmes, D. E., Bond, D. R., Lowy, D. A., Ans, S., Fertig, K. P., and Lovley, D. R. *Nat. Biotechnol.*, 20:821–825, 2002.

[224] Nielsen, M. E., Reimers, C. E., and Stecher III, H. A. *Environ. Sci. Technol.*, 41: 7895–7900, 2007.

[225] Nielsen, M. E., Reimers, C. E., White, H. K., Sharmab, S., and Girguis, P. R. *Energy Environ. Sci.*, 1:584–593, 2008.

[226] Barbir, F. *PEM Fuel Cells: Theory and Practice*. Elsevier/Academic Press, London, 2005.

[227] BP statistical review of world energy, June 2012. Online: `http://www.bp.com/assets/bp_internet/globalbp/globalbp_uk_english/reports_and_publications/statistical_energy_review_2011/STAGING/local_assets/pdf/statistical_review_of_world_energy_full_report_2012.pdf` retrieved: 5 Sep 2012.

[228] BP energy outlook 2030, January 2012. Online: `http://www.bp.com/liveassets/bp_internet/globalbp/STAGING/global_assets/downloads/O/2012_2030_energy_outlook_booklet.pdf` retrieved on: 5 Sep 2012.

[229] Feng, Y., Wang, X., Logan, B. E., and Lee, H. *Appl. Microbiol. Technol.*, 78:873–880, 2008.

[230] Katuri, K. P. and Scott, K. *Biotechnol. Bioeng.*, 107:52–58, 2010.

[231] Ahn, Y. and Logan, B. E. *Bioresour. Technol.*, 101:469–475, 2010.

[232] Tender, L. M., Gray, S. A., Groveman, E., Lowy, D. A., Kauffman, P., Melhado, J., Tyce, R. C., Flynn, D., Petrecca, R., and Dobarro, J. *J. Power Sources*, 179: 571–575, 2008.

[233] Shah, A. A., , Sui, P. C., Kim, G. S., and Ye, S. *J. Power Sources*, 166:1–21, 2007.

[234] Shah, A. A. and Walsh, F. C. *J. Power Sources*, 185:287–301, 2008.

[235] Bartlett, P. N. and Pratt, K. F. E. *J. Elecroanal. Chem.*, 397:61–78, 1995.

[236] Kano, K. and Ikeda, T. *Anal. Sci.*, 16:1013–1021, 2000.

[237] Ikeda, T. and Kano, K. *J. Biosci. Bioeng.*, 92(1):9–18, 2001.

[238] Calabrese-Barton, S. *Electrochim. Acta*, 50:2145–2153, 2005.

[239] Zeng, Y., Choo, Y. F., Kim, H.-H., and Wu, P. *J. Power Sources*, 195:79–89, 2010.

[240] Marcus, A. K., Torres, C. I., and Rittmann, E. *Biotechnol. Bioeng.*, 98(6):1171–1182, 2007.

[241] Tayhas, G. and Palmore, R. chapter Biofuel Cells. John Wiley & Sons, Ltd, 2008.

[242] Osman, M. H., Shah, A. A., and Walsh, F. C. *Biosens. and Bioelectron.*, 26:3087–3102, 2011.

[243] Osman, M. H., Shah, A. A., and Walsh, F. C. *Biosens. and Bioelectron.*, 26:953–963, 2010.

[244] Michaelis, L. and Menten, M. L. *Biochem. Z.*, 49:333–369, 1913.

[245] Johnson, K. A. and Goody, R. S. *Biochem.*, 50:8264–8269, 2011.

[246] Briggs, G. E. and Haldane, J. B. S. *Biochem. J.*, 19:338–339, 1925.

[247] Hui, T.-W., Wong, K.-Y., and Shiu, K.-K. *Electroanalysis*, 8(6):597–601, 1996.

[248] Sokic-Lazic, D., Arechederra, R. L., Treu, B. L., and Minteer, S. D. *Electroanalysis*, 22(7):757–764, 2010.

[249] Palmore, G. T. R., Bertschy, H., Bergens, S. H., and Whitesides, G. M. *J. Electroanal. Chem.*, 443:155–161, 1998.

[250] Addo, P. K., Arechederra, R. L., and Minteer, S. D. *Electroanalysis*, 22(7-8):807–812, 2010.

[251] Sato, F., Togo, M., Islam, M. K., Matsue, T., Kosuge, J., Fukasaku, N., Kurosawa, S., and Nishizawa, M. *Electrochem. Commun.*, 7:643–647, 2005.

[252] Takagi, K., Kano, K., and Ikeda, T. *J. Electroanal. Chem.*, 445:211–219, 1998.

[253] Antiochia, R., Gallina, A., Lavagnini, I., and Magno, F. *Electroanalysis*, 14(18): 1256–1261, 2002.

[254] Sugiyama, T., Goto, Y., Matsumoto, R., Sakai, H., Tokita, Y., and Hatazawa, T. *Biosens. and Bioelectron.*, 26:452–457, 2010.

[255] Wohlfahrt, G., Trivic, S., Zeremski, J., Pericin, D., and Leskovac, V. *Mol. Cell. Biochem.*, 260:69–83, 2004.

[256] Montornes, J. M., Vreeke, M. S., and Katakis, I. chapter Glucose Biosensors. John Wiley & Sons, Ltd, 2008.

[257] Rusling, J. F., Wang, B., and Yun, S. chapter Electrochemistry of Redox Enzymes. John Wiley & Sons, Ltd, 2008.

[258] Ogino, Y., Takagi, K., Kano, K., and Ikeda, T. *J. Electroanal. Chem.*, 396:517–524, 1995.

[259] Tsujimura, S., Kawaharada, M., Nakagawa, T., Kano, K., and Ikeda, T. *Electrochem. Commun.*, 5:138–141, 2003.

[260] Tsujimura, S., Kano, K., and Ikeda, T. *J. Electroanal. Chem.*, 576:113–120, 2005.

[261] Tsujimura, S., Kamitaka, Y., and Kano, K. *Fuel Cell*, 7(6):463–469, 2007.

[262] Ikeda, T. *Chem. Rec.*, 4:192–203, 2004.

[263] Ikeda, T., Tatsumi, H., Katano, H., Wanibuchi, M., Hibi, T., and Kajino, T. *Anal. Sci.*, 24:237–241, 2008.

[264] Habrioux, A., Napporn, T., Servat, K., Tingry, S., and Kokoh, K. B. *Electrochim. Acta*, 55:7701–7705, 2010.

[265] Tokita, Y., Nakagawa, T., Sakai, H., Sugiyama, T., Matsumoto, R., and Hatazawa, T. *ECS Trans.*, 13(21):89–97, 2008.

[266] Sakai, H., Nakagawa, T., Mita, H., Matsumoto, R., Sugiyama, T., Kumita, H., Tokita, Y., and Hatazawa, T. *ECS Trans.*, 16(38):9–15, 2009.

[267] Gorton, L. and Bartlett, P. N. chapter NAD(P)-Based Biosensors. John Wiley & Sons, Ltd, 2008.

[268] Buffinton, G. D., karin Öllinger, brunmark, A., and Cadenas, E. *Biochem. J.*, 257: 561–571, 1989.

[269] Kano, H., Tatsumi, H., Hibi, T., Ikeda, T., and Tsukatani, T. *Anal. Sci.*, 24:1415–1419, 2008.

[270] Nakagawa, T., Tsujimura, S., Kano, K., and Ikeda, T. *Chem. Lett.*, 32(1):54–55, 2003.

[271] Manjon, A., Obon, J. M., Casanova, P., Fernandez, V. M., and Ilborra, J. L. *Biotechnol. Lett.*, 24:1227–1232, 2002.

[272] Alonso, L., Palmero, S., Muñoz, E., Sanllorente, S., and Garcia-Garcia, M. A. *Elecroanal.*, 12(10):757–762, 2000.

[273] Blaedel, W. J. and Engstrom, R. C. *Anal. Chem*, 50(3):476–479, 1978.

[274] Bird, B., Stewart, W., and Lightfoot, E. *Transport Phenomena*. John Wiley and Sons, 2002.

[275] Marrero, T. R. and Mason, E. A. *J. Phys. Chem. Ref. Data*, 1(1):3–118, 1972.

[276] Fischback, M. B., December 2006. Maser of Science thesis.

[277] Ha, S., Adams, B., and Masel, R. I. *J. Power Sources*, 128:119–124, 2004.

[278] Rustling, J. F., Wang, B., and eok Yun, S. chapter Electrochemistry of Redox Enzymes, pages 39–86. Wiley, 2008.

[279] Tang, Y., Wu, Y., and Wang, Z. *J. Electrochem. Soc.*, 148(4):133–138, 2001.

[280] Shim, Y. B. and Park, S. M. *J. Electroanal. Chem.*, 425:201–207, 1997.

[281] Leskovac, V., Trivic, S., Wohlfahrt, G., Kandrac, J., and Pericin, D. *Int. J. Biochem. Cell Biol.*, 37:731–750, 2005.

[282] Springer, T. E., Zawodinski, T. A., and Gottesfeld, S. *J. Electrochem. Soc.*, 138: A2334–A2341, 1991.

[283] Motupally, S., Becker, A. J., and Weidner, J. W. *J. Electrochem. Soc.*, 147:A3171–A3177, 2000.

[284] Gyss, C. and Bourdillon, C. *Anal. Chem.*, 59:2350–2355, 1987.

[285] Andersson, M., Axelsson, A., and Zacchi, G. *Int. J. Pharm.*, 157:199–208, 1997.

[286] Shaidarova, L. G., Gedmina, A. V., Chelnokova, I. A., and Budnikov, G. K. *J. Anal. Chem.*, 59(11):1025–1031, 2004.

[287] Chatterjee, M., Chatterjee, A., Ghosh, S., and Basumallick, I. *Electrochim. Acta*, 54:7299–7304, 2009.

[288] Lee, W.-Y., Park, G.-G., Yang, T.-H., Yoon, Y.-G., and Kim, C.-S. *Int. J. Hydrog. Energ.*, 29(9):961–966, 2004.

[289] Arriagada, J., Olausson, P., and Selimovic, A. *J. Power Sources*, 112(1):54–60, 2002.

[290] Milewski, J. and Świrski, K. *Int. J. Hydrog. Energ.*, 34(13):5546–5553, 2009.

[291] Rasmussen, C. E. and Williams, C. K. I. *Gaussian Processes for Machine Learning*. The MIT Press, 2006.

[292] Williams, C. K. Prediction with gaussian processes: From linear regression to linear prediction and beyond. In *Learning in graphical models*, pages 599–621. Springer, 1998.

[293] Shah, A. A. and Nair, P. B. Fuel cell modelling using reduced basis Gaussian process regression. 2013. Submitted for publication.

Appendix: Journal publications

Electrochimica Acta 112 (2013) 386–393

Contents lists available at ScienceDirect

Electrochimica Acta

journal homepage: www.elsevier.com/locate/electacta

Mathematical modelling of an enzymatic fuel cell with an air-breathing cathode

M.H. Osman[a], A.A. Shah[b,*], R.G.A. Wills[a], F.C. Walsh[a]

[a] Electrochemical Engineering Laboratory, School of Engineering Sciences, University of Southampton, Highfield, Southampton SO17 1BJ, UK
[b] School of Engineering, University of Warwick, Coventry CV47AL, UK

ARTICLE INFO

Article history:
Received 28 March 2013
Received in revised form 6 August 2013
Accepted 6 August 2013
Available online 25 August 2013

Keywords:
Enzymatic fuel cell
Diffusional mediator
Biological anode
Two-substrate mechanism
Modelling and simulation

ABSTRACT

Multi-dimensional steady-state and dynamic models for an enzymatic fuel cell are developed. In the model system, the biocatalyst (glucose oxidase) is immobilized in a porous electrically conducting anode, while glucose and a mediator are supplied from a solution. A platinum air-breathing cathode and a Nafion membrane complete the cell unit. Detailed mass and charge balances are combined with a model for the ping-pong reaction mechanism in the anode, together with oxygen reduction in the cathode. The effects of enzyme oxidation by dissolved oxygen in the anode (a competing side reaction) are also included. The model is validated against experimental polarization and power curves, and the steady-state performance under different conditions is analyzed and discussed. The simulation results demonstrate some of the possible limitations of enzymatic fuel cells and provide insights into the spatial distributions of the reactants, potentials and current.

1. Introduction

Biofuel cells have been defined as systems capable of direct chemical to electrical energy conversion via biochemical pathways [1–6]. Direct electrochemical conversion is a desirable feature since it avoids the thermodynamic limitations associated with combustion, in addition to being more environmentally friendly.

Enzymatic fuel cells can yield low power densities as a consequence of slow rates of electron transfer from the enzyme active site to the electrode [7]. They can also suffer from short lifetimes as a result of poor stability of the enzyme when it functions in a foreign environment. Much of the current research is directed at alleviating these problems, with particular focus on new methods and materials for enzyme-electrode (and possibly mediator) integration, often in highly ordered three-dimensional structures. Developments in the overall system design have also led to more efficient systems. For example, removing the separator membrane without a significant loss in the power output, and the emergence of single chamber, air-breathing systems using compact membrane electrode assemblies (MEAs).

Mathematical models can reduce the burden on laboratory-based design, testing and characterization. At the cell level, models can capture the potential, reactant, and temperature distribution, as well as global information such as the cell potential. For many important quantities, local information such as potential and current density profiles can only be gained from detailed and rigorously validated models, particularly during *in-situ* operation. For these reasons, a great deal of effort has been invested in modelling polymer electrolyte membrane (PEM) and solid oxide fuel cells and solid-oxide fuel cells [8]. Numerical modelling of enzymatic and microbial fuel cells, on the other hand, is not a well-developed area [9,10]. With a few notable exceptions [11–13], models are highly simplified, neglecting crucial features such as transience, spatial non-uniformity, ion migration, fluid flow and heat transport. In this paper, a transient, two-dimensional model for a glucose-oxidase based fuel cell is developed. The ping-pong mechanism of the biocatalyzed reactions is treated explicitly and the model is validated against experimental results. The approach can be applied to other biofuel cell systems and in a companion paper a model of a fully biological (anode and cathode) fuel cell is developed.

2. Fuel cell model

2.1. Reaction kinetics

The system under consideration was reported by Fischback et al. [14] (see also [15,16]). The developed miniature fuel cell (12 mm × 12 mm × 9 mm) comprised a Nafion membrane/cathode electrode assembly (MCEA) stacked with an enzymatic (glucose oxidase) carbon felt anode, as depicted in Fig. 1. Glucose oxidase was covalently attached to functionalized carbon nano-tubes (CNTs) before excess GOx was made to precipitate near the CNTs. Finally, a cross-linking

* Corresponding author. Tel.: +44 023 8059 8520; fax: +44 023 8059 3131.
E-mail address: Akeel.Shah@warwick.ac.uk (A.A. Shah).

0013-4686/$ – see front matter © 2013 Elsevier Ltd. All rights reserved.
http://dx.doi.org/10.1016/j.electacta.2013.08.044

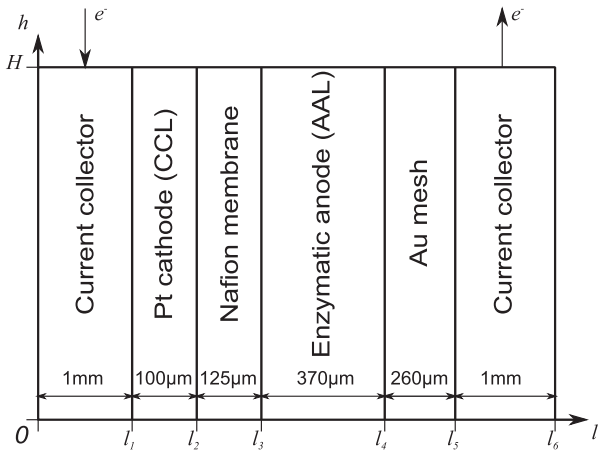

Fig. 1. A schematic of the modelled cell [14].

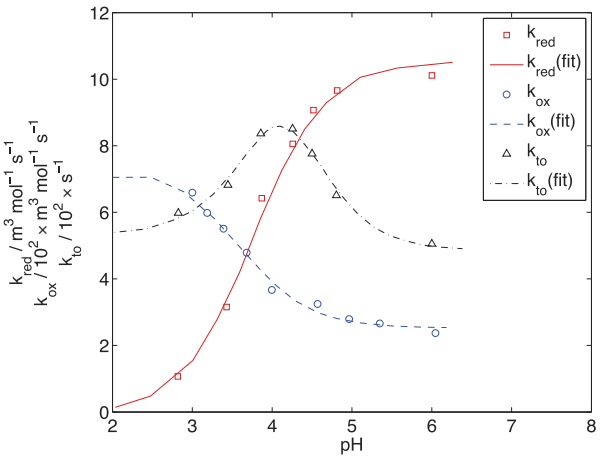

Fig. 2. The pH dependence of enzymatic rate constants (determined from the results in [23,24]).

agent was added to form crosslinked enzyme clusters on the surface of the CNTs. This mixture was then cast on a carbon felt. The anode was placed between the MCEA and a gold mesh, for improved electrical conductivity. The current collectors were made from titanium plates, with current being drawn from the top side (Fig. 1). Slits were machined into these plates to provide the anolyte on the anode side and air on the cathode side. The anode was continuously fed with a solution containing glucose and the mediator benzoquinone. The air-breathing Pt/Nafion cathode was prepared by applying a Nafion/Pt-black layer on a Nafion 115 membrane [14]. The fuel cell was capable of operating continuously at maximum power for 16 h with no significant drop in performance.

For a mediated enzymatic anode, the two chemical reactions occurring are the two-substrate 'ping-pong' reactions involving the reduction and oxidation of the enzyme [17–19]:

$$\text{Enzyme } \textit{reduction}: \quad E_{ox} + S \xrightarrow{k_{red}} E_{red} + P \tag{1}$$

$$\text{Enzyme } \textit{oxidation}: \quad E_{red} + M_{ox} \xrightarrow{k_{ox}} E_{ox} + M_{red} \tag{2}$$

where E_{ox} and E_{red} (i.e., FAD and $FADH_2$) are the oxidized and reduced states of the enzyme (i.e., glucose oxidase) respectively. M_{ox} and M_{red} are the oxidized and reduced forms of the quinone mediator: benzoquinone and hydroquinone respectively [17]. S and P are the glucose substrate and glucono-lactone product, respectively. A third electrochemical reaction regenerates the mediator at the electrode:

$$M_{red} \overset{k_{anod}}{\rightleftharpoons} M_{ox} + 2H^+ + 2e^- \tag{3}$$

This reaction is assumed to be a two-proton/two-electron process [20]. There is disagreement in the literature on the chemical pathway of the benzoquinone reduction reaction, and the stability of some of the intermediate radicals [21]. Ions formed by a single-electron transfer are found to be more stable in unbuffered solutions for pH > 2.5 [22]. In this work, the hydroquinone oxidation is assumed to proceed by reaction (3).

When studying the influence of a third substrate, dissolved oxygen (O_d), which competes with the mediator for the oxidation of the GOx, a third enzymatic reaction is included:

$$E_{red} + O_d \xrightarrow{k_{O_d}} E_{ox} + H_2O_2 \tag{4}$$

Unless stated otherwise, the competing enzyme oxidation reaction (Eq. (4)) is neglected.

The anode is treated as an electrically conducting porous matrix in which the immobilized enzyme resides and participates in the bio-electrochemical reactions. Applying steady-state approximations to the intermediate enzyme complexes (i.e., Michaelis–Mentin kinetics), the reaction rates of the two enzymatic reactions (1) and (2) can be expressed as (in the anode active layer (AAL) only):

$$R_{red} = k_{red}\, c_{gluc}\, c_{E_{ox}} \tag{5}$$

$$R_{ox} = k_{ox}\, c_{M_{ox}}\, c_{E_{red}} \tag{6}$$

respectively, where c_i represents the concentration of species i ('gluc' representing glucose). k_{red} and k_{ox} are the pH dependent bimolecular rate constants, which were interpolated from the experimental data in [23,24] (see Fig. 2).

When assuming the presence of dissolved oxygen the rate of enzyme oxidation by the third substrate is expressed as:

$$R_{O_d} = k_{O_d} c_{O_d} c_{E_{red}} \tag{7}$$

The rate of reaction (3), occurring on the carbon anode, is expressed in Butler–Volmer form, assuming a two-electron reaction:

$$R_{anod} = k_{anod}\; c_{M_{red}}^{\alpha_a} c_{M_{ox}}^{\alpha_c} \left[\exp\left(\frac{2\alpha_c F\eta_a}{RT}\right) - \exp\left(\frac{-2\alpha_a F\eta_a}{RT}\right)\right] \tag{8}$$

where k_{anod} is the rate constant (s^{-1}), η_a is the anode overpotential, α_a and α_c are the anodic and cathodic charge transfer coefficients, respectively, T is the system temperature, F is Faraday's constant and R is the molar gas constant.

In the cathode catalyst layer (CCL), oxygen is assumed to undergo a four-electron reduction to water on Pt:

$$O_2 + 4H^+ + 4e^- \overset{k_{cath}}{\rightleftharpoons} 2H_2O_{(d)} \tag{9}$$

This is the most common assumption made in fuel cell modelling when considering air-breathing cathodes. For alkaline conditions, or for conditions close to neutral pH, this model may not be valid. In the present case, however, the pH remains below 4.75 for all cases considered. The pH of the anolyte was measured by Fischback et al. [14], who recorded values of 3.2 and 3.48 before and after operation, respectively. The same conditions were used as the basis for the simulations. Given the location of the reaction sites (simultaneous contact between ionomer, Pt and carbon [25,26]) it is assumed that the water enters the ionomer phase, i.e., is in a dissolved form (denoted with a subscript '(d)'). The rate of reaction (9)

Table 1
Source terms for mass balances (16), (20) and (21), and the charge balances (32) and (33).

Source term	Cathode catalyst layer	Anode enzyme layer
S_{O_2}	$-R_{cath}$	–
$S_{H_2O_{(v)}}$	$\nu h_{dv}(c_d - c_d^{eq})$	–
$S_{H_2O_{(d)}}$	$2R_{cath} - \nu h_{dv}(c_d - c_d^{eq})$	–
S_{H^+}	$-4R_{cath}$	$2R_{anod}$
$S_{M_{red}}$	–	$-(R_{anod} - R_{ox})$
$S_{M_{ox}}$	–	$(R_{anod} - R_{ox})$
S_{gluc}	–	$-R_{red}$
S_{ϕ_s}	$4FR_{cath}$	$-2FR_{anod}$

is expressed in Butler–Volmer form, assuming equal charge transfer coefficients:

$$R_{cath} = \frac{i_{O_2}^{ref}}{F}\left(\frac{c_{O_2}}{c_{O_2}^0}\right)\left[\exp\left(\frac{-2F\eta_a}{RT}\right) - \exp\left(\frac{2F\eta_a}{RT}\right)\right] \tag{10}$$

where $i_{O_2}^{ref}$ is the reference exchange current density and η_c is the cathode overpotential.

The overpotentials are defined as ($j = c$ for the cathode and $j = a$ for the anode):

$$\eta_j = \phi_s - \phi_e - E_j^0 \tag{11}$$

where ϕ_e and ϕ_s are the ionic and electron potentials. The half-cell equilibrium potentials are calculated from the Nernst equation:

$$E_a^0 = E_a^{0\prime} - \frac{RT}{2F}\ln\left(\frac{c_{M_{red}}}{c_{M_{ox}}}\right) - 0.06 \times \text{pH} \tag{12}$$

$$E_c^0 = E_c^{0\prime} - 0.06 \times \text{pH} \tag{13}$$

where $E_j^{0\prime}$ are the standard potentials referenced at pH = 0, with a change of 60 mV per pH unit.

2.2. Reactant mass balances

The mass balance for the reduced immobilized enzyme in the absence of dissolved oxygen is as follows:

$$\frac{\partial c_{E_{red}}}{\partial t} = R_{red} - R_{ox} \tag{14}$$

In the presence of dissolved oxygen, the source term is modified to: $R_{red} - R_{ox} - R_{O_d}$. The fixed total concentration of enzyme, c_{E_Σ}, is distributed between the two states: oxidized (GOx-FAD) and reduced (GOx-$FADH_2$):

$$c_{E_\Sigma} = c_{E_{red}} + c_{E_{ox}} \tag{15}$$

Having calculated the reduced enzyme concentration (Eq. (14)), and knowing the total enzyme concentration, the oxidized enzyme concentration can then be calculated using Eq. (15).

The mass balance for a mobile species i in the porous regions (AAL, gold mesh and CCL) takes into account the accumulation of reactant species, transport by diffusion, electro-migration under a potential field ϕ_e (Nernst-Planck equation) and generation/consumption during the reactions:

$$\epsilon\frac{\partial c_i}{\partial t} + \nabla\cdot\left(-D_i^{\text{eff}}\nabla c_i - \frac{z_i F D_i^{\text{eff}} c_i}{RT}\nabla\phi_e\right) = S_i \tag{16}$$

where c_i, D_i^{eff}, z_i and S_i are the concentration, effective diffusion coefficient, charge, and source term for species i. ϵ is the porosity of the porous region: $\epsilon = \epsilon_{al}$ in the AAL, $\epsilon = \epsilon_{Au}$ in the gold mesh and $\epsilon = \epsilon_{cl}$ in the CCL. The source terms, arising from the reactions and phase changes, are given in Table 1.

In the anolyte, the mobile species are glucose, M_{red}, M_{ox}, $H_2O_{(l)}$, H^+, a negatively charged counter ion, and in some cases $O_{2(d)}$. The pH is defined as: $\text{pH} = -\log_{10}(c_{H^+})$ (in mol L^{-1}). Assuming that protons are the only cations in the anolyte, electro-neutrality is maintained by the counter ions, which, for simplicity, are assumed to have a unit charge. Denoting the counter ions by A^-, electroneutrality, which is given by:

$$\sum_i z_i c_i = 0 \tag{17}$$

then demands that $c_{A^-} = c_{H^+}$. In the CCL, Eq. (16) applies to O_2 and $H_2O_{(v)}$ in the CCL. In each of the regions, the effective diffusion coefficient for each species is approximated using a Bruggeman correction:

$$D_i^{\text{eff}} = \epsilon^{3/2} D_i \tag{18}$$

where D_i is the corresponding free-space value.

The mass balances for the species within the membrane and the ionomer (polymer electrolyte) of the CCL, namely water and protons, are treated separately, using the model of Springer et al. [27] developed for PEM fuel cells. The water moves as protonated water complexes, with the number of water molecules per proton characterized by a 'drag number' [27]:

$$n_{drag} = \frac{5\lambda}{44} \tag{19}$$

where λ is the membrane water content, i.e., mol H_2O per mol SO_3^-. For convenience, the dissolved water concentration is normalized with respect to the fixed charge site concentration of the membrane, ν, to define $c_d = c_{H_2O_{(d)}}/\nu$. The normalized-water and proton concentrations are then given by:

$$\epsilon\frac{\partial c_d}{\partial t} + \nabla\cdot\left(-D_d^{\text{eff}}\nabla c_d - \frac{n_{drag}}{\nu}\frac{\sigma_e}{F}\nabla\phi_e\right) = S_i \tag{20}$$

$$\epsilon\frac{\partial c_{H^+}}{\partial t} + \nabla\cdot\left(-D_{H^+}^{\text{eff}}\nabla c_{H^+} - \frac{\sigma_e}{F}\nabla\phi_e\right) = S_i \tag{21}$$

respectively. In these equations, ϵ represents the volume fraction for dissolved-water and proton transport: $\epsilon = 1$ in the membrane and $\epsilon = \epsilon_{clp}$ (the volume fraction of ionomer) in the CCL. The electromigration terms in Eqs. (20) and (21) formally reduce to the familiar Nernst-Planck form through the relation between ion mobility and conductivity. The conductivity is obtained from an empirical relation [27]:

$$\sigma_e = \exp\left[1286\left(\frac{1}{303} - \frac{1}{T}\right)\right](0.514\lambda - 0.326) \tag{22}$$

The membrane water content is related to the dissolved water concentration as follows, with a correction for swelling of the hydrated membrane [25]:

$$\lambda = \frac{c_d}{1 - 0.0216 c_d} \tag{23}$$

The diffusion coefficient of dissolved water depends on λ through the following empirical relation [28]:

$$D_d^{\text{eff}} = \begin{cases} \epsilon^{3/2}(3.1\times10^{-7}\lambda(\exp^{0.28\lambda} - 1)\exp^{-2436/T}) & (0 < \lambda \le 3) \\ \epsilon^{3/2}(4.17\times10^{-8}\lambda(1 + 161\exp^{-\lambda})\exp^{-2436/T}) & (3 < \lambda \le 22) \end{cases} \tag{24}$$

The mass transfer of water between the vapour and dissolved phases (in the CCL) is driven by the deviation from the equilibrium concentration of dissolved water, c_d^{eq}. The corresponding equilibrium water content, λ^{eq} is related to the water vapour activity in the CCL, a_w by [25]:

$$\lambda^{eq} = 0.3 + 10.8 a_w - 16 a_w^2 + 14.1 a_w^3 \tag{25}$$

The water activity (equilibrium relative humidity) is defined as:

$$a_w = \frac{c_{H_2O_{(v)}} RT}{P_{sat}} \tag{26}$$

where P_{sat} is the saturation pressure at a temperature T [27]:

$$\log_{10} P_{sat} = -2.1794 + 0.02953\Delta T - 9.1837 \times 10^{-5}\Delta T^2 + 1.4454 \times 10^{-7}\Delta T^3 \tag{27}$$

in which $\Delta T = T - 273$. The contributions of the phase change to the source terms of vapour and dissolved water are given in Table 1. The proportionality constant, h_{dv}, representing the coefficient of adsorption/desorption between the vapour and dissolved phases, is given by [25]:

$$h_{dv} = \begin{cases} \kappa_a \lambda & (c_d - c_d^{eq} < 0) \\ \kappa_d \lambda & (c_d - c_d^{eq} < 0) \end{cases} \tag{28}$$

in which κ_a and κ_d are adsorption and desorption coefficients.

2.3. Charge balances

The flow of a charged species i gives rise to a current density $\vec{j}_i = z_i F \vec{N}_i$, where z_i is the charge and $\vec{N}_i$ is the molar flux (driven by diffusion and electro-migration in the present case). Therefore, the total current density in the anolyte, $\vec{j}_e$ satisfies:

$$\vec{j}_e = \sum_i \vec{j}_i = -\sigma_e \nabla \phi_e - F \sum z_i D_i^{eff} \nabla c_i \tag{29}$$

in which the effective conductivity σ_e is given by:

$$\sigma_e = \frac{F^2}{RT} \sum z_i^2 D_i^{eff} c_i \tag{30}$$

The ionic current in the Nafion membrane and the proton-conducting ionomer of the CCL is governed by Ohm's law:

$$\vec{j}_e = -\epsilon^{3/2} \sigma_e \nabla \phi_e \tag{31}$$

where σ_e is defined in Eq. (22) and ϵ represents the volume fraction of the the proton-conducting phase: $\epsilon = 1$ in the membrane and $\epsilon = \epsilon_{clp}$ (the volume fraction of ionomer) in the CCL. A steady-state charge balance in the ion-conducting regions is given by:

$$-\nabla \cdot \vec{j}_e = -S_\phi \tag{32}$$

in which the charge source S_ϕ is defined in Table 1. This source term is zero in regions where electrochemical reactions do not occur.

The electronic current, $\vec{j}_s$ is governed by Ohm's law. Conservation of charge within the porous regions ($\nabla \cdot \vec{j}_s + \nabla \cdot \vec{j}_e = 0$) leads to:

$$-\nabla \cdot \vec{j}_s = -\nabla \cdot (\epsilon^{3/2} \sigma_s \nabla \phi_s) = S_\phi \tag{33}$$

in which σ_s is the conductivity of the electron conducting phase and ϵ is its volume fraction: $\epsilon = 1 - \epsilon_{al}$ in the AAL, $\epsilon = 1 - \epsilon_{Au}$ in the gold mesh, $\epsilon = 1$ in the current collectors and $\epsilon = 1 - \epsilon_{cl} - \epsilon_{clp}$ in the CCL.

2.4. Initial and boundary conditions

The cell can be modelled as either operating in galvanostatic mode or potentiostatic mode. In the first case, it was assumed that a fixed current was drawn outwards from the top edge of the cathode current collector and into the cell at the top edge of the anode current collector:

$$-\vec{n} \cdot (-\sigma_s \nabla \phi_s) = \begin{cases} -\left(\frac{H}{l_1}\right) j_{cell} & (0 \le l \le l_1;\ h = H) \\ \left(\frac{H}{l_6 - l_5}\right) j_{cell} & (l_5 \le l \le l_6;\ h = H) \end{cases} \tag{34}$$

where j_{cell} is the fixed, applied current density, relative to the anode geometrical area and $\vec{n}$ is the unit normal vector pointing into the membrane. All other external boundaries were assumed to be insulated. The cell potential was evaluated as the difference between the averages of the electronic potential of the cathode and anode, evaluated at the top boundaries of the current collectors:

$$E_{cell} = \overline{\phi}_{s,c} - \overline{\phi}_{s,a} \tag{35}$$

in which the bar denotes a spatial average. For operation in potentiostatic mode, a cell potential was imposed (applied through equipotential surfaces at the top boundaries of the two current collectors):

$$\phi_s = \begin{cases} E_{cell} & (0 \le l \le l_1;\ h = H) \\ 0 & (l_5 \le l \le l_6;\ h = H) \end{cases} \tag{36}$$

The current density, j_{cell} (expressed relative to the electrode area) measured at the the top of the current collector:

$$j_{cell} = \frac{1}{H} \int_0^{l_1} \left(-\sigma_s \frac{\partial \phi_s}{\partial h}\right) dx \tag{37}$$

The concentrations of gaseous species at the air inlet ($l = l_1$), and the concentration of soluble species at the anolyte inlet ($l = l_5$) were assumed to be constant and equal to the initial concentrations:

$$c_i = c_i^0 \quad (l = l_1, l_5) \tag{38}$$

At the membrane/anode interface ($l = l_3$), the water in the anode solution was constrained in order to maintain a membrane water content of $\lambda = 22$ (fully liquid saturated, as would be expected for contact with an aqueous solution). The mass balance of water across this interface was maintained by setting the flux of liquid water into the membrane equal to that of the dissolved water at that boundary:

$$-\vec{n} \cdot \left(-D_{H_2O_{(l)}}^{eff} \nabla c_{H_2O_{(l)}}\right) = -\nu D_d^{eff} \frac{\partial c_d}{\partial l} - \frac{5\lambda}{44F} \sigma_e \frac{\partial \phi_e}{\partial l} \quad (l = l_3) \tag{39}$$

At time $t = 0$ the total enzyme concentration is assumed to be distributed equally between the reduced and oxidized states such that the initial concentration of oxidized enzyme is:

$$c_{E_{ox}}^0 = \frac{c_{E_\Sigma}}{2} \tag{40}$$

3. Results and discussion

In order to match the simulation results to the experimental data, a number of fitting parameters were used, a standard procedure for models of complex systems. The default parameter values are given in Table 2. The dimensions of the gold mesh, current collectors and and Pt/Nafion cathode were assumed since specific details of the materials were not provided in Fischback et al. [14]. The AAL thickness is 370 μm [15]. The values used did not qualitatively affect the results. The three fitting parameters were the unknown total concentration of the enzyme (c_{E_Σ}), and two electrochemical rate constants for the anode mediator and cathode oxygen reduction (k_{anod} and $i_{O_2}^{ref}$ respectively). The parameter estimation (implemented in Matlab) was performed through a least-squares fit of the simulation results to the experimental polarization data (minimization of the total square error).

Table 2
The default parameters values used in the simulations.

Parameter	Description	Value
T	System temperature	298 K
c_{E_Σ}	Total enzyme concentration (fitted)	1.77×10^{-3} mol m^{-3}
$c^0_{M_{red}}/c^0_{M_{ox}}$	Initial reduced/oxidized mediator concentration [14]	5 mol m^{-3}
c^0_{gluc}	Initial glucose concentration [14]	200 mol m^{-3}
$c^0_{H^+}$	Initial proton concentration (3.2 pH [14])	0.63 mol m^{-3}
$c^0_{H_2O_{(v)}}$	Initial water vapour concentration	0.89 mol m^{-3}
$c^0_{O_2}$	Initial oxygen concentration	8.58 mol m^{-3}
$c^0_{H_2O_{(l)}}$	Initial liquid water concentration	55.5 kmol m^{-3}
c^{*0}_d	Initial (normalized) dissolved water concentration	17.22
D_{H^+}	Diffusion coefficient of protons in anolyte	2×10^{-9} m^2 s^{-1}
D_{M_r}/D_{M_o}	Mediator diffusion coefficient [31]	2×10^{-9} m^2 s^{-1}
D_{gluc}	Diffusion coefficient of glucose [32]	0.7×10^{-9} m^2 s^{-1}
$D_{H_2O_{(l)}}/D_{O_d}$	Diffusion coefficient of liquid water/dissolved oxygen	2×10^{-9} m^2 s^{-1}
$D_{H_2O_{(v)}}/D_{O_2}$	Diffusion coefficient of water vapour/gaseous oxygen	1×10^{-5} m^2 s^{-1}
k_{O_d}	Rate constant of enzyme-dissolved oxygen reaction [24]	2×10^{3} m^3 mol-1 s^{-1}
κ_a (κ_d)	Water adsorption (desorption) coefficient [25]	1.11 (3.33) [$\times10^{-6}$ s^{-1}]
k_{anod}	Rate constant for mediator oxidation (fitted)	0.15 s^{-1}
α_a	Anodic charge transfer coefficient (estimated)	0.57
α_c	Cathodic charge transfer coefficient (estimated)	0.43
$i^{ref}_{O_2}$	Reference current density of oxygen reduction (fitted)	0.093 A m^{-3}
$E^{0\prime}_a$	Benzoquinone equilibrium potential [33]	0.7 V
$E^{0\prime}_c$	Oxygen reduction equilibrium potential (fitted)	0.955 V
ϵ_{cl}	Void fraction in cathode catalyst layer (CCL)	0.2
ϵ_{clp}	Polymer (ionically conducting) fraction in CCL	0.6
ϵ_{al}	Void fraction of carbon felt anode [34]	0.9
ϵ_{Au}	Void fraction of gold mesh	0.6
σ_{al}	Carbon felt electronic conductivity [34]	30 S m^{-1}
σ_{cc} (σ_{Au})	Ti current collector (gold mesh) electronic conductivity	2 (45) [$\times10^6$ S m^{-1}]

To obtain polarization curves (current density vs. cell potential), the potentiostatic model was solved at steady-state. The results were consistent with transient operation simulations, in which the cell potential was decreased in steps, maintaining the value at each step for 10 min intervals and measuring the current at the end of the interval (the same procedure was used in the experiments [14]). The 10 min interval is long enough for transient results to reach steady-state values. The results were also in agreement with equivalent galvanostatic simulations.

Fig. 3 compares the polarization curves from the experimental cell to those from the numerical model. The match is very good, indicating that the model is able to capture the physical processes in the cell to a good degree of accuracy. The short-circuit current (SCC) density is equal to 17.5 A m^{-2}, the open-circuit potential is 0.33 V, and the maximum power density is 1.27 W m^{-2}, at approximately 0.15 V. The cell performance can be characterized by two main factors: a relatively large drop in the reversible open-circuit potential (150 mV, of which approximately 100 mV is due to the decrease in E^0_c as a result of the pH rise), and a relatively large anodic overpotential at the membrane boundary, l_3, compared to the average η_a which remains less than 5 mV at all currents.

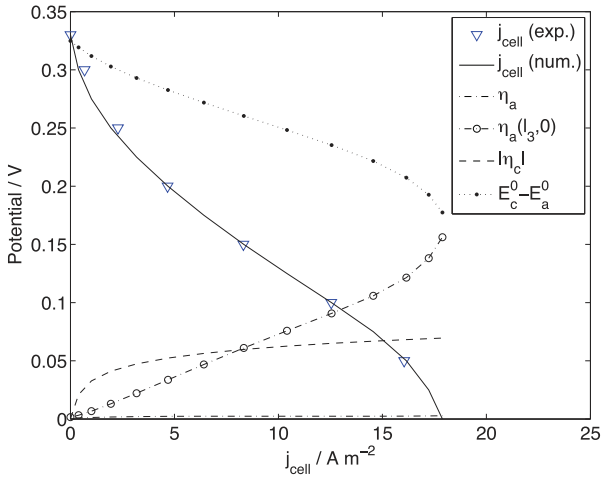

Fig. 3. Simulated and experimentally determined polarization and power curves. The parameter values used in these simulations are given in Table 2.

Fig. 4 shows the mole fractions of the mediator and the enzymes *vs.* the cell current density. The overall performance of the cell is strongly dependent on the reduced enzyme fraction at the membrane boundary, l_3, which quickly drops to 0.5 at 8 A m^{-2}. The anode-averaged reduced fraction of enzyme shows a linear relationship with current and at short-circuit conditions the low mole fraction of M_{red} at the membrane boundary (l_3) is due to both the diffusion limit of M_{red} and the depletion of E_{red}, whose local and average mole fractions are around 0.25 and 0.1 at short circuit conditions. The limiting factor of mediator mass transport is evident from the profile of the reduced mediator fraction across the anode (Fig. 5), which reaches a maximum of 0.82 near the anode inlet, l_4, but drops to nearly 0.15 at the membrane boundary. Profiles of M_{ox} are not shown since the sum of the reduced and oxidized states is equal to the total mediator concentration when the two species have equal diffusion coefficients. Variations along the h direction were negligible and are not, therefore, reported.

Fig. 6 shows the variation in the pH across the cell at $h=0$ for different operating cell potentials. The negligible drop in pH across the MCEA indicates that the rise in cathodic pH is not caused by proton mass transport limitations through the Nafion but is instead

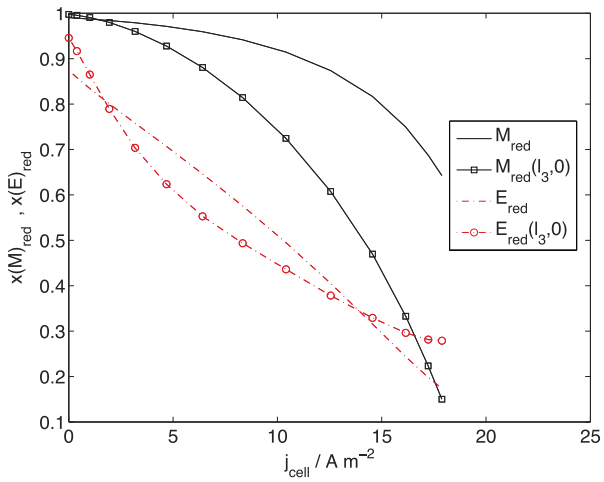

Fig. 4. The enzyme and mediator mole fractions *vs.* cell current density. The parameter values used in these simulations are given in Table 2.

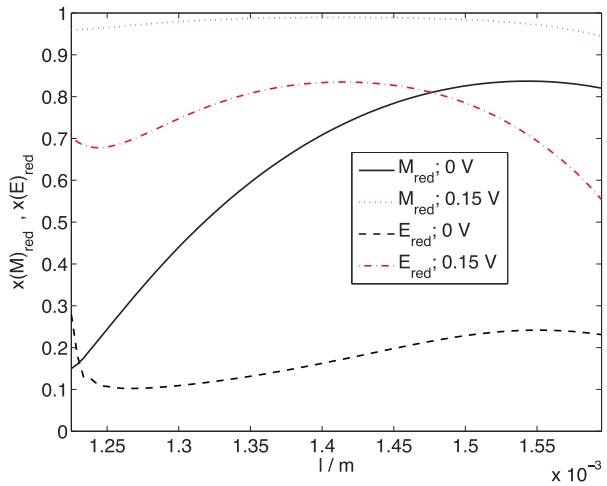

Fig. 5. The enzyme and mediator mole fraction profiles across the anode at different cell potentials. The parameter values used in these simulations are given in Table 2.

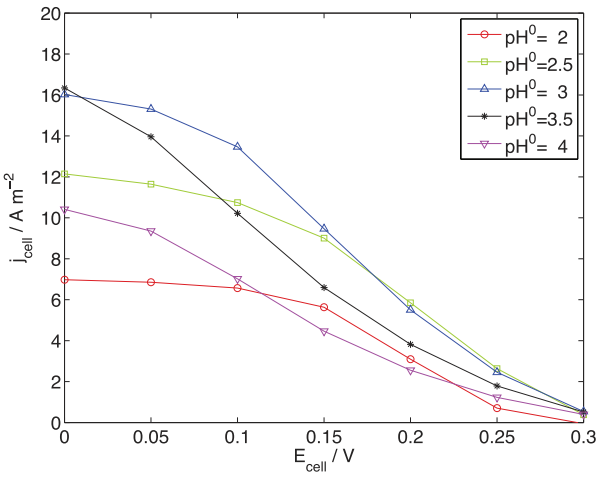

Fig. 7. Polarization curves for different initial pH values. The other parameter values used in these simulations are given in Table 2.

due to a limitation in the rate of proton generation from the anodic reaction, which is confined to a very thin region near the membrane, as evident from the sharp rise in pH at the boundary l_3. The anodic overpotential drops from nearly 150 mV at l_3 to less than 5 mV in a thin region of approximately 35 μm thickness, an indication that the electrochemical reaction is confined to a region in the vicinity of the membrane that is less than 10% of the anode thickness.

The activity of free GOx at pH = 7 is one order of magnitude greater than that at 3.2 pH, measured by UV–vis spectroscopy [14]. These results were obtained using o-dianisidine as the redox indicator which is recycled using a second enzyme, horseradish peroxidase (HRP). In this GOx-HRP setup, the two substrates for GOx are glucose and molecular oxygen, while the product is hydrogen peroxide. The rate of GOx is indirectly obtained by measuring the rate of peroxide reaction with the redox indicator, dianisidine. The pH profiles of enzyme activities are known to depend on the specific mediator used, and those obtained using the GOx-HRP system will generally be different from those used in the fuel cell. To study the effect of pH on the GOx activity with the benzoquinone mediator, the initial pH was varied between 2 to 4. The polarization and power curves for different pH^0 are shown in Fig. 7. With

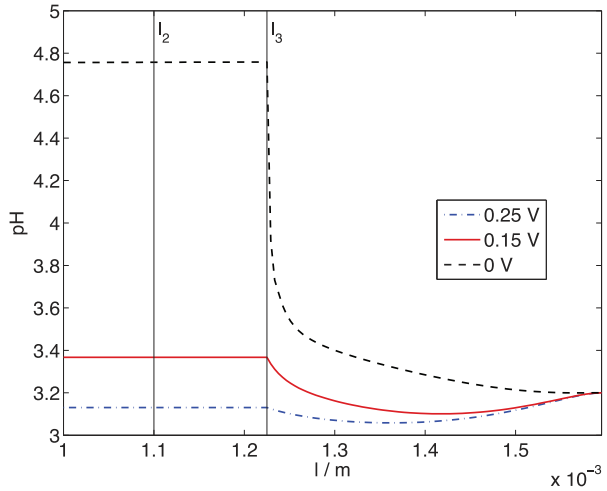

Fig. 6. The pH variation across the cell at different cell potentials. The parameter values used in these simulations are given in Table 2.

increasing pH up to 3, j_{cell} is higher for all cell potentials. At even greater values of pH the cell performance quickly deteriorates. Fig. 8 shows the maximum power and current *vs.* initial pH. The optimum value for maximum power production is around pH = 3. The enzyme reduction and oxidation rates increase and decrease respectively with an increasing pH (Fig. 2), which results in an increase in the reduced enzyme fraction at higher pH values. From pH = 2 to pH = 3, the cell current is higher at all potentials but the reduced mediator fraction still increases with pH. This suggests that the rate of M_{red} production is limited by the amount of (reduced) enzyme and not the rate constant k_{ox}, which decreases at higher pH, but remains two orders of magnitude greater than k_{red}. For pH > 3, the maximum power decreases due to a depletion of M_{ox} (excess of M_{red}), which reduces the concentration dependent term in the Butler–Volmer expression 8 and in turn leads to an increase in the anodic overpotential.

When using enzymes such as GOx that are reactive towards oxygen, it is common practice to bubble the solution with nitrogen to remove traces of the dissolved substrate. Any dissolved oxygen in the solution competes with the mediator for oxidation of the enzyme, according to Eq. (4). Assuming the solution is fully saturated with oxygen ($c^0_{O_d}$ =0.5 mol m^{-3}), the effect of the competing reaction (4) on the cell performance is negligible, even though the rate of reaction E_{red} with molecular oxygen is more than two-fold that of E_{red} with the mediator. At sufficiently high enzyme concentrations (10^{-3} mol m^{-3} in this case), the competing side reaction will proceed to consume the dissolved oxygen with a negligible effect on the current output or the enzyme/mediator mole fractions. Even at 10% of the fitted enzyme concentration, the presence of a third competing substrate has an insignificant effect on the cell performance. When the dissolved oxygen concentration is increased to almost ten-fold the saturation value, the oxygen side reaction begins to affect the availability of E_{red}, which in turn reduces the fraction of M_{red} and the output cell current, as shown in Fig. 9(a).

One major research focus in enzymatic fuel cells is an increase in enzyme loading while maintaining long-term stability. Fischback et al. [14] demonstrated that cross-linked GOx clusters on carbon nano-tubes lead to a high enzyme loading, while retaining the initial activity for 250 days. Fig. 10 shows the dependence of the simulated maximum power and current densities on the total enzyme concentration. The fitted concentration corresponds to the maximum power output. At 10% of the default enzyme concentration, the maximum power output drops to 40% of the maximum

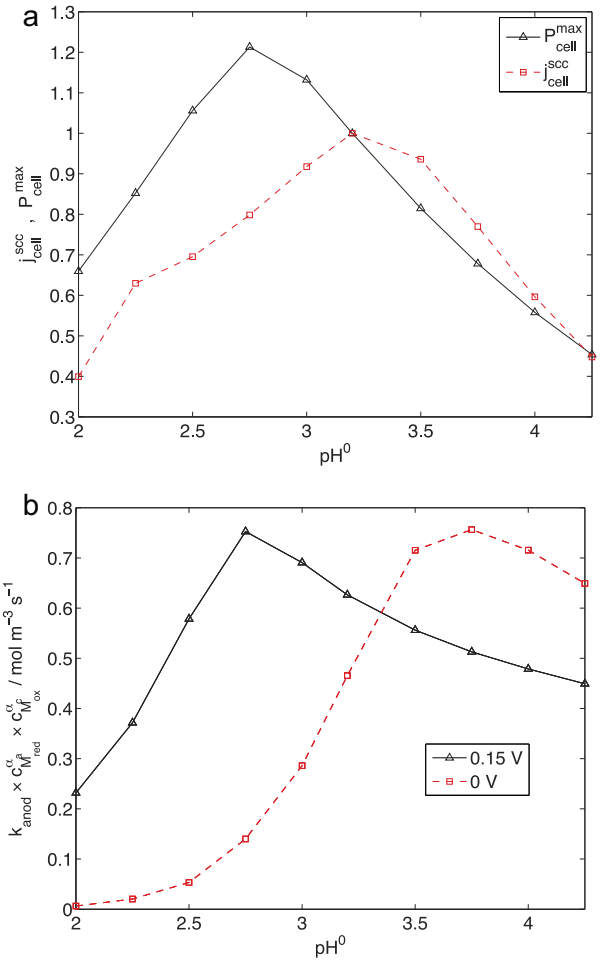

Fig. 8. (a) The maximum power output and short-circuit current (normalized by the default case values corresponding to pH = 3.2); (b) the electrochemical reaction rate for different cell potentials (evaluated at (l_3, 0)) *vs.* the initial pH. The other parameter values used in these simulations are given in Table 2.

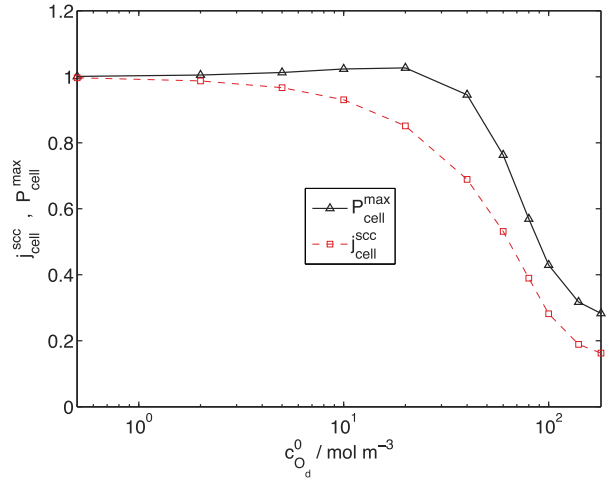

Fig. 9. The maximum power output and short-circuit current (normalized by the default values corresponding to $c^0_{O_d} = 0$) *vs.* the dissolved oxygen concentration. The other parameter values used in these simulations are given in Table 2.

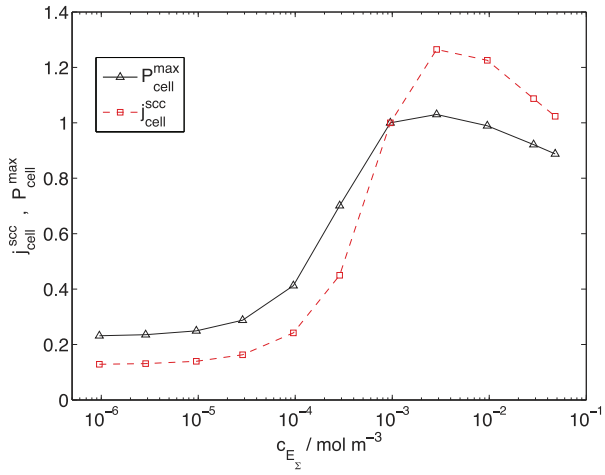

Fig. 10. The maximum power output and short-circuit current (normalized by the default fitted case) *vs.* the total enzyme concentration. The other parameter values used in these simulations are given in Table 2.

value, while at higher enzyme concentrations (greater than 5 to 10 times the default value) the maximum power and current actually decrease. The cause of this deteriorating performance is similar to that seen in the case of operation at high pH values; the increased biological reaction rates (Eqs. (1) and (2)) lead to a depletion in M_{ox}, which in turn leads to a rise in the anodic overpotential (due to the Butler–Volmer form of the current density/reaction rate 8). Thus, increasing the enzyme loading beyond a certain (optimal) value is not beneficial to performance unless the electrochemical limit of the cell is simultaneously altered (e.g., using a different mediator).

4. Conclusions

Very few detailed models of biofuel cells have been developed, despite the considerable efforts directed towards the development of these technologies. In this paper, a detailed, dynamic model of a biofuel cell based on an enzymatic anode and air-breathing cathode was developed and presented. Comparisons to experimental data have demonstrated that the model is able to capture the complex cell process to a good degree of accuracy. The model developed can simulate steady-state as well as dynamic performance, under galvanostatic or potentiostatic conditions.

The simulations presented have revealed details regarding the spatial distributions in the cell. The overall performance of the cell is strongly influenced by the reduced enzyme fraction in the vicinity of the membrane and the diffusion limitation associated with the mediator. The spatial variations in the h (vertical direction) in Fig. 1 were shown to be small when compared to variations in the l (through plane) direction. There is also a strong dependence on the local pH in the anode. For pH > 3, the maximum power is decreased due to a depletion of M_{ox}. A similar result was obtained when the enzyme loading was increased beyond an optimal value, demonstrating that the cell in this case is limited electrochemically.

References

[1] R.A. Bullen, T.C. Arnot, J.B. Lakeman, F.C. Walsh, Biofuel cells and their development, Biosens. Bioelectron. 21 (2006) 2015.
[2] M.J. Cooney, V. Svoboda, C. Lau, G. Martin, S.D. Minteer, Enzymatic Biofuel Cells, Energy Environ. Sci. 1 (2008) 320.
[3] I. Willner, Y.M. Yan, B. Willner, R. Tel-Vered, Integrated Enzyme-Based Biofuel Cells-A Review, Fuel Cell 9 (2009) 7.
[4] I. Ivanov, T. Vidakovi-Koch, K. Sundmacher, Recent advances in enzymatic fuel cells: experiments and modelling, Energies 3 (2010) 803.

[5] E. Katz, A.N. Shipway, I. Willner, Biochemical fuel cells, in: W. Vielstich, H. A. Gasteiger, A. Lamm, (Eds.), Handbook of Fuel Cells – Fundamentals, Technology and Applications, John Wiley & Sons Ltd., New York, 2003.
[6] A.K. Shukla, P. Suresh, S. Berchmans, A. Rajendran, Biological fuel cells and their applications, Curr. Sci. Ind. 87 (2004) 455.
[7] J. Kim, H. Jia, P. Wang, Challenges in biocatalysis for enzyme-based biofuel cells, Biotechnol. Adv. 24 (2006) 296.
[8] A.A. Shah, K.H. Luo, T.R. Ralph, F.C. Walsh, Recent trends and developments in polymer electrolyte membrane fuel cell modelling, Electrochim. Acta 56 (2011) 3731.
[9] M.H. Osman, A.A. Shah, F.C. Walsh, Recent progress and continuing challenges in bio-fuel cells. Part I: Enzymatic, Biosens. Bioelectron. 26 (2011) 3087.
[10] M.H. Osman, A.A. Shah, F.C. Walsh, Recent progress and continuing challenges in bio-fuel cells. Part II: Microbial, Biosens. Bioelectron. 26 (2010) 953.
[11] C. Picioreanu, I.M. Head, K.P. Katuri, M.C.M. van Loosdrecht, K. Scott, A computational model for biofilm-based microbial fuel cells, Water Res. 41 (2007) 2921.
[12] C. Picioreanu, M.C.M. van Loosdrecht, T.P. Curtis, K. Scott, Model based evaluation of the effect of pH and electrode geometry on microbial fuel cell performance, Bioelectrochemistry 78 (2010) 8.
[13] A.S. Bedekar, J.J. Feng, S. Krishnamoorthy, K.G. Lim, G.T.R. Palmore, S. Sundaram, Oxygen limitation in microfluidic biofuel cells, Chem. Eng. Comm. 195 (2008) 256.
[14] M.B. Fischback, J.K. Youn, X. Zhao, P. Wang, H.G. Park, H.N. Chang, J. Kim, S. Ha, Miniature Biofuel Cells with Improved Stability under Continuous Operation, Electroanalysis 18 (2006) 2016.
[15] Michael B. Fischback, Introduction and Characterization of an Innovative Biofuel Cell Platform with Improved Stability Through Novel Enzyme Immobilization Techniques, Washington State University, December 2006 (Master's Thesis).
[16] S. Ha, B. Adams, R.I. Masel, A miniature air breathing direct formic acid fuel cell, J. Power Sources 128 (2004) 119.
[17] T.W. Hui, K.Y. Wong, K.K. Shiu, Kinetics of o-benzoquinone mediated oxidation of glucose by glucose-oxidase at edge plane pyrolytic-graphite electrode, Electroanalysis 8 (1996) 597.
[18] P.N. Bartlett, C.S. Toh, E.J. Calvo, V. Flexer, Chapter 8: modelling biosensor re-sponses, in: P.N. Bartlett (Ed.), Bioelectrochemistry: Fundamentals, Experimental Techniques and Applications, John Wiley & Sons, Ltd., Chichester, UK, 2008.
[19] K. Kano, T. Ikeda, Fundamentals and practices of mediated bioelectrocatalysis, Anal. Sci. 16 (2000) 1013.
[20] J.F. Rustling, B. Wang, S. Yun, Chapter 2. Electrochemistry of redox enzymes, in: P.N. Bartlett (Ed.), Bioelectrochemistry: Fundamentals, Experimental Techniques and Applications, John Wiley & Sons, Ltd., Chichester, UK, 2008.
[21] Y. Tang, Y. Wu, Z. Wang, Spectroelectrochemistry for Electroreduction of p-Benzoquinone in Unbuffered Aqueous Solution, J. Electrochem. Soc. 148 (2001) 133.
[22] Y.B. Shim, S.M. Park, Spectroelectrochemical studies of p-benzoquinone reduction in aqueous media, J. Electroanal. Chem. 425 (1997) 201.
[23] V. Leskovac, S. Trivic, G. Wohlfahrt, J. Kandrac, D. Pericin, Glucose oxidase from Aspergillus niger: the mechanism of action with molecular oxygen, quinones, and one-electron acceptors, Int. J. Biochem. Cell Biol. 37 (2005) 731.
[24] G. Wohlfahrt, S. Trivic, J. Zeremski, D. Pericin, V. Leskovac, The chemical mechanism of action of glucose oxidase from Aspergillus niger, Mol. Cell. Biochem. 260 (2004) 69.
[25] A.A. Shah, G.S. Kim, P.C. Sui, D. Harvey, Transient non-isothermal model of a polymer electrolyte fuel cell, J. Power Sources 163 (2007) 793.
[26] A.A. Shah, G.S. Kim, W. Gervais, A. Young, K. Promislow, J. Li, S. Ye, The effects of water and microstructure on the performance of polymer electrolyte fuel cells, J. Power Sources 160 (2006) 1251.
[27] T.E. Springer, T.A. Zawodinski, S. Gottesfeld, Polymer Electrolyte Fuel Cell Model, J. Electrochem. Soc. 138 (1991) A2334.
[28] S. Motupally, A.J. Becker, J.W. Weidner, Diffusion of Water through Nafion(r) 115 Membranes, J. Electrochem. Soc. 147 (2000) A3171.
[31] C. Gyss, C. Bourdillon, Enzymatic electrocatalysis as a strategy for electrochemical detection in heterogeneous immunoassays, Anal. Chem. 59 (1987) 2350.
[32] M. Andersson, A. Axelsson, G. Zacchi, Diffusion of glucose and insulin in a swelling N-isopropylacrylamide gel, Int. J. Pharm. 157 (1997) 199.
[33] L.G. Shaidarova, A.V. Gedmina, I.A. Chelnokova, G.K. Budnikov, Electrocatalytic Oxidation of Hydroquinone and Pyrocatechol at an Electrode Modified with a Polyvinyl Pyridine Film with Electrodeposited Rhodium and Its Use in the Analysis of Pharmaceuticals, J. Anal. Chem. 59 (2004) 1025.
[34] M. Chatterjee, A. Chatterjee, S. Ghosh, I. Basumallick, Electro-oxidation of ethanol and ethylene glycol on carbon-supported nano-Pt and -PtRu catalyst in acid solution, Electrochim. Acta 54 (2009) 7299.

F806 *Journal of The Electrochemical Society*, **160** (8) F806-F814 (2013)
0013-4651/2013/160(8)/F806/9/$31.00 © The Electrochemical Society

Detailed Mathematical Model of an Enzymatic Fuel Cell

M. H. Osman,[a] A. A. Shah,[b,z] and R. G. A. Wills[a]

[a]*Energy Technology Research Group,School of Engineering Sciences, University of Southampton, Highfields, Southampton SO17 1BJ, United Kingdom*
[b]*School of Engineering, University of Warwick, Coventry CV4 7AL, United Kingdom*

In this paper, two-dimensional steady-state and dynamic models for an enzymatic fuel cell are developed. The anode consists of a biocatalyst (an enzyme cascade of glucose dehydrogenase and diaphorase with VK3 mediator) immobilized in a porous electrically-conducting anode, while glucose and the phosphate buffer are supplied from a solution. An air-breathing bilirubin oxidase/ferricyanide cathode and a cellophane membrane complete the cell unit. Detailed mass and charge balances are combined with a model for the reaction mechanism in the electrodes. The model is validated against experimental polarization data, demonstrating good agreement, and the dynamic performance is discussed. The VK3 equilibrium potential is varied and its effect on the enzymatic system and power output is examined.
 [DOI: 10.1149/1.059308jes]

Manuscript submitted March 11, 2013; revised manuscript received May 6, 2013. Published May 16, 2013.

Biofuel cells operate on the same principles as conventional fuel cells, directly converting chemical energy in a fuel and oxidant into electrical energy. Despite the significantly lower power outputs of biofuel cells compared to conventional cells, they have a number of highly attractive properties: they use renewable bio-catalysts, the can operate under benign pH and temperature conditions, are they able to operate on a much broader range of fuels, tolerating limited impurities in the feedstock.[1–3] Enzymatic fuel cells (EFCs) employ enzymes in isolated and purified forms, which enables the construction of relatively well-defined systems that exhibit a high specificity toward the desired reactions, and avoids the use of dangerous micro-organisms such as *e-coli*.

The concept of biological electron transfer has been applied successfully in biosensors, which are widely available commercially. Much of the interest in enzymatic fuel cells (EFCs) has been motivated by in-vivo medical applications, which require very low power densities. Recent developments, however, have shown that power densities approaching the mW cm^{-2} scale are feasible, with multi-stack designs capable of powering small portable electronic devices.[4] These developments, and the increasing sophistication in assembling efficient bioelectrochemical electrodes are the results of both a greater understanding of the controlling factors in biological redox interactions, and improved techniques in physical electrochemistry that allow ex situ characterization of the electrodes.[5]

Modelling and simulation could play vital roles in further understanding and developing biofuel cells.[2,3] Carefully validated models can be used in conjunction with laboratory studies to investigate the reaction environment, design new electrode architectures and accelerate the development of practical systems. To date, however, only a small number of models have been developed. With few notable exceptions,[6–13] these models are highly simplified, neglecting crucial features such as the dynamics, spatial non-uniformities, ion migration, fluid flow and heat transport. In contrast, the modeling and simulation of batteries and conventional fuel cells, such the polymer electrolyte membrane (PEM) fuel cell,[14] are mature areas of research.

In this paper, a multi-dimensional, transient framework for modeling EFCs is developed. The complex design of the particular cell chosen allows for a general framework to be developed; it contains a biological anode and a biological cathode, as well as a multiple enzyme system in the anode. Detailed mass and charge balances are combined with models for the multistep reaction mechanisms in the electrodes. The model results are rigorously fitted to half-cell experimental data and validated against whole cell data, demonstrating excellent agreement. The framework developed is general and can be applied to other EFC systems.

[z]E-mail: Akeel.Shah@warwick.ac.uk

Model Development

The model presented here is of a system reported by Sakai et al.[4]. The bioanode was composed of immobilized layers of: a hydrophilic cationic polymer, poly-lysine; two enzymes, glucose dehydrogenase (GDH) and diaphorase (DI); their intermediate cofactor, NADH; an electrode mediator, menadione (vitamin K3); and a hydrophilic anionic polymer, polyacrylic acid sodium salt. Solutions of each component were added in the order mentioned on four stacked carbon fiber sheets (10 mm square, 2.11 mm total thickness), and drying of the anode followed each step.

Similarly, the air-breathing biocathode, made of two similar carbon sheets (0.905 mm thick), employed a ferricyanide mediator ($K_3[Fe(CN)_6]$), poly-lysine as an electrolyte, and bilirubin oxidase (BOD). The hydrophilic polymer poly-lysine coated the carbon fiber and BOD was subsequently immobilized on the poly-lysine. The two electrodes were separated by a permeable cellophane membrane, and titanium meshes were used as current collectors. The anode side of the cell was fed with a solution containing a phosphate buffer (1 M, pH 7) and glucose (0.4 M).

Different configurations were constructed to study the separate half cells. The single unit design studied, along with the reaction mechanism is presented in Figure 1. The thickness of the Ti meshes and cellophane were assumed to be 1 mm and 60 μm.

The use of multiple enzyme electrodes as a way to increase the overall efficiency in biofuel cells is receiving increasing attention.[15] It has been used to achieve the complete oxidation of fuels such as methanol[16,17] or glycerol[18] to carbon dioxide. Other systems, such as the diaphorase/NAD^+-dependent dehydrogenases[19–23] are used to complement the individual properties of each enzyme. The optimum pH for GDH is near neutral, while the activity of dissolved glucose oxidase (GOx) in solution is more favorable under slightly acidic conditions.[24] The optimum pH does depend on the chosen mediator and the immobilization method, as is the case for an anode using GOx wired to a redox polymer which is capable of producing maximum current at a wide range of pH from 6 to 10.[25] A fuel cell utilizing Dehydrogenases are incapable of utilizing dioxygen, a natural electron acceptor of glucose oxidase.[26] The dependence on the NAD^+ cofactor makes it necessary to use an intermediate enzyme for NADH oxidation since the direct chemical (*via* a mediator) or electrochemical regeneration of the cofactor proceed at low rates and large overpotentials.[27,21] The use of diaphorase is an efficient method to accelerate NADH oxidation.[28,21] With a great variety of NAD^+-dependent dehydrogenases, the system modeled in this paper can be adapted readily to operate on different types of fuels.

Bilirubin oxidase, a multi-copper enzyme like laccase, can catalyze the four electron reduction of O_2 to water in the presence of a suitable electron donor. This group of enzymes is superior to Pt in cathodes since the electrochemical reduction proceeds at a lower overpotential,[29] without formation of hydrogen peroxide. While

Journal of The Electrochemical Society, **160** (8) F806-F814 (2013) F807

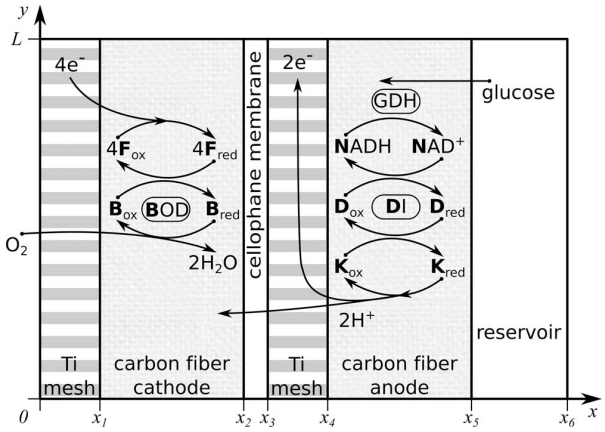

Figure 1. Schematic representation of the fuel cell and the reaction mechanisms.

laccase exhibits very little activity above pH 5, BOD yields a high mediated biocatalytic current at neutral pH.[30–35]

It is noted that research and development by Sony has increased the power output by using a lower potential anode mediator that is less reactive with DI,[36] by replacing the sodium phosphate with an imidazole buffer,[37] and by adding another enzyme to break down the gluconic acid product, alongside other electrode and enzyme modifications.

Reaction kinetics.— Glucose dehydrogenase catalyzes the oxidation of glucose in the presence of NAD^+ *via* the following reaction:[38]

$$GN: \quad \mathrm{G} + \mathrm{N}_{ox} \rightarrow \mathrm{N}_{red} + \mathrm{H}^+ + \mathrm{P} \qquad [1]$$

where N_{ox} and N_{red} represent NAD^+ and NADH respectively. G represents glucose, and P is the product, glucono-lactone. The forward reaction rate can be expressed as follows:

$$R_{GN} = \frac{k_{GDH}}{1 + \mathrm{MM}_G/c_G + \mathrm{MM}_N/c_{\mathrm{N}_{ox}}} \qquad [2]$$

in which MM_G and MM_N are the Michaelis-Menten constants, and c_G and $c_{N_{ox}}$ are the concentrations of glucose and NAD^+, respectively. k_{GDH} is the enzymatic rate, calculated by dividing the experimentally measured enzyme unit, U, by the total anodic volume. Reaction 1 asssumes a simplified or lumped single displacement, in which the glucose substrate and NADH cofactor would bind to the enzyme before GDH catalyzes the proton transfer. The exact mechanism (ordered or random) and the seperate sequential steps are not included, though they may be important for a more accurate description. With the current lack of detail regarding the exact kinetics, the reaction mechanism is simplified and the rate is simply expressed using the extended Michaelis-Menten model for 2 substrates, i.e. a single enzyme turnover rate.

The reactions of diaphorase with the NADH and the mediator K3 follow a 'ping-pong' mechanism involving the oxidized and reduced forms of the diaphorase enzyme (D_{ox} and D_{red}, respectively), as shown below:[22]

$$ND: \quad \mathrm{D}_{ox} + \mathrm{N}_{red} + \mathrm{H}^+ \rightleftarrows \mathrm{D}_{red} + \mathrm{N}_{ox} \qquad [3]$$

$$DK: \quad \mathrm{D}_{red} + \mathrm{K}_{ox} \rightleftarrows \mathrm{D}_{ox} + \mathrm{K}_{red} \qquad [4]$$

where K_{ox} and K_{red} are the oxidized and reduced forms of the mediator, K3 (2-methyl-1,4-naphthoquinone).

Following Takagi et al.[21], the reaction kinetics of the diaphorase enzymes with their electron mediators (reactions 3 and 4) can be written in a Butler-Volmer form:

$$R_{ND} = k_{DI}\left[c_{\mathrm{D}_{ox}} c_{\mathrm{N}_{red}} \exp\left(\frac{2\beta_D F(E_D^0 - E_N^0)}{RT}\right) - c_{\mathrm{D}_{red}} c_{\mathrm{N}_{ox}} \exp\left(\frac{2\alpha_D F(E_D^0 - E_N^0)}{RT}\right)\right] \qquad [5]$$

$$R_{DK} = k_{DI}\left[c_{\mathrm{D}_{red}} c_{\mathrm{K}_{ox}} \exp\left(\frac{2\alpha_D F(E_K^0 - E_D^0)}{RT}\right) - c_{\mathrm{D}_{ox}} c_{\mathrm{K}_{red}} \exp\left(\frac{2\beta_D F(E_K^0 - E_D^0)}{RT}\right)\right] \qquad [6]$$

in which c_i is the concentration of species i, k_{DI} is the (common) rate constant, α_D and β_D are the oxidation and reduction charge-transfer coefficients, respectively, and E_N^0, E_K^0 and E_D^0 are the equilibrium redox potentials for the NADH, K3 mediator and the diaphorase enzyme, respectively. The latter can be calculated using the Nernst equation (equation 17 presented below). The factor of two in the exponential terms represents the number of electrons transferred. The direct electrochemical oxidation of diaphorase, and the mediated electron transfer between NADH and the oxidized K3 are relatively small.[28] They are, therefore, neglected.

The final electrochemical reaction transferring the electrons to the anode is:

$$K: \quad \mathrm{K}_{red} \rightleftarrows \mathrm{K}_{ox} + 2\mathrm{H}^+ + 2e^- \qquad [7]$$

The rate of this reaction can be expressed in Butler-Volmer form as follows:

$$R_K = a_a^s k_K c_{\mathrm{K}_{red}}^{\alpha_K} c_{\mathrm{K}_{ox}}^{(1-\alpha_K)} \times \left[\exp\left(\frac{2(1-\alpha_K)F\eta_a}{RT}\right) - \exp\left(\frac{-2\alpha_K F\eta_a}{RT}\right)\right] \qquad [8]$$

in which a_a^s is the specific surface area of the anode, k_K is the rate constant, α_K is the charge transfer coefficient, and η_a is the anodic overpotential, defined as:

$$\eta_a = \phi_s - \phi_e - E_K^0 \qquad [9]$$

In this expression, ϕ_s and ϕ_e are the electronic and ionic potentials, respectively.

At the cathode, the action of BOD can be divided into a two step mechanism of irreversible reactions:[30]

$$OB: \quad \mathrm{O}_2 + 4\mathrm{H}^+ + \mathrm{B}_{red} \rightarrow \mathrm{B}_{ox} + 2\mathrm{H}_2\mathrm{O} \qquad [10]$$

$$BF: \quad 4\mathrm{F}_{red} + \mathrm{B}_{ox} \rightarrow 4\mathrm{F}_{ox} + \mathrm{B}_{red} \qquad [11]$$

where F_{red} and F_{ox} are the reduced and oxidized forms of the ferro/ferri-cyanide mediator couple ($[Fe(CN)_6]^{-4}$ and $[Fe(CN)_6]^{-3}$, respectively), and B_{red} and B_{ox} are the reduced and oxidized forms of the BOD enzyme, respectively. The rates of reactions 10 and 11 are assumed to take the following forms:

$$R_{OB} = k_{BOD}\, c_{\mathrm{B}_{red}} \left(\frac{c_{\mathrm{H}^+}}{c_{\mathrm{H}^+}^0}\right)\left(\frac{c_{\mathrm{O}_2}}{c_{\mathrm{O}_2}^0}\right) \qquad [12]$$

$$R_{BF} = k_{BOD}\, c_{\mathrm{B}_{ox}} \left(\frac{c_{\mathrm{F}_{red}}}{c_{\mathrm{F}}^0}\right) \qquad [13]$$

where c_i is the concentration of species i and c_i^0 is the reference concentration of species i. The mediator is regenerated at the electrode surface by a one electron transfer:

$$F: \quad \mathrm{F}_{ox} + e^- \rightleftarrows \mathrm{F}_{red} \qquad [14]$$

F808 *Journal of The Electrochemical Society*, **160** (8) F806-F814 (2013)

Table I. Reaction kinetics parameters.

Constant	Description	Value
$E_N^{0\prime}$	Standard equilibrium potential of NADH	−0.54 V 22
$E_D^{0\prime}$	Standard equilibrium potential of diaphorase	−0.456 V 22
$E_K^{0\prime}$	Standard equilibrium potential of K3	−0.23 V 22, 39
$E_F^{0\prime}$	Standard equilibrium potential of ferricyanide	0.29 V 40, 41
k_{GDH}	Estimated rate constant for GDH	0.8 mM s^{-1}
MM_G	Glucose michaelis-menten constant (GDH)	2 mM 42
MM_N	NAD^+ michaelis-menten constant (GDH)	2 mM
k_{DI}	Rate constant for diaphorase	15 mM s^{-1} 21
α_D	Diaphorase oxidation charge-transfer coefficient	0.5 21
β_D	Diaphorase reduction charge-transfer coefficient	0.2 21
k_{BOD}	Rate constant of BOD reactions	205 s^{-1} 33
k_F	Exchange rate for ferri/ferro-cyanide (reaction 14)	5.5×10^{-7} m s^{-1}
k_K	Exchange rate for K3 mediator (reaction 7)	2.9×10^{-8} m s^{-1} 43
α_F	Transfer coefficient for ferricyanide (reaction 14)	0.25 44
α_K	Transfer coefficient for K3 (reaction 7)	0.87

The rate of this electrochemical reaction can be expressed in Butler-Volmer form as shown below:

$$R_F = a_c^s\, k_F\, c_{\mathrm{F}_{red}}^{\alpha_K}\, c_{\mathrm{F}_{ox}}^{(1-\alpha_K)} \left[\exp\left(\frac{-\alpha_F F \eta_c}{RT}\right) - \exp\left(\frac{(1-\alpha_F) F \eta_c}{RT}\right)\right] \quad [15]$$

in which a_c^s is the cathode specific surface area, k_F is the rate constant, α_F is the transfer coefficient, and η_c is the cathode overpotential, defined as:

$$\eta_c = \phi_s - \phi_e - E_F^0 \quad [16]$$

E_F^0 is the equilibrium potential for reaction 14.

The equilibrium potentials for the redox reactions, E_i^0 are approximated using the Nernst equation, i.e., in terms of deviations from the standard values, $E_i^{0\prime}$ (referenced to Ag/AgCl electrode at reference pH 7 in Table I):

$$E_i^0 = E_i^{0\prime} - \frac{RT}{n_e F} \log\left(\frac{c_{i_{red}}}{c_{i_{ox}}}\right) - 0.03\, n_{\mathrm{H}}(\mathrm{pH} - 7) \quad [17]$$

the number of electrons and protons transferred are denoted by n_e and n_{H}, respectively. For the NADH/NAD^+ couple, $n_e = 2$ and $n_{\mathrm{H}} = 1$ (reactions 1 and 3). For the mediator K (reaction 7), $n_e = n_{\mathrm{H}} = 2$. For the diaphorase enzyme (reactions 3 and 4), $n_e = n_{\mathrm{H}} = 2$; one free proton and one proton attached to N_{red}. For the mediator F (reaction 11), $n_e = 1$ and $n_{\mathrm{H}} = 0$. The reaction rate constants are listed in Table I.

Reactant mass balances.— It is assumed that the carbon fiber anode and the carbon fiber cathode were fully impregnated with the respective ionomer, enzyme(s) and mediator. This amounts to an assumption of uniform (but different) volume fractions of each constituent in the electrode.

The anode electrolyte was composed of glucose and a phosphate buffer (concentration $c_{Bfr} = 1$ M). With a pH ranging from near neutral to slightly basic, the ionic species of the buffer considered here (negative log dissociation constant $\mathrm{pK}_a \equiv 7.21$) are the weak acid $H_2PO_4^-$ (denoted 'HA'), the conjugate base HPO_4^{2-} (denoted 'A'), sodium ions (Na^+), and free protons (H^+). Buffer solutions resist changes in pH by maintaining an equilibrium between the weak acid and conjugate base, via the dissociation reaction $\mathrm{HA} \rightleftarrows \mathrm{A} + \mathrm{H}^+$.

Mass balances for glucose, A and HA that take into account transport by diffusion and electro-migration (in the case of the charged species), together with consumption or generation via the reactions, can be written as follows:

$$\epsilon \frac{\partial c_i}{\partial t} + \nabla \cdot \left(-D_i^{\mathrm{eff}} \nabla c_i - \frac{z_i F D_i^{\mathrm{eff}} c_i}{RT} \nabla \phi_e\right) = S_i \quad [18]$$

in which c_i, D_i^{eff}, z_i and S_i are the concentration, effective diffusion coefficient, charge and source term for species i. ϵ is the volume fraction occupied by the phase in which the species moves. In the anode, the species moves through the electrolyte solution, so that $\epsilon = \epsilon_{CF}$, the carbon felt porosity. Similarly, $\epsilon = \epsilon_{Ti}$ in the anode Ti mesh, in which the source terms are zero. In the cathode $\epsilon = \epsilon_{EL}$, the volume fraction of poly-lysine electrolyte. Finally, in the membrane $\epsilon = 1$. In each of the regions, the effective diffusion coefficient for each species is approximated using a Bruggeman correction:

$$D_i^{\mathrm{eff}} = \epsilon^{3/2} D_i \quad [19]$$

where D_i is the corresponding free-space value.

Using equation 18 to solve for HA and A, the pH and the concentration of protons are determined by:

$$-\log_{10}(c_{\mathrm{H}^+}) \equiv \mathrm{pH} = \mathrm{pK}_a + \log_{10}\left(\frac{c_A}{c_{HA}}\right) \quad [20]$$

The sodium concentration is then found from the electro-neutrality condition in the electrolyte:

$$\sum_i z_i c_i = 0 \quad [21]$$

A mass balance for oxygen (in gaseous phase) in the cathode carbon fiber and the Ti mesh can be written as follows:

$$\epsilon \frac{\partial c_{\mathrm{O}_2}}{\partial t} - \epsilon^{3/2} D_{\mathrm{O}_2} \nabla^2 c_{\mathrm{O}_2} = S_{\mathrm{O}_2} \quad [22]$$

in which c_{O_2}, D_{O_2} and S_{O_2} are the concentration, free-space diffusion coefficient, charge and source term for O_2, respectively, and ϵ is the porosity of the relevant region. In the carbon fiber cathode, $\epsilon = \epsilon_{CF} - \epsilon_{EL}$ and the in the Ti mesh, $\epsilon = \epsilon_{Ti}$. Note that a Bruggeman correction is again used.

For the immobilized enzymes and mediators in both carbon electrodes, the molar flux is equal to zero, and equation (18) simplifies to:

$$\frac{\partial c_i}{\partial t} = S_i \quad [23]$$

where c_i is the concentration of N_{red}, D_{red}, K_{red}, B_{ox}, or F_{ox}. The concentrations of the opposite states are found from the fixed total concentration each species i, c_i^0:

$$c_{i_{red}} + c_{i_{ox}} = c_i^0 \quad [24]$$

The source terms appearing in equation 18, 22 and 23 can be found in Table II. The parameters appearing in these mass balances can be found in Table III.

Table II. Source terms in mass and charge balances.

Source term	Cathode	Anode
S_G	–	$-R_{GN}$
$S_{N_{red}}$	–	$R_{GN}-R_{ND}$
$S_{D_{red}}$	–	$R_{ND}-R_{DK}$
$S_{K_{red}}$	–	$R_{DK}-R_K$
S_{O_2}	$-R_{OB}$	–
$S_{B_{ox}}$	$R_{OB}-R_{BF}$	–
$S_{F_{ox}}$	$4R_{BF}-R_F$	–
S_{HA}	$-4R_{OB}$	$R_{GN}-R_{ND}+2R_K$
S_ϕ	$-F\,R_F$	$2F\,R_K$

Charge balances.— The flow of a charged species i in the electrolyte gives rise to a current density $\vec{j}_i = z_i F \vec{N}_i$, where z_i is the charge and $\vec{N}_i$ is the molar flux (driven by diffusion and electromigration in the present case). Therefore, the total current density in the electrolyte, $\vec{j}_e$ satisfies:

$$\vec{j}_e = \sum_i \vec{j}_i = -\sigma_e \nabla\phi_e - F\sum z_i D_i^{\text{eff}} \nabla c_i \qquad [25]$$

where the effective conductivity σ_e is given by:

$$\sigma_e = \epsilon^{3/2}\frac{F^2}{RT}\sum z_i^2 D_i^{\text{eff}} c_i \qquad [26]$$

in which $\epsilon = \epsilon_{CF}$ (the free space) in the anode carbon fiber electrode, $\epsilon = \epsilon_{EL}$ in the cathode carbon fiber electrode, $\epsilon = \epsilon_{Ti}$ in the anode titanium mesh, and $\epsilon = 1$ in the cellophane membrane. The charge balances in these ion-conducting regions are now given by:

$$-\nabla\cdot\vec{j}_e = -S_\phi \qquad [27]$$

where the charge source terms S_ϕ are defined in Table II. This source term represents the volumetric transfer current density and is, therefore, equal to zero in regions where electrochemical reactions do not occur.

The electronic current, $\vec{j}_s$ is governed by Ohm's law. Conservation of charge within the porous regions ($\nabla\cdot\vec{j}_s + \nabla\cdot\vec{j}_e = 0$) leads to:

$$-\nabla\cdot\vec{j}_s = -\nabla\cdot\left(\epsilon^{3/2}\sigma_s\nabla\phi_s\right) = S_\phi \qquad [28]$$

Table III. Mass and charge balance parameters.

Constant	Description	Value
c_G^0	Initial glucose concentration	0.4 M 4
c_{HA}^0	Initial weak acid concentration	0.618 M
c_A^0	Initial weak acid concentration	0.382 M
c_N^0	Total (NADH + NAD^+) concentration	0.119 M 4
c_K^0	Total K3 concentration	77 mM 4
c_D^0	Total diaphorase concentration	31.6 nM
c_B^0	Total BOD concentration	6.26 *mu*M
c_F^0	Total ferricyanide concentration	88.4 mM 4
D_{O_2}	Oxygen gas diffusion coefficient	2×10^{-5} m^2 s^{-1} 45
D_i	Diffusion coefficient of electrolyte ions	2×10^{-9} m^2 s^{-1}
D_G	Glucose diffusion coefficient	2×10^{-9} m^2 s^{-1}
ϵ_{Ti}	Porosity of titanium mesh	0.9
ϵ_{CF}	Porosity of carbon felt	0.7
ϵ_{EL}	Electrolyte volume fraction in cathode	0.5
σ_{Ti}	Conductivity of titanium	2×10^6 S m^{-1}
σ_{CF}	Conductivity of carbon fiber sheet	1250 S m^{-1}
a_a^s	Anode specific surface area	9600 m^{-1} 4
a_c^s	Cathode specific surface area	11000 m^{-1} 4

where σ_s is the conductivity of the electron conducting phase of volume fraction ϵ: $\epsilon = 1-\epsilon_{CF}$ in the CF electrodes and $\epsilon = 1-\epsilon_{Ti}$ in the titanium mesh.

The dynamic model developed above is transformed into a steady-state model by neglecting the time derivative and the initial conditions presented below.

Initial and boundary conditions.— The cell is considered to be operated in potentiostatic mode, i.e., a cell voltage, V_{cell} was imposed (applied through equipotential surfaces at the top boundaries of the two Ti mesh current collectors shown in Figure 1):

$$\phi_s = \begin{cases} V_{cell} & (0 \le x \le x_1;\ y = L) \\ 0 & (x_3 \le x \le x_4;\ y = L) \end{cases} \qquad [29]$$

The output current density relative to the electrode area, j_{cell}, is measured along the top surface of the Ti mesh current collector in the cathode (see Figure 1), where the current is purely electronic:

$$j_{cell} = \left(\frac{1}{L}\right)\int_0^{x_1}\left(-\sigma_s\frac{\partial\phi_s}{\partial y}\right)dx \qquad [30]$$

The electronic current is carried in the Ti meshes and carbon fiber electrodes. With the exception of the two equipotential surfaces specified above, all exterior boundaries are electrically insulating:

$$-\vec{n}\cdot(-\sigma_s\nabla\phi_s) = 0 \qquad [31]$$

in which $\vec{n}$ is the normal unit vector pointing outwards. Similarly, insulation conditions apply at the exterior boundaries for the ionic current ($x = x_1, x_6;\ y = 0, L$).

The (homogeneous) initial conditions for the immobilized species in the electrodes are assumed to correspond to equilibrium conditions:

$$c_{i_{red}} = c_{i_{ox}} = c_i^0 \qquad [32]$$

The concentration of oxygen at the air inlet, $x = 0$, and the concentrations of the soluble anolyte species (glucose, acid, base) at the inlet to the anode electrode, $x = x_6$ (0.5 mm from the anode edge, x_5), are given by (consistent with the initial concentrations):

$$c_i = c_i^0 \quad (x = 0, x_6) \qquad [33]$$

For the soluble anolyte species, insulation conditions (no mass flux) are imposed at all other exterior boundaries (x_1, $y = 0, L$):

$$-\vec{n}\cdot\left(-D_i^{\text{eff}}\nabla c_i - \frac{z_i F D_i^{\text{eff}} c_i}{RT}\nabla\phi_e\right) = 0 \qquad [34]$$

Similarly, insulation conditions are imposed at the exterior boundaries of gaseous oxygen (x_2, $y = 0, L$). Continuity of mass and charge flux is applied at all interior boundaries.

Results and Discussion

The system of equations described above was solved using COMSOL Multiphysics. The multiphysics modules used were the diffusion and convection, to solve for the species concentrations, and the general partial differential equation solver, to solve for the potentials. In order to match the simulation results to the experimental data of Sakai et al.[4] the following parameters were estimated using a rigorous nonlinear least-squares analysis implemeted by applying the MATLAB function `lsqcurvefit` and using the default settings (values for these parameters were not available):

1. In the anode: the *initial* DI concentration, c_D^0, and the K3 transfer coefficient, α_K.
2. In the cathode: the *initial* concentration, c_B^0, the mediator exchange rate, k_F.

These constants were estimated by comparing separate half-cell model (not detailed here) simulations half-cell experimental data contained in the Supplementary Data of Sakai et al.[4] (shown in Figure 2(a)). The parameter estimation (implemented in Matlab) was

F810 *Journal of The Electrochemical Society*, **160** (8) F806-F814 (2013)

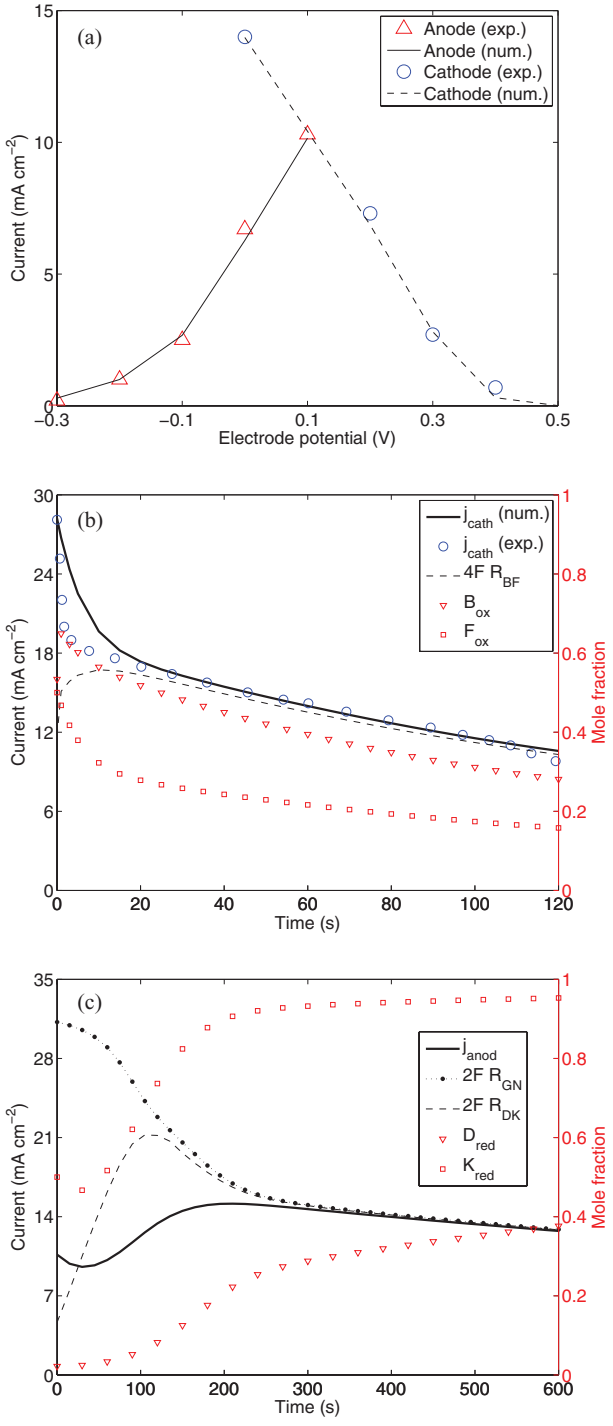

Figure 2. (a) Fitted half-cell simulations together with the corresponding experimental results; (b) the transient half-cell response of the cathode at 0 V and (c) the transient half-cell response of the anode at 0.1 V. The model parameters are as given in Tables I and III.

performed through a nonlinear least-squares fit of the simulation results to the half-cell polarization data (minimization of the least-square error) and the quality of the eventual fit is depicted in Figure 2. The estimated parameter values are given in Tables I and III. The glucose dehydrogenase rate constant, k_{GDH}, was estimated to be 10% of the experimentally reported GDH activity in solution, and the fitted total BOD concentration, c_B^0, was approximately 1% of the reported amount of immobilized enzyme.[4] The value of MM_N was arbitrarily chosen equal to that of glucose. The effect of a reduction in MM_N by a factor of 10 (the value in [4]), on the half-cell and whole-cell polarization curves was found to be negligible. This order of magnitude decrease did, however, slightly alter the diaphorase mole fraction distribution. The reason for the negligible variations is the high GDH rate (the N_{red} fraction exceeds 0.85 at all cell voltages), while reducing MM_N increases the GDH rate and the N_{red} fraction even further but has little effect on the diaphorase and K mediator. When approximating the total amount of enzyme in the ping-pong mechanism, values were found to be lower than the experimental values due to both a lower activity of the immobilized enzyme, and the definition of the total enzyme, which excludes the enzyme-substrate complexes (equation 24). In both cases, these values are in agreement with the reduction of immobilized enzymatic activity reported in the literature.

To understand the limitations and transient behavior of the full cell, it is useful to first investigate the performance of each half cell. Figure 2(b) compares the numerically simulated cathodic half-cell current density j_{cath} (at 0 V *v.s* reference electrode) for the first two minutes to the reported experimental half cell data. The simulated initial cathodic current density is approximately 28 mA cm^{-2} and drops rapidly to around 18 mA cm^{-2}. This indicates a relatively faster electrochemical rate compared to the enzymatic regeneration of the oxidized mediator, F_{ox}. The difference between the simulated and experimental curves (a more rapid drop in the current density in the latter case) is probably due to the fact that the BOD enzyme and the active carbon-fiber surface area are separated by a poly-L-lysine layer (not included in the model), and in reality the mediator at the carbon fiber side is rapidly depleted. After the initial drop, the current continues to steadily decrease from 18 to 10 mA cm^{-2} after 2 minutes of potentiostatic operation. This slower decrease is due to proton depletion in the cathode, leading to a reduction in the concentration of oxidized enzyme and consequently a drop in the oxidized mediator concentration, accompanied by a significant drop in the current density. After 10 minutes of operation, the cathodic current approaches the steady-state value of 3 mA cm^{-2}, which represents the proton mass transport limit in the cathode.

Numerical simulations of the anodic half-cell current density at 0.1 V potentiostatic operation are depicted in Figure 2(c). Corresponding experimental results were not available for comparison. The initial anodic current density remains at around 10 mA cm^{-2} during the first minute, and is limited by both a relatively slower electrochemical rate of the K3 mediator and an initially low diaphorase reaction rate. The equilibrium potential difference between DI and K3 is a factor of 2.7 greater than that between DI and NAD$^+$, leading to a higher rate of reaction DK than that of ND ((5) and (6)). Hence, the diaphorase species is in an almost completely oxidized state in the initial stages (as indicated by the low value of D_{red}). As the initially high GDH rate (see reaction (1)) increases the concentration of N_{red}, the diaphorase rates also increase and the anodic current reaches almost 15 mA cm^{-2} after 3 minutes of operation at 0.1 V. The steady drop in current that follows is due to a pH decrease in the anode.

The results discussed below pertain to the full-cell model. The default model parameters used in the simulations are given in Tables I and III.

A potential sweep was simulated by increasing V_{cell} in steps of 0.1 V from 0 to 0.8 V. The cell voltage was held constant at each potential for 60 s, and the current density and other quantities were estimated at the end of each 60 s constant-voltage period, as in the equivalent laboratory experiments.[4] The numerical simulations and the experimental data are plotted in Figure 3, which shows that the model captures the experimental data extremely well (using the parameters obtained from the least-squares fitting described above). The experimental error in the maximum power density of 1.45 mW cm^{-2} at 0.3 V was reported to be $\pm$ 0.24 mW cm^{-2} ($\pm$ 0.8 mA cm^{-2}). Both the experimental and simulated polarization curves suggest a short-circuit current density of around 11 mA cm^{-2} (after 60 s at $V_{cell} = 0$ V).

Journal of The Electrochemical Society, **160** (8) F806-F814 (2013) F811

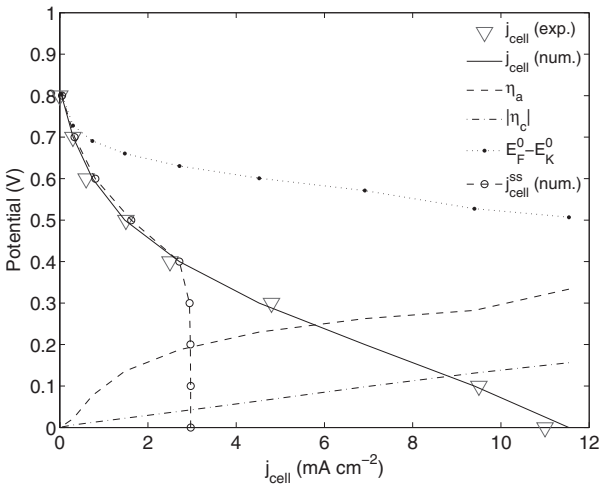

Figure 3. A comparison of the simulated and experimental polarization curves obtained from a potential sweep (V_{cell} = 0.1, 0.2, . . . , 0.8 with 60 s hold at each potential), using the model parameters in Tables I and III. Also shown are the electrode overpotentials and the cell equilibrium potential.

The simulated anode and cathode overpotentials are also displayed in Figure 3. These plots show that the transient cell performance is influenced more by the anode than the cathode. The limiting anode process is discussed in detail below. The steady-state current is limited by proton mass transport to 3 mA cm^{-2} at cell voltages lower than 0.4 V.

Since the mediators and enzymes are immobilized, their concentrations are determined solely by the relevant reaction rates (Table II). The electrode averaged mole fractions of the reactants ($c_{i_{ox}}/c_i^0$ or $c_{i_{red}}/c_i^0$) as functions of the current density during the potential sweep are shown in Figure 4. Deviations from the equilibrium value (0.5) of the mole fraction of a reduced or oxidized species is an indicator of its net rate of production/consumption. The mole fraction of N_{red} is greater than 0.8 at all current densities. From the relative concentrations in Figure 4 (and from the reaction rate calculations directly), it is possible to distinguish two regions of anodic performance.

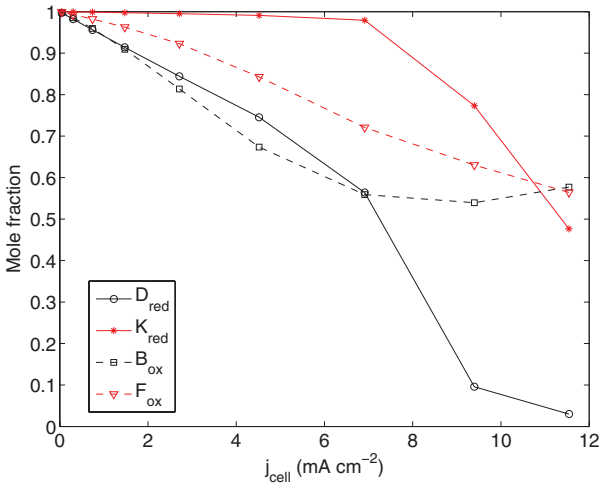

Figure 4. Normalized concentrations vs. j_{cell} for a potential sweep (V_{cell} = 0.1, 0.2, . . . , 0.8 with 60 s hold at each potential), using the model parameters in Tables I and III.

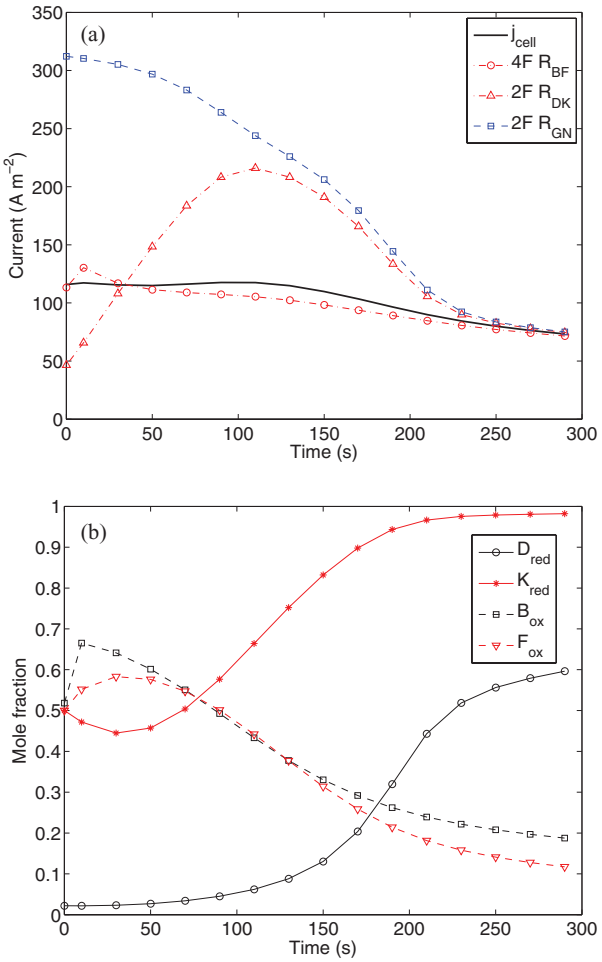

Figure 5. Time evolution at short-circuit (V_{cell} = 0 V) of: (a) j_{cell} and the enzymatic reaction rates and (b) the averaged mole fractions. The model parameters are as given in Tables I and III.

1. For current densities below 7 mA cm^{-2}, the rates of the reactions can be ordered as follows: $R_{ND} > R_{DK} > R_K$ (see reactions 3, 4 and 7). In this region, K_{red} is in excess.
2. For current densities in the range 7−11.5 mA cm^{-2}, the rates of the reactions can be ordered as follows: $R_{ND} < R_{DK}$ and $R_{DK} > R_K$. This leads to a decrease in the mole fraction of D_{red} below 0.5, while the mole fraction of K_{red} remains above the equilibrium value of 0.5.

If higher short-circuit current densities could be achieved by the mediator reaction 7, with rate R_K, a third region would exist where the rates of the reactions can be ordered as follows: $R_{ND} < R_{DK} < R_K$. In this range, only N_{red} remains in excess, while the mole fraction of K_{red} drops below 0.5 and the reduced diaphorase fraction approaches zero.

While the potential sweep results with 1 minute intervals show that the short-circuit current is limited to the maximum anodic current, longer operating times indicate that the the BOD reactions 10 and 11 are also limiting. Figure 5(a) shows the evolution of the cell current density and of the current densities associated with reactions 1, (4) and (11) for V_{cell} = 0 V. After 2 minutes of operation, j_{cell} begins to decrease due to a relatively low value of R_{BF}. This can also be seen from the decrease in the oxidized mole fractions ($c_{i_{ox}}/c_i^0$) of the enzyme and mediator in the cathode, as shown in Figure 5(b). As the rate of reaction 11 continues to fall, the mediator F_{ox} is increasingly

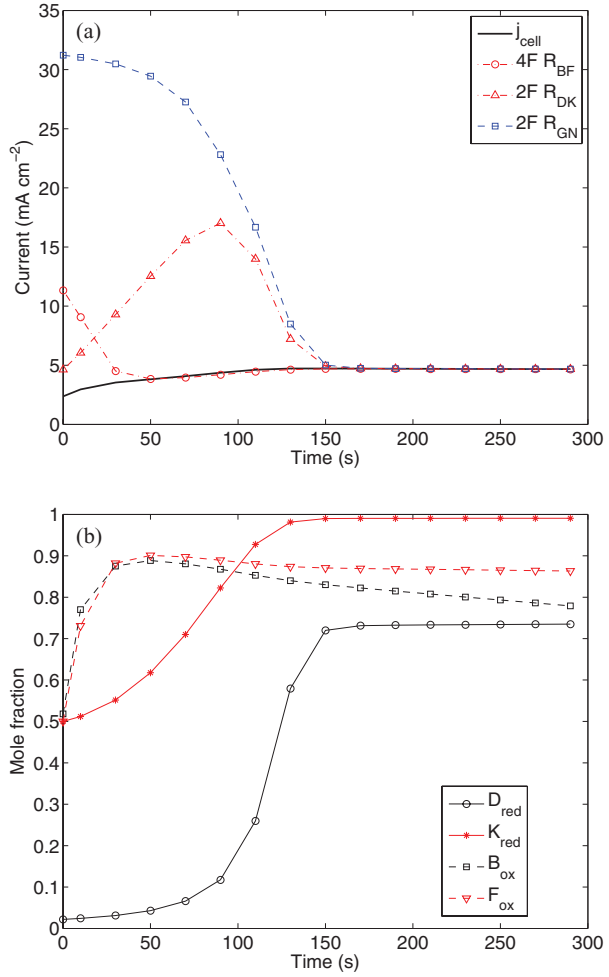

Figure 6. Time evolution at $V_{cell} = 0.3$ V of: (a) j_{cell} and the enzymatic rates and (b) the averaged mole fractions. The model parameters are as given in Tables I and III.

depleted, which lowers the rate of electron transfer step (14). At this cell voltage, the cathodic pH rapidly increases to a value in excess of 8 after 5 minutes of operation.

When calculating the oxidized and reduced enzyme concentrations using the ping-pong mechanism, the low enzyme concentrations, compared to those of the mediators and cofactors, limit the deviation from equilibrium of the two enzyme reactions. $S_{D_{red}}$, and $S_{B_{ox}}$ remain very close to zero, or undergo a rapid and short-lived change that rapidly alters the distribution in the enzyme state. For this reason, separate rates for reactions 3/4 and 10/11, i.e., R_{ND}/R_{DK} and R_{OB}/R_{BF}, are not shown (they are approximately equal except for short durations), and the enzyme state is interpreted from the enzyme mole fractions.

When the cell is operated at 0.3 V, j_{cell} is limited by the rate of the electron transfer step (7) involving the K3 mediator in the anode (Figure 6), as discussed above in relation to the half cell results; Figure 6(a) clearly demonstrates that the enzymatic reaction rates are not limiting. As shown in Figure 6(b), after 3 minutes of operation the mole fractions of reduced diaphorase and K3 mediator in the anode and the mole fractions of oxidized BOD and mediator in the cathode exceed values of 0.7, indicating that the electron transfer steps (7) and (14) are slow.

The cell performance for longer operating times is still limited by the pH increase in the cathode (as found in the half-cells results), though the rise in pH at low current densities is slower. Figure 7

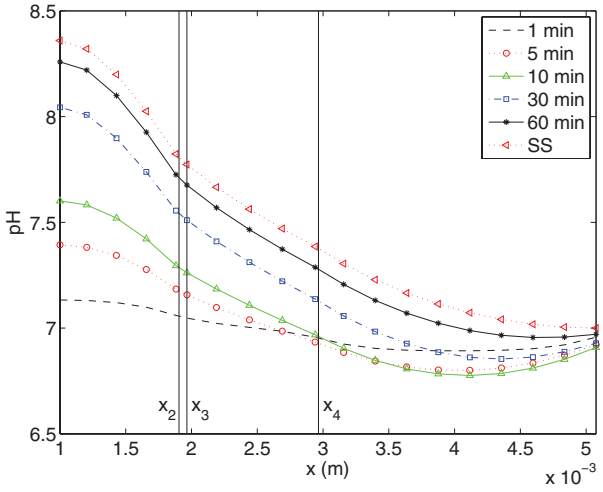

Figure 7. The pH variation across the cell ($x_1 \leq x \leq x_5$ in Figure 1) for $V_{cell} = 0.3$ V at different times during transient simulation and also at steady-state. The model parameters are as given in Tables I and III.

shows the pH variation across the cell ($x_1 \leq x \leq x_5$ as defined in Figure 1) at $V_{cell} = 0.3$ V. Steady-state and transient simulations longer than 1 hour show that the limiting current is around 3 mA cm^{-2} for all cell voltages below 0.4. The pH rise in the cathode reduces the oxidized fractions of BOD and cathode mediator. The drop in the F_{ox} concentration, particularly close to the Ti mesh/carbon fiber interface ($x = x_1$), leads to a large increase in the cathodic overpotential. The limiting current does not change considerably if the anode reservoir boundary conditions are changed to accommodate a time-varying, acidic buffer in a 3 mL reservoir.

Figure 8 shows the variation in the cathodic overpotentials at different times ($x_1 \leq x \leq x_2$ in Figure 1). In these simulations the cell is operated at short-circuit (0 V). Similar to the previous results pertaining to $V_{cell} = 0.3$ V, after 30 mins of operation the depletion of oxidized species in the cathode is greater at the air side ($x = x_1$). The electrochemical reaction is then concentrated at the membrane side of the cathode where the proton and F_{ox} concentrations are relatively high. After 30 mins of operation, the overpotential at x_2 is almost 30 mV more negative than the value at x_1. The variation in the overpotential across the anode is less pronounced, although the electrochemical

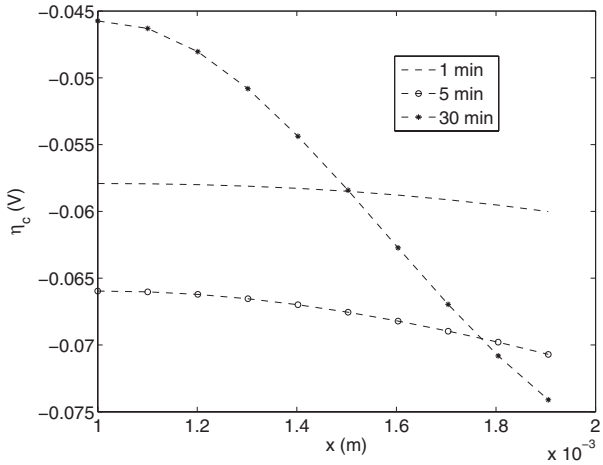

Figure 8. Overpotential in the cathode ($x_1 \leq x \leq x_2$ in Figure 1) at $V_{cell} = 0$ V. The model parameters are as given in Tables I and III.

Journal of The Electrochemical Society, **160** (8) F806-F814 (2013) F813

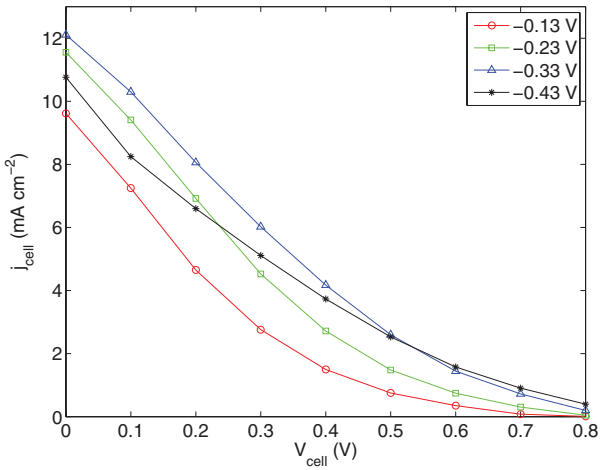

Figure 9. Polarization curves obtained from potential sweeps (V_{cell} = 0.1, 0.2, . . . , 0.8, with 60 s hold at each potential) for different mediator potentials, $E_K^{0\prime}$. The other model parameters are as given in Tables I and III.

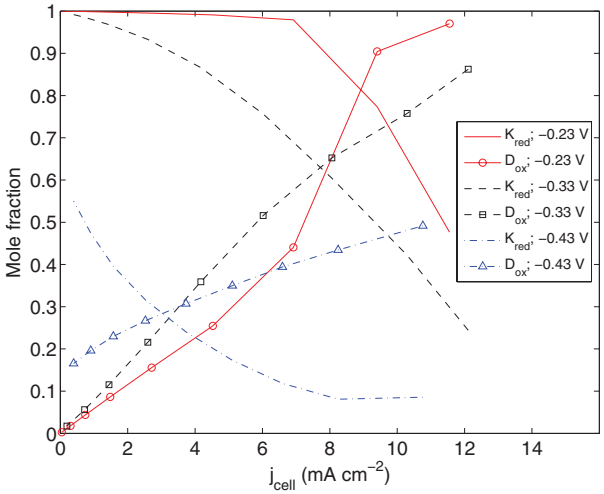

Figure 11. Concentrations of K_{red}, D_{ox} versus current for different mediator potentials, $E_K^{0\prime}$, from potential sweeps of V_{cell} = 0.1, 0.2, . . . , 0.8, with 60 s hold at each potential. The other model parameters are as given in Tables I and III.

reaction is slightly more active on the current-collector side of the anode, which is favorable for proton generation and migration to the cathode. Variations in the species concentrations and in the potentials across in the y direction were found to be negligible and are not therefore shown.

The choice of K3 as a mediator for DI is based on its high reactivity, which is partly due to its equilibrium potential, around 0.22 V higher than DI. A mediator with a lower potential will be less reactive with DI (lower R_{DK}) but, on the other hand, would increase the reversible open-circuit cell voltage. Figure 9 shows the potential sweep curves (V_{cell} = 0, 0.1, 0.2, . . . , 0.8 V, with hold for 60 s at each potential difference) for four cells with different hypothetical $E_K^{0\prime}$ = −0.13, −0.23 (default value), −0.33 and −0.43 V; the last potential is only 26 mV more positive than that of diaphorase. With the exception of this last case, the cell current density is higher at all voltages as $E_K^{0\prime}$ is made more negative. When the standard equilibrium potentials of DI and K3 are almost equal ($E_K^{0\prime}$ = −0.43 V), however, j_{cell} is lower in almost the entire range of cell voltages compared to $E_K^{0\prime}$ = −0.33 V. The net effect on the output power density curves is shown in Figure 10. Clearly, the optimum peak power is achieved when $E_K^{0\prime} \approx -0.33$ V, rather than the default value of −0.23 V.

Figure 11 shows the mole fractions of the oxidized DI and reduced K3 at three mediator equilibrium potentials. For increasingly negative values of $E_K^{0\prime}$, K_{red} is lower for any given current density. At values of $E_K^{0\prime}$ more positive than −0.23 V, the rate R_{DK} of reaction 4 increases and the fraction of reduced K3 mediator remains high at all current densities. The point of cross-over (0.5 mole fraction) in the state of the K3 mediator changes from 11.5 to 1 mA cm^{-2} as $E_K^{0\prime}$ is lowered from −0.23 V to−0.43 V. The oxidized DI enzyme fraction at short-circuit is also lowered as the mediator equilibrium potential is reduced. When $E_K^{0\prime}$ = −0.43 V, the rate R_{DK} decreases significantly compared to R_{ND}, and the fraction of oxidized DI enzyme remains below its equilibrium value (0.5) at all current densities.

In a bioanode, the oxidized electrode mediator is continually consumed by the enzyme. At low electrical currents this results in a near-zero oxidized fraction, effectively reducing the exchange current

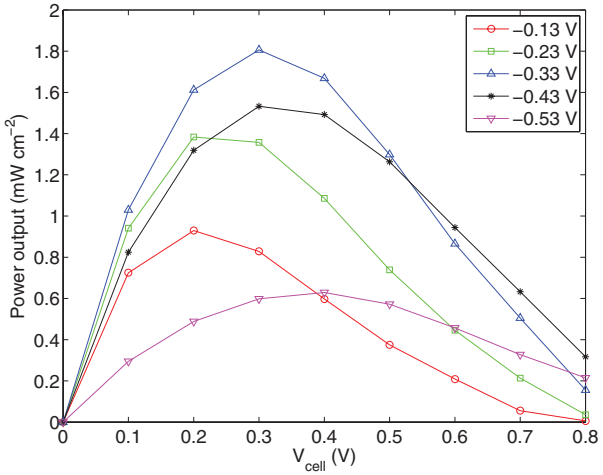

Figure 10. The power density curves obtained for different mediator potentials, $E_K^{0\prime}$, from potential sweeps of V_{cell} = 0.1, 0.2, . . . , 0.8, with 60 s hold at each potential. The other model parameters are as given in Tables I and III.

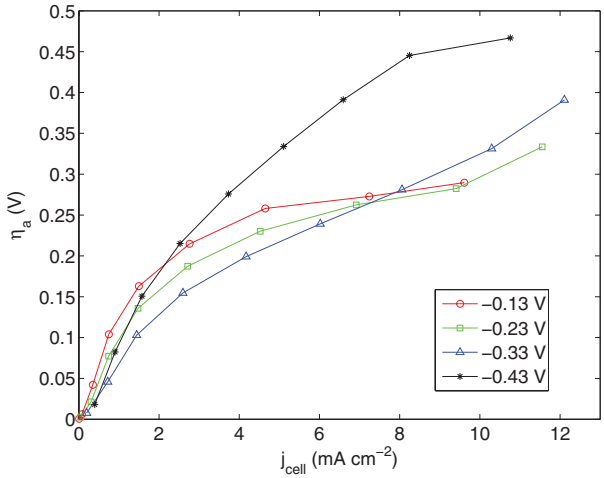

Figure 12. Anodic overpotential versus current for different mediator potentials, $E_K^{0\prime}$, from potential sweeps of V_{cell} = 0.1, 0.2, . . . , 0.8, with 60 s hold at each potential. The other model parameters are as given in Tables I and III.

density (equation 15). This effect is seen in the anodic overpotential in Figure 12 and explains the poor performance using the default value of R_{DK}. If the rate constant K_{red} is in less excess at low current and the electrochemical reaction is effectively faster.

Conclusions

Very few detailed models of biofuel cells have been developed, despite the considerable efforts directed toward the development of these technologies. In this paper, a detailed, dynamic model of a complete biofuel cell based on an enzyme cascade anode and biocathode was presented. Comparisons to experimental data have demonstrated that the model is able to capture the complex physical and bio-electrochemical phenomena within the cell to a good degree of accuracy.

The simulations presented have revealed details regarding the spatial and temporal behavior of the cell. These details depend to some extent on the values of the fitting parameters used. With the availability of rate constants and other measurable parameters, the methodology can provide more accurate predictions. The model presented here can be extended to other enzymatic and microbial systems, applying the same principles of mass, charge and momentum conservation. Perhaps the most challenging aspect of biofuel cell modeling lies in capturing the loss of biochemical activity that is an inevitable feature of these systems. In future work, the long-time performance of biofuel cell systems will be investigated.

Other improvements planned for this model include incorporating the acid dissociation constants of the electrode polymers in calculating the pH, and introducing the electrolyte thin film in the gas-diffusion cathode. The former addition is aimed at capturing the initial experimental pH which differs from that of the buffer, while the latter addition would lead to more accurate predictions of the cathodic current density. It would also permit a study of the effect of the carbon fiber diameter and film thickness on the performance of the electrode.

References

1. G. T. R. Palmore, Chapter 10. *Biofuel Cells, in Bioelectrochemistry: Fundamentals, Experimental Techniques and Applications* (ed P. N. Bartlett), John Wiley & Sons, Ltd, Chichester, UK, 2008.
2. M. H. Osman, A. A. Shah, and F. C. Walsh, *Biosens. and Bioelectron.*, **26**, 3087 (2011).
3. M. H. Osman, A. A. Shah, and F. C. Walsh, *Biosens. and Bioelectron.*, **26**, 953 (2010).
4. H. Sakai, T. Nakagawa, Y. Tokita, T. Hatazawa, T. Ikeda, S. Tsujimura, and K. Kano, *Energy Environ. Sci.*, **2**, 133 (2009).
5. *Electrochemistry of Redox Enzymes, in Bioelectrochemistry: Fundamentals, Experimental Techniques and Applications* (ed P. N. Bartlett), John Wiley & Sons, Ltd, Chichester, UK, 2008.
6. T. Tamaki, T. Ito, and T. Yamaguchi, *Fuel Cells*, **9**, 37 (2009).
7. C. Picioreanu, M. C. M. van Loosdrecht, T. P. Curtis, and K. Scott, *Bioelectrochem.*, **78**, 8 (2010).
8. C. Picioreanu, K. P. Katuri, M. C. M. van Loosdrecht, I. M. Head, and K. Scott, *J. Appl. Electrochem.*, **40**, 151 (2010).
9. C. Picioreanu, I. M. Head, K. P. Katuri, M. C. M. van Loosdrecht, and K. Scott, *Water Res.*, **41**, 2921 (2007).
10. A. S. Bedekar, J. J. Feng, S. Krishnamoorthy, K. G. Lim, G. T. R. Palmore, and S. Sundaram, *Chem. Eng. Comm.*, **195**, 256 (2008).
11. E. Kjeang, D. Sinton, and D. A. Harrington, *J. Power Sources*, **158**, 1 (2006).
12. P. Kar, H. Wen, H. Li, S. D. Minteer, and S. Calabrese-Barton, *J. Electrochem. Soc.*, **158**, B580 (2011).
13. N. Martens and E. A. H. Hall, *Anal. Chem.*, **66**, 2763 (1994).
14. A. A. Shah, T. R. Ralph, and F. C. Walsh, *J. Electrochem. Soc.*, **156**, B465 (2009).
15. D. Sokic-Lazic, R. L. Arechederra, B. L. Treu, and S. D. Minteer, *Electroanalysis*, **22**, 757 (2010).
16. G. T. R. Palmore, H. Bertschy, S. H. Bergens, and G. M. Whitesides, *J. Electroanal. Chem.*, **443**, 155 (1998).
17. P. K. Addo, R. L. Arechederra, and S. D. Minteer, *Electroanalysis*, **22**, 807 (2010).
18. R. L. Arechederra and S. D. Minteer, *Fuel Cells*, **9**, 63 (2009).
19. M. Togo, A. Takamura, T. Asai, H. Kaji, and M. Nishizawa, *Electrochim. Acta*, **52**, 4669 (2007).
20. F. Sato, M. Togo, M. K. Islam, T. Matsue, J. Kosuge, N. Fukasaku, S. Kurosawa, and M. Nishizawa, *Electrochem. Commun.*, **7**, 643 (2005).
21. K. Takagi, K. Kano, and T. Ikeda, *J. Electroanal. Chem.*, **445**, 211 (1998).
22. R. Antiochia, A. Gallina, I. Lavagnini, and F. Magno, *Electroanalysis*, **14**, 1256 (2002).
23. T. Sugiyama, Y. Goto, R. Matsumoto, H. Sakai, Y. Tokita, and T. Hatazawa, *Biosens. and Bioelectron.*, **26**, 452 (2010).
24. G. Wohlfahrt, S. Trivic, J. Zeremski, D. Pericin, and V. Leskovac, *Mol. Cell. Biochem.*, **260**, 69 (2004).
25. Nicolas Mano, Fei Mao, and Adam Heller, *J. Elecrtoanal. Chem.*, **574**, 347 (2005).
26. J. M. Montornes, M. S. Vreeke, and I. Katakis, Chapter 5. *Glucose Biosensors, in Bioelectrochemistry: Fundamentals, Experimental Techniques and Applications* (ed P. N. Bartlett), John Wiley & Sons, Ltd, Chichester, UK, 2008.
27. J. F. Rusling, B. Wang, and S. Yun, Chapter 2. *Electrochemistry of Redox Enzymes, in Bioelectrochemistry: Fundamentals, Experimental Techniques and Applications* (ed P. N. Bartlett), John Wiley & Sons, Ltd, Chichester, UK, 2008.
28. Y. Ogino, K. Takagi, K. Kano, and T. Ikeda, *J. Electroanal. Chem.*, **396**, 517 (1995).
29. V. Soukharev, N. Mano, and A. Heller, *J. Am. Chem. Soc.*, **126**, 8368 (2004).
30. S. Tsujimura, M. Kawaharada, T. Nakagawa, K. Kano, and T. Ikeda, *Electrochem. Commun.*, **5**, 138 (2003).
31. S. Tsujimura, K. Kano, and T. Ikeda, *J. Electroanal. Chem.*, **576**, 113 (2005).
32. S. Tsujimura, Y. Kamitaka, and K. Kano, *Fuel Cells*, **7**, 463 (2007).
33. T. Ikeda, *Chem. Rec.*, **4**, 192 (2004).
34. T. Ikeda, H. Tatsumi, H. Katano, M. Wanibuchi, T. Hibi, and T. Kajino, *Anal. Sci.*, **24**, 237 (2008).
35. A. Habrioux, T. Napporn, K. Servat, S. Tingry, and K. B. Kokoh, *Electrochim. Acta*, **55**, 7701 (2010).
36. Y. Tokita, T. Nakagawa, H. Sakai, T. Sugiyama, R. Matsumoto, and T. Hatazawa, *ECS Trans.*, **13**, 89 (2008).
37. H. Sakai, T. Nakagawa, H. Mita, R. Matsumoto, T. Sugiyama, H. Kumita, Y. Tokita, and T. Hatazawa, *ECS Trans.*, **16**, 9 (2009).
38. L. Gorton and P. N. Bartlett, Chapter 4. NAD(P)-Based Biosensors, in Bioelectrochemistry: Fundamentals, Experimental Techniques and Applications (ed P. N. Bartlett), John Wiley & Sons, Ltd, Chichester, UK, 2008.
39. G. D. Buffinton, K. Öllinger, A. Brunmark, and E. Cadenas, *Biochem. J.*, **257**, 561 (1989).
40. H. Kano, H. Tatsumi, T. Hibi, T. Ikeda, and T. Tsukatani, *Anal. Sci.*, **24**, 1415 (2008).
41. T. Nakagawa, S. Tsujimura, K. Kano, and T. Ikeda, *Chem. Lett.*, **32**, 54 (2003).
42. A. Manjon, J. M. Obon, P. Casanova, V. M. Fernandez, and J. L. Ilborra, *Biotechnol. Lett.*, **24**, 1227 (2002).
43. L. Alonso, S. Palmero, E. Muñoz, S. Sanllorente, and M. Angeles Garcia-Garcia, *Elecroanal.*, **12**, 757 (2000).
44. W. J. Blaedel and R. C. Engstrom, *Anal. Chem*, **50**, 476 (1978).
45. T. R. Marrero and E. A. Mason, *J. Phys. Chem. Ref. Data*, **1**, 3 (1972).

Biosensors and Bioelectronics 26 (2011) 3087–3102

Contents lists available at ScienceDirect

Biosensors and Bioelectronics

journal homepage: www.elsevier.com/locate/bios

Review

Recent progress and continuing challenges in bio-fuel cells. Part I: Enzymatic cells

M.H. Osman, A.A. Shah*, F.C. Walsh

Energy Technology Research Group, School of Engineering Sciences, University of Southampton, University Road, Highfield, Southampton, Hants SO17 1BJ, UK

ARTICLE INFO

Article history:
Received 26 October 2010
Received in revised form
30 November 2010
Accepted 4 January 2011
Available online 6 January 2011

Keywords:
Bio-fuel cells
Enzymatic
Challenges
Immobilization
Materials
Applications

ABSTRACT

Recent developments in bio-fuel cell technology are reviewed. A general introduction to bio-fuel cells, including their operating principles and applications, is provided. New materials and methods for the immobilisation of enzymes and mediators on electrodes, including the use of nanostructured electrodes are considered. Fuel, mediator and enzyme materials (anode and cathode), as well as cell configurations are discussed. A detailed summary of recently developed enzymatic fuel cell systems, including performance measurements, is conveniently provided in tabular form. The current scientific and engineering challenges involved in developing practical bio-fuel cell systems are described, with particular emphasis on a fundamental understanding of the reaction environment, the performance and stability requirements, modularity and scalability. In a companion review (Part II), new developments in microbial fuel cell technologies are reviewed in the context of fuel sources, electron transfer mechanisms, anode materials and enhanced O_2 reduction.

Contents

1. Introduction

Bio-fuel cells have been defined, in the broadest sense, as systems capable of direct chemical to electrical energy conversion via biochemical pathways (Bullen et al., 2006; Katz et al., 2003; Shukla et al., 2004). Direct electrochemical conversion is a desirable feature since it avoids the thermodynamic limitations associated with combustion, in addition to being more environmentally friendly. The conversion is achieved by coupling an oxidation reaction supplying electrons at the anode with a reduction reaction utilizing electrons at the cathode. These two reaction are electronically separated inside the system to force electrons to flow through an external circuit, while ion movement inside the system maintains charge balance and completes the electrical circuit (see Fig. 1 for an example).

Conventional inorganic fuel cells such as the polymer–electrolyte, direct-methanol and solid-oxide systems (Larminie and Dicks, 2003) rely on expensive rare metal catalysts and/or operate on reformed fossil fuels. In bio-fuel cells (BFCs), the chemical reactions are driven by diverse and abundant bio-fuels and biological catalysts. The production/consumption cycle of bio-fuels is considered to be carbon neutral and, in principle, more

* Corresponding author. Tel.: +44 23 8059 8520; fax: +44 23 8059 3131.
E-mail address: A.Shah@soton.ac.uk (A.A. Shah).

0956-5663/$ – see front matter © 2011 Published by Elsevier B.V.
doi:10.1016/j.bios.2011.01.004

Nomenclature

Abbreviations

ABTS	2,2′-azinobis (3-ethylbenzothiazoline-6-sulfonate) diammonnium salt
AlcDH	alcohol dehydrogenase
AldDH	aldehyde dehydrogenase
BFC	biofuel cell
BOD	bilirubin oxidase
CDH	cellobiose dehydrogenase
CF	carbon fiber
CoTMPP	cobalt tetramethylphenylporphyrin
DET	direct electron transfer
EFC	enzymatic fuel cell
FAD	flavin adenine dinucleotide
FDH	fructose dehydrogenase
GDH	glucose dehydrogenase
GOx	glucose oxidase
HQS	8-hydroxyquinoline-5-sulfonic acid
KB	Ketjen black
CP	carbon paper
LDH	lactate dehydrogenase
MEA	membrane-electrode assembly
MEC	microbial electrolysis cell
MFC	microbial fuel cell
MP	microperoxidase
MWCNT	multi-walled carbon nanotubes
NAD	nicotinamide adenine dinucleotide
NR	neutral red
OCV	open circuit voltage
PANI	polyaniline
PBS	phosphate buffer solution
PLL	poly-L-lysine
PPy	polypyrrole
PQQ	pyrroloquinoline quinone
PVP	polyvinylpyrrolidone
SCC	short circuit current
SWCNT	single wall carbon nanotube
TBAB	tetrabutylammoniumbromide

Symbols

E^0	formal potential (V)
j	current density (mA cm^{-2})
K_M	Michaelis constant (mol L^{-1} M)
P	power density
R	resistance (Ω)
$[S]$	substrate concentration (M)
E_{cell}	cell voltage (V)
v	enzymatic reaction rate

sustainable than that of conventional fuel cells (Lovley, 2006). Moreover, biocatalysts could offer significant cost advantages over traditional precious-metal catalysts through economies of scale. The neutral pH and low temperature of operation represents further advantages (Bullen et al., 2006; Shukla et al., 2004).

This review considers major developments in enzymatic and microbial fuel cells over the past five years. Earlier developments will be reviewed briefly to provide context. For more detailed reviews of this work, the reader is referred to Bullen et al. (2006); Davis and Higson (2007); Kim et al. (2006). The review is divided into two parts, the present part focussing on enzymatic systems and Part II on microbial systems (Osman et al., 2010). An introduction to biofuel cells is provided in the next section.

2. The operating principles of a bio-fuel cell

Almost all biochemical processes are catalyzed by enzymes. A group of these proteins, oxidoreductases, are responsible for reactions involving electron transfer, and are the most commonly used enzymes. Different subclasses of oxidoreductases are defined based on the type of substrate they act on, as well as the reaction mechanism (e.g. dehydrogenases, oxidases, and peroxidases).

Bio-fuel cells can be classified according to the biocatalyst. Systems using specific isolated enzymes for at least part of their operation are known as enzymatic fuel cells (EFCs), while those utilizing whole organisms containing complete enzyme pathways are know as microbial fuel cells (MFC). A third, intermediate group based on organelles, namely mitochondria, has recently emerged (Arechederra et al., 2009). Several operational differences between these bio-fuel cell types can be identified immediately. Isolated enzymes are substrate specific, while the diverse enzyme contents of whole organisms can be used for a wide range of fuels. Moreover, a complete breakdown of the organic fuel to carbon dioxide and water is usually only possible with several reaction steps (several enzyme catalysts). This is more easily achieved in MFCs, though it also can be achieved in EFCs with an appropriate combination and cascading of specific enzymes (Arechederra and Minteer, 2009).

A short lifetime is an inherent characteristic of enzymes, even in their natural environment (Kim et al., 2006). This drawback is not as severe in MFCs since the organisms are able to regenerate the required enzymes as part of their natural functioning. These living systems are also able to grow and adapt, a common and advantageous phenomenon observed in MFCs (Kim et al., 2007). Fishilevich et al. (2009) recently developed a microbial fuel cell in which GOx was displayed on the surface of yeast in the anode compartment, with glucose as the fuel and methylene blue as a mediator. The use of micro-organism display in this manner opens up the possibility of self-regenerating enzyme systems from the continuous growth and expression of enzymes on organism surfaces (Boder and Wittrup, 1997).

The microorganism used is either a specific isolated species or a mixed culture. It can be applied directly on the electrodes or used in a suspension, or else the system may be inoculated with a mixed culture in a nutrient solution under specific conditions that will allow it to form a biofilm on the electrode. Due to the living nature of organisms, MFC systems have an initial transient operating period of bacterial growth and adaptation to the electron transport mechanism (to and from the electrodes). EFCs, on the other hand, have a faster response time due to the simpler chemical pathways involved.

Ideally, the cell voltage for a BFC is independent of the current drawn. In practice, the reversible cell voltage is not realized even under open-circuit (zero current) conditions due to a number of losses incurred when the cell is operated. The difference between actual cell voltage (V_{cell}) and the theoretical reversible cell voltage for the overall cell reaction (E_{cell}) at a generated current density j (current I divided by the cross-sectional area of the electrodes, A), is termed the overvoltage. As depicted in Fig. 2, there are three major losses that contribute towards the overvoltage (or 'overpotential', η, for a single electrode): activation overpotentials, ohmic losses and mass-transport (concentration) overpotentials (Clauwaert et al., 2008). The cell voltage at zero current (open-circuit voltage, OCV) E_{OCV} can also deviate from E_{cell} as a result of internal currents and fuel crossover. At steady state, and assuming spatially distributed reactants, the cell voltage can be approximated as follows:

$$V_{cell} = E_{cell} - j\sum_i \rho_i l_i - \eta_{act} - \eta_{conc} \quad (1)$$

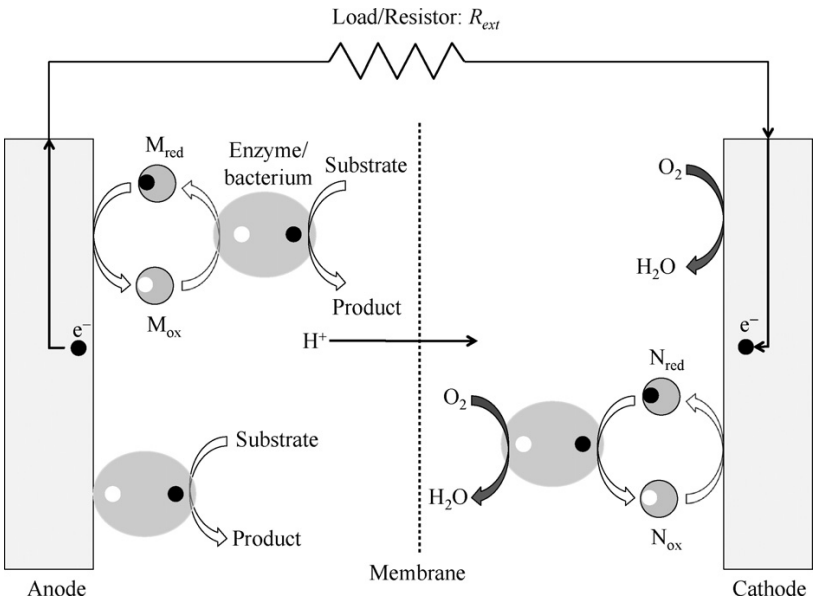

Fig. 1. An example of a biofuel cell with oxygen reduction at the cathode. Oxidation of the substrate is catalysed by the enzymes/bacteria (preferably immobilised on the electrodes), releasing protons and electrons. The electrons released are either transferred directly to the electrode or are transferred via redox mediators, M. Oxygen reduction at the cathode can take place directly on the electrode or via enzymes/bacteria, possibly facilitated by mediators, N. The mediators can be freely suspended or immobilised on the electrode to enhance electron transfer.

where the second term on the right-hand side represents ohmic losses and the final two terms denote the activation and concentration overpotentials, respectively (sums of the contributions from the two electrodes). The reversible potential E_{cell} can be calculated from the Gibbs free energy change for the anodic and cathodic reactions.

At low currents, activation (charge transfer) losses dominate; they arise from the energy barrier to charge transfer, from the mediator or bacteria/enzyme to the electrodes. These overpotentials (separate for the two electrodes) can be approximated if expressions for the reaction rates are known, e.g. a Tafel's or Bultler–Volmer's relation. Activation losses can be reduced by improving the electrode catalysis, increasing the electrode surface area, and by optimising the operating conditions (e.g. temperature and pH).

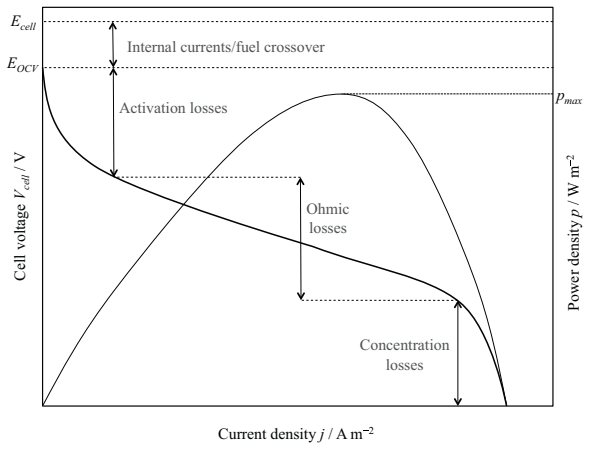

Fig. 2. Typical variations of the cell voltage and power of an operating fuel cell with current density. The major losses of cell voltage and the approximate ranges of current density in which they occur are indicated.

Ohmic losses are due to the resistance to charge transport through the various components in the cell, including contact resistances. They include both ionic and electronic resistances through the current collectors, electrolytes, membrane and electrodes, as well as the interfaces between these components. Assigning a characteristic resistivity ρ_i and thickness l_i to each component i, the ohmic losses may be approximated using Ohm's law, as in Eq. (1). To keep ohmic losses to a minimum, the membrane must possess a low resistance, the gap between the electrodes should be optimal and the components must be well contacted. The solution conductivity can also be increased by varying its composition, but this must not affect the functioning of the bacteria/enzymes.

Concentration losses are caused by resistance to mass transport, leading to large concentration gradients, notably in the vicinity of the electrode surface. These losses tend to dominate at high current densities. They can be lowered by ensuring that the solutions are well-mixed (e.g. by stirring or recirculation) or, in the case of an air-breathing cathode, that the ingress of O_2 is not severely restricted. The electrical power density, P of a BFC is defined as the product of the cell voltage and the generated current density: $P = IV_{cell} = V_{cell}^2/R_{ext}$, where R_{ext} is a known, fixed external resistance. The power density can be calculated by normalising the power with respect to the electrode cross-sectional area or the electrode volume. A typical profile for the power density, $p = P/A = jV_{cell}$, as a function of current density is shown in Fig. 2.

One of the most important measures of performance of a BFC is the coulombic efficiency, which is defined as ratio of coulombs transferred from the substrate to the anode, to the theoretical maximum coulombs produced if all of the substrate is oxidized ($\times 100\%$) (Liu et al., 2005a). The major causes of reduced coulombic efficiency are (a) the occurrence of alternative reactions that do not result in current production; (b) build-up of biomass; and (c) crossover of the substrate or mixing of the anodic and cathodic reagents, a particular problem in membrane-less systems (Clauwaert et al., 2008).

The operating voltage of a fuel cell has an upper limit dictated by the difference in potential between the oxidant and reductant

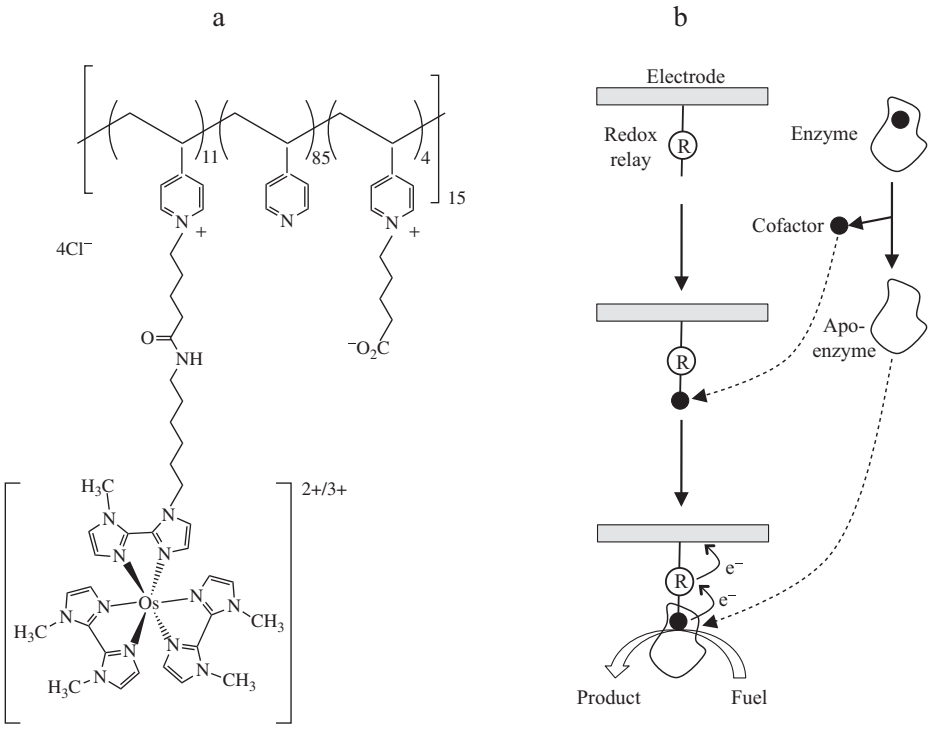

Fig. 3. The structure of polyvinylpyridine-[Os(N,N′-dialkylated-2, 2′-biimidazole)$_3$]$^{2+/3+}$ (Mao et al., 2003). A tris-dialkylated *N*, *N*′-biimidazole Os$^{2+/3+}$ complex was tethered to the backbone of a PVP polymer via 13-atom spacers. (b) Illustration of the concept of enzyme reconstitution. An electron relay unit (molecule, redox polymer or nanoparticle) is linked to an electrode. The cofactor of the enzyme is eliminated and tethered to the relay unit. The apoenzyme is then reconstituted on the relay-cofactor monolayer. Adapted from Zayats et al. (2008).

and the potential difference between the final electron donor and initial acceptor at the electrodes. In bio-fuel cells, this upper limit is determined largely by the redox potential of the active sites acting on the substrate. If mediators (redox active species) are used to shuttle the electrons to/from the electrode, inevitable thermodynamic losses will occur; the mediators require a potential that is shifted from that of the active site to promote electron transfer. Mediated electron transfer can, however, yield higher currents when the mediator concentration is sufficiently large (Kamitaka et al., 2007).

Many reports have categorized BFCs into direct and mediated electron transfer (DET and MET respectively), with often differing definitions. Systems utilizing non-diffusive mediators that are attached along with enzymes on electrodes, or those utilizing mixtures of carbon nanotubes and redox polymers, for instance, can be considered both direct and mediated. Other reports have classified systems based on the materials and methods used for electrode preparation, such as apoenzyme reconstruction, immobilization in redox polymers and the use of nanostructured elements (Kim et al., 2006; Willner et al., 2009; Sarma et al., 2009). In this review, discussion will be divided according to the methods and purposes.

MET usually refers to cases where a mediator is used to enhance electron transfer between the electrochemically active part of the enzyme and the electrode. Conversely, the transfer of electrons directly from the enzyme to the electrode is termed as DET. The vast majority of enzymes are not capable of DET (Sucheta et al., 1993; Ghindilis et al., 1997; Ferapontova et al., 2003; Tasca et al., 2008a) so that most systems employ a mediator, which is usually enzyme specific. For glucose oxidation on glucose oxidase (GOx), examples of mediators are ferrocene monocarboxylic acid, pyrroloquinoline quinone (PQQ), methylene blue, ferrocenecarboxaldehyde and ferrocenemethanol (Harper and Anderson, 2010). The potential applications of bio-fuel cells are diverse. Non-electrochemical applications of bacterial reactions for the production of hydrogen through fermentation, or methane via methanogens are known technologies. Although these bioreactors may be connected to conventional fuel cells for electricity production, either as an external unit supplying the fuel (Ishikawa et al., 2006), or by incorporating the fuel production process with the oxidation reaction on the same anode (Niessen et al., 2005), the biological pathway remains separate from the process of electricity production.

3. Secondary fuel production

Microbial electrolysis cells (MECs) are similar in configuration to microbial fuel cells but require an electrical energy input to initiate a normally unfavorable reaction producing a secondary fuel. For example, hydrogen can be produced on an anaerobic cathode by the reduction of protons (the product of acetic acid oxidation at the anode) (Liu et al., 2005b; Rozendal et al., 2006; Call and Logan, 2008). The electrode reactions can be written as (Liu et al., 2005b):

$$\text{Anode}: CH_3COOH + 2H_2O \rightarrow 2CO_2 + 8e^- + 8H^+ \quad (2)$$

$$\text{Cathode}: 8H^+ + 8e^- \rightarrow 4H_2 \quad (3)$$

which can be combined with the fermentation of glucose into acetate to produce hydrogen.

In another example Cheng et al. (2009) produced methane at a cathode by 'electromethanogenesis' combined with the oxidation of an organic fuel at the anode. Several reports have suggested a mechanism of methane production in microbial electrochemical cells from acetate through acetoclastic methanogenesis, or

from the intermediate hydrogen product. The work of Cheng et al. (2009) presents preliminary evidence that methane can be produced from microorganisms (combined with CO_2 capture). MECs that use electricity for the production of a secondary fuel may be used with renewable energy systems to generate usable fuels that are easily transported and stored. Call and Logan (2008) have projected that such systems can provide hydrogen gas at $0.62 per kg compared to $3.8 per kg by water electrolysis. Another class of microbial electrochemical cells not strictly adhering to the definition of a fuel cell is that based on phototroph organisms that use light energy to produce electricity. A two-step approach where *Rhodobacter sphaeroides* converts sunlight and an organic substrate into hydrogen gas, which is then oxidized at a Pt anode, has achieved power densities up to 0.079 mW cm^{-2} (Cho et al., 2008; Rosenbaum et al., 2005) in a single compartment cell. In an approach relying solely on light energy, Furukawa et al. (2006) designed a miniature fuel cell that replicated the photosynthetic/metabolic processes to provide direct electrical energy in light/dark conditions, via alternate conversion between CO_2, H_2O and electricity. Cao et al. (2008) used an enriched consortium of phototrophic bacteria from a wastewater treatment plant in a two-chamber MFC. A maximum power density of 0.265 mW cm^{-2} was obtained. A sediment type MFC using mixed communities of photosynthetic and heterotrophic microorganisms, capable of power production in both light and dark without the need of organic substrate additions, was recently reported by He et al. (2009).

4. Applications of bio-fuel cells

An immediately obvious area of application is static power generation, with microbial fuel cells being the more likely candidate. These systems can be fuelled by widely available, carbon-neutral complex fuels such as cellulose (Ishii et al., 2008; Niessen et al., 2005). Alternatively, they can form the basis for waste treatment systems, combined with energy generation from the organic matter found in sewage. In this application area, MFCs will have to compete with traditional anaerobic digesters producing methane or hydrogen. At present, this is not possible considering target power densities of around 1 kW m^{-3} for economic competitiveness (Watanabe, 2008; Rabaey and Verstraete, 2005). Despite these drawbacks, direct electrical output with high efficiency, low operating temperatures, and good organic treatment efficiency, with the possibility of operating on low strength wastewater, are some of the advantages of MFCs (Watanabe, 2008; Rabaey and Verstraete, 2005). Moreover, bio-electrodes can be used for the oxidation/reduction of specific target substrates (such as nitrate, iron and sulfate) in waste removal or metal extraction from minerals (He and Angenent, 2006). The operation of MFCs on marine sediment to power remote marine instruments has also been explored in several reports.

For applications on a smaller scale, BFCs operating on high energy density fuels have the potential to power portable electronic devices, though current power densities are still far from the target figures of ~100 mW (Sakai et al., 2009). *In vivo* application of bio-fuel cells, either for powering small implantable devices or as biosensors, are more promising for the short term due to their low power requirements. Short life times are, however, a major issue.

5. Biofuel cell designs and configurations

The classical design of an BFC is based on two chambers containing the anode and cathode, separated by a ion-selective membrane (Bullen et al., 2006). Such cells can be operated in either batch or continuous mode. For wastewater treatment (MFCs), an up-flow, two-chamber design was developed by He et al. (2005), operating in continuous mode. The system exhibited a high internal resistance of 84 Ω. A membrane-less version was constructed by Jang et al. (2004), with, however, a considerably higher internal resistance of 3.9 MΩ. Removing the membrane can lead to higher power outputs but the cells must be carefully designed for high reaction selectivity in order to avoid low coulombic efficiencies (due to transport of oxygen to the anode). For scale up and reduced cost, on the other hand, the concept of a membrane-less, single chamber design is highly attractive. Moreover, the use of a ferricyanide solution and aeration in the cathode compartment are not desirable. Park and Zeikus (2003) developed an MFC with a Mn^{4+} graphite anode and air cathode containing an internal, proton-permeable porcelain layer. Liu and Logan (2004) simplified the design by using a carbon-paper air-breathing-cathode (direct O_2 reduction, catalysed by platinum) without a membrane in a tubular arrangement. The cell exhibited a higher power density than an equivalent membrane-containing cell but with a much reduced coulombic efficiency. An alternative arrangement was developed by Rabaey and Verstraete (2005), in which a granular graphite matrix anode was housed in a tubular, sealed membrane covered by a woven-graphite cathode (soaked in a ferricyanide solution).

Immobilisation of the enzymes/mediators opens up the possibility of single compartment EFCs. There are, however, very few examples of membrane-less or separator-free EFCs. The first single-chamber EFC was developed by Katz et al. (1999b), consisting of two immiscible electrolytes separated by a liquid–liquid interface, allowing DET to take place. GOx apo-enzyme was reconstituted a PQQ-flavin adenine dinucleotide phosphate (FAD) monolayer associated with an Au electrode (see Section 7). The cathode consisted of an Au electrode onto which a microperoxidase-11 monolayer was assembled and for which cumene peroxide was used as the oxidiser. Ramanavicius et al. (2005) constructed a single-chamber EFC operating with immobilised alcohol dehydrogenase (AlcDH) on a carbon-rod anode and co-immobilized GOx/microperoxidase on a carbon-rod cathode. The power density, around 10 nW cm^{-2}, was low and the operational half-life was only 2.5 days. A DET, single-chamber H_2/O_2 cell with hydrogenase at the anode and fungal laccase at the cathode was constructed by Vincent et al. (2005), again, however, with a low power density. A more systematic selection of the enzymes and electrode materials by Kamitaka et al. (2007) led to a single-chamber, membrane-less fructose/O_2 cell capable of power densities on the order of 1 mW cm^{-2}; fructose dehydrogenase (FDH) was immobilised on a Ketjen–Black (KB) modified carbon paper and multi-copper oxidases were immobilised on a carbon paper cathode modified with KB and a carbon aerogel. Coman et al. (2008) instead used cellobiose dehydrogenase (CDH) and lacasse for a glucose/O_2 system, which was capable of only 5 μW cm^{-2}. More recently, Wang et al. (2009) immobilised GOx (anode) and laccase (cathode) on porous silicon substrates with pre-deposited carbon nanotubes to form a membrane-less, mediator-free glucose EFC. Again, the power density (1.38 μW cm^{-2}) was low and decreased by a factor of almost 5 after 24 h.

6. Enzymatic fuel cells

The two major problems in enzyme-based systems are the short lifetime of the enzyme caused by a reduction in its stability when functioning in a foreign environment, and the low power densities resulting from a low electron transfer rate from the enzyme active site to the electrode (Kim et al., 2006). The bulk of the research in enzymatic fuel cells has been directed at enzyme/electrode integration methods that alleviate these problems. The short lifetime (a few hours) is an inherent characteristic of enzymes even in their

natural environment, but the lifetime may be increased to a few days by immobilization (Kim et al., 2006).

Enzymes used in fuel cells are of the oxidoreductase family (capable of catalysing oxidation and reduction reactions). They can be categorised into three groups, according to the type of electrical communication (Heller, 1992) or to their associated redox cofactors. The first group consists of PQQ-dependent dehydrogenases, e.g. AlcDH, glucose dehydrogenase and glycerol dehydrogenase. Each is structurally different, but most have multiple metal centers and the coenzyme PQQ is bound to the enzyme. The second group includes those with a nicotinamide adenine dinucleotide ($NADH/NAD^+$) or nicotinamide adenine dinucleotide phosphate ($NADPH/NADP^+$) cofactor, e.g. glucose dehydrogenase and AlcDH. In this case, the redox center is usually loosely bound and may diffuse away. This allows the enzyme to transfer electrons to the electrode by the diffusing center, although the diffusing enzyme site may be lost, especially in continuous flow systems. Covalent linking of such enzymes needs to maintain a flexible link, allowing reversible movement between the protein structure and the electron acceptor. Enzymes in the third category have a tightly bound FAD redox cofactor that is buried deep inside the protein structure, which makes extraction of the electrons difficult. The most commonly used enzyme, GOx, belongs to this group. In an aqueous solution, the redox potential of FAD at the enzyme active site is negative, making it ideal for the anode side of a biofuel cell if DET can be achieved. However, systems employing GOx are typically mediated, although it is possible to achieve DET using nanostructured electrodes as discussed later (Xiao et al., 2003; Zayats et al., 2005; Cai and Chen, 2004; Patolsky et al., 2004).

For biological cathodes, the enzymes are typically multi-copper oxidases, which are capable of a four-electron reduction of O_2 to water and have a high specificity towards this reaction (Solomon et al., 1996). Examples include plant and fungal laccases (Chen et al., 2001) and BOD (Mano et al., 2003). Laccases are generally employed under slightly acidic conditions, while BOD has activity in more alkaline media, which allows it to be used at neutral pH. Cytochrome oxidase and cytochrome *c* have also been employed. In the case of H_2O_2 reduction, microperoxidase (Willner et al., 1998a; Katz et al., 1999b) and horseradish peroxidase (Pizzariello et al., 2002) are commonly used as enzymes.

7. Enzyme and mediator immobilization

Immobilisation of the enzyme can has several advantages, including isolation of the enzyme for reaction, increased selectivity, improved mass transfer and long-term stability (Cao, 2005). It also has the advantage of separating the enzyme from the mixture containing the substrate, allowing for more modular cell designs. On the other hand, it can affect the stability and/or activity of the enzyme, it can introduce additional mass-transfer limitations on the substrate and it involves additional costs. Stability is clearly a key consideration. The stability of the immobilised enzyme will depend on the nature and strength of the bonds to the support material, the conditions required for immobilisation, the degree of confinement and the conditions under which the enzyme reactions occur in a functioning electrode. The method of immobilization must be selected carefully to avoid denaturing of the enzymes and loss of structural freedom required for their activity (Moehlenbrock and Minteer, 2008; Cooney et al., 2008).

The main immobilisation techniques for biosensors and EFCs are (Tischer and Wedekind, 2000): physical surface adsorption with diffusional mediators, or mediators co-adsorbed with an enzyme; entrapment in conducting polymer matrices or gels; wiring or covalent attachment to functionalised polymers; and apoenzyme reconstruction. Nano-structured elements can also be used as substrates for binding, or incorporated with one of the aforementioned techniques for enhanced electrical conductivity and stability.

The simplest method of enzyme immobilization is physical adsorption or entrapment. Enzymes can be adsorbed, for example, onto conductive particles such as carbon black or graphite powder (Pizzariello et al., 2002). The methods are straightforward and cost-effective. If the binding forces (primarily electrostatic) between the enzyme and the support are too weak, however, the enzymes can desorb and contaminate the solution; if they are too strong, denaturation can occur during the immobilisation process. Entrapment involves the confinement of the enzyme within a polymer matrix, a sol–gel (Kandimalla et al., 2006), a redox hydrogel (Gregg and Heller, 1991) or behind a semi-permeable membrane. The structure must permit a sufficient degree of enzyme movement, while simultaneously preventing any leaching of the enzyme and/or mediator.

Isolated enzymes can be covalently bonded to supports (e.g. porous glass, cellulose, ceramics, and metallic oxides) via different functional groups on the support and enzyme, often in the presence of enzyme inhibitors. Reagents are used to activate the functional groups on the support. The functional groups on the enzyme, which include amino, carboxylic acid and hydroxyl groups, should not be essential for catalytic activity. The conditions for this type of immobilization are important since they determine the level of enzyme activity retention. Cross-linking consists of joining enzymes to form three dimensional aggregates via covalent bonding between active groups within the enzymes. The aggregates exhibit low mechanical stability and the retained enzymatic activity can be low using this method (Sheldon, 2007).

Covalent bonding and cross-linking are commonly used to immobilise enzymes on self-assembled monolayers (SAMs) (Gooding and Hibbert, 1999). In the context of biosensors, the most studied SAMs are those formed by alkanethiols chemisorbed from solution onto gold surfaces (Dubois and Nuzzo, 1992). Despite the many advantages of these SAMs (simplicity of preparation, densely packed structures and control over functional groups at the monolayer surface), they are prone to instability (Schoenfisch and Pemberton, 1998; Delamarche et al., 1994; Gooding et al., 2003). To improve stability, several research groups have used covalent modification of carbon surfaces via electrochemically reductive adsorption of aryldiazonium salts (Allongue et al., 1997; Saby et al., 1997; Kariuki and McDermott, 2001; Brooksby and Downward, 2004). The resulting monolayers are highly stable over a wide potential window (Allongue et al., 1997). In recent studies, gold, graphite and glassy-carbon (GC) electrodes were functionalised using aryldiazonium salts bearing carboxylic acid groups (Pellissier et al., 2008; Boland et al., 2009a). Pellissier et al. (2008) grafted a GOx layer on a GC electrode modified using this method, through coupling with peripheral amine groups of the GOx. This enzyme layer was used as an anchoring base onto which a cross-linked enzyme layer was subsequently deposited, before testing the electrode using a GC rod counter electrode. The authors demonstrated that these modified electrodes retained much of their activity after 6 weeks, while control electrodes prepared by depositing the cross-linker and GOx directly onto the GC had lost all activity within only 1 week.

Sol–gel glass is produced by the hydrolysis and polycondensation of organometallic compounds (typically silicon alkoxides) at low temperature (Lin and Brown, 1997). Enzymes can be introduced during the formation of the sol–gel (the 'sol–gel process'), leaving them entrapped around siloxane polymer chains within an inorganic oxide network. The final matrix structure can be controlled by the pH, the temperature, the choice of solvent and the choice of catalyst, amongst other considerations. The main advantages of this method in the context of biosensor and biofuel applications are: simplicity of preparation; the ability to control

Table 1
Summary of key enzymatic fuel cell developments

Anode	Cathode	Electrolytes/membrane	P_{max} (cw cm^{-2})	V or j at P_{max}	OCV (V)	Remarks	Reference
Mitochondria immob. in modified Nafion on C-electrode	Air-breathing **Pt**-C/membrane assembly	10 mM, 7.45 PBS, 6 M $NaNO_3$, 100 mM **pyruvate**, 1 g L^{-1} ADP	0.0315†, 0.024 (average)	0.1† mA cm^{-2}	–	Air cathode/ membrane assembly	Arechederra et al. (2009)
AlcDH/AldDH/oxalate oxidase in modified Nafion on C-paper	Air-breathing **Pt** –C/membrane assembly	7.15 pH PBS, 6 M $NaNO_3$ 100 mM **glycerol**	1.32	2† mA cm^{-2} (0.66 V†)	–	Air cathode/membrane assemble	Arechederra and Minteer (2009)
GOx /HQS (mediator) in PPy on Carbon rod	**Laccase** /ABTS (mediator) in PPy on porous carbon tube	5 pH PBS, 10 mM **glucose**, N_2 purged, 37 °C, separate O_2 solution circulated inside cathode	0.027	0.25 V	0.41†		Brunel et al. (2007)
CDH adsorbed on graphite	**Laccase** adsorbed on graphite	0.1 M citrate buffer, 4.5 pH, 5 mM **glucose**, air saturated	5×10^{-3}	0.5 V	0.73	Membrane/mediator-less. Enzyme desorption causes current/power loss.	Coman et al. (2008)
5 bilayers of AuNPs/**GDH** on three dimensional ordered macroporous, cystamine treated Au electrode	Similar to anode, using **laccase** as catalyst	0.1 M, 6 pH PBS, 5 mM NADH, 30 mM **glucose**	0.178	0.226 V	0.32	SCC = 0.752 mA cm^{-2}	Deng et al. (2008)
Cross-linked clusters of **GOx** and CNTs on CF electrode (0.332 cm^2)	Air breathing **Pt** –C cathode (0.332 cm^2)	Un-buffered, 200 mM **glucose**, 10 mM benzoquinone	0.12	0.1 V	0.33	MEA assembly. Better initial performance but degrades quickly in buffered solutions due to cation interference with proton transport.	Fischback et al. (2006)
GDH on poly(brilliant cresyl blue)/SWCNT/GC rod (3 mm diameter)	Cross-linked **BOD** on SWCNT on same carbon electrode	0.1 M PBS, 7 pH, 10 mM NAD^+, 40 mM **glucose**, ambient air	0.054	0.5 V	0.73	Membrane-Less. 5% P loss in first day. 46% loss in one week	Gao et al. (2007)
GOx 'wired' through PVP-Os complex with cross-linking on 2 cm long, 7 μm diam. CF	**BOD** 'wired' through PAA-PVI-Os complex with cross-linking on similar electrode	20 mM PBS, 7.24 pH, 0.14 M NaCl, 15 mM **glucose**, 37 °C	0.315	0.46†V	–	Membrane-less. Commercial enzyme stock purified before usage. Operating cell for 1 week at 0.52 V lost 6% of power output per day	Gao et al. (2009)
Au$_{70}$Pt$_{30}$ bi-metallic nanoparticles on inner surface of carbon tube (4.4 cm^2, 1.4 cm diam.)	**BOD** /ABTS in modified Nafion on inner surface of porous carbon tube (6 mm diam.)	7.4 pH, PBS, 0.7 M **glucose**, 37 °C	0.19, 0.09 (10 mM glucose)	0.52 V, 0.4 V (10 mM glucose)	0.89†	Abiotic anode. Concentric design. Membrane-less	Habrioux et al. (2009)
FDH adsorbed on Ketjen's black (0.282 cm^2)	**Laccase** adsorbed on carbon aerogel particles (0.282 cm^2)	McIlvaine buffer, 5 pH, 200 mM **fructose**, O_2 saturated, 25 °C	0.85 (stirred), 0.39 (unstirred)	0.41 V	0.79	SCC = 2.8 mA cm^{-2} (stirred), 1.1 mA cm^{-2} (unstirred). Power drops to 63% after 12 hours. 4 cells in series operate 1.8 V LED for ~60 days.	Kamitaka et al. (2007)
GOx /HQS immobilized in polypyrrole nanowires (0.15 cm^2)	**BOD** /ABTS in polypyrrole film (0.35 cm^2)	7.4 pH, PBS, 15 mM **glucose**	0.28	0.15 V	0.35	SCC = 2.9 mA cm^{-2} and maximum power density with 200 nm diam. 16 μm length nanowires. Membrane-Less	Kim et al. (2009)

Table 1 (*Continued*)

Anode	Cathode	Electrolytes/membrane	P_{max} (cw cm^{-2})	V or j at P_{max}	OCV (V)	Remarks	Reference
GOx covalently attached to 3-methylthiophene (3MT) and thiophene-3-acetic acid (T3A) copolymer	**BOD** covalently attached to same copolymer	0.1 M PBS, 7 pH and either 0.1 M **glucose**, 1 mM *N*, *N*, *N*′, *N*′-tetramethyl-p-phenylenediamine, N_2 saturated or 1 mM ABTS, O_2 saturated in either compartment separated by Nafion membrane	0.15	0.35 V	0.61	Anodic current decreased to 50% while cathodic current decreased to 75% the initial values after 1 month	Kuwahara et al. (2009)
Au electrode-cystamine-PQQ-**LDH** monolayer	Au electrode-cystamine-**microperoxidase 11**	Anolyte: 0.1 M tris buffer, 7 pH, 20 mM $CaCl_2$, 20 mM NAD^+, 20 mM **lactate**. Catholyte 0.1 M PBS, 7 pH, 1 mM H_2O_2, ABTS. Nafion separator.	0.142	0.1† V	0.34†	LDH immobilization carried in presence of $CaCl_2$ promoter, NAD^+, and lactate found to increase power by 26% compared to immobilization without.	Lee et al. (2009)
Latex draw chemical structure **GOx** /single-stranded DNA-wrapped SWCNT on cystamine dihydrochloride treated Au electrode (0.0314 cm^2)	Similar immobilization for **laccase**	0.1 M PBS, 7 pH, **glucose**, O_2, 25 °C	0.442	0.46 V	1.5†	Cell operated for more 5 days with power in excess of 0.43 mW cm^{-2}. DNA-wrapped SWCNT found to increase enzyme loading.	Lee et al. (2010)
Polyethylene glycol diglycidyl ether) **GOx** /SWCNTs in silica gel	**BOD** /SWCNT in silica gel	Anolyte: 4 mM ferrocene methanol, 100 mM **glucose**. Catholyte: 8 mM ABTS, O_2 saturated. Room temperature. Nafion separator.	0.12, 0.086 (ambient air)	0.24 V, 0.21 V (ambient air)	0.48		Lim et al. (2007)
Penicillium pinophilum sourced **GOx** /PVP-Os complex, cross-linked, on 2 cm long, 7 μm diam. CF	**Laccase** /PVP-Os complex, cross-linked on 2 cm long, 7 μm diam. CF	20 mM citrate buffer, 5 pH, 37 °C, 5 mM **glucose**	0.28	0.88 V	–	GOx sourced from *P. pinophilum* allows higher power density at lower fuel concentration than tradition *A. niger* but unstable at neutral pH. 3% power loss per day for first 2 weeks.	Mano (2008)
GDH /NAD^+ in Ketjen's black on GC (0.07 cm^2)	**BOD** in Ketjen's black	PBS, 50 mM **glucose**, O_2 saturated	0.052	0.3 V	0.64	SCC = 0.223 mA cm^{-2}. Membrane/mediator-less	Miyake et al. (2009)
AldDH adsorbed on graphite electrode	**AlcOD/microperoxidase-8** adsorbed on graphite electrode	50 mM sodium acetate, 6 pH, 100 mM KCl, 2 mM **ethanol**	1.5×10^{-3}	–	0.24	Ethanol as substrate for both half-reactions. Power decreases to half initial value after 26 h of operation	Ramanavicius et al. (2008)

4 layers of (CF/ poly-L-lysine/ **GDH** /diaphorase/NADH/vitamin K_3/polyacrylic acid sodium salt) (1 cm^2 each)	Air-breathing, 2 layer of (CF sheet/ $K_3[Fe(CN)_6]$/PLL/ **BOD**) (1 cm^2 each)	0.1 M, 7 pH, (PBS), room temperature, 0.4 M **glucose**. Electrodes stacked with cellophane membrane in a single assembly.	1.45	0.3 V	0.8	SCC = 11 mA cm^{-2}.	Sakai et al. (2009)
CDH / polyvinylpyridine- Os complex/SWCNTs on graphite rods (3.05 mm diam.) with cross-linking	**Pt** –C (area ≫ anode area)	PBS, 7.4 pH, 37 °C, 0.1 M **glucose**, O_2 purged, non-quiescent	0.157	0.28 V	0.5		Tasca et al. (2008b)
PLL-K_3/diaphorase/**GDH** on GC (0.07 cm^2)	Poly-dimethylsiloxane coated **Pt** cathode	PBS, 7 pH, 5 mM **glucose**, 1 mM NAD^+, 37 °C	0.032	0.29 V	0.55	Current drops to half initial value after 18 h	Togo et al. (2007)
AlcDH/ AldDH / NAD^+/ modified Nafion on polymethylene green anode	**BOD** /modified Nafion on 1 cm^2 CF paper. Dried then soaked in $Ru(bpy)_3{}^{2+}$ mediator	7.15 pH, PBS, 1 mM **ethanol**, 1 mM NAD^+, room temperature	0.39, 0.83 (with Nafion membrane)	–	0.51, 0.68 (with Nafion)	Power increases to a maximum of 0.46 mW cm^{-2} then rapidly drops after 20 days.	Topcagic and Minteer (2006)
LDH /modified Nafion with $CaCl_2$ on CF paper (1 cm^2)	**Pt** –C black	Anolyte: 7.15 pH, PBS, 25 mM **lactate**. Catholyte: 1 M NaCl, dissolved O_2, 20 °C. Nafion Separator	0.022	–	0.85	Testing over 45 days without any claimed degradation in performance	Treu and Minteer (2008)
Porous Si-functionalised SWCNT-**GOx**	Porous Si-functionalised SWCNT-**laccase**	PBS, 4 mM **glucose**, air bubbling, stirred. 5 mm inter-electrode distance	1.38×10^{-3}	99 mV	–	Lower power density (0.35×19^{-3} mW cm^{-2}) at higher voltage (0.357 V) when SWCNTs grown by chemical deposition followed by carboxyl group attachment rather then electrophoretic deposition of pre-functionalised SWCNTs.	Wang et al. (2009)
Covalently linked SWCNT-NAD^+ deposited on classy carbon. **AlcDH** attached to NAD^+ through affinity, and cross-linked	Thioanaline modified **BOD** copolymerized with thioanaline capped **Pt** nanoparticles on Au electrode with thioanaline monolayer with crosslinking.	0.1 M PBS, 7 pH, 40 mM **ethanol** l, O_2 saturated	0.2	0.55† V	0.62	Maximum power at 0.37 mA cm^{-2}	Yan et al. (2009)
GOx / MWCNTs/Nafion on carbon felt (0.33 cm^2)	Air-breathing **Pt** cathode	100 mM **glucose**, 10 mM 1.4-benzoquinone. Nafion/electrode assembly	0.077	0.51 V	0.57	–	Zheng et al. (2008)

† Values not explicitly reported, but estimated from graphical results.

the porosity; the chemical and mechanical stability of the gel; and negligible swelling (Lin and Brown, 1997; Wang, 1999).

A method to co-immobilise the enzyme and mediator (designed to prevent mediator leaching) was developed by Heller and co-workers, who used soluble redox hydrogels to construct biosensors and, subsequently, miniature biofuel cells (Chen et al., 2001; Mano et al., 2002b; Soukharev et al., 2004; Heller, 2004, 2006). In this method the enzyme is complexed with a redox polyelectrolyte forming a water soluble adduct, which is cross-linked on the electrode surface. The cross-linked polymer swells on contact with water to form a hydrogel, to which the enzymes are covalently bound. The enzymes are electrically connected to the electrode by a redox network and are said to be 'wired'; electron conduction is predominantly controlled by collisional electron transfer between the reduced and oxidized (transition metal-based) redox centers tethered to the polymer backbone. Popular choices for the polymer backbone are polyvinylimidazole, polyallylamine and polyvinylpyridine (PVP) and the redox centres are typically osmium (Os) or ruthenium complexes (Gregg and Heller, 1991). Os complexes are particularly useful due to the ease with which the redox potential can be tuned by chemical modification of the complex (Kavanagh et al., 2009). They can be tethered flexibly to polymer backbones, improving the electron transfer kinetics between the enzyme and electrode (Stoica et al., 2009). The mechanical strength of the hydrogels and the electron transfer rate can be improved by using spacers that connect the redox-active centers to the cross-linked networks. These spacers provide additional flexibility and improved collisional electron transfer. The lengths of the spacers are important; optimally between 8 and 15 atoms (Heller, 2006; Mano et al., 2005; Mao et al., 2003). The redox potentials of the hydrogels are determined by the transition metal ion of their complex and by its ligands, so they can be tailored to a specific enzyme/reaction combination (Heller, 2006; Kim et al., 2003). An example of a redox polymer structure, developed by Mao et al. (2003), is given in Fig. 3(a). The authors tethered a tris-dialkylated N,N′-biimidazole $Os^{2+/3+}$ complex to the backbone of a PVP polymer via 13-atom spacers. An order of magnitude increase in the apparent electron diffusion coefficient was observed when compared to a structure without spacers, used earlier by the authors. Furthermore, oxidation of glucose was found to occur at potentials close to the reversible potential of the FAD/$FADH_2$ centers of the enzyme.

Realising DET using GOx is difficult due to the deeply embedded nature of the active FAD sites. The same applies for PQQ and heme containing enzymes. In an attempt to overcome this issue, Willner and co-workers introduced a method based on reconstituting apo-enzymes on functionalised electrodes (Willner et al., 1996, 1998a,b; Xiao et al., 2003) (see Fig. 3(b) for an illustration). In one example, gold nanoparticles were linked to a gold electrode by a dithiol bridge, while amino-FAD was linked to the particles (Xiao et al., 2003). The FAD cofactor units were extracted from GOx to give the apo-enzyme, which was reconstituted on the FAD-functionalised particles. The gold nanoparticles were seen to act as electron relays between the FAD redox site and the electrode. Similarly, PQQ-dependent GDH was electrically wired by the reconstitution of apo-GDH on PQQ-functionalised nanoparticles (Zayats et al., 2005). Patolsky et al. (2004) instead reconstituted apo-GOx on FAD units linked to the ends of single wall carbon nanotubes (SWCNTs) assembled on a gold electrode, motivated by the efficient DET between SWCNTs and absorbed GOx redox active sites (Guiseppi-Elie et al., 2002; Cai and Chen, 2004). The authors deduced that the SWCNTs behaved as electrical contacts between the active site of the enzyme and the electrode. Such electrodes, using either single-walled or multi-walled CNTs (Ivnitski et al., 2006; Zhang et al., 2003) display good stability and sensitivity (Cai and Chen, 2004; Wang et al., 2003; Lin et al., 2004).

A summary of recent key developments in EFCs are presented in Table 1. They are discussed in detail in the sequel.

7.1. Physical immobilisation of enzymes and mediators

Tasca et al. (2008a) investigated the direct electron transfer (DET) capabilities of different CDHs adsorbed on a graphite electrode in the presence or absence of SWCNTs. SWCNTs were found to increase the electrocatalytic current, the onset of which was shifted to more negative potentials. CDH is composed of a large flavin-associated domain and a smaller heme-binding domain that allows direct electron transfer to the electrode. A membrane-less fuel cell was constructed using *Phanerochaete sordida* CDH coadsorbed with SWCNTs, together with a Pt/C cathode. A solution with 0.1 M, 4.5 pH citrate buffer containing O_2 and 5 mM lactose was used. The open circuit voltage was 590 mV and a maximum power density of 0.032 mW cm^{-2} at 430 mV was obtained. CDH was also adsorbed on graphite in a fuel cell with laccase immobilized in a polymer (Coman et al., 2008). The power density (0.005 mW cm^{-2}) was lower than the SWCNT system of Tasca et al. (2008a), but the cell voltages achieved were slightly higher.

In a similar fashion to CDH, FDH contains a heme group that should in principle allow direct electron transfer to the electrode. Previous investigations, however, were not successful in achieving practical currents. Kamitaka et al. (2007) immobilized FDH from *Gluconobacter* sp. by adsorption on a Ketjen's black (KB) modified carbon-paper anode that was capable of 4 mA cm^{-2}. Combined with a laccase biocatalyst from *Trametes* sp. adsorbed on a carbon aerogel cathode, a membrane-less bio-fuel cell was constructed and operated at room temperature in an O_2 saturated, 5 pH McIlvaine buffer containing 200 mM fructose. Under stirred conditions, to alleviate the O_2 mass transfer limitation, a maximum power density of 0.85 mW cm^{-2} at 410 mV was obtained and the open circuit voltage was recorded as 790 mV. The power output decreased to 63% of the maximum after 12 h of continuous operation. Under low power conditions, 4 cells connected in series continuously powered a small light-emitting diode for 60 days. Since the cell was operated at low power output for two months, the short lifetime was unlikely to be due to enzyme desorption but rather to a loss of activity during continuous operation at a high current density.

Though stirring is not usually desired in real applications, it is often used in systems to improve mass transport and increase the power output. Katz et al. (2005) investigated the effects of a constant magnetic field applied parallel to the electrode surface in surface-confined bio-electrocatalytic systems. In the two systems of GOx-FAD-PQQ and lactate dehydrogenase (LDH)/NAD^+-PQQ, in which the current was limited by mass transport, it was found that the current increased by a factor of three when a magnetic field (0.92 T) was applied. This improvement was brought on by a magnetohydrodynamic effect, engendering a magnetic force on the ions in solution, and thus decreasing the hydrodynamic layer thickness and increasing the current density.

Glucose dehydrogenase (GDH) was later immobilized with its cofactor, NAD^+ on KB, supported on a GC rod (Miyake et al., 2009). Together with a BOD/KB cathode, the constructed fuel cell was operated in an O_2 saturated phosphate buffer solution (PBS) containing 50 mM glucose. It achieved a maximum power density of 0.052 mW cm^{-2} at 0.3 V with an open circuit voltage (OCV) of 0.642 V.

Physical adsorption is attractive due to its simplicity, although enzyme retention is usually problematic. A review of systems employing simple adsorption shows that, despite exhibiting 'normal' cell voltages, they have low power densities compared to alternative systems based on the same biocatalysts. This indicates either poor electron transport despite the direct capabilities, or is

possibly a result of the low maximum enzyme loadings that can be achieved.

7.2. Enzyme immobilisation in polymers

Early hydrogel-modified electrodes in EFCs performed well over a period of a few days but suffered long-term stability issues (Calabrese-Barton et al., 2004). Amongst the causes of lost activity were (a) leaching of components from the cross-linked matrix and (b) hydrogel loss (Binyamin and Heller, 1999; Boland et al., 2009b). A recently developed method for improving stability consists of anchoring the hydrogel to the electrode surface via covalently attached tether groups (Boland et al., 2009b; Lehr et al., 2010). Boland et al. (2009b) compared the current densities and stabilities of pre-treated and bare graphite and Au electrodes. The pre-treated graphite electrodes were functionalised to yield the amine functional groups by electrochemical reduction of a diazonium salt from 1,4-phenylenediamine. An Os-based redox polymer was then cross-linked on the bare and pre-treated electrodes, with GOx on the anode and BOD on the cathode. For both electrodes, retention of activity was vastly improved by pre-treatment, although the test times of 48 h were still rather short. The authors postulated that the improved stability was due to the presence of amine groups on the pre-treated surfaces; these groups are amenable to anchoring of the hydrogel through reaction with the oxirane ring of the crosslinker.

Recently, Sakai et al. (2009) prepared an anode by successively applying solutions of poly-L-lysine (PLL), GDH, diaphorase, NADH, vitamin K_3 and polyacrylic acid sodium salt to four separate carbon fiber (CF) sheets. A membrane electrode assembly (MEA) was constructed by combining the anode with a cellophane membrane and an air-breathing cathode, fabricated by successively treating two CF sheets with $K_3[Fe(CN)_6]$, PLL and BOD solutions. A bio-fuel cell containing the MEA and a 0.1 M, 7 pH PBS at room temperature with 0.4 M glucose yielded a power density of 1.45 mW cm^{-2} at 0.3 V with an OCV of 0.8 V and a short circuit current (SCC) of 11 mA cm^{-2}. The diaphorase biocatalyst was used for a reduced overpotential oxidation of NADH with vitamin K_3 as the electron mediator. Two cells were then connected in series to operate a small toy car (16.5 g) for more than 2 h continuously. The assembled unit had a power output of 100 mW, a volume of 80 cm^3, and a weight of 39.7 g, of which 16.1 g was the fuel solution.

LDH is one of the many PQQ dependent enzymes capable of DET through a heme group (Treu and Minteer, 2008). Treu and Minteer (2008) isolated PQQ-dependent LDH bound to the outer membrane of *Gluconobacter* and purified them through ion exchange chromatography. The enzyme was immobilized with a tetrabutylammoniumbromide (TBAB)-modified Nafion solution on CF paper. $CaCl_2$ was also used in the immobilization since Ca^{2+} ions are used to coordinate the PQQ cofactor with the apoenzyme. The anode was combined with a Pt cathode and a Nafion membrane.

Khani et al. (2006) explored the use of alginate polymer beads in a low cost, simple method for enhanced enzyme retention. It was found that the use of pure alginate or alginate/carbon beads for the immobilization of GOx and laccase maintained 75% and 91% of the enzymatic activities, respectively, and doubled the active half-life of the enzymes. The rates of activity loss for entrapped laccase and BOD were 0.6% and 1.14% per day, respectively. While the turnover rate of GOx improved with the alginate beads (compared to a solution), the opposite was true for laccase. The Michaelis–Menten constant for GOx in the alginate beads increased by almost a factor of four, an effect that was explained by the limited substrate concentration near the enzymes.

Polymers containing redox mediator metal complexes have been used in the immobilization of GOx (Mano et al., 2005; Mano, 2008; Gao et al., 2009), lacasse (Calabrese-Barton et al., 2001; Soukharev et al., 2004; Barriere et al., 2004; Gallaway and Calabrese Barton, 2008) and BOD (Mano et al., 2002a). Mano (2008) used Os based metal complexes attached to a PVP polymer in addition to a crosslinking agent to wire GOx and laccase to two 7 μm diameter ×2 cm long GC electrodes. The GOx was sourced from *P. pinophilum* rather than the traditional *Aspergillus niger* since it has a lower Michaelis constant (which is needed for operating the miniature fuel cell in a glucose concentration similar to that found in physiological conditions, 5–8 mM). In a 20 mM citrate buffer with 5 mM glucose at 5 pH (optimum for GOx) and 37 °C, the fuel cell was capable of producing 0.28 mW cm^{-2} at 0.88 V, and operated continuously for 1 month at a power loss of 3% per day for the first 2 weeks. At neutral pH, however, *Penicillium pinophilum* is unstable and denaturation of the enzyme was found to occur; the optimum pH was in the range 4–6.

Gao et al. (2009) investigated the performance of different polymer backbones and a 7.24 pH PBS, GOx from *A. niger*, containing 15 mM glucose and atmospheric O_2. The main purpose of this study was to investigate the effect of purifying the enzyme. Commercial enzyme stocks usually contain other chemical elements whose exact composition is unknown. Purification of the stock was found to improve the specific activity and the performance of a fuel cell compared to non-purified enzymes.

Organic polymers have also been used to covalently attach enzymes. In the work by Kuwahara et al. (2009), 3-methylthiophene and thiophene-3-acetic acid were co-polymerised into a film on a gold coated alumina plate. Subsequently, GOx and BOD were covalently attached to the carboxyl groups of the polymer. Appropriate mediators were used in the two PBS (7 pH) solutions separated by a Nafion membrane. The anolyte was saturated with nitrogen and contained 0.1 M glucose while the catholyte was saturated with O_2. The OCV and maximum current density, both higher with BOD/copolymer than with Pt/C cathodes, were 0.61 V and 0.15 mW cm^{-2} at 0.35 V. Periodic measurements of the separate half-cell currents showed that the anodic current decreased by 50% over one month, while the cathodic current decreased by 25%.

Brunel et al. (2007) made a membrane-less bio-fuel cell using porous tubes supplied internally with O_2 and containing the biocatalyst at the outer surfaces exposed to the anolyte. GOx and its mediator, 8-hydroxyquinoline-5-sulfonic (HQS) acid, were co-immobilized in polypyrrole (PPy) polymer and the cathode was similarly prepared using laccase and its mediator, 2,2′-azinobis (3-ethylbenzothiazoline-6-sulfonate) diammonium salt (ABTS), on a porous carbon tube. A solution of nitrogen saturated PBS and 10 mM glucose at 37 ° C was used. A separate solution containing dissolved O_2 was circulated inside the cathode. At a pH of 5, a maximum power density of 0.027 mW cm^{-2} at 0.24 V was obtained. This decreased to 0.020 mW cm^{-2} at 7 pH. Some degree of leakage of the ABTS mediator was observed. The cell was tested intermittently after being stored at 4 ° C and retained 80% of its initial power density after 1 month.

Tamaki and Yamaguchi (2006) have immobilised a quinone mediator on a flexible spacer to polymer grafted on carbon black (Tamaki and Yamaguchi, 2006; Tamaki et al., 2007). The electrode was then immersed in GOx solution, and a cross-linking agent was applied after drying. The aim was to create a three-dimensional structure where the electron conduction was divided between the carbon particles and the redox polymers.

The DET of GOx has been established using a simple anode fabrication method and without the use of nanomaterials. In the work by Wang and Chen (2009), GOx was immobilized in PLL on a GC electrode, before a layer of Nafion was applied. Electrochemical tests on the Nafion-PLL-GOx anode showed reversible electrochemical behavior of the GOx and a performance similar to that using nanomaterials.

Rather than using polymers applied as films, Kim et al. (2009) prepared an anode using PPy nanowires to immobilize GOx and its mediator, HQS, on a nanoporous anodized aluminum oxide electrode. Different nanowire lengths, diameters, and electrode base preparation methods were tested, along with a single cathode made by immobilizing a mixture of laccase and its mediator, ABTS, in a PPy film on a gold electrode. With increasing nanowire length, the cell showed a decrease in OCV and an increase in the power density, which reached 0.28 mW cm^{-2} (at 0.15 V) using a 200 nm diameter $\times$16 μm length wire. This system suffered from low operating and open-circuit cell voltages, probably due to the high resistance of the long nanowires. The voltage was found to increase using 350 nm long wires grown directly on the Au surface, but the current and power output would be expected to decrease due to a decrease in the available surface area for enzyme immobilization.

7.3. Reconstructed apoenzymes and sol–gels

Monolayers of enzymes covalently bonded through redox relay molecules have been used for the construction of anodes (Zayats et al., 2008, and references therein). Lee et al. (2009) attached NAD$^+$-dependent LDH to PQQ electron mediators, which were in turn attached to a gold electrode by a cystamine monolayer. The novelty of the method introduced was that the final step of covalent attachment of LDH was performed in the presence of the NAD$^+$ cofactor, lactate substrate, and Ca^{2+}, which helped to promote a favorable orientation of the LDH after immobilization. The bioelectrochemical oxidation reactions of NADH, mediated by PQQ and leading to an electron transfer to the anode are (Shukla et al., 2004):

$$NADH + PQQ + H^+ \rightarrow NAD^+ + PQQH_2 \quad (4)$$

$$PQQH_2 \rightarrow PQQ + 2\,H^+ + 2\,e^- \text{ (to anode)} \quad (5)$$

The anode was combined with a cathode composed of microperoxidase (MP-11) attached to a monolayer of cystamine on a gold electrode. The anolyte consisted of 0.1 M, 7 pH, tris buffer containing optimized solution concentrations of 10 mM $CaCl_2$, 10 mM NAD$^+$ and 5 M lactate, while the catholyte consisted of a 0.1 M, 7 pH, PBS containing 1 mM hydrogen peroxide as the electron acceptor and ABTS as the mediator. The two compartments were separated by a Nafion membrane and the cell was operated at room temperature. The maximum power density obtained was 0.142 mW cm^{-2}. No mention was made of the cell voltage but a reading from the power and polarization plots shows that the OCV was around 0.34 V, and the maximum power density was achieved at around 0.1 V; relatively low when compared to the difference in the formal potential of the two mediators, 0.585 V ($E^0_{ABTS} = 0.46$ (Zebda et al., 2009b) and $E^0_{PQQ} = -0.125$ (Katz et al., 1999a)).

Sol–gel was employed by Lim et al. (2007) for the encapsulation of GOx, using tetramethoxy silane as the precursor for the silica gel incorporating both the biocatalysts (GOx and BOD) and SWCNTs. Ferrocene methanol and ABTS were the mediators in the membrane-separated anodic and cathodic compartments, respectively. Both compartments contained phosphate buffer solutions, with 100 mM of glucose at the anode side and saturated O_2 at the cathode side. Operating at room temperature, the fuel cell achieved a maximum power density of 0.120 mW cm^{-2} at 0.24 V, with an OCV of 0.48 V. Immobilization in a hydrogel removed any effects associated with orientation of the enzymes. Mobile enzymes diffuse in the gel, increasing the number of active enzymes and thus increasing the current, which may reach three times that for a monolayer (Tsujimura et al., 2005). The performance was poor when compared to other systems using the same biocatalysts and operating at a similar pH and fuel concentration.

7.4. Nanostructured electrodes

In recent years, the use of nanotechnology to develop biofuel cell electrodes has become widespread. Nano-structured materials have been shown to be appropriate hosts for enzyme immobilization, providing a greater surface area for attachment and improving enzyme kinetics (Kim et al., 2006). They can also be used as electrical 'wires' between the electrode and the active redox centre of the enzyme.

Lee et al. (2010) compared a fuel cell constructed using GOx and laccase with a cell containing SWCNT and a cell containing DNA-wrapped SWCNT. The use of single-stranded DNA-wrapped SWCNTs was found to increase the GOx loading to 73.3 μg mm^{-2} compared to approximately 19 μg mm^{-2} for both SWCNT/FAD-GOx and cystamine/PQQ/FAD-GOx anodes. The electron conductivity at the three anodes was also studied and the results showed that the two electrodes containing SWCNT had similar conductivities, which were an order of magnitude greater than that of the cystamine/PQQ/FAD-GOx anode. A membrane-less fuel cell employing DNA-wrapped SWCNTs for immobilization of GOx and laccase and operating in a PBS (7 pH, 25 °C) using glucose and O_2 (the fuel concentration was unspecified) achieved a maximum power density of 0.442 mW cm^{-2} at 0.46 V, with an OCV of approximately 1.5 V. The authors suggested that DNA wrapping contributes towards decreasing the shear stress between the enzyme and the SWCNT, in addition to acting as the primary electron transfer mediator. These results are, however, questionable since the high OCV cannot be explained in terms of the redox potentials of the two biocatalysts ($E^0_{GOx} \approx -0.34$ V and $E^0_{laccase} \approx 0.54$ V *vs.* SCE (Zebda et al., 2009b)). The power density obtained using this pair of mediator-less biocatalysts was higher than those obtained with the same catalysts either entrapped in polymers with mediators (Brunel et al., 2007), or wired through mediator activated polymers (Mano, 2008). Moreover, this system (Lee et al., 2010) was operated at neutral pH, a condition that is not optimal for *Trametes versicolor* laccase activity.

These disadvantages of using laccase have been found to be source dependent. Those sourced from *Melanocarpus albomyces*, for instance, display optimum activity close to neutral conditions (Kavanagh et al., 2009). Kavanagh et al. immobilised laccase with an Os containing polymer, while the anode contained suspended, mediated GOx. The maximum power density was 0.052 mW cm^{-2} at 0.21 V with and OCV of 0.55 V. Ivnitski et al. (2006) prepared a GOx anode using multi-walled carbon nanotubes (MWCNTs), which were grown using cobalt nanoparticles deposited on a carbon paper (CP). A mixture of GOx and polyethyleneimine was then applied to the electrode, followed by a casting of Nafion. The positively charged polycation acts as a binder between the negatively charged GOx and the CP/MWCNT electrode.

Fischback et al. (2006) used enzymes in cross-linked clusters covalently immobilized on functionalised CNTs, which were than cast on a carbon felt. The preparation procedure involved immobilizing single GOx enzymes on functionalised CNTs, before adding ammonium sulfate to form enzyme clusters from the remaining freely suspended GOx. These clusters around the CNTs were then cross-linked and applied with Nafion on a carbon felt electrode. The anode was combined with a proton exchange membrane and an air-breathing Pt cathode. The cell was tested in the absence of a buffer, with an ammonium buffer and with a sodium buffer. In the absence of a buffer, the initial performance was poor, but the cell remained stable over a longer period of time and maintained almost constant power output. The maximum power density was 0.120 mW cm^{-2} at 0.1 V with an OCV of 0.33 V. The buffered cells underwent a degradation in performance due to the presence of cations, which hinder the passage of protons through the membrane. Cross-linked enzyme clusters have previously been shown

by the same group to provide good stability and high activity retention (up to 250 days). While an un-buffered solution was found to give better performance due to a lack of interference with proton transport, it may also have led to the low operating voltage (low solution conductivity). The use of an alternative membrane in the buffered cells to alleviate the problem of hindered proton transport, while not increasing the internal resistance, was not investigated.

Deng et al. (2008) applied several coatings of AuNP/enzyme bilayers on macroporous gold electrodes initially treated with cystamine. Using GDH and laccase as enzymes, a membrane-less fuel cell was constructed. The cell was studied with respect to the number of bilayers and compared to one with flat gold electrodes and one bilayer. A maximum power density of 0.178 mW cm^{-2} at 226 mV was achieved using five bilayers while the OCV was 0.32 mV. The current and power density were found to increase with the first 5 layers and in all cases were higher than with flat electrodes. A higher OCV (0.52 V) was observed with flat gold electrodes, and was attributed by the authors to a difference in the O_2 reduction potential compared to that for the macroporous cathode. However, CVs of these two anodes showed that a current peak occurred at a slightly higher potential with the flat electrode, indicating that the lower cell voltage is due to both electrode potentials, possibly as a consequence of the higher electrical resistance of the macroporous materials.

SWCNTs on GC have been used to attach AlcDH to covalently linked NAD^+ (Yan et al., 2009). This anode was combined with a cathode containing both Pt and BOD in a copolymer cross-linked matrix and the cell was operated with 0.1 M PBS and 40 mM of ethanol at a pH of 7.0 (Fig. 4). A maximum power density of 0.2 mW cm^{-2} at 0.55 V and 0.37 mA cm^{-2} with an OCV of 0.62 V were attained. While CNTs are employed for their good conductivity and large surface area for depositing the enzymes, Zhou et al. (2009) showed that a higher voltage and power density can be obtained with a mesoporous carbon based material.

Ideally, enzymatic electrodes for power generation should maximize enzyme loading, activity and stability, while also minimizing inefficiencies due to substrate mass transport limitations and slow electron transfer from the enzyme to the electrode. While increasing bond strength (physical adsorption/entrapment, ionic bonding, and covalent bonding) improves enzyme retention, deactivation is also more probable (Sheldon, 2007). Simple physical binding or entrapment in polymers is sometimes complemented by ionic binding, but this imposes an operating pH depending on the type of enzyme used and the ionomer charge. Addition of a cross-linking agent is a simple and widely used method to improve the stability and increase both the concentration of the enzyme and its activity (Sheldon, 2007).

The random enzyme orientation, when physically adsorbed or covalently bonded, is unfavourable for efficient electron communication with the active site. The reconstruction of apo-enzymes around the active site bound to a redox relay provides excellent electrical communication. Monolayers of these electrically contacted enzymes have a high turnover number and sensitivity, although the enzyme loading is limited by the electrode surface area. This limitation can be relieved by a similar enzyme reconstitution but on an electrically active thin polymer film (Zayats et al., 2008). Immobilization of mediators and enzymes on polymer films is a simple and practical method for biofuel cell electrodes; however, the effective diffusion coefficient of the mediator (and hence the electron transport rate) is several orders of magnitude lower than that of a typical diffusional mediator (Kim et al., 2006).

The increasing use of nanostructures (such as nanoparticles, nanofibers and CNTs) has a twofold advantage: providing a greater surface area for the biocatalysts and enhancing their stability and activity (Kim et al., 2008). These procedures are, on the other hand, relatively costly. Some reports have claimed that CNTs can have an adverse effects on the enzyme kinetics (Zhao et al., 2009), indicating that the use of these structures requires a careful selection of enzymes, electrode materials and attachment methods. More generally, a careful optimization of the nanostructure size is required, since small pores can lead to mass transport limitations for the mediator/substrate and large pores can lead to leaching of the enzyme (Kim et al., 2006).

7.5. Fuel oxidation

In many enzymatic fuel cells, both the cathode and anode are enzyme-based, with the aim of combining the benefits of higher stability and the good catalytic activity of inorganic materials, together with improved O_2 reduction kinetics via biocatalysts at low temperatures (Choi et al., 2009; Habrioux et al., 2007, 2009). Habrioux et al. (2009) used Au–Pt nanoparticles supported in a Nafion/carbon-black mix, together with BOD and its mediator ABTS co-immobilized in a Nafion film to construct a concentric bio-fuel cell. A maximum power density of 0.19 mW cm^{-2} at 0.52 V was achieved at 37 °C and 7.4 pH using 0.7 M glucose. An appreciable power density of 0.09 mW cm^{-2} could still be achieved at a lower glucose concentration of 10 mM.

Most fuels used in EFCs are either saccharides, such as glucose, lactose, fructose and cellobiose, or alcohols such as ethanol. Recently, glycerol has been considered due to its high energy density and abundance (it is a byproduct of biodiesel) (Arechederra et al., 2007; Arechederra and Minteer, 2009). In a study by Arechederra et al. (2007), a cascade of two PQQ-dependent enzymes, AlcDH and aldehyde dehydrogenase (AldDH) was immobilized in modified Nafion on a CP/Pt cathode, and the assembled fuel cell produced a maximum power density of up to 1.21 mW cm^{-2}. This cell was further developed by adding a third enzyme, oxalate oxidase (Arechederra and Minteer, 2009), which allowed the complete oxidation of glycerol and slightly increased the maximum power density to 1.32 mW cm^{-2} with 100 mM of glycerol. However, the cell was less tolerant to high fuel concentrations compared to the original cell.

Another enzyme cascade system was reported by Topcagic and Minteer (2006). Ethanol was oxidized to acetate by AlcDH and AldDH and dissolved O_2 was reduced by BOD immobilized with two consecutive mediators in Nafion. In a membrane-less system employing 7.15 pH PBS with 1 mM ethanol and 1 mM NAD^+ as the anodic mediator, an OCV of 0.51 V and a maximum power density of 0.39 mW cm^{-2} were achieved. Both the voltage and power were lower than an equivalent cell employing a Nafion membrane separator. Ramanavicius et al. (2008) developed a fuel cell that used ethanol as the substrate for both half reactions, with an AlcOD/MP cascade on the cathode and AlcDH on the anode. The maximum power density was 1.5×10^{-3} mW cm^{-2} with an OCV of 0.24 V.

In addition to the development of enzyme/electrode preparation methods, several studies have been aimed at optimising systems according to the buffer type and concentration, redox polymer composition, and binder-to-enzyme ratios (Sakai et al., 2009; Kjeang et al., 2006; Kontani et al., 2009; Mano et al., 2005; Stoica et al., 2009). Most of the choices were specific to the setup used and are of limited use for other designs. In the case of microfluidic fuel cells, numerical optimization of the channel dimensions has been performed by several groups (Zebda et al., 2009a,b; Togo et al., 2008).

Membrane-less fuel cells have several attractive features, including structural simplicity, reduced cost, and a greater scope for miniaturization. There are, however, several requirements for such systems: specificity of the two half reactions occurring, such that the substrates/products of one do not interfere with the other, and acceptable operating conditions common to both biocatalysts (Stoica et al., 2009). A number of membrane-less systems have been

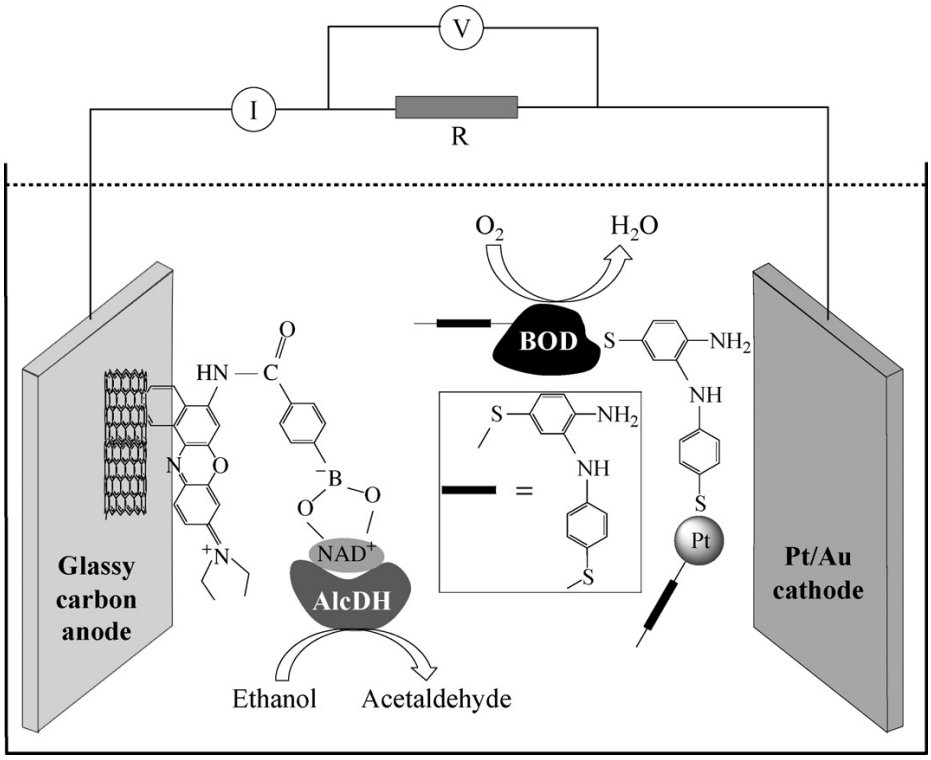

Fig. 4. A schematic representation of a membrane-less bio-fuel cell employing bioelectrocatalytic electrodes composed of (a) alcohol dehydrogenase (AlcDH) reconstituted on a relay-NAD^+ monolayer associated with carbon nanotubes (anode); and (b) a platinum-nanoparticle/bilirubin-oxidase (BOD) crosslinked composite on a Au/Pt electrode (cathode). Adapted from Yan et al. (2009).

developed, exhibiting varying degrees of electrical performance. In systems based on DET using CDH/laccase (Coman et al., 2008), CDH/BOD (Coman et al., 2009), or GOx/laccase (Wang et al., 2009), power densities of only a few $\mu W\,cm^{-2}$ have been realised. The first two systems employing CDH exhibited relatively high operating and open cell voltages, and hence the low power was due to a low current, specifically the anodic current. This was potentially due to unfavorable orientation of CDH after immobilization; CDM has one FAD domain and one heme domain allowing DET to the electrode. Membrane-less systems employing mediators, and either GDH/BOD (Gao et al., 2007), AlcDH/BOD (Topcagic and Minteer, 2006), GDH/laccase (Deng et al., 2008), or FDH/laccase (Kamitaka et al., 2007), can have power densities 1–2 orders of magnitude higher than those yielded by DET. The absence of soluble mediators, however, remains an essential feature of the flow type fuel cells proposed for *in vivo* applications.

8. Summary and outlook

In the last few years, enzymatic fuel cells have approached power densities of $\sim 1\,mW\,cm^{-2}$. For portable electronic applications, high energy density fuels such as ethanol (Topcagic and Minteer, 2006) and glycerol (Arechederra and Minteer, 2009) show great promise. Developments in the overall system design have also led to more efficient systems. For example, removing the separator membrane without significant loss in power output, and the emergence of single chamber, air-breathing systems using compact MEAs. For many proposed applications, however, further substantial improvements in performance are required (higher power densities and energy efficiencies).

For both MFC and EFC, electrode materials need to be more catalytic while maintaining their performance, particularly in the face of problems caused by fouling of the active surfaces and loss of enzyme activity. It is also important to study time-dependent performance over practical periods, particularly with a focus on long-term changes in the enzyme activity.

A greater understanding and characterisation of the reaction environment can be achieved through studies of the reactant and charge distribution, mass transport and mass transfer, as well as the bio-electrochemical reaction kinetics. Carefully validated models can be used in conjunction with laboratory studies to investigate these processes (particularly *in situ*) and to accelerate the development of practical systems. To date, only a small number of models have been developed for specific systems (Bartlett and Pratt, 1995; Kano and Ikeda, 2000; Ikeda and Kano, 2001; Gallaway and Calabrese Barton, 2008; Calabrese-Barton, 2005; Kjeang et al., 2006; Zeng et al., 2010; Marcus et al., 2007; Picioreanu et al., 2007, 2010). Models for other electrochemical cells, including polymer electrolyte membrane (PEM) fuel cells and batteries (Shah and Walsh, 2008; Shah et al., 2009, 2008) are ideal templates for further developing BFC models.

A vitally important aspect of bio-fuel cell performance and stability is the immobilization of the enzyme/mediator on the electrode. Maintaining a continuous supply of fuel to the active sites and ensuring an efficient electron-transfer process from the enzyme/bacteria to the electrode via the mediator are crucial. While previous research was mainly targeted at developing the enzyme chemistries (Bullen et al., 2006), the past 5 years can be marked by efforts to develop new methods and materials for integrated enzyme electrodes that maximize enzyme loading and move from the classic two-dimensional loading to highly ordered three-

dimensional structures with improved enzyme stabilization (Kim et al., 2008). These use of nanostructures shows great promise, though it should be kept in mind that for application purposes the materials must be safe and cost effective, and the fabrication techniques must be practical.

From an engineering perspective, cells with chemistries that allow single-compartment operation and possess constructional simplicity would be highly advantageous. It is important that low-cost, modular and scalable designs are developed, particularly if they are to form the basis for multi-plate (e.g. bipolar) cell stacks. At the present time, there are very few examples of BFC stacks (Aelterman et al., 2006; Sakai et al., 2009). In this respect, much could be learned from the rapid progress in PEM fuel cell MEA/stack performance over the past two decades (Barbir, 2005). Cell construction has been improved to optimise the cell voltage through comprehensive modelling/experimental studies of the electrode overpotentials and all cell resistances; there is a vast body of literature on the electrical, thermal, transport and mechanical properties of electrode, plate and membrane materials.

References

Aelterman, P., Rabaey, K., Pham, H.T., Boon, N., Verstraete, W., 2006. Environ. Sci. Technol. 40, 3388–3394.
Allongue, P., Delamar, M., Desbat, B., Fagebaume, O., Hitmi, R., Pinson, J., Savéant, J.M., 1997. J. Am. Chem. Soc. 119, 201–207.
Arechederra, R.L., Boehm, K., Minteer, S.D., 2009. Electrochim. Acta 54, 7268–7273.
Arechederra, R.L., Minteer, S.D., 2009. Fuel Cells 9, 63–69.
Arechederra, R.L., Treu, B.L., Minteer, S.D., 2007. J. Power Sources 173, 156–161.
Barbir, F., 2005. PEM Fuel Cells: Theory and Practice. Elsevier/Academic Press, London.
Barriere, F., Ferry, Y., Rochefort, D., Leech, D., 2004. Electrochem. Commun. 237, 237–241.
Bartlett, P.N., Pratt, K.F.E., 1995. J. Electroanal. Chem. 397, 61–78.
Binyamin, G., Heller, A., 1999. J. Electrochem. Soc. 146, 2965–2967.
Boder, E.T., Wittrup, K.D., 1997. Nat. Biotechnol. 15, 553–557.
Boland, S., Foster, K., Leech, D., 2009a. Electrochim. Acta 54, 1986–1991.
Boland, S., Jenkins, P., Kavanagh, P., Leech, D., 2009b. J. Electroanal. Chem. 626, 111–115.
Brooksby, P.A., Downward, A.J., 2004. Langmuir 20, 5038–5045.
Brunel, L., Denele, J., Servat, K., Kokoh, K.B., Jolivalt, C., Innocent, C., Cretin, M., Rolland, M., Tingry, S., 2007. Electrochem. Commun. 9, 331–336.
Bullen, R.A., Arnot, T.C., Lakeman, J.B., Walsh, F.C., 2006. Biosens. Bioelectron. 21, 2015–2045.
Cai, C., Chen, J., 2004. Anal. Biochem. 332, 75–83.
Calabrese-Barton, S., 2005. Electrochim. Acta 50, 2145–2153.
Calabrese-Barton, S., Kim, H.H., Binyamin, G., Zhang, Y.C., Heller, A., 2001. J. Am. Chem. Soc. 123, 5802–5803.
Calabrese-Barton, S.A., Gallaway, J.W., Atanassov, P., 2004. Chem. Rev. 104, 4867–4886.
Call, D., Logan, B.E., 2008. Environ. Sci. Technol. 42, 3401–3406.
Cao, L., 2005. Curr. Opin. Biotechnol. 9, 217–226.
Cao, X., Huang, X., Boon, N., Liang, P., Fan, M., 2008. Electrochem. Commun. 10, 1392–1395.
Chen, T., Calabrese-Barton, S., Binyamin, G., Gao, Z., Zhang, Y., Kim, H.H., Heller, A., 2001. J. Am. Chem. Soc. 123, 8630–8631.
Cheng, S., Xing, D., Call, D.F., Logan, B.E., 2009. Environ. Sci. Technol. 43, 3953–3958.
Cho, Y.K., Donohue, T.J., Tejedor, I., Anderson, M.A., McMahon, K.D., Noguera, D.R., 2008. J. Appl. Microbiol. 104, 640–650.
Choi, Y., Wang, G., Nayfeh, M.H., Tung Yau, S., 2009. Biosens. Bioelectron. 24, 3103–3107.
Clauwaert, P., Aelterman, P., Pham, T.H., De Schamphelaire, L., Carballa, M., Rabaey, K., Verstraete, W., 2008. Appl. Microbiol. Biotechnol. 79, 901–913.
Coman, V., Ludwig, R., Harreither, W., Haltrich, D., Gorton, L., Ruzgas, T., Shleev, S., 2009. Fuel Cells 10, 9–16.
Coman, V., Vaz-Domínguez, C., Ludwig, R., Harreither, W., Haltrich, D., DeLacey, A., Ruzgas, T., Gorton, L., Shleev, S., 2008. Phys. Chem. Chem. Phys. 10, 6093–6096.
Cooney, M.J., Svoboda, V., Lau, C., Martin, G., Minteer, S.D., 2008. Energy Environ. Sci. 1, 320–337.
Davis, F., Higson, S.P.J., 2007. Biosens. Bioelectron. 22, 1224–1235.
Delamarche, E., Michel, B., Kang, H., Gerber, C., 1994. Langmuir 10, 4103–4108.
Deng, L., Wang, F., Chen, H., Shang, L., Wang, L., Wang, T., Dong, S., 2008. Biosens. Bioelectron. 24, 329–333.
Dubois, L.H., Nuzzo, R.G., 1992. Ann. Rev. Phys. Chem. 43, 437–463.
Ferapontova, E.E., Ruzgas, T., Gorton, L., 2003. Anal. Chem. 75, 4841–4850.
Fischback, M.B., Youn, J.K., Zhao, X., Wang, P., Park, H.G., Chang, H.N., Kim, J., Ha, S., 2006. Electroanalysis 18, 2016–2022.
Fishilevich, S., Amir, L., Fridman, Y., Aharoni, A., Alfonta, L., 2009. J. Am. Chem. Soc. 131, 12052–12053.
Furukawa, Y., Moriuchi, T., Morishima, K., 2006. J. Micromech. Microeng. 16, 220–S225.
Gallaway, J.W., Calabrese Barton, S.A., 2008. J. Am. Chem. Soc. 130, 8527–8536.
Gao, F., Courjean, O., Mano, N., 2009. Biosens. Bioelectron. 25, 356–361.
Gao, F., Yan, Y., Su, L., Wang, L., Mao, L., 2007. Electrochem. Commun. 9, 989–996.
Ghindilis, A.L., Atanassov, P., Wilkins, E., 1997. Electroanalysis 9, 661–674.
Gooding, J.J., Hibbert, D.B., 1999. Trac-Trend Anal. Chem. 18, 525–533.
Gooding, J.J., Mearns, F., Yang, W., Liu, J., 2003. Electroanalysis 15, 81–96.
Gregg, B.A., Heller, A., 1991. J. Phys. Chem. 95, 5970–5975.
Guiseppi-Elie, A., Lei, C., Baughman, R.H., 2002. Nanotechnology 13, 559–564.
Habrioux, A., Servat, K., Tingry, S., Kokoh, K.B., 2009. Electrochem. Commun. 11, 111–113.
Habrioux, A., Sibert, E., Servat, K., Vogel, W., Kokoh, K., Alonso-Vante, N., 2007. J. Phys. Chem. B 111, 10329–10333.
Harper, A., Anderson, M.R., 2010. Sensors 10, 8248–8274.
He, Z., Angenent, L.T., 2006. Electroanalysis 18, 2009–2015.
He, Z., Kan, J., Mansfeld, F., Angenent, L.T., Nealson, K.H., 2009. Environ. Sci. Technol. 43, 1648–1654.
He, Z., Minteer, S.D., Angenent, L.T., 2005. Environ. Sci. Technol. 39, 5262–5267.
Heller, A., 1992. J. Phys. Chem. 96, 3579–3587.
Heller, A., 2004. Phys. Chem. Chem. Phys. 6, 209–216.
Heller, A., 2006. Curr. Opin. Chem. Biol. 10, 664–672.
Ikeda, T., Kano, K., 2001. J. Biosci. Bioeng. 92, 9–18.
Ishii, S., Shimoyama, T., Hotta, Y., Watanabe, K., 2008. BMC Microbiol. 8, 6.
Ishikawa, M., Yamamura, S., Takamura, Y., Sode, K., Tamiya, E., Tomiyama, M., 2006. Int. J. Hydrogen Energy 31, 1484–1489.
Ivnitski, D., Branch, B., Atanassov, P., Apblett, C., 2006. Electrochem. Commun. 8, 1204–1210.
Jang, J.K., Pham, T.H., Chang, I.S., Kang, K.H., Moon, H., Cho, K.S., Kim, B.H., 2004. Proc. Biochem. 39, 1007–1012.
Kamitaka, Y., Tsujimura, S., Setoyama, N., Kajino, T., Kano, K., 2007. Phys. Chem. Chem. Phys. 9, 1793–1801.
Kandimalla, V.B., Tripathi, V.S., Ju, H.X., 2006. Crit. Rev. Anal. Chem. 36, 73–106.
Kano, K., Ikeda, T., 2000. Anal. Sci. 16, 1013–1021.
Kariuki, J.K., McDermott, M.T., 2001. Langmuir 17, 5947–5951.
Katz, E., Filanovsky, B., Willner, I., 1999a. New J. Chem. 23, 481–487.
Katz, E., Lioubashevski, O., Willner, I., 2005. J. Am. Chem. Soc. 127, 3979–3988.
Katz, E., Shipway, A., Willner, I., 2003. Handbook of Fuel Cells—Fundamentals, Technology and Applications. John Wiley & Sons Ltd (Chapter 21—biochemical fuel cells).
Katz, E., Willner, I., Kotlyar, A.B., 1999b. J. Electroanal. Chem. 479, 64–68.
Kavanagh, P., Boland, S., Jenkins, P., Leech, D., 2009. Fuel Cells 9, 79–84.
Khani, Z., Jolivalt, C., Cretin, M., Tingry, S., Innocent, C., 2006. Biotechnol. Lett. 28, 1779–1786.
Kim, B.H., Chang, I.S., Gadd, G.M., 2007. Appl. Microbiol. Biotechnol. 76, 485–494.
Kim, H.H., Mano, N., Zhang, Y., Heller, A., 2003. J. Electrochem. Soc. 150, 209–213.
Kim, J., Grate, J., Wang, P., 2008. Trends Biotechnol. 26, 639–646.
Kim, J., Jia, H., Wang, P., 2006. Biotechnol. Adv. 24, 296–308.
Kim, J., Kim, S.I., Hwa Yoo, K., 2009. Biosens. Bioelectron. 25, 335–350.
Kjeang, E., Sinton, D., Harrington, D., 2006. J. Power Sources 158, 1–12.
Kontani, R., Tsujimura, S., Kano, K., 2009. Bioelectrochemistry 76, 10–13.
Kuwahara, T., Homma, T., Kondo, M., Shimomura, M., 2009. Syn. Met. 159, 1859–1864.
Larminie, J., Dicks, A., 2003. Fuel Cell Systems Explained. John Wiley & Sons.
Lee, J.Y., Shin, H.Y., Kang, S.W., Park, C., Kim, S.W., 2010. J. Power Sources 195, 750–755.
Lee, J.Y., Shin, H.Y., Lee, J.H., Song, Y.S., Kang, S., Park, C., Kim, J.B., Kim, S.W., 2009. J. Molec. Catal. B 59, 274–278.
Lehr, J., Williamson, B.E., Barrière, F., Downward, A.J., 2010. Bioelectrochemistry 79, 142–146.
Lim, J., Malati, P., Bonet, F., Dunn, B., 2007. J. Electrochem. Soc. 154, A140–A145.
Lin, J., Brown, C.W., 1997. Trends Anal. Chem. 16, 200–211.
Lin, Y., Lu, F., Tu, Y., Ren, Z., 2004. Nano Lett. 4, 191–195.
Liu, H., Cheng, S., Logan, B.E., 2005a. Environ. Sci. Technol. 39, 5488–5493.
Liu, H., Grot, S., Logan, B.E., 2005b. Environ. Sci. Technol. 39, 4317–4320.
Liu, H., Logan, B.E., 2004. Environ. Sci. Technol. 38, 4040–4046.
Lovley, D.R., 2006. Curr. Opin. Biotechnol. 17, 327–332.
Mano, N., 2008. Chem. Commun. 19, 2221–2223.
Mano, N., Fernandez, J.L., Kim, Y., Shin, W., Bard, A.J., Heller, A., 2003. J. Am. Chem. Soc. 125, 15290–15291.
Mano, N., Kim, H.H., Zhang, Y.C., Heller, A., 2002a. J. Am. Chem. Soc. 124, 6480–6486.
Mano, N., Mao, F., Heller, A., 2002b. J. Am. Chem. Soc. 124, 12962–12963.
Mano, N., Mao, F., Heller, A., 2005. J. Electroanal. Chem. 574, 347–357.
Mao, F., Mano, N., Heller, A., 2003. J. Am. Chem. Soc. 125, 4951–4957.
Marcus, A.K., Torres, C.I., Rittmann, E., 2007. Biotechnol. Bioeng. 98, 1171–1182.
Miyake, T., Oike, M., Yoshino, S., Yatagawa, Y., Haneda, K., Kaji, H., Nishizawa, M., 2009. Chem. Phys. Lett. 480, 123–126.
Moehlenbrock, M.J., Minteer, S.D., 2008. Chem. Soc. Rev. 37, 1188–1196.
Niessen, J., Schröder, U., Harnisch, F., Scholz, F., 2005. Lett. Appl. Microbiol. 41, 286–290.
Osman, H., Shah, A.A., Walsh, F.C., 2010. Biosens. Bioelectron. 26, 953–963.
Park, D.H., Zeikus, J.G., 2003. Biotechnol. Bioeng. 81, 348–355.
Patolsky, F., Weizmann, Y., Willner, I., 2004. Ang. Chem. 43, 2113–2117.

Pellissier, M., Barrière, F., Downward, A.J., Leech, D., 2008. Electrochem. Commun. 10, 835–838.
Picioreanu, C., Head, I.M., Katuri, K.P., van-Loosdrecht, M.C.M., Scott, K., 2007. Water Res. 41, 2921–2940.
Picioreanu, C., van Loosdrecht, M.C.M., Curtis, T.P., Scott, K., 2010. Bioelectrochemistry 78, 8–24.
Pizzariello, A., Stredansky, M., Miertus, S., 2002. Bioelectrochemistry 56, 99–105.
Rabaey, K., Verstraete, W., 2005. Trends Biotechnol. 23, 291–298.
Ramanavicius, A., Kausaite, A., Ramanaviciene, A., 2008. Biosens. Bioelectron. 24, 761–766.
Ramanavicius, A., Kausaitea, A., Ramanaviciene, A., 2005. Biosens. Bioelectron. 20, 1962–1967.
Rosenbaum, M., Schroöder, U., Scholz, F., 2005. Environ. Sci. Technol. 39, 6328–6333.
Rozendal, R.A., Hamelers, H.V.M., Euverink, G.J.W., 2006. Int. J. Hydrogen Energy 31, 1632–1640.
Saby, C., Ortiz, B., Champagne, G.Y., Bélanger, D., 1997. Langmuir 13, 6805–6813.
Sakai, H., Nakagawa, T., Tokita, Y., Hatazawa, T., Ikeda, T., Tsujimura, S., Kano, K., 2009. Energy Environ. Sci. 2, 133–138.
Sarma, A.K., Vatsyayan, P., Goswami, P., Minteer, S.D., 2009. Biosens. Bioelectron. 24, 2313–2322.
Schoenfisch, M.H., Pemberton, J.E., 1998. J. Am. Chem. Soc. 120, 4502–4513.
Shah, A.A., Ralph, T.R., Walsh, F.C., 2009. J. Electrochem. Soc. 156, B465–B484.
Shah, A.A., Walsh, F.C., 2008. J. Power Sources 185, 287–301.
Shah, A.A., Watt-Smith, M., Walsh, F., 2008. Electrochim. Acta 53, 8087–8100.
Sheldon, R.A., 2007. Adv. Synth. Catal. 349, 1289–1307.
Shukla, A.K., Suresh, P., Berchmans, S., Rajendran, A., 2004. Curr. Sci. 87, 455–468.
Solomon, E.I., Sundaram, U.M., Machonkin, T.E., 1996. Chem. Rev. 96, 2563–2606.
Soukharev, V., Mano, N., Heller, A., 2004. J. Am. Chem. Soc. 126, 8368–8369.
Stoica, L., Dimcheva, N., Ackermann, Y., Karnicka, K., Guschin, D.A., Kulesza, P.J., Rogalski, J., Haltrich, D., Ludwig, R., Gorton, L., Schuhmann, W., 2009. Fuel Cells 9, 53–62.
Sucheta, A., Cammack, R., Weiner, J., Armstrong, F.A., 1993. Biochemistry 32, 5455–5465.
Tamaki, T., Ito, T., Yamaguchi, T., 2007. J. Phys. Chem. B 111, 10312–10319.
Tamaki, T., Yamaguchi, T., 2006. Ind. Eng. Chem. Res. 45, 3050–3058.
Tasca, F., Gorton, L., Harreither, W., Haltrich, D., Ludwig, R., Nöll, G., 2008a. J. Phys. Chem. C 112, 9956–9961.
Tasca, F., Gorton, L., Harreither, W., Haltrich, D., Ludwig, R., Nöll, G., 2008b. J. Phys. Chem. C 112, 13668–13673.
Tischer, W., Wedekind, F., 2000. In: Wolf-Dieter, F., (Ed.), Biocatalysis—From Discovery To, Applications, Springer-Verlag. 95–126.
Togo, M., Takamura, A., Asai, T., Kaji, H., Nishizawa, M., 2007. Electrochim. Acta 52, 4669–4674.
Togo, M., Takamura, A., Asai, T., Kaji, H., Nishizawa, M., 2008. J. Power Sources 178, 53–58.
Topcagic, S., Minteer, S.D., 2006. Electrochim. Acta 51, 2168–2172.
Treu, B.L., Minteer, S.D., 2008. Bioelectrochem. 74, 73–77.
Tsujimura, S., Kano, K., Ikeda, T., 2005. Electroanal. Chem. 576, 113–120.
Vincent, K.A., Cracknell, J.A., Lenz, O., Zebger, I., Friedrich, B., Armstrong, F.A., 2005. Proc. Natl. Acad. Sci. U. S. A. 102, 16951–16954.
Wang, D., Chen, L., 2009. Electrochim. Acta 54, 4316–4320.
Wang, J., 1999. Anal. Chim. Acta 399, 21–27.
Wang, J., Musameh, M., Lin, Y., 2003. J. Am. Chem. Soc. 125, 2408–2409.
Wang, S.C., Yang, F., Silva, M., Zarow, A., 2009. Electrochem. Commun. 11, 34–37.
Watanabe, K., 2008. J. Biosci. Bioeng. 106, 528–536.
Willner, I., Arad, G., Katz, E., 1998a. Bioelectrochem. Bioener. 44, 209–214.
Willner, I., Heleg-Shabtai, V., Blonder, R., Katz, E., Tao, G., 1996. J. Am. Chem. Soc. 118, 10321–10322.
Willner, I., Katz, E., Patolsky, F., Bückmann, A.F., 1998b. J. Chem. Soc., Perkin Trans. 2, 1817–1822.
Willner, I., Yan, Y.M., Willner, B., Tel-Vered, R., 2009. Fuel Cells 9, 7–24.
Xiao, Y., Patolsky, F., Katz, E., Hainfeld, J.F., Willner, I., 2003. Science 21, 1877–1881.
Yan, Y.M., Baravik, I., Tel-Vered, R., Willner, I., 2009. Adv. Mater. 21, 4275–4279.
Zayats, M., Katz, E., Willner, I., 2005. J. Am. Chem. Soc. 127, 12400–12406.
Zayats, M., Willner, B., Willner, I., 2008. Electroanalysis 20, 583–601.
Zebda, A., Renaud, L., Cretin, M., Innocent, C., Pichot, F., Ferrigno, R., Tingry, S., 2009a. J. Power Sources 193, 602–606.
Zebda, A., Renaud, L., Cretin, M., Pichot, F., Innocent, C., Ferrigno, R., Tingry, S., 2009b. Electrochem. Commun. 11, 592–595.
Zeng, Y., Choo, Y.F., Kim, H.H., Wu, P., 2010. J. Power Sources 195, 79–89.
Zhang, S.G.W.Q., Wang, R., Yoona, S.F., 2003. Biochem. Biophys. Res. Commun. 311, 572–576.
Zhao, X., Jia, H., Kim, J., Wang, P., 2009. Biotechnol. Bioeng. 104, 1068–1074.
Zheng, W., Zhou, H.M., Zheng, Y.F., Wang, N., 2008. Chem. Phys. Lett. 457, 381–385.
Zhou, M., Deng, L., Wen, D., Shang, L., Jin, L., Dong, S., 2009. Biosens. Bioelectron. 24, 2904–2908.

Biosensors and Bioelectronics 26 (2010) 953–963

Contents lists available at ScienceDirect

Biosensors and Bioelectronics

journal homepage: www.elsevier.com/locate/bios

Review

Recent progress and continuing challenges in bio-fuel cells. Part II: Microbial

M.H. Osman, A.A. Shah*, F.C. Walsh

Energy Technology Research Group, School of Engineering Sciences, University of Southampton, Highfield, Southampton SO17 1BJ, UK

ARTICLE INFO

Article history:
Received 10 June 2010
Received in revised form 15 August 2010
Accepted 17 August 2010
Available online 24 August 2010

Keywords:
Bio-fuel cells
Microbial
Electron transfer
Materials
Challenges
Review

ABSTRACT

Recent key developments in microbial fuel cell technology are reviewed. Fuel sources, electron transfer mechanisms, anode materials and enhanced O_2 reduction are discussed in detail. A summary of recently developed microbial fuel cell systems, including performance measurements, is conveniently provided in tabular form. The current challenges involved in developing practical bio-fuel cell systems are described, with particular emphasis on a fundamental understanding of the reaction environment, the performance and stability requirements, modularity and scalability. This review is the second part of a review of bio-fuel cells. In Part 1 a general introduction to bio-fuel cells, including their operating principles and applications, was provided and enzymatic fuel cell technology was reviewed.

Contents

1. Introduction

Bio-fuel cells can be defined as systems capable of direct chemical to electrical energy conversion *via* biochemical pathways (Bullen et al., 2006; Katz et al., 2003; Shukla et al., 2004). The conversion is achieved by coupling an oxidation reaction supplying electrons at the anode with a reduction reaction utilizing electrons at the cathode. The reactions are electronically separated inside the system to force electrons to flow through an external circuit, while ion movement inside the system maintains charge balance and completes the electrical circuit.

Conventional inorganic fuel cells such as the polymer–electrolyte, direct-methanol and solid-oxide systems (Larminie and Dicks, 2003) have reached an advanced state in their development. These systems rely on expensive rare metal catalysts, operate on reformed fossil fuels and suffer from a host of degradation and fuel-storage issues. Bio-fuel cells (BFC), on the other hand, are considered to be in the early stages of development. The chemical reactions are driven by diverse and abundant bio-fuels (Pant et al., 2010) and biological catalysts. The production/consumption cycle of bio-fuels is considered to

Abbreviations: AQDS, anthraquinone-1,6-disulfonic acid; ABTS, 2,2′-azinobis (3-ethylbenzothiazoline-6-sulfonate) diammonnium salt; AlcDH, alcohol dehydrogenase; AldDH, aldehyde dehydrogenase; BES, 2-bromoethanesulfonate; BFC, bio-fuel cell; BUG, benthic unattended generator; CE, coulombic efficiency; CoTMPP, cobalt tetramethylphenylporphyrin; CP, carbon paper; DET, direct electron transfer; EDTA, ethylenediaminetetraacetic acid; EFC, enzymatic fuel cell; ET, electron transfer; MEA, membrane-electrode assembly; MET, mediated electron transfer; MFC, microbial fuel cell; NQ, 1,4-naphthoquinone; NR, neutral red; PEM, polymer electrolyte membrane; PEMFC, polymer electrolyte membrane fuel cell; PTFE, polytetrafluoroethylene.

* Corresponding author. Tel.: +44 23 8059 8520; fax: +44 23 8059 3131.
E-mail address: A.Shah@soton.ac.uk (A.A. Shah).

0956-5663/$ – see front matter © 2010 Elsevier B.V. All rights reserved.
doi:10.1016/j.bios.2010.08.057

be carbon neutral and, in principle, more sustainable than that of conventional fuel cells (Lovley, 2006). Moreover, biocatalysts could offer significant cost advantages over traditional precious-metal catalysts through economies of scale. The neutral pH and low temperature of operation represent further advantages (Bullen et al., 2006; Shukla et al., 2004).

Bio-fuel cells can be classified according to the biocatalyst. Systems using specific isolated enzymes for at least part of their operation are known as enzymatic fuel cells (EFCs), while those utilizing whole organisms containing complete enzyme pathways are know as microbial fuel cells (MFC). The micro-organism is either a specific isolated species or a mixed culture, which can be applied directly on the electrodes or used in a suspension. Alternatively, the system may be inoculated with a mixed culture in a nutrient solution under specific conditions that will allow it to form a biofilm on the electrode (Mohan et al., 2008). Many authors instead categorize BFCs according to the nature of the electron transfer (ET). Micro-organisms can either transfer electrons directly (direct physical contact with the electrode) or *via* mediators. These processes are termed, respectively, direct electron transfer (DET) and mediated electron transfer (MET). The definitions of these terms can, however, differ (Bullen et al., 2006). Systems utilizing non-diffusive mediators that are used to attach enzymes on electrodes, or those utilizing both carbon nano-tubes and redox polymers, for instance, can be considered both direct and mediated. This grouping will not be adopted here; rather, discussion will be divided according to the methods and purposes.

In MFCs, the organisms are able to regenerate the required enzymes as part of their natural functioning (Kim et al., 2007a,b), offering an advantage over EFCs, which, on the other hand, have a faster response time owing to the simpler chemical pathways. In a companion review (Part I), the operating principles and applications of bio-fuel cells were described and developments in enzymatic fuel cells were reviewed. In the present review, developments in MFC technology are reviewed and the current challenges involved in developing practical bio-fuel cell systems are described.

2. Microbial fuel cells

A summary of the key developments in microbial fuel cells is presented in Table 1. They are discussed in detail below.

2.1. Exoelectrogenesis

The use of whole cells for the biocatalysis of fuels is advantageous since it eliminates the need for enzyme isolation and allows multiple enzymes (and hence multiple fuels) to function together in conditions close to their natural environment. The working principle of MFCs is to force the microbes to shift from aerobic respiration to an aerobic respiration, in which the electrons produced during oxidation of the fuel are donated by some means to the electrode (electrode respiration or exoelectrogenesis (Logan, 2009)). The effect of O_2 (a natural electron acceptor) diffusion to the anode is known to lower the coulombic efficiency and several reports have noted a corresponding decrease in the power output. A more recent study on the effect of O_2 presence in the anode compartment (Oh et al., 2009) concluded that the dissolved O_2 level does not affect the power output since O_2 is scavenged by aerobic digestion. During this process, however, bacterial activity primarily takes the form of aerobic respiration of the substrate, and the voltage and power recover only after the O_2 concentration falls below a critical level. Other methods of maintaining anaerobic conditions include the use of O_2 chemical scavengers such as cysteine (Logan et al., 2005).

Forcing anoxic conditions in the anode compartment does not necessitate that the bacterium will take the respiration chemical pathway, while donating the electrons to the electrode. Bacteria will undergo the process that maximizes their energy gain, which is proportional to the potential difference between the oxidation reaction and the terminal electron acceptor. If the anodic potential is too low, organisms will switch to fermentation, which can extract only one-third of the electrons available in the substrate (Rabaey and Verstraete, 2005). One recent report comparing different fuels concluded that non-fermentable substrates (*e.g.* acetate) have higher coulombic and energy efficiencies compared to fermentable substrates such as glucose (Sool Lee et al., 2008). Hence, a careful balance of the anode potential is required; it must high enough that organisms do not switch to fermentation, yet sufficiently low to maintain a high cell voltage and power output.

Several studies have investigated the effect of the anode potential on bacterial growth and power production (Oh et al., 2009; Aelterman et al., 2008; Cheng et al., 2008). At high anode potentials (by-poising), bacterial growth is encouraged, the startup time is reduced, and the overall current is reduced (Aelterman et al., 2008). It has been argued, however, that there is a critical potential beyond which bacteria can no longer generate significantly more electrons due to the shortage of suitable electron acceptors (Cheng et al., 2008).

The microbial cultures in fuel cells can either be suspended in the anode solution or immobilized on the electrode surface. It has been reported that the immobilization of *P. vulgaris* on graphite felt electrodes by either culturing the bacteria on the anode or chemically linking them *via* amide bonds decreases the response time of a system to fuel addition (Allen and Bennetto, 1993). Having the biocatalyst in solution limits the operation of the system to batch-mode where fuel quantities are added at different intervals, unless the mediator is regularly replenished, increasing the cost of the system. A comparison of this operating mode with continuous-flow operation showed that the power output and efficiency were lower (Allen and Bennetto, 1993). In continuous-feed systems, biofilm forming species are preferred since they can either use the electrode directly (through physical contact) or transfer electrons through the biofilm *via* mobile mediators (Rabaey and Verstraete, 2005). Batch-mode operation, on the other hand, offers the advantage of greater mediator influence (Rabaey et al., 2005b), particularly when mediator producing bacteria are used; this promotes accumulation of the mediators in the anodic compartment (Rabaey and Verstraete, 2005).

Clauwaert et al. (2007) constructed an MFC using the effluent of a used MFC as inoculum for a graphite granule anode. The power density in batch operation (83 $\mu W\,cm^{-3}$) was higher than in continuous operation (65 $\mu W\,cm^{-3}$), yet the coulombic efficiency (CE) was much lower (20–40% compared to 90%).

2.2. Electron transport

One of the most difficult aspects of microbial fuel cell development is tapping into the intracellular electron transport system and diverting the generated electrons from their natural electron acceptors outside the cell to the anode. The ET can be achieved either through the use of artificial or natural (produced by the bacterium) mediators or by direct contact with the electrode *via* membrane associated cytochromes. Direct contact through "nanowires" or pili produced by the bacteria has recently been attempted (Logan, 2009, and references there in). This method was established in *Geobacter sulfurreducens*, where the deletion of the gene responsible for pili production stopped the current generation (Richter et al., 2008).

When mediators are used as electron shuttles, they are required to: (i) have fast kinetics for both oxidation at the anode and reduction inside the organism; (ii) easily penetrate the cell membrane; (iii) be chemically stable and not interfere with other metabolic

Table 1
Summary of key microbial fuel cell developments.

Anode	Cathode	Electrolytes, membrane	P_{max} (mW cm^{-2}) (mW cm^{-3})	V or j at P_{max}	OCV (V)	Remarks	Reference
Graphite rod (5 mm diameter), graphite granules (1.5–5 mm diameter) inoculated with aerobic/anaerobic sludge mixture	Same graphite rod/granules as anode	Anolyte: 0.75^{-1} gL^{-1} acetate Catholyte: 50 mM $K_3Fe(CN)_3$, 100 mM KH_2PO_4 buffer, 1 M NaOH, 7 pH, room temperature. Ultrex membrane	0.263 mW cm^{-3} (six parallel cells), 0.308 mW cm^{-3} (series)	0.35 V (parallel), 2.28 V (series)	0.67 (parallel), 4.16 (series)	QE = 77.8% and 12.4% for parallel and series, respectively. Figures based on void volume fraction in cell. Maximum power occurs after 200 days of operation	Aelterman et al. (2006)
C-cloth (7 cm^2) inoculated with domestic wastewater (7.3–7.6 pH, 200–300 mgL^{-1} COD)	Pt/C-cloth (7 cm^2), with four PTFE diffusion layers on air side	Per liter: (5 mg glucose, PBS: 0.31 g NH_4Cl, 4.97 g $NaH_2PO_4H_2O$, 2.75 g $Na_2HPO_4H_2O$, 0.13 g KCl), and 12.5 mL each of metal and vitamin solution, 30 °C	0.0766 mW cm^{-3}	–	0.3	CE = 20–27%	Cheng et al. (2006b)
Granular graphite inside tube, with previous MFC effluent as inoculum	Graphite felt biocathode on outside of tube	Electrolytes (per liter): (4.4 g KH_2PO_4, 3.4 g K_2HPO_4, 2 g $NaHCO_3$, 0.5 g NaCl, 0.2 g $MgSO_4{\cdot}7H_2O$, 0.0146 g $CaCl_2$) circulated with 2 g L^{-1} of sodium acetate re-added to anodic circuit upon depletion. Ultrex membrane on inner tube surface	0.083 mW cm^{-3} (batch), 0.065 mW cm^{-3} (continuous)	0.34 V (continuous)	–	CE = 20–40% (batch), 90% (continuous)	Clauwaert et al. (2007)
Carbon cloth (1 cm^2), inoculated with pre-acclimated mixed culture from previous MFC	Two air-breathing: Pt on carbon cloth (7 cm^2 each) with PTFE layers	200 mM PBS, with 30 mM acetate and per liter: (0.31 g NH_4Cl, 0.13 g KCl, 5.84 g $NaH_2PO_4{\cdot}H_2O$, 15.5 g $Na_2HPO_4{\cdot}7H_2O$. And 12.5 mL of minerals and vitamin) in batch operation mode	0.686 mW cm^{-2} (anode area), 0.098 mW m^{-2} (reactor cross-section)	2.62 mA cm^{-2} (anodic)	0.7–0.8		Fan et al. (2008)
Either: (i) plain porous carbon paper (22.5 cm^2) or (ii) iron-oxide coated. Both inoculated with anaerobic sewage sludge or (iii) plain carbon paper with anode biofilm from previous MFC applied	Pt	Anolyte: 7 pH, buffer (per liter): 0.31 g NH_4Cl, 0.13 g KCl, 2.69 g $NaH_2PO_4{\cdot}H_2O$, 4.33 g Na_2HPO_4 and acetate. Stirred. Catholyte: 50 mM PBS, 7 pH, air sparged. Nafion separator. 30 °C	(i) 0.8×10^{-3} mW cm^{-2}, (ii) 3×10^{-3} mW cm^{-2}, (iii) 4×10^{-3} mW cm^{-2}	(iii) 0.2 V	–	CE = (i) 40% and (ii) 80%.	Kim et al. (2005)
Carbon cloth (757 cm^2 total surface area), inoculated with wastewater in presence of nutrients and acetate	Pt on Carbon cloth (161 cm^2 total surface area) with 4 diffusion layers on the side open to air chamber	Nutrient solution with 800 mg L^{-1} acetate in batch-mode. Membrane-less	0.016 mW m^{-3}, 0.052 mW cm^{-2}	0.18 mA cm^{-2}	–	CE = 38–52%. Power increases to 0.022 mW cm^{-3} (0.069 mW cm^{-2}) with continuous-flow mode. Purpose to show higher power output in scaled-up cell when conditions of higher electrode area to reactor volume and shorter inter-electrode distance are satisfied	Liu et al. (2008)

Table 1 (*Continued*)

Anode	Cathode	Electrolytes, membrane	P_{max} (mW cm^{-2}) (mW cm^{-3})	V or j at P_{max}	OCV (V)	Remarks	Reference
Either: (i) Graphite fiber brush (9600 m^2/m^3 reactor volume), or (ii) same brush electrode (4200 m^2/m^3 reactor volume). Both inoculated using pre-acclimated bacteria from previous MFC	Air-breathing. (i) Cobalt tetramethylphenylporphyric or (ii) Pt. Both on carbon paper with four diffusion layers	Batch-fed: 50 mM PBS, and (per liter): 4.09 g Na_2HPO_4, 2.93 g $NaH_2PO_4{\cdot}H_2O$, and 1 g of either (i) acetate, 30 °C or (ii) glucose, 23 °C.	(i) 0.24 mW cm^{-2}, 0.073 mW cm^{-3} and (ii) 0.143 mW cm^{-2}, 2.3×10^{-3} mW cm^{-3}	(i) 0.82 mA cm^{-2}	(i) 0.57	CE = (i) 40–60% and (ii)23%. Power densities normalized by cathode area and liquid volume	Logan et al. (2007)
Geobacter sulfurreducens PCA. Carbon cloth (0.806 cm^2)	Air-breathing Pt on CF electrode (6.45 cm^2)	10 mM acetate, circulated. Nafion separator	0.19 mW cm^{-2}, 0.043 mW cm^{-3}	0.46 mA cm^{-2}		When anode volume chamber volume decreased from 7 to 0.336 mL volumetric power density increased to 2.15 kW m^{-3}.	Nevin et al. (2008)
Hasenula anomala (yeast) adsorbed on either (i) graphite felt, or (ii) Polymer-Pt composite coated graphite	Graphite	Anolyte: PBS with nutrient broth, Catholyte: 0.1 M ferricyanide. Nafion separator	(i) 2.34×10^{-3} mW cm^{-3} and (ii) 2.9×10^{-3} mW cm^{-3}	–	–	–	Prasad et al. (2007)
Pseudomonas aeruginosa on rough graphite plate anodes (30 cm^2)	–	Anolyte: glucose, 0.5 g L^{-1} day^{-1}. Catholyte: 100 mM PBS, 100 mM potassium hexacyanoferrate, aerated at minimum of 6 mg L^{-1}	0.167×10^{-3} mW cm^{-2}	–	–	No mediator addition. Bacterial strain produces pyocyanin mediator that can also be used by other organisms for electron mediation, enhancing the performance of mixed cultures when present	Rabaey et al. (2005a,b)
Shewanella oneidensis in solution with graphite felt electrode (2 cm^2, 1.2 cm^3 compartment volume)	Graphite felt electrode (2 cm^2, 1.2 cm^3 compartment volume)	Anolyte: (i) Suspended *S. oneidensis* with 10–30 mM sodium lactate, optionally with: (ii) saturated O_2 content of influent, (iii) 100 M AQDS mediator, (iv) both O_2 and mediator. Catholyte: 7.4 PBS, 50 mM ferricyanide. Nafion membrane	(i) 0.3 mW cm^{-2}, 0.5 mW cm^{-2} (ii) 0.2 mW cm^{-2}, 0.333 mW cm^{-3} (iii) 0.4 mW cm^{-2}, 0.666 mW cm^{-3}, (iv) 0.27 mW cm^{-2}, 0.45 mW cm^{-3}	(i) 0.6 mA cm^{-2} (ii) 0.4 mA cm^{-2} (iii) 1 mA cm^{-2} (iv) 0.7 mA cm^{-2}	(i) 0.75, (ii) 0.7, (iii) 0.7, (iv) 0.8	CE = (ii) 3–5.5%. SCC = (i) 1 mA cm^{-2}, (ii) 0.6 mA cm^{-2}, (iii) 1.79 mA cm^{-2}, (iv) 1.2 mA cm^{-2}	Ringeisen et al. (2007)
Glassy carbon (10 cm^2), mixed culture from compost	Suspended *Trametes versicolor* laccase	Anolyte: 10 mM of glucose and lactate. Catholyte: 0.1 M acetate buffer, 2 mM ABT, 5 pH, air saturated. 100 mM NaCl salt bridge	4.6×10^{-3} mW cm^{-2}	0.5 V	1.1	Low power density due to cell design. Immobilizing laccase in hydrogel in the absence of mediator produces little power. No change in power after 2 days of operation	Schaetzle et al. (2009)
Carbon felt, inoculated with mixed bacterial culture	Pt on carbon cloth (57 cm^2) with four PTFE diffusion layer. Open to air chamber	Per liter: (0.1 g KCl, 0.2 g NH_4Cl, 0.6 g NaH_2PO_4) and fed with 20 mL of model organic waste containing starch, Bacto peptone and fish extract at 3:1:1 ratio.	0.13 mW cm^{-3} (12 series cells), 0.09 mW cm^{-2}		0.56	CE = 28–48%. Treatment efficiency of 93% at organic loading rate of 5.8 g L^{-1} per day	Shimoyama et al. (2008)

Graphite fiber brush (2235 cm^2 surface), *Rhodopseudomonas palustris* DX-1 biofilm	Air-breathing, Pt on carbon paper with four PTFE diffusion layers	200 mM PBS, 1 g L^{-1} acetate, 23 °C	0.272 mW cm^{-2}, 0.087 mW cm^{-3}	0.99 mA cm^{-2}	0.56	Power density based on cross-sectional area of anode. Under dark conditions, power density slightly less (0.272 mW cm^{-2}). Electron transfer was not through self-produced mediators, probably by direct communication with electrode. CE = 40–60%	Xing et al. (2008)
CF brush, inoculated with pre-acclimated mixed culture from MFC	Air-breathing, Pt on carbon cloth with four PTFE diffusion layers	50 mM PBS with minerals, vitamin and acetate (1 g L^{-1}), 23 °C. Anion-exchange membrane placed against cathode and supported with a stainless steel mesh	0.046 mW cm^{-3}	0.34 mA cm^{-2}	0.24	Anion-exchange membrane significantly improves electrical performance by reducing the large pH gradients, and lowering internal resistance. CE 1g 90% for current densities greater than 0.2 mA cm^{-2}. Using two cathode/anion permeable membranes increases power density to 0.098 mW cm^{-3}	Zhang et al. (2009)

pathways; (iv) not adsorb on the bacteria or anode, and (v) have a potential that matches that of the reductive metabolite (Shukla et al., 2004).

Different types of mediators, such as thionine, quinone, phenazines, Fe(III) ethylenediaminetetraacetic acid (EDTA), methylene blue, and neutral red (NR), have been used in MFCs. The redox mediators can be immobilized on the anode. In the work by Park and Zeikus (2003), the authors compared the electrical performance of two cell designs: the first with a soluble NR mediator and a woven graphite electrode and the second having covalently-linked NR on a woven graphite anode. The current in the cell containing an immobilized mediator was a factor of three higher than the current in the cell using soluble NR. Similar results were obtained when a Mn^{4+} mediator was incorporated into the anode by coordination bonding to the silica content of the graphite. On the cathode side, Fe^{3+} was incorporated into the graphite electrode following the procedure used for Mn^{4+} in the anode. The inner surface of the cathode was coated with a 1 mm thick proton permeable layer of porcelain. Electrons reaching the cathode from the external circuit reduce the Fe(III) to Fe(II), which in turn is oxidized to Fe(III) by O_2. Operating on a bacterial culture from a sewage sludge, and using glucose as the substrate, the fuel cell with the Mn^{4+} anode achieved a power density of 78.7 $\mu W\,cm^{-2}$ based on the theoretical surface area of the graphite felt. Graphite felt was chosen over simple graphite plates due to its higher surface area, though materials with small pore sizes usually raise concerns when used as anodes in MFCs since bacterial attachment and growth may cause blockage, leaving the active sites inaccessible to the substrate.

An alternative to using artificial mediators was made possible after the discovery that some species, *e.g. Clostridium butyricum* (Park et al., 2001) and *Pseudomonas aeruginosa* (Rabaey et al., 2005a), produce their own mediators. The latter species is known to produce phenazine derivatives that are capable of mediating ET from the bacterium to the electrode. An MFC developed by Rabaey et al. (2004) using this species was capable of achieving a CE of 83% without the need for artificial mediators. The use of these species is not restricted to the originating micro-organism; their presence in mixed cultures, or with other species not capable of DET, may enhance the electron transfer capabilities of other bacterial species (Xing et al., 2008).

Perhaps more practical bacterial species with enhanced ET capabilities are the metal reducing bacterium, namely *Rhodoferax ferrireducens* (Chaudhuri and Lovley, 2003), *Geobacter sulfurreducens* species (Bond and Lovley, 2003; Richter et al., 2008) and *Shewanella oneidensis* (Ringeisen et al., 2007). The direct electronic communication abilities of these species with the electrode is due to the presence of enzymes on their outer membrane that can transfer the electrons directly to the anode.

Ringeisen et al. (2007) used *Shewanella oneidensis* with a ferricyanide cathode to demonstrate the ability of this species to generate power in the absence of a mediator and in the presence of O_2. Power densities of 0.2 $mW\,cm^{-2}$ and 0.33 $mW\,cm^{-3}$ were achieved, though these could be doubled in the absence of O_2 or with the addition of a mediator. Nevin et al. (2008) used *Geobacter sulfurreducens* PCA on a carbon cloth in an acetate solution along with an air-breathing Pt cathode to construct a two-chamber fuel cell. The power densities were 0.19 $mW\,cm^{-2}$ and 0.043 $mW\,cm^{-3}$ when the anode chamber volume was 7 mL.

Direct ET through membrane bound enzymes has also been demonstrated for *Hasenula anomala*, a eukaryotic yeast cell (Prasad et al., 2007), in a two-chamber mediatorless MFC with the microorganism immobilized by physical adsorption. In this work, a maximum power density of 2.9 $\mu W\,cm^{-3}$ was obtained with a polyaniline-Pt coated graphite anode, using ferricyanide in the catholyte.

Xing et al. (2008) used a strain of *Rhodopseudomonas palustris*, a species that has previously been used for hydrogen production, to construct a fuel cell that was capable of achieving a maximum power density of 0.272 $mW\,cm^{-2}$ (at 0.99 $mA\,cm^{-2}$) in light conditions and 0.264 $mW\,cm^{-2}$ in dark conditions, with respective coulombic efficiencies of 50% and 60%. The electrodes consisted of a graphite brush anode with a 30% wet-proofed carbon cloth/Pt cathode (7 cm^2) of four diffusion layers. Acetate (1 $g\,L^{-1}$) was used as the electron donor in a phosphate buffer solution. The electrical performance was higher than that with a mixed culture using the same system (Xing et al., 2008).

2.3. Biocatalyst source

The selection of the biocatalyst source and enrichment of the biocatalyst are important for optimising the performance of MFCs. The dominant opinion until recently was that pure cultures are better suited to the study of specific organisms (and their electrochemical performance) than they are to maximizing power generation. Mixed cultures, in contrast, are better suited for practical applications, especially when mixed fuels are used, as in wastewater treatment applications (Kim et al., 2007a). Recently, however, power densities from certain pure cultures are now comparable to those obtained from the use of mixed cultures (Ringeisen et al., 2007; Xing et al., 2008).

It has been observed that the bacterial population in the anodic biofilm changes during operation (Kim et al., 2007a, and references there in), with the domination of specific classes such as *Geobacter* (Nevin et al., 2008). Aelterman et al. (2006) studied culture composition at different times during the operation of a MFC. After an initial period of stabilization, species from the *Proteobacteria* (*e.g. Geobacter*, *Shewanella*, and *Pseudomonas*) were dominant, while at maximum power generation, members of the *Bacilli* class (*e.g. Clostridium*) were dominant. The change in culture composition was also accompanied by a decrease in the internal resistance (Aelterman et al., 2006). Different sources of mixed bacterial cultures have been used as inoculums in MFCs with the most common being anaerobic sewage sludge (Aelterman et al., 2006; Kim et al., 2005; Liu et al., 2008), or bacterial cultures obtained from used MFCs (Clauwaert et al., 2007; Fan et al., 2008; Logan et al., 2007; Zhang et al., 2009). Other sources such as soil and garden compost have also been investigated (Schaetzle et al., 2009).

The question of whether microbial communities will evolve and selectively adapt to a MFC environment gave rise to a study by Kim et al. (2005), where the effects of different inoculation techniques on the performance of a two-chamber MFC were investigated. Fig. 1 shows selected results from this study. Inocula were sourced from an anaerobic sewage sludge that was filtered and added to acetate for use as an enrichment medium, which was then replaced with a nutrient buffer for use in different settings. The performance of cells using these enriched inocula were compared to the performance of a controlled MFC with CP electrodes inoculated with the untreated sludge (the latter cell yielded a maximum power density 0.4 $\mu W\,cm^{-2}$). A large proportion of the microorganisms in anaerobic sludge is believed to be methanogens, which lead to undesirable methane formation reactions that consume the substrate with no electricity generation, thus lowering the CE. Addition of 2-bromoethanesulfonate (BES), an inhibitor of methanogenic activity, was found to significantly increase the CE from 40% in the absence of BES to 70% with a correspondingly large reduction in the concentration of methane from 40 to 2%. It has recently been demonstrated that BES, which is a mild irritant to the skin, eyes and respiratory system, can inhibit the bioactivity of methanogens even at very low doses of 0.1–0.27 mM, while having no effect on exoelectrogens (Chae et al., 2010). The authors of this report conducted batch-cycle experiments, discov-

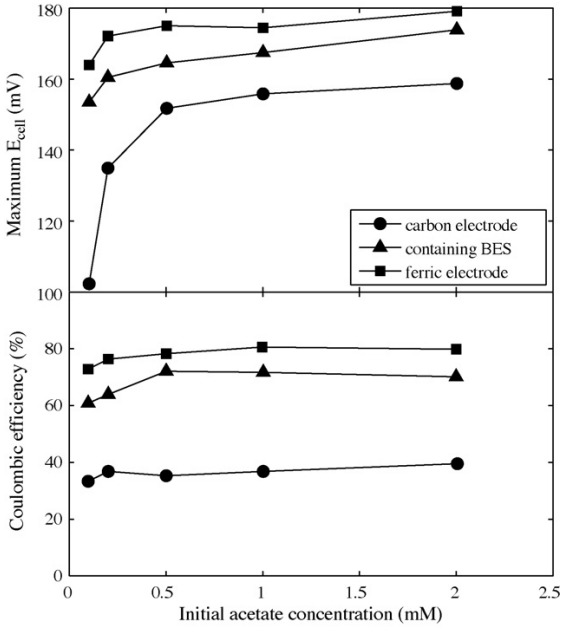

Fig. 1. The effect of initial acetate concentration on the maximum voltage and CE in MFCs using a carbon electrode (●), a carbon electrode that contains BES only during the initial stage of enrichment of the microbial culture on wastewater (△), and a ferric electrode (■) (Kim et al., 2005). Estimates of the errors were not provided by the authors.

ering that methane production was inhibited for several cycles after a single injection of BES, suggesting that it need only be injected intermittently.

In another experiment, to promote the activity of iron-reducing bacteria that are known to be capable of both direct ET and growth in the presence of acetate, Kim et al. employed an iron-oxide coated carbon paper anode. This was found to increase the power density and CE to 3 $\mu W\,cm^{-2}$ and 80%, respectively. These increases were accompanied by a faster response to substrate addition, indicating a direct ET between the iron-reducing bacteria and the electrode. Iron-reducing bacteria selectively attached to the electrode and preferentially (over methanogenic bacteria) reacted with the acetate. To further exploit the improved performance brought about by iron-reducing bacteria, their concentration was increased by successively enriching the inoculum in ferric citrate and acetate solution. This serial enrichment actually caused a negative effect on the performance and an MFC with the pre-enriched iron-reducing bacteria yielded only 0.2 $\mu W\,cm^{-2}$. The best performance was achieved with a biofilm scraped from the anode of a functioning MFC and applied to the new anode (4 $\mu W\,cm^{-2}$). None of these different techniques were found to have any effect on the startup time. While the study was useful in comparing different inoculation techniques, the power densities obtained were low, possibly due to the high internal resistance of the design.

2.4. Anode materials

Careful selection of anode materials is important due to its effect on both the microbial attachment and the ET (Watanabe, 2008). Carbon or graphite based materials are frequently selected for anodes due to their large surface area, high conductivity, biocompatibility and chemical stability (Logan et al., 2006). A recent report has demonstrated that gold, though impractical form a commerical perspective, could potentially be used as an anode with *Geobacter sulfurreducens*, yielding a performance similar to that with graphite (Richter et al., 2008). A successful coupling of a bare gold electrode with *Shewanella putrefaciens* was only achieved by modifying the electrode with an alkanethiol self-assembled monolayer having a carboxylic acid functional head group (Crittenden et al., 2006), as a result of strong hydrogen bonding between the carboxylic acid groups and the cytochromes in the bacteria. This covalent linking functioned as an electrical connection between the bacteria and the electrode, and the modified electrode produced significantly higher currents than with glassy carbon. The influence of chain length and of other functional groups was also investigated. When five methylene units were added to the self-assembled monolayer, the current output was reduced, while the use of a methyl group yielded no current at all.

In another report, the anode was modified to immobilize a derivative of the anthraquinone-1,6-disulfonic acid (AQDS) mediator (Adachi et al., 2008) (adsorption of AQDS, as well as 1,4-naphthoquinone (NQ), on graphite to construct bio-fuel cell anodes was previously explored by Lowy et al. (2006)). Polyethyleneimine was used to bind the mediator and *Geobacter sulfurreducens* to a graphite electrode. The lifetime of this anode was reported to be more than four months (without decomposition or decrease in the current).

Numerous reports have investigated the modification of anodes with conductive polymers, mainly the organic polyanilines (Watanabe, 2008, and references therin). This type of modification increases the current density, though it is also susceptible to microbial attack and degradation (Watanabe, 2008).

2.5. O_2 reduction

The complementary reduction reaction occurring at the cathode is usually achieved with O_2 as the electron acceptor. Alternative electron acceptors are hexacyanoferrate (Aelterman et al., 2006; Pham et al., 2008), ferricyanide (Ringeisen et al., 2006, 2007), permanganate (You et al., 2006) and H_2O_2. Fuel cells using these compounds show significantly improved performance compared to O_2 based systems, as a consequence of the lower reduction potential and increased ionic strength. Due to their inherently slow oxidation kinetics, however, they need to be regenerated continually (Logan et al., 2006; Chae et al., 2008). Although ferricyanide has been employed as a mediator in conjunction with O_2 as an electron acceptor in an enzymatic fuel cell (Kim et al., 2009), it is doubtful that the ferricyanide functions only as a mediator, given its superior reduction kinetics compared to O_2.

The reduction of O_2 on non-catalyzed carbon based surfaces is very inefficient, occurring at an overpotential of almost 1 V below the formal reduction potential (Freguia et al., 2010). In addition to enhancing the reaction kinetics, catalysts such as platinum also decrease the critical O_2 concentration (concentration below which the reaction ceases), thus preventing O_2 diffusion to the anode (Pham et al., 2004). The relatively well developed knowledge of O_2 reduction on platinum has been successfully applied to improve the operation of low temperature polymer electrolyte membrane fuel cells (PEMFCs), which typically operate at temperatures below 100 °C.

The high cost of platinum and the possibility of poisoning by species such as CO (He and Angenent, 2006) have motivated a search for alternative O_2 reduction catalysts that can function under physiological conditions and yield a similar level of performance. Cheng et al. (2006a) investigated the performance of a single-chamber air-breathing MFC using either cobalt tetramethylphenylporphyrin (CoTMPP) or Pt. Using carbon cloth electrodes of (7 cm^2 projected area) and a Pt loading of 0.5 mg cm^{-2}, the cell produced a maximum power density of 480 mW cm^{-2}. Replacing the Pt cathode with 0.6 mg cm^{-2} CoTMPP/Nafion binder

produced similar potentials but the power was reduced by 12%, with little loss in activity over 25 cycles. Comparing the CoTMPP cell to a cell with either a lower Pt loading of 0.1 mg cm^{-2} or one using PTFE binder, demonstrated consistently higher power densities.

Enzymes or whole micro-organisms could provide cost-effective and sustainable biocatalysts for O_2 reduction. A review of biocathode development up to 2006 was provided by He and Angenent (2006). Schaetzle et al. (2009) implemented a bio-fuel cell using a mixed culture from soil/garden compost on a glassy carbon anode, along with laccase in a hydrogel applied at a platinum cathode with soluble 2,2′-azinobis-(3-ethylbenzothiazoline-6-sulfonate) (ABTS) as a mediator. Compared to the performance using a virgin platinum electrode, the enzyme cathode led to increases in the power density and OCV from 0.46 μW cm^{-2} (at 0.2 V) and 0.6 V to 4.63 μW cm^{-2} (at 0.5 V) and 1.1 V, respectively. It must be pointed out that laccase applied as a hydrogel on a platinum cathode will be permeable to both the mediator and to O^{-2}, making it difficult to isolate the effect of the platinum from that of the enzyme in the performance figures.

Recently, whole micro-organisms that can use the cathode as an electron donor have been investigated for use in MFCs. Clauwaert et al. (2007) combined the anode of a tubular MFC with a new mixed culture, open-air, graphite felt cathode. Under continuous-feed operation, the 0.183 L MFC generated a volumetric power density of 65 μW cm^{-3} at 0.344 V with a CE of 90%. Under batch-fed mode the power density was 28% higher but the CE ranged between 20% and 40%. The application of a layer of manganese oxide on the cathode was observed to lower the startup time by 30% without affecting the steady-state performance. In the absence of ammonium or nitrate, the cell was operated for 7 months. Similar improvements in MFC performance and reductions in the internal resistance were also observed by Chen et al. (2008).

2.6. Reactor design

Different design concepts and configurations have been developed to optimise the arrangement of the three basic components, anode, cathode and separator, in a functioning system (Zhang et al., 2009; Fan et al., 2007a). Four different categories can be identified (Watanabe, 2008):

1. the classic two-chamber setup where both the anode and cathode are placed in liquid electrolytes separated by an ion exchange membrane;
2. a single-chamber air-breathing MFC with the anode placed in the electrolyte and the cathode unit (with or without a separator) placed between open-air and the anolyte (Park and Zeikus, 2003; Liu and Logan, 2004; Cheng et al., 2006b; Logan et al., 2007);
3. a single-chamber MFC where all three components are arranged into a single unit similar to the membrane electrode assembly (MEA) of PEMFC (Fan et al., 2007a);
4. a cassette-electrode arrangement where two MEAs are arranged to have a common aerated chamber on the inside and are exposed to a common anolyte on the outside (Shimoyama et al., 2008).

An air-breathing cathode is desirable since it eliminates the need for an aerated catholyte, thus simplifying the system design, as well as reducing costs and energy requirements. Such a system was first developed by Park and Zeikus (2003), using mediator-immobilized graphite electrodes. A 1 mm proton-conducting porcelain layer was applied to the inside of the cathode, which was impermeable to the liquid anolyte. This design was found to produce a maximum power density (0.0788 mW cm^{-2}) which is similar to that of a more complex two-chamber configuration.

The effect of a proton exchange membrane was later investigated by Liu and Logan (2004), who found that removing the PEM (and slightly reducing the Pt loading) increased the power density by 88% when using glucose as a substrate and by 420% when using wastewater. The CE, however, was significantly reduced as a consequence of increased O^{-2} diffusion to the anode. It is now believed that using an air-breathing cathode without a PEM increases the power output. The removal of the PEM causes a reduction in the internal resistance of the system, although care should be taken with microbial biofilm formation on the cathode (Liu and Logan, 2004).

Condensation in an air-breathing cathode leads to a two-phase flow. Cheng et al. (2006b) found that the addition of hydrophobic layers on the air side of the cathode mitigated flooding of the catalyst layer. At the same time, the CE was increased through a reduction in the rate of O^{-2} diffusion to the anode. Additional layers of hydrophobic PTFE will continue to increase the CE, though it is not desirable to reduce the O^{-2} diffusion beyond the limit of the reaction requirements. Cheng et al. (2006b) found the optimum number of PTFE layers (applied to a carbon cloth) to be four. The power density in this case was increased by more than 40% (0.0766 mW cm^{-2}) and the CE increased from ~15% to more than 20% compared to a cathode without PTFE layers.

It has recently been suggested that internal resistance due to restricted proton-transport is the dominant limiting factor in most MFC designs (Watanabe, 2008; Kim et al., 2007a; He et al., 2006; Eun Oh and Logan, 2006), though some disagreement exists over the exact source of this resistance. Watanabe (2008) reasoned that since proton diffusion is always slower than ET in the external circuit, proton-transport limitations dominate kinetic and reactant-transport limitations. While proton-transport limitations are often disregarded on the basis that MFCs use the same PEM as chemical fuel cells but with current densities a few orders of magnitude lower (Kim et al., 2007a), new evidence suggests that a comparison to PEMFCs is not valid due to differences in the pH and electrolyte composition (Kim et al., 2007a; Fan et al., 2007b). In MFCs, there is a much higher concentration of cations (other than protons) that hinder proton diffusion through the membrane. The presence of these cations results in an increased pH in the catholyte and a decreased pH in the anolyte, which affects the solution conductivity and the overall cell performance (Rozendal et al., 2006) (restricted proton migration through the membrane decreases the pH in the anode solution, while simultaneously increasing the pH in the cathode solution, where protons are continuously consumed by oxygen reduction). Subsequent studies have suggested that anion-exchange and bipolar membranes have better characteristics than cation exchange membranes in terms of pH management and electrical performance (Zhang et al., 2009; Kim et al., 2007b; Rozendal et al., 2008).

One of the practical difficulties faced in MFC design is the increased internal resistance with scale-up. Increasing the surface area increases the power output only when the system is not limited by a high internal resistance (Logan et al., 2007). Several early reports showed that increasing the reactor volume decreases the power density (Clauwaert et al., 2007; Fan et al., 2007a), even when the inter-electrode gap is kept constant. In contrast, Liu et al. (2008) recently found that a high ratio of electrode area to reactor volume and a simultaneous decrease in the inter-electrode gap when scaling up a reactor from 28 to 520 mL increased the power density.

Logan et al. (2007) designed a new graphite brush anode by winding graphite fibers around a central conductive, non-corrosive metal rod. The 2.5 cm diameter × 2.5 cm length anode (specific area 9600 m^{-1}) was used with an air-breathing carbon paper cathode containing 40% CoTMPP catalyst in a cube-design MFC. The design achieved power densities of 0.24 mW cm^{-2} (based on the projected

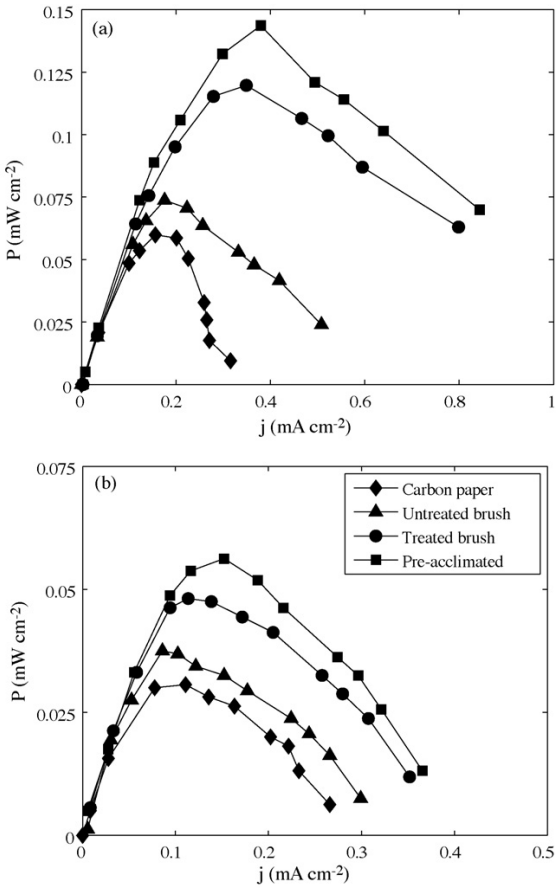

Fig. 2. Power density curves for bottle-MFCs in (A) 200 mM PBS and (B) 50 mM PBS (Logan et al., 2007). Estimates of the errors were not provided by the authors.

cathode area) and 0.073 mW cm^{-3} (based on the liquid volume) with a maximum CE of 60%. The specific area of the graphite-bush anode is much higher than that of traditional graphite foam or cloth. The internal resistance of the graphite-bush fuel cell (R_{int} = 8 Ω) was lower than the equivalent resistance using a plain carbon paper electrode. Moreover, power production was not affected by biofilm growth. This anode design represents a promising concept that should, in principle, allow efficient scaling of MFCs with a wide scope for optimization (fiber density, length, and winds per unit length) (Logan et al., 2007). A second bottle-MFC using a different anode was also constructed. The effects of the different electrode preparation methods and the buffer concentration are shown in Fig. 2.

The total power output can be increased and shifted to a higher voltage and current when individual cells are connected in series or in parallel (Aelterman et al., 2006). With a series connection, however, voltage reversal in individual cells may occur, shifting the anode potential to positive values. This phenomenon is encountered when either high currents are drawn from the weaker cell with limited biocatalytic conversion performance, or during sudden changes in fuel demand, as occurs at startup (Kim et al., 2007a; Oh et al., 2009; Aelterman et al., 2006). The increased potential could be accompanied by O_2 evolution in the anode. The problem can be alleviated by avoiding low substrate conditions (*e.g.* batch-fed operation) (Logan, 2010), and by ensuring that all cultures are properly enriched before operating at a high current.

Microbial fuel cells that can harvest electricity from the organic matter in aquatic sediments have been developed by Reimers, Tender and co-workers (Tender et al., 2001; Reimers et al., 2002). These systems, termed Benthic Unattended Generators (BUGs), can be used to power electronic devices in romote locations. The anode is buried in the marine/freshwater sediment and is connected to a cathode that is suspended in the aerobic water. *Desulfuromonas* species are considered to be the predominant species on anodes submerged in marine sediments, while *Geobacter* dominate in freshwater (Lovley, 2006). In a more recent design, the anode is enclosed in a so-called benthic chamber buried in the sediment, which improves mass transport of pore water to the anode by advection, either naturally or through pumping, and leads to significantly higher power densities (Nielsen et al., 2007, 2008).

3. Challenges in the development of practical bio-fuel cells

Despite the rapid progress in bio-fuel cells, cost-effective, modular designs that can be handled safely (and are environmentally friendly) are still some way from being realised. Two promising applications for the near future are (domestic and industrial) wastewater treatment/electricity production (Feng et al., 2008; Katuri and Scott, 2010; Ahn and Logan, 2010), and providing power to marine instruments, such as a meteorological buoy, using BMFCs (Tender et al., 2008). Several of the critical challenges to be overcome in the development of MFC technology are listed below.

1. A step-change improvement in performance is required for many applications. This includes much higher power densities and energy efficiencies.
2. Electrode materials need to be more catalytic while maintaining their performance in the face of problems caused by fouling of the active surfaces, loss of enzyme activity, corrosion and other degradation mechanisms.
3. Cell construction needs to be improved to maximize the cell voltage by paying appropriate attention to electrode overpotentials and all cell resistances, including those arising in the positive and negative electrodes, the separator/membrane and the electrolytes.
4. Time dependent performance (and hence energy density) must be studied over practical periods (<1000 h) due to long-term changes in the enzyme activity, electrode fouling, membrane blockage, the build-up of metabolites and the breakdown of products. Sludge production can block flow paths as well as foul electrodes and membranes.
5. Many investigations have naturally involved small, laboratory-scale units cells. The importance of the reaction environment and of scale-up necessitate studies of (i) the fluid flow and active species transport/mass transfer, (ii) the bio-electrochemical reaction kinetics and (iii) the distributions of the current density, charge and reactant concentrations (including that of dissolved O_2). Fractional conversion in larger, multi-plate (*e.g.* bipolar) cell stacks is also of importance. Cells with chemistries that allow single-compartment operation and possess constructional simplicity would be highly advantageous.
6. A crucial aspect of bio-fuel cell development is the immobilization of the enzyme/mediator on the electrode. Maintaining a continuous supply of fuel to the active sites and ensuring an efficient electron transfer process from the enzyme/bacteria to the electrode *via* the mediator are crucial. The development of new techniques for immobilization, including on nano-structures substrates, could provide significant improvements in both performance and stability. These techniques must be both practical and cost-effective.

7. It is important that mathematical models are developed to reduce the burden on laboratory-based design, testing and characterization. At the cell level, models must be able to capture the distributions of charge, potentials and concentrations as well as global information such as the cell voltage, as in PEM fuel cell modelling (Shah et al., 2007; Shah and Walsh, 2008; Shah et al., 2009). In many cases, particularly for *in situ* operation, local information can only be gained from detailed and rigorously-validated models. Although a small number of models have been developed for specific systems Bartlett and Pratt (1995), Kano and Ikeda (2000), Ikeda and Kano (2001), Gallaway and Barton (2008), Calabrese-Barton (2005), Kjeang et al. (2006), Zeng et al. (2010), Marcus et al. (2007), Picioreanu et al. (2007, 2010), with the exception Picioreanu et al. (2010) they are highly simplified and neglect crucial features such as transient performance, spatial non-uniformities, conductive losses, potential profiles, ion migration, fluid flow and a heat balance.

4. Conclusions

In this review, recent developments in microbial fuel cell technology have been reviewed and current challenges associated with the further development of enzymatic and microbial fuel cells have been identified.

Research targets for microbial fuel cells are generally different from those for enzymatic fuel cells. MFC systems are typically discussed in the context of large-scale applications using wastewater or mixed organic compounds as fuels. Power densities have rapidly increased in the last few years to a few $W\,m^{-2}$ and over $1\,kW\,m^{-3}$ (of reactor volume). Most of the systems developed are <1 L in volume, though new understanding of the important parameters affecting reactor scale-up has successfully led to larger scale systems with similar performance characteristics. These developments have also been enabled by better insight into the species and processes responsible for electricity generation in biofilms. A direct electrical output with high efficiency, low operating temperatures, and good organic treatment efficiency (with the possibility of operating on low-strength wastewater) make MFCs ideal for waste treatment technologies (Watanabe, 2008; Rabaey and Verstraete, 2005).

References

Adachi, M., Shimomura, T., Komatsu, M., Yakuwa, H., Miya, A., 2008. Chem. Commun. 7, 2055–2057.
Aelterman, P., Freguia, S., Keller, J., Verstraete, W., Rabaey, K., 2008. Appl. Microbiol. Biotechnol. 78, 409–418.
Aelterman, P., Rabaey, K., Pham, H.T., Boon, N., Verstraete, W., 2006. Environ. Sci. Technol. 40, 3388–3394.
Ahn, Y., Logan, B.E., 2010. Bioresour. Technol. 101, 469–475.
Allen, R.M., Bennetto, H.P., 1993. Appl. Biochem. Biotechnol. 39–40, 27–40.
Bartlett, P.N., Pratt, K.F.E., 1995. J. Electroanal. Chem. 397, 61–78.
Bond, D., Lovley, D., 2003. Appl. Environ. Microbiol. 69, 1548–1555.
Bullen, R.A., Arnot, T.C., Lakeman, J.B., Walsh, F.C., 2006. Biosens. Bioelectron. 21, 2015–2045.
Calabrese-Barton, S., 2005. Electrochim. Acta 50, 2145–2153.
Chae, K.J., Choi, M., Ajayi, F.F., Park, W., Chang, I.S., Kim, I.S., 2008. Energy Fuels 22, 169–176.
Chae, K.J., Choi, M.J., Kim, K., Ajayi, F.F., Park, W., Kim, C.W., Kim, I.S., 2010. Bioresour. Technol. 101, 5350–5357.
Chaudhuri, S., Lovley, D., 2003. Nat. Biotechnol. 21, 1229–1232.
Chen, G.W., Choi, S.J., Lee, T.H., Lee, G.Y., Cha, J.H., Kim, W., 2008. Appl. Microbiol. Biotechnol. 79, 379–388.
Cheng, K.Y., Ho, G., Cord-Ruwisch, R., 2008. Environ. Sci. Technol. 42, 3828–3834.
Cheng, S., Liu, H., Logan, B.E., 2006a. Environ. Sci. Technol. 40, 364–369.
Cheng, S., Liu, H., Logan, B.E., 2006b. Electrochem. Commun. 8, 489–494.
Clauwaert, P., van-der Ha Nico Boon, D., Verbeken, K., Verhaege, M., Rabaey, K., Verstraete, W., 2007. Environ. Sci. Technol. 41, 7564–7569.
Crittenden, S.R., Sund, C.J., Sumner, J., 2006. Langmuir 22, 9473–9476.
Fan, Y., Hu, H., Liu, H., 2007a. J. Power Sources 171, 348–354.
Fan, Y., Hu, H., Liu, H., 2007b. Environ. Sci. Technol. 41, 8154–8158.
Fan, Y., Sharbrough, E., Liu, H., 2008. Environ. Sci. Technol. 42, 8101–8107.
Feng, Y., Wang, X., Logan, B.E., Lee, H., 2008. Appl. Microbiol. Technol. 78, 873–880.
Freguia, S., Tsujimura, S., Kano, K., 2010. Electrochim. Acta 55, 813–818.
Gallaway, J.W., Barton, S.A.C., 2008. J. Am. Chem. Soc. 130, 8527–8536.
He, Z., Angenent, L.T., 2006. Electroanalysis 18, 2009–2015.
He, Z., Wagner, N., Minteer, S.D., Angenent, L., 2006. Environ. Sci. Technol. 40, 5212–5217.
Ikeda, T., Kano, K., 2001. J. Biosci. Bioeng. 92, 9–18.
Kano, K., Ikeda, T., 2000. Anal. Sci. 16, 1013–1021.
Katuri, K.P., Scott, K., 2010. Biotechnol. Bioeng. 107, 52–58.
Katz, E., Shipway, A., Willner, I., 2003. Handbook of Fuel Cells – Fundamentals, Technology and Applications. John Wiley & Sons Ltd (Chapter 21 – Biochemical fuel cells).
Kim, B.H., Chang, I.S., Gadd, G.M., 2007a. Appl. Microbiol. Biotechnol. 76, 485–494.
Kim, J., Parkey, J., Rhodes, C., Gonzalez-Martin, A., 2009. J. Solid State Electrochem. 13, 1043–1050.
Kim, J.R., Cheng, S., Eun Oh, S., Logan, B.E., 2007b. Environ. Sci. Technol. 41, 1004–1009.
Kim, J.R., Min, B., Logan, B.E., 2005. Appl. Microbiol. Biotechnol. 68, 23–30.
Kjeang, E., Sinton, D., Harrington, D., 2006. J. Power Sources 158, 1–12.
Larminie, J., Dicks, A., 2003. Fuel Cell Systems Explained. John Wiley & Sons.
Sool Lee, H., Parameswaran, P., Kato-Marcus, A., Torres, C.I., Rittmann, B.E., 2008. Water Res. 42, 1501–1510.
Liu, H., Cheng, S., Huang, L., Logan, B., 2008. J. Power Sources 179, 274–279.
Liu, H., Logan, B., 2004. Environ. Sci. Technol. 38, 4040–4046.
Logan, B.E., 2009. Nat. Rev.: Microbiol. 7, 375–381.
Logan, B.E., 2010. Appl. Microbiol. Biotechnol. 85, 1665–1671.
Logan, B.E., Cheng, S., Watson, V., Estadt, G., 2007. Environ. Sci. Technol. 41, 3341–3346.
Logan, B.E., Hamelers, B., Rozendal, R., Schröder, U., Keller, J., Freguia, S., Aelterman, P., Verstraete, W., Rabaey, K., 2006. J. Am. Chem. Soc. 40, 5181–5192.
Logan, B.E., Murano, C., Scott, K., Gray, N.D., Head, I.M., 2005. Water Res. 39, 942–952.
Lovley, D.R., 2006. Curr. Opin. Biotechnol. 17, 327–332.
Lowy, D., Tender, L.M., Zeikus, J.G., Park, D.H., Lovley, D.R., 2006. Biosens. Bioelectron. 21, 2058–2063.
Marcus, A.K., Torres, C.I., Rittmann, E., 2007. Biotechnol. Bioeng. 98, 1171–1182.
Mohan, S.V., Raghavulu, S.V., Sarma, P.N., 2008. Biosens. Bioelectron. 24, 41–47.
Nevin, K.P., Richter, H., Covalla, S.F., Johnson, J.P., Woodard, T.L., Orloff, A.L., Jia, H., Zhang, M., Lovley, D.R., 2008. Environ. Microbiol. 10, 2505–2514.
Nielsen, M.E., Reimers, C.E., Stecher III, H.A., 2007. Environ. Sci. Technol. 41, 7895–7900.
Nielsen, M.E., Reimers, C.E., White, H.K., Sharmab, S., Girguis, P.R., 2008. Energy Environ. Sci. 1, 584–593.
Eun Oh, S., Logan, B.E., 2006. Appl. Microbiol. Biotechnol. 70, 162–169.
Oh, S.E., Kim, J.R., Joo, J.H., Logan, B.E., 2009. Water Sci. Technol. 60, 1311–1317.
Pant, D., Van Bogaert, G., Diels, L., Vanbroekhoven, K., 2010. Bioresour. Technol. 101, 1533–1543.
Park, D.H., Zeikus, J.G., 2003. Biotechnol. Bioeng. 81, 348–355.
Park, H.S., Kim, B.H., Kim, H.S., Kim, H.J., Kim, G.J., Kim, M., Chang, I.S., Park, Y.K., Chang, H.I., 2001. Anaerobe 7, 297–306.
Pham, H.T., Jang, J.K., Kim, I.S., 2004. J. Microbiol. Biotechnol. 14, 324–329.
Pham, T.H., Boon, N., Aelterman, P., Clauwaert, P., Schamphelaire, L.D., Vanhaecke, L., Maeyer, K.D., Höfte, M., Verstraete, W., Rabaey, K., 2008. Appl. Microbiol. Biotechnol. 77, 1119–1129.
Picioreanu, C., Head, I.M., Katuri, K.P., van-Loosdrecht, M.C.M., Scott, K., 2007. Water Res. 41, 2921–2940.
Picioreanu, C., van Loosdrecht, M.C.M., Curtis, T.P., Scott, K., 2010. Bioelectrochemistry 78, 8–24.
Prasad, D., Arun, S., Murugesan, M., Padmanaban, S., Satyanarayanan, R.S., Berchmans, S., Yegnaraman, V., 2007. Biosens. Bioelectron. 22, 2604–2610.
Rabaey, K., Boon, N., Höfte, M., Verstraete, W., 2005a. Environ. Sci. Technol. 39, 3401.
Rabaey, K., Boon, N., Sicilia, S., Verhaege, M., Verstraete, W., 2004. Appl. Environ. Microbiol. 70, 5373–5382.
Rabaey, K., Ossieur, W., Verhaege, M., Verstraete, W., 2005b. Water Sci. Technol. 52, 515–523.
Rabaey, K., Verstraete, W., 2005. Trends Biotechnol. 23, 291–298.
Reimers, C.E., Tender, L.M., Stecher, H.A., Holmes, D.E., Bond, D.R., Lowy, D.A., Ans, S., Fertig, K.P., Lovley, D.R., 2002. Nat. Biotechnol. 20, 821–825.
Richter, H., McCarthy, K., Nevin, K., Johnson, J., Rotello, V., Lovley, D., 2008. Langmuir 24, 4376–4379.
Ringeisen, B.R., Henderson, E., Wu, P.K., Pietron, J., Ray, R., Little, B., Biffinger, J., Jones-Meehan, J., 2006. Environ. Sci. Technol. 40, 2629–2634.
Ringeisen, B.R., Ray, R., Little, B., 2007. J. Power Sources 165, 591–597.
Rozendal, R.A., Hamelers, H.V.M., Buisman, C.J.N., 2006. Environ. Sci. Technol. 40, 5206–5211.
Rozendal, R.A., Sleutels, T.H.J.A., Hamelers, H.V.M., Buisman, C.J.N., 2008. Water Sci. Technol. 57, 1757–1762.
Schaetzle, O., Barrière, F., Schröder, U., 2009. Energy Environ. Sci. 2, 96–99.
Shah, A.A., Ralph, T.R., Walsh, F.C., 2009. J. Electrochem. Soc. 156, B465–B484.
Shah, A.A., Sui, P.C., Kim, G.S., Ye, S., 2007. J. Power Sources 166, 1–21.
Shah, A.A., Walsh, F.C., 2008. J. Power Sources 185, 287–301.
Shimoyama, T., Komukai, S., Yamazawa, A., Ueno, Y., Logan, B.E., Watanabe, K., 2008. Environ. Biotechnol. 80, 325–330.
Shukla, A.K., Suresh, P., Berchmans, S., Rajendran, A., 2004. Curr. Sci. 87, 455–468.
Tender, L.M., Gray, S.A., Groveman, E., Lowy, D.A., Kauffman, P., Melhado, J., Tyce, R.C., Flynn, D., Petrecca, R., Dobarro, J., 2008. J. Power Sources 179, 571–575.

Tender, L.M., Reimers, C.E., Fertig, S., Wang, W., 2001. Environ. Sci. Technol. 35, 192–195.
Watanabe, K., 2008. J. Biosci. Bioeng. 106, 528–536.
Xing, D., Zuo, Y., Cheng, S., Regan, J.M., Logan, B.E., 2008. Environ. Sci. Technol. 42, 4146–4151.
You, S., Zhao, Q., Zhang, J., Jiang, J., Zhao, S., 2006. J. Power Sources 162, 1409–14115.
Zeng, Y., Choo, Y.F., Kim, H.H., Wu, P., 2010. J. Power Sources 195, 79–89.
Zhang, X., Cheng, S., Huang, X., Logan, B.E., 2009. Biosens. Bioelectron. 11, 2177–2180.